AMIRA International

JUNE 2000

CONFIDENTIAL

PROGRESS REPORT NO. 1

Geological, Tectonic and Metallogenic Relations of South China

P603

CODES SRC
Centre for Ore Deposit Research

University of Tasmania
Australia

AMIRA INTERNATIONAL ACN 004448266
LEVEL 9, 128 EXHIBITION STREET, MELBOURNE, VIC 3000 AUSTRALIA
TEL: (61) 3 9679 9999, FAX: (61) 3 9679 9900, WEB: WWW.AMIRA.COM.AU

CONFIDENTIAL

Contents

Geological, Tectonic and Metallogenic Relations of South China (P603)

Research Team:

Khin Zaw
Eleanor Bruce
Clive Burrett
Ron Berry
Ross Large

Geological, Tectonic and Metallogenic Relations of South China (P603)

10.30-10:40 am	Introduction (Alan Goode)
10.40-11.00 am	Aims, background and progress (Khin Zaw)
11.00-11:15 am	TEA/COFFEE
11:15-11:45 pm	Tectonics of China (Clive Burrett)
11:45-12:15 pm	Metallogenic relations of China and deposit compilation (Khin Zaw)
12:15-1:00 pm	GIS up-date (Eleanor Bruce)
1.00-2.00 pm	LUNCH
2:00-2:30 pm	Future program (Khin Zaw)
2:30-3:00 pm	General discussions and comments (Sponsors))

Geological, Tectonic and Metallogenic Relations in South China (P603)

- **Aims of the Project**
  - To establish a GIS (ARC/INFO, ArcView and MapInfo) integrated, comprehensive digital geoscience data set and mineral deposit database for south China focussing on the distribution of ore deposits building on the successful AMIRA project P390A for mainland SE Asia

    (Project-related GIS vs Custodial GIS)
  - To undertake a tectonic and metallogenic analysis of the selected mineralised belts in the region, with particular emphasis on geological features, structural relationships, and regional metal zonation based on the GIS database, and geochronological data
  - To develop a geotectonic and metallogenic model for the evolution and origin of mineralised belts in these regions.

CODES SRC

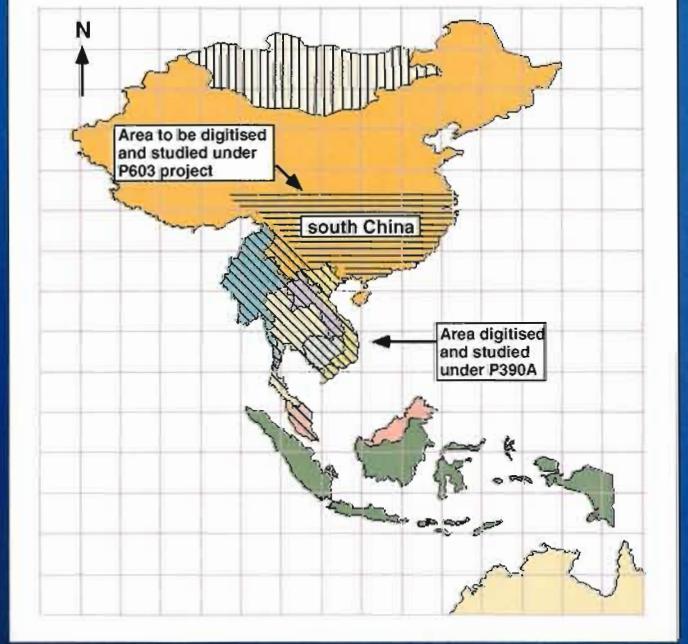

CODES SRC

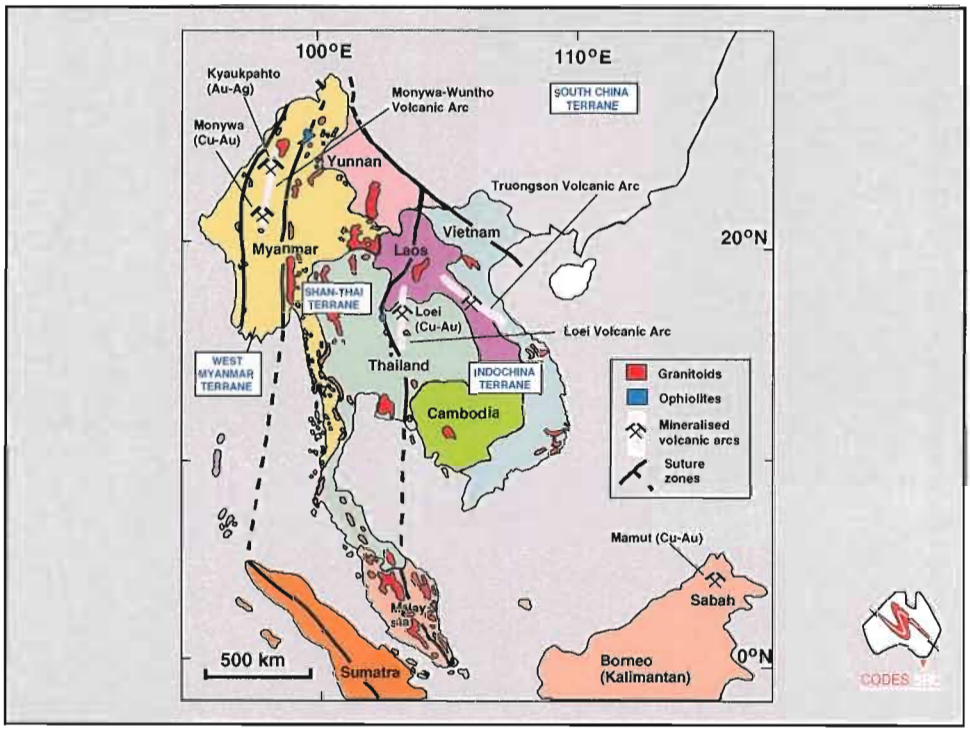
100°E
110°E
20°N
0°N
Kyaukpahto (Au-Ag)
Monywa (Cu-Au)
Monywa-Wuntho Volcanic Arc
SOUTH CHINA TERRANE
Yunnan
Truongson Volcanic Arc
Vietnam
Myanmar
Laos
SHAN-THAI TERRANE
Loei (Cu-Au)
Loei Volcanic Arc
WEST MYANMAR TERRANE
Thailand
INDOCHINA TERRANE
Cambodia
Granitoids
Ophiolites
Mineralised volcanic arcs
Suture zones
Mamut (Cu-Au)
Sabah
Malay Basin
500 km
Sumatra
Borneo (Kalimantan)
CODES SRC

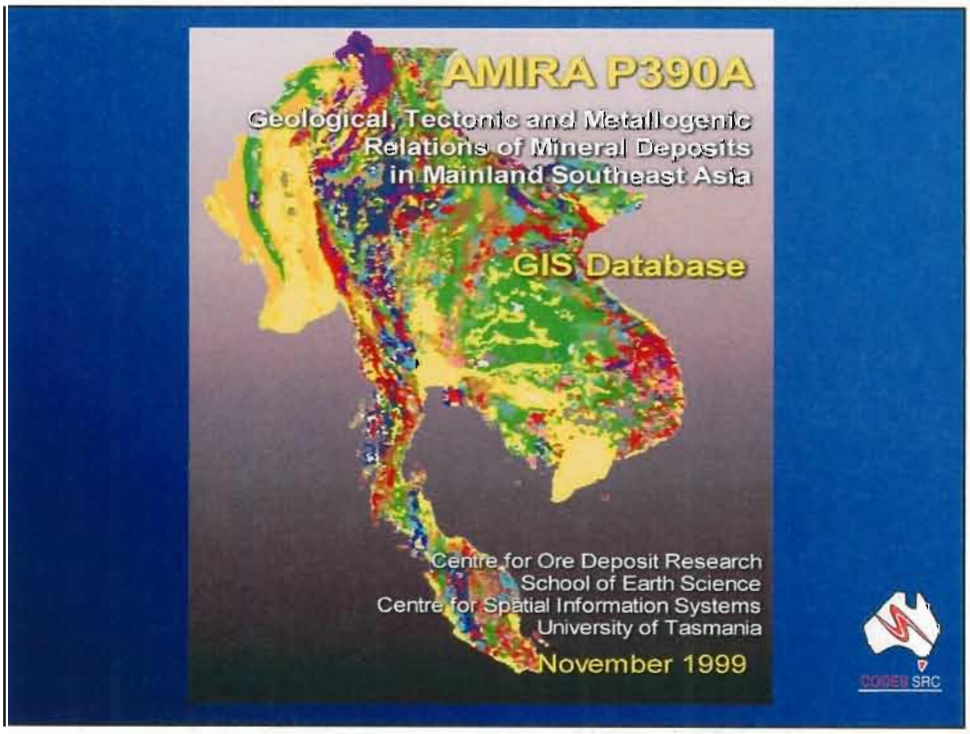
AMIRA P390A
Geological, Tectonic and Metallogenic Relations of Mineral Deposits in Mainland Southeast Asia
GIS Database
Centre for Ore Deposit Research
School of Earth Science
Centre for Spatial Information Systems
University of Tasmania
November 1999
CODES SRC

GIS compilation

Myanmar	1,000,000 scale geological map published by Myanmar Government in 1977
Laos	1,000,000 scale geological map by British Geological Survey in 1990
Cambodia	500,000 scale geological map published by UN-ESCAP in 1993
Thailand	1,000,000 scale geological map published by Department of Mineral Resources, Thailand in 1982
Malaysia	500,000 scale geological map published by Geological Survey of Malaya in 1985
Vietnam	1,500,000 scale geological map published by UN-ESCAP in 1990
Yunnan	1,000,000 scale geological map published by Chinese Government in 1983

SRC

Deposit Database

◆ Myanmar	-	736 occurrences
◆ Laos PDR	-	533 occurrences
◆ Cambodia	-	113 occurrences
◆ Thailand	-	1562 occurrences
◆ Malaysia	-	624 occurrences
◆ Vietnam	-	130 occurrences
◆ SW Yunnan	-	32 occurrences
Total	-	3730 occurrences

CODES SRC

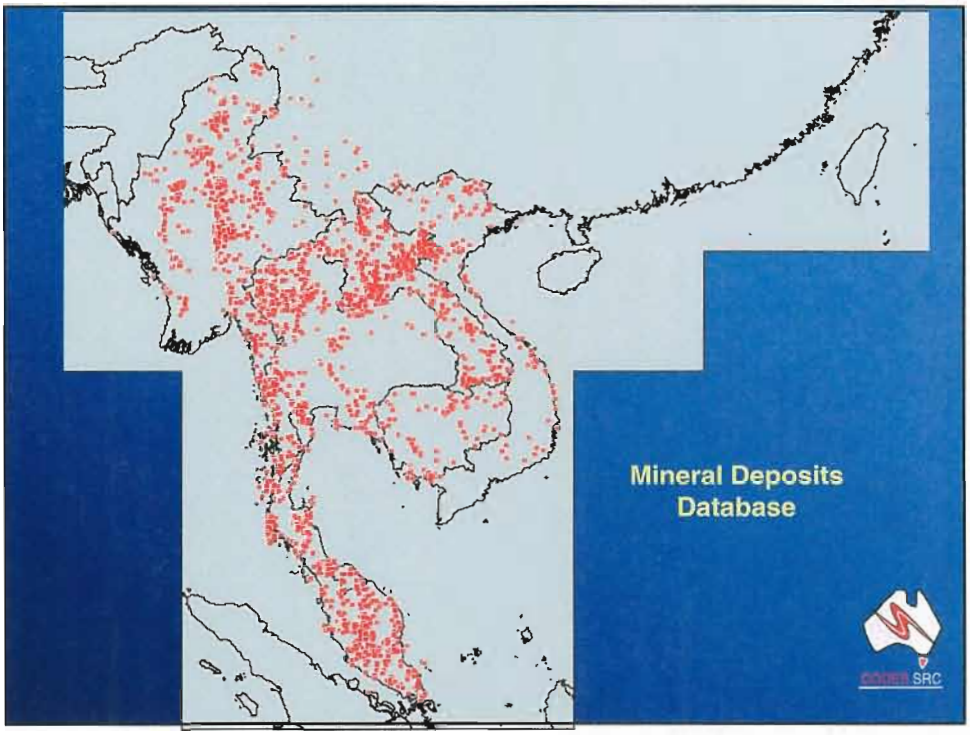
Mineral Deposits
Database
CODES SRC

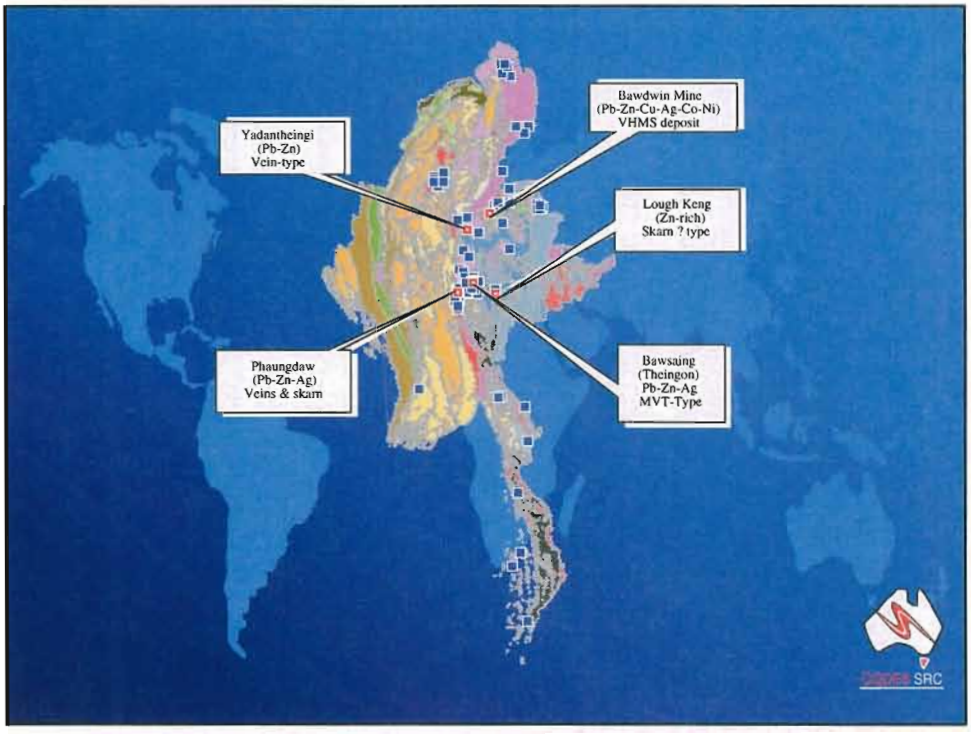
Yadantheingi
(Pb-Zn)
Vein-type
Bawdwin Mine
(Pb-Zn-Cu-Ag-Co-Ni)
VHMS deposit
Lough Keng
(Zn-rich)
Skarn ? type
Phaungdaw
(Pb-Zn-Ag)
Veins & skarn
Bawsaing
(Theingon)
Pb-Zn-Ag
MVT-Type
CODES SRC

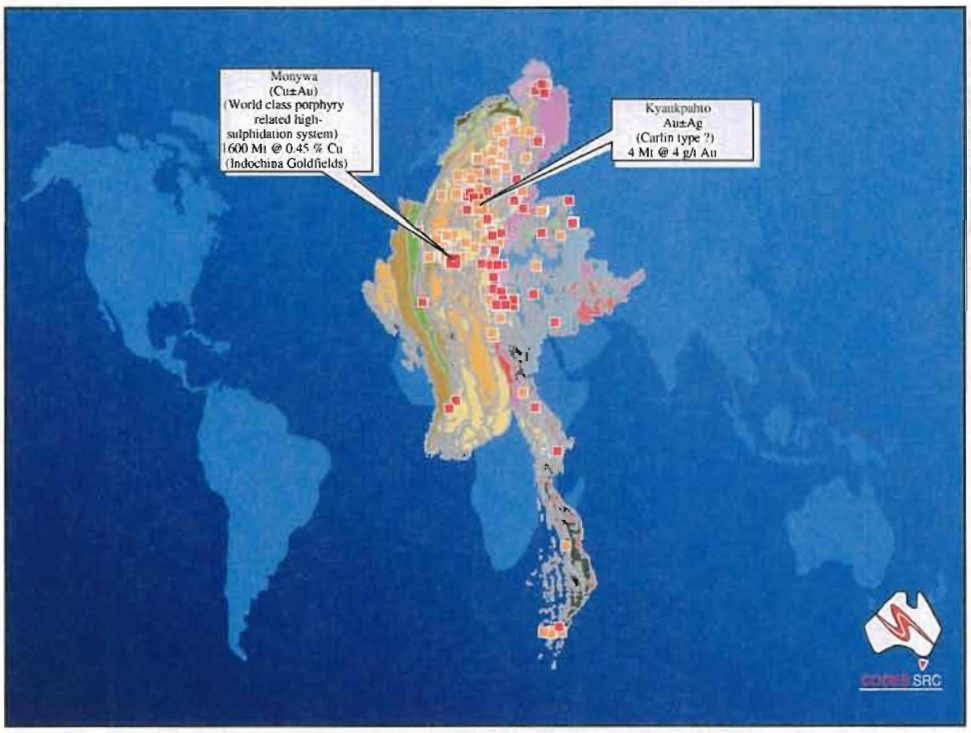
Monywa
(Cu±Au)
(World class porphyry
related high-
sulphidation system)
1600 Mt @ 0.45 % Cu
(Indochina Goldfields)
Kyaukpahto
Au±Ag
(Carlin type ?)
4 Mt @ 4 g/t Au
CODES SRC

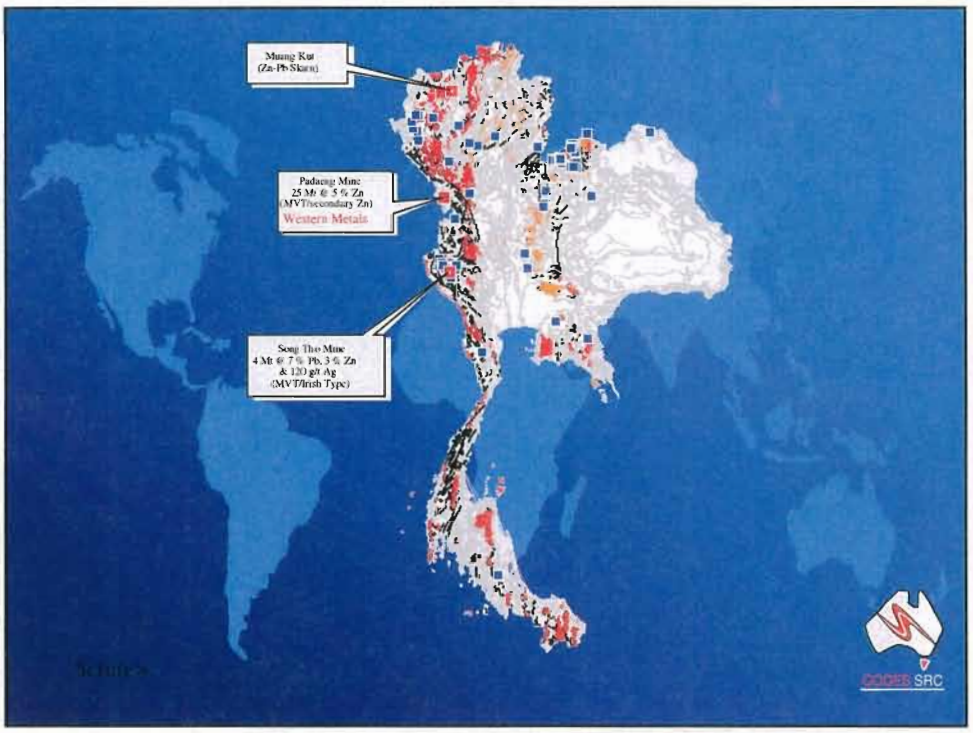
Muang Kut
(Zn-Pb Skarn)
Padaeng Mine
25 Mt @ 5 % Zn
(MVT/secondary Zn)
Western Metals
Song Thao Mine
4 Mt @ 7 % Pb, 3 % Zn
& 120 g/t Ag
(MVT/Irish Type)
CODES SRC

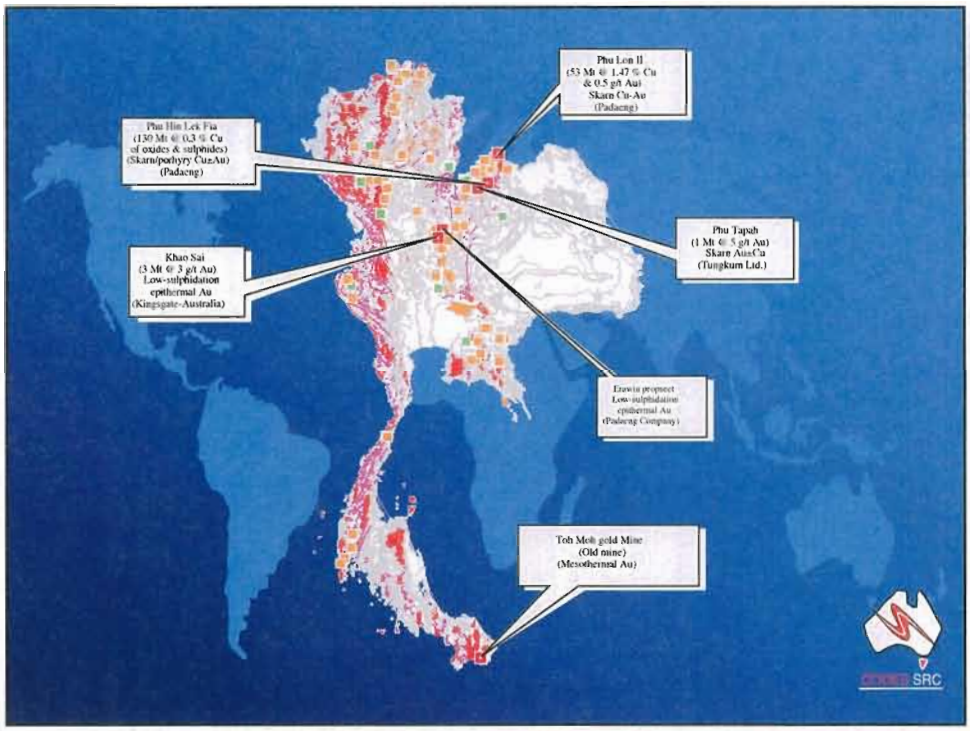
Phu Lon II
(53 Mt @ 1.47 % Cu
& 0.5 g/t Au)
Skarn Cu-Au
(Padaeng)
Phu Hin Lek Fia
(130 Mt @ 0.3 % Cu
of oxides & sulphides)
(Skarn/porhyry CuzAu)
(Padaeng)
Phu Tapah
(1 Mt @ 5 g/t Au)
Skarn Au±Ca
(Tungkum Ltd.)
Khao Sai
(3 Mt @ 3 g/t Au)
Low-sulphidation
epithermal Au
(Kingsgate-Australia)
Erawin prospect
Low-sulphidation
epithermal Au
(Padaeng Company)
Toh Meh gold Mine
(Old mine)
(Mesothermal Au)
CODES SRC

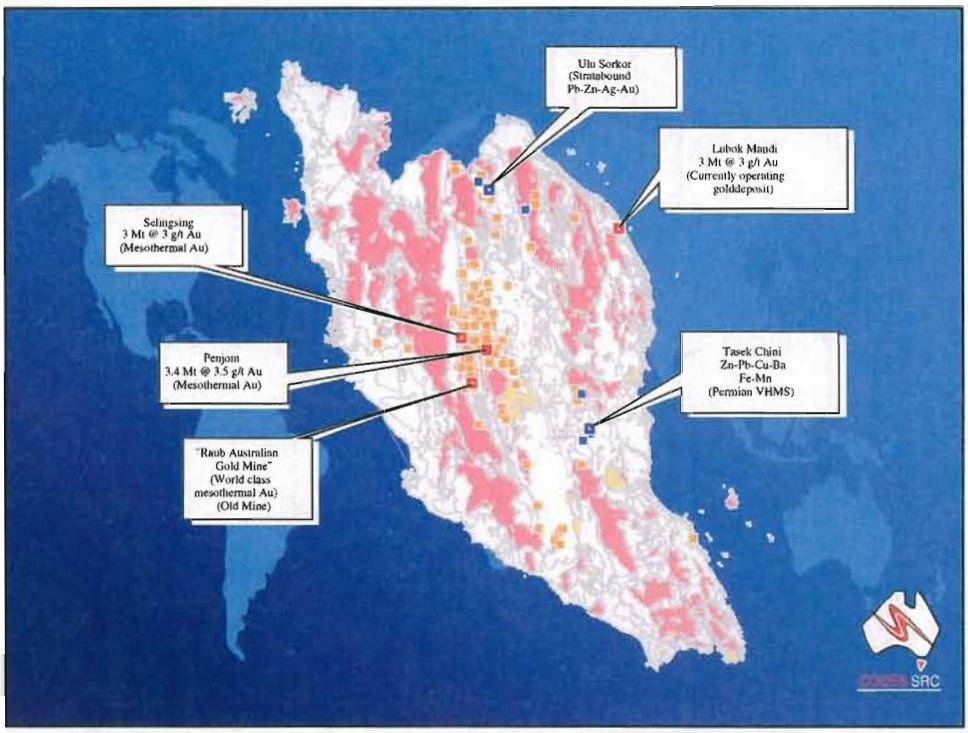
Ulu Sorkor
(Stratabound
Pb-Zn-Ag-Au)
Lubok Mandi
3 Mt @ 3 g/t Au
(Currently operating
golddeposit)
Selingsing
3 Mt @ 3 g/t Au
(Mesothermal Au)
Penjom
3.4 Mt @ 3.5 g/t Au
(Mesothermal Au)
Tasek Chini
Zn-Pb-Cu-Ba
Fe-Mn
(Permian VHMS)
"Raub Australian
Gold Mine"
(World class
mesothermal Au)
(Old Mine)
CODES SRC

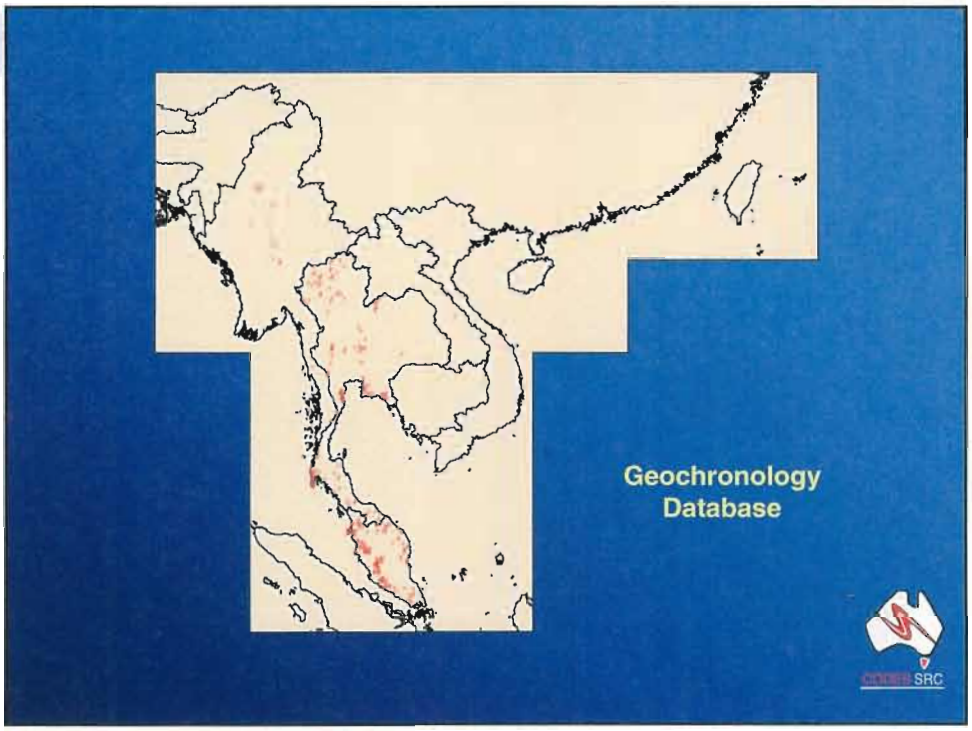
Geochronology
Database
CODES SRC

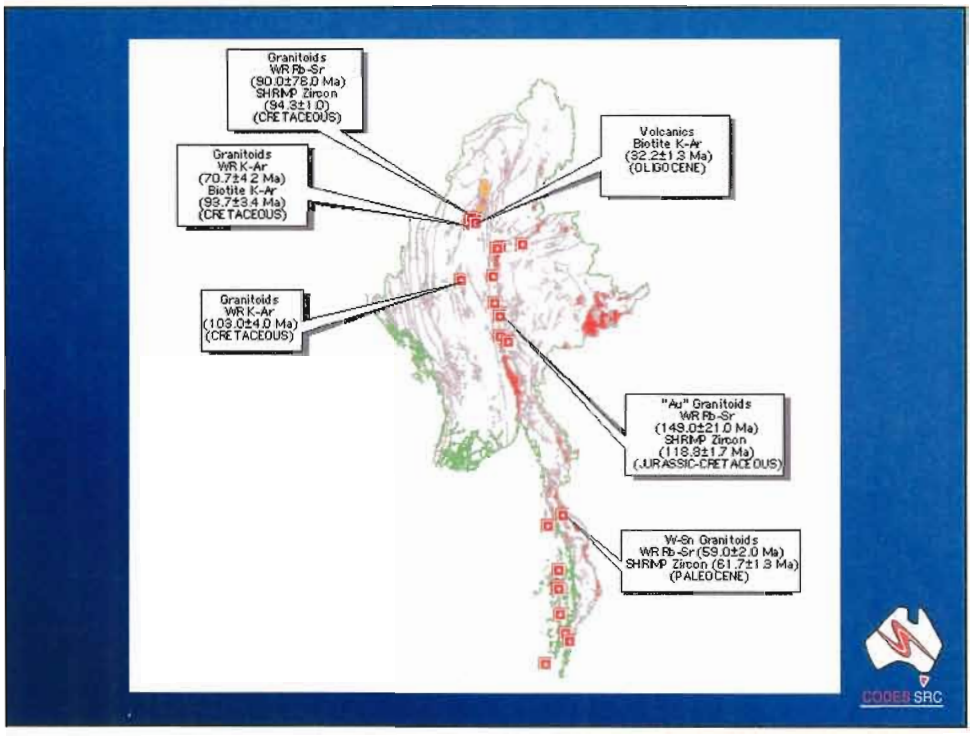
Granitoids
WR Rb-Sr
(90.0±7.8.0 Ma)
SHRIMP Zircon
(94.3±1.0)
(CRETACEOUS)
Granitoids
WR K-Ar
(70.7±4.2 Ma)
Biotite K-Ar
(99.7±3.4 Ma)
(CRETACEOUS)
Granitoids
WR K-Ar
(103.0±4.0 Ma)
(CRETACEOUS)
Volcanics
Biotite K-Ar
(32.2±1.3 Ma)
(OLIGOCENE)
"Au" Granitoids
WR Rb-Sr
(149.0±21.0 Ma)
SHRIMP Zircon
(118.3±1.7 Ma)
(JURASSIC-CRETACEOUS)
W-Sn Granitoids
WR Rb-Sr (59.0±2.0 Ma)
SHRIMP Zircon (61.7±1.3 Ma)
(PALEOCENE)
CODES SRC

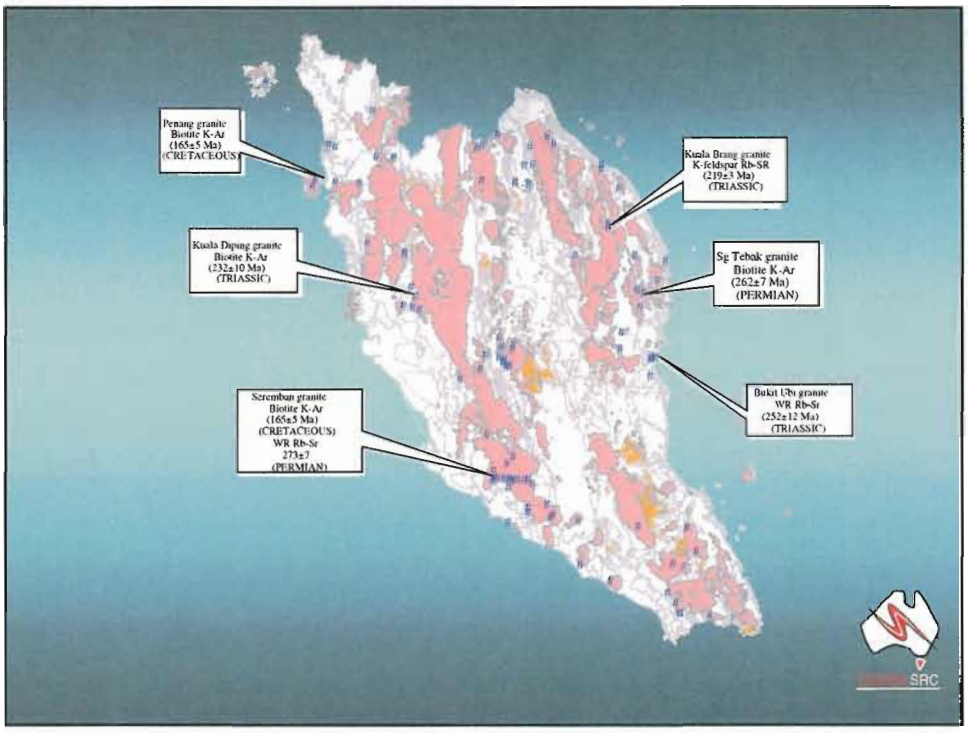
Penang granite
Biotite K-Ar
(165±5 Ma)
(CRETACEOUS)
Kuala Dipang granite
Biotite K-Ar
(232±10 Ma)
(TRIASSIC)
Seremban granite
Biotite K-Ar
(165±5 Ma)
(CRETACEOUS)
WR Rb-Sr
273±7
(PERMIAN)
Kuala Berang granite
K-feldspar Rb-SR
(219±3 Ma)
(TRIASSIC)
Sg Tebak granite
Biotite K-Ar
(262±7 Ma)
(PERMIAN)
Bukit Ubi granite
WR Rb-Sr
(252±12 Ma)
(TRIASSIC)
SRC

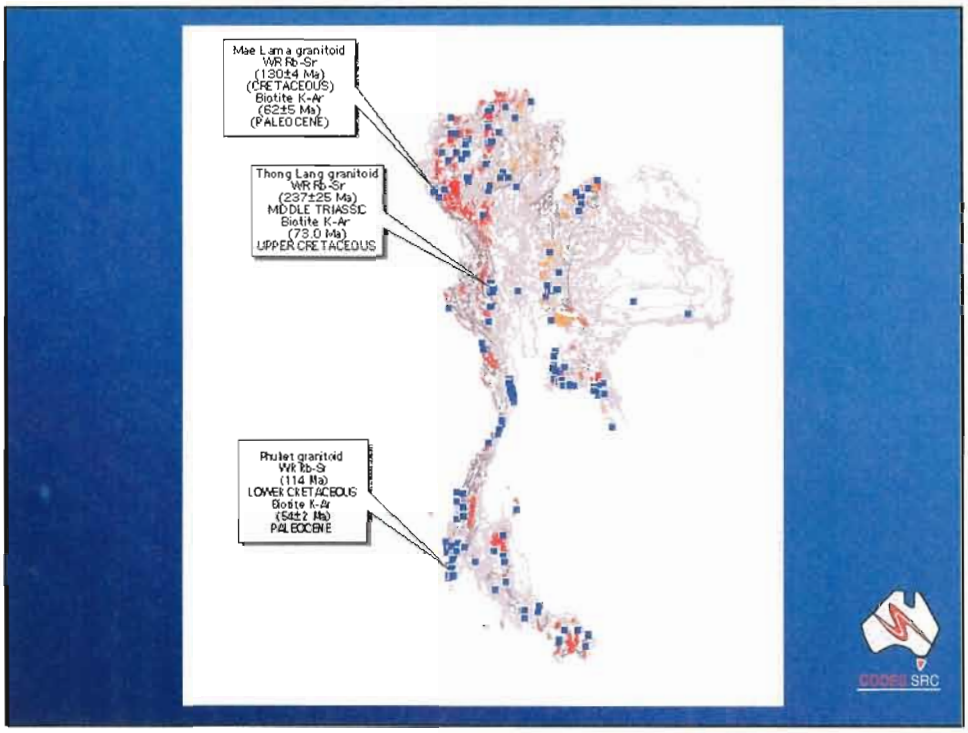
Mae Lama granitoid
WR Rb-Sr
(130±4 Ma)
(CRETACEOUS)
Biotite K-Ar
(62±5 Ma)
(PALEOCENE)
Thong Lang granitoid
WR Rb-Sr
(237±25 Ma)
MIDDLE TRIASSIC
Biotite K-Ar
(73.0 Ma)
UPPER CRETACEOUS
Phulet granitoid
WR Rb-Sr
(114 Ma)
LOWER CRETACEOUS
Biotite K-Ar
(54±2 Ma)
PALEOCENE
SRC

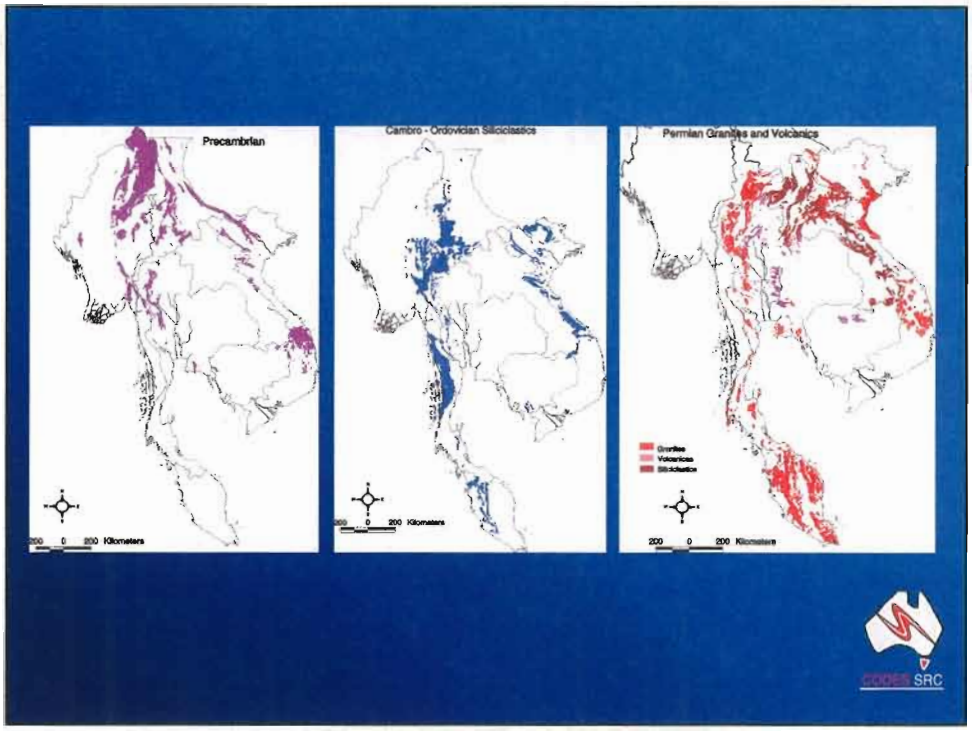
Precambrian
Cambro - Ordovician Siliciclastics
Permian Granites and Volcanics
Granites
Volcanics
Siliciclastics
200 0 200 Kilometers
CODES SRC

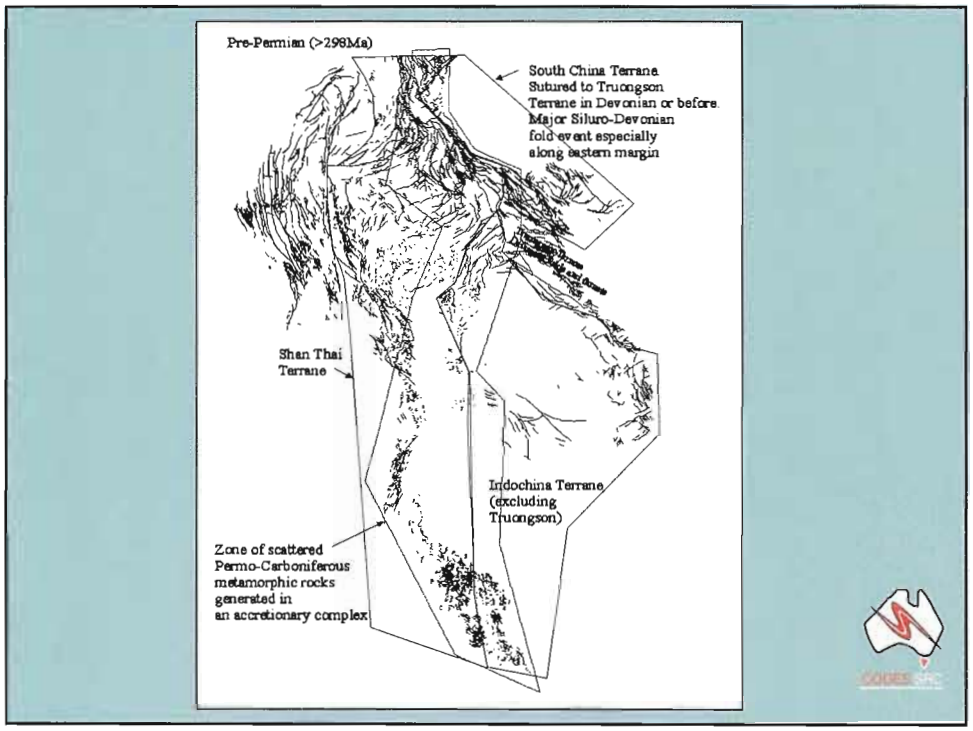
Pre-Permian (>298Ma)
South China Terrane
Sutured to Truongson
Terrane in Devonian or before.
Major Siluro-Devonian
fold event especially
along eastern margin
Shan Thai
Terrane
Indochina Terrane
(excluding
Truongson)
Zone of scattered
Permo-Carboniferous
metamorphic rocks
generated in
an accretionary complex
CODES SRC

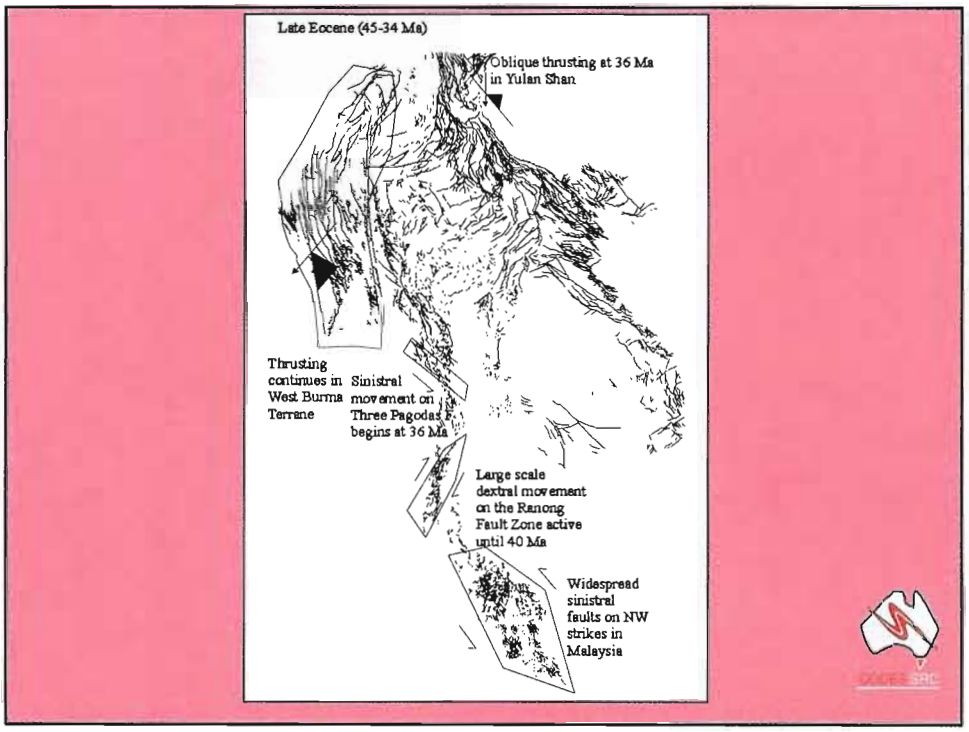
Late Eocene (45-34 Ma)
Oblique thrusting at 36 Ma in Yulan Shan
Thrusting continues in West Burma Terrane
Sinistral movement on Three Pagodas F. begins at 36 Ma
Large scale dextral movement on the Ranong Fault Zone active until 40 Ma
Widespread sinistral faults on NW strikes in Malaysia

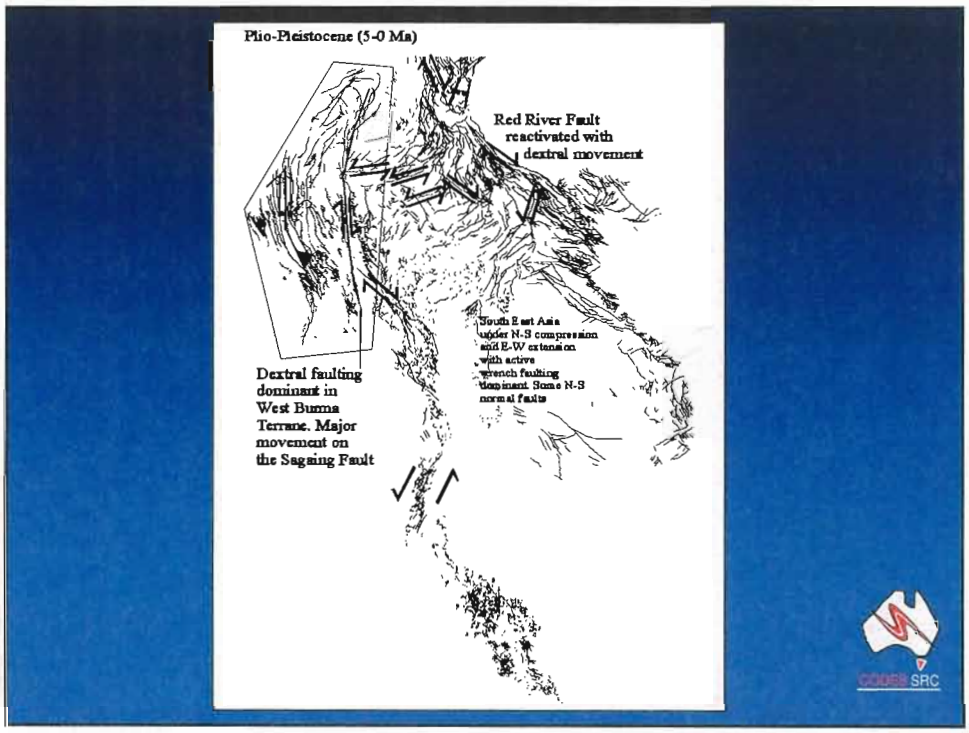
Plio-Pleistocene (5-0 Ma)
Red River Fault reactivated with dextral movement
South East Asia under N-S compression and E-W extension with active wrench faulting dominant. Some N-S normal faults
Dextral faulting dominant in West Burma Terrane. Major movement on the Sagaing Fault

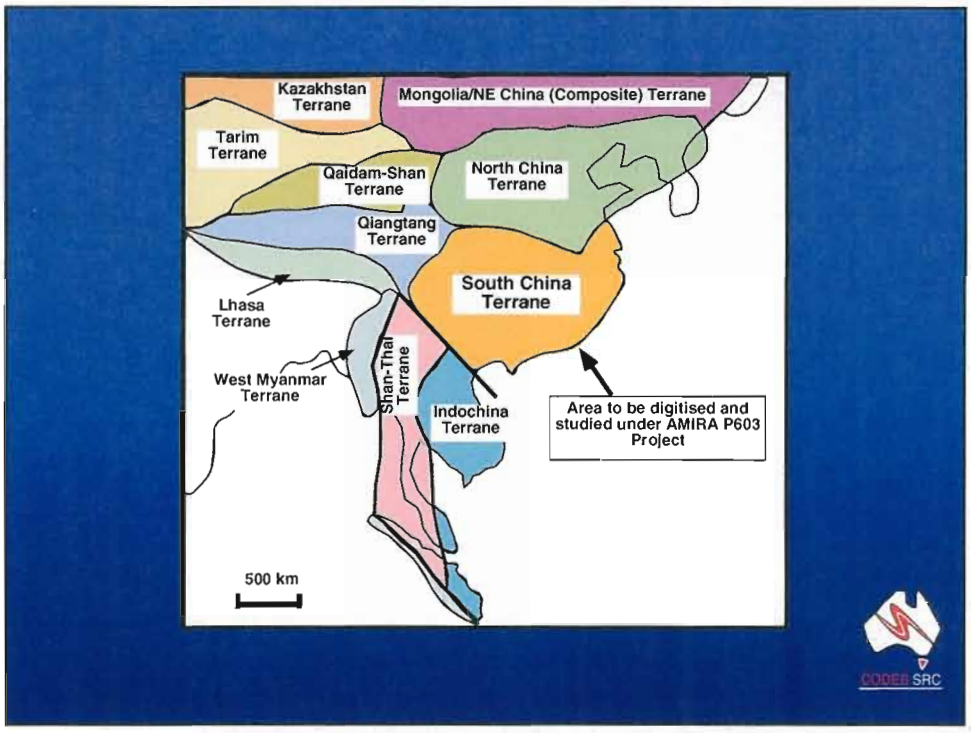
Kazakhstan Terrane
Mongolia/NE China (Composite) Terrane
Tarim Terrane
Qaidam-Shan Terrane
North China Terrane
Qiangtang Terrane
South China Terrane
Lhasa Terrane
West Myanmar Terrane
Shan-Thai Terrane
Indochina Terrane
Area to be digitised and studied under AMIRA P603 Project
500 km
CODES SRC

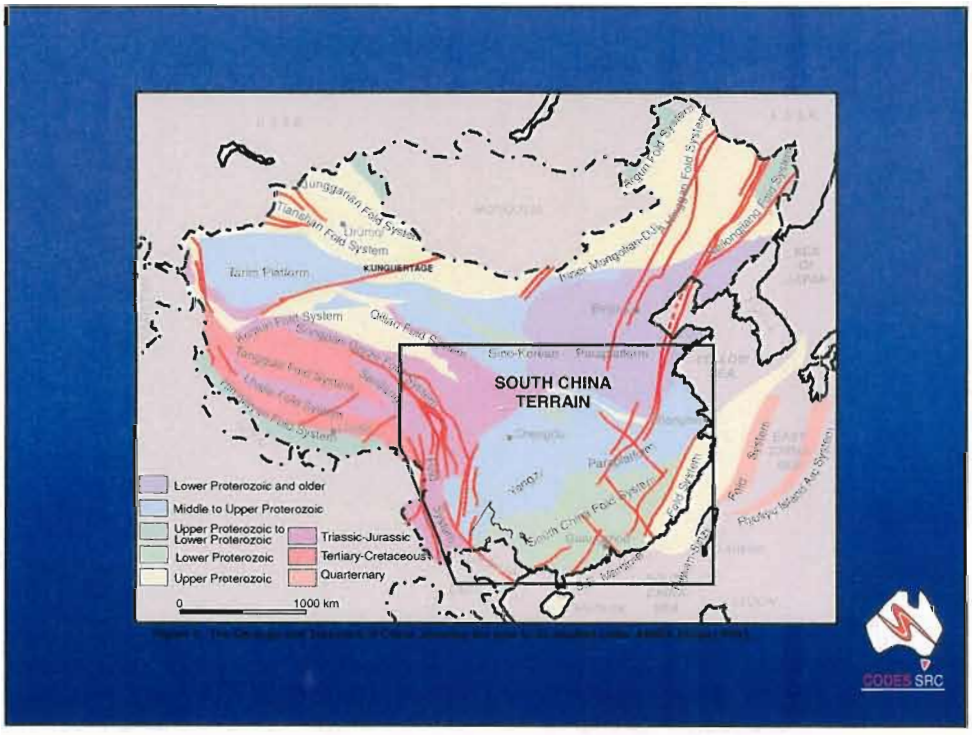
SOUTH CHINA TERRAIN
Lower Proterozoic and older
Middle to Upper Proterozoic
Upper Proterozoic to Lower Proterozoic
Lower Proterozoic
Upper Proterozoic
Triassic-Jurassic
Tertiary-Cretaceous
Quarternary
0
1000 km
CODES SRC

Table 1. Proposed program showing general time frame and reporting for the project.

1999-2000	2000-2001	2001-2002
--------Literature review, data collection & data compilation ----------		
---------Input of existing data into GIS & Field checking ----------		
	-------Tectonic, Palaeogeographic and Metallogenic Interpretation -------	
---Reporting --Reporting ---Reporting---Reporting ---Reporting---Reporting--		

CODES SRC

Province	Proposed program	1999-2000	2000-2001	2001-2002
Yunnan & Sichuan	Geology coverage Deposit database			
Guangxi & Guizhou	Geology coverage Deposit database			
Guangdong & Hunan	Geology coverage Deposit database			
Hubei & Jiangxi	Geology coverage Deposit database			
Fujian & Shandong	Geology coverage Deposit database			
Anhui & Jiansu	Geology coverage Deposit database			
Zhejing & Shanghai	Geology coverage Deposit database			

Amira P603

Geological, Tectonic and Metallogenic Relations of Mineral Deposits in Mainland South China

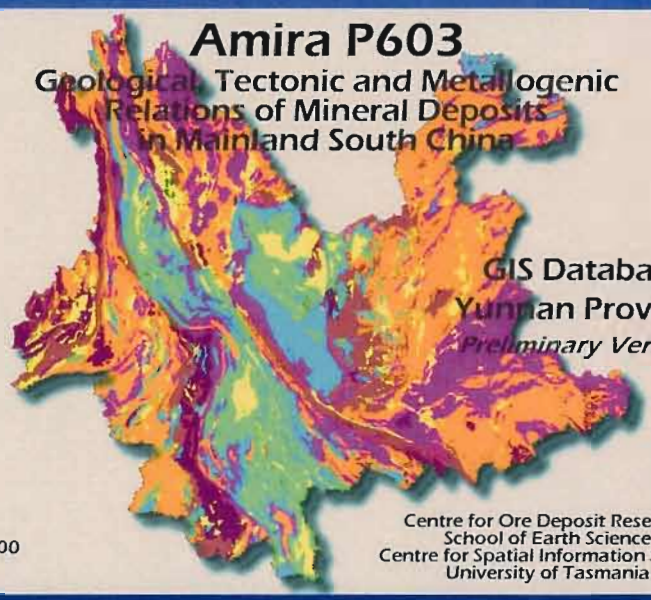

GIS Database

Yunnan Province

Preliminary Version

June 2000

Centre for Ore Deposit Research
School of Earth Science
Centre for Spatial Information Science
University of Tasmania

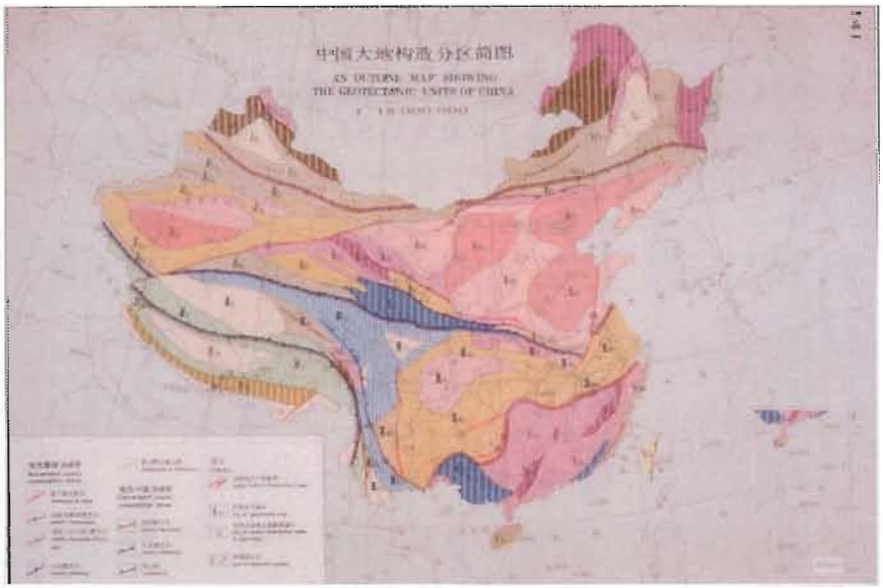
中国大地构造分区简图
THE GEOTECTONIC UNITS OF CHINA


9
QINLING OCEAN
SOUTH CHINA OCEAN
YANGTZE LAND
INTERMEDIATE TYPE
MOBILE TYPE
华南中元古代（1.9亿年前）古地理图
PALAEOGEOGRAPHIC MAP OF THE MIDDLE PROTEROZOIC
(PRIOR TO 1000 m.y. BP) OF SOUTH CHINA

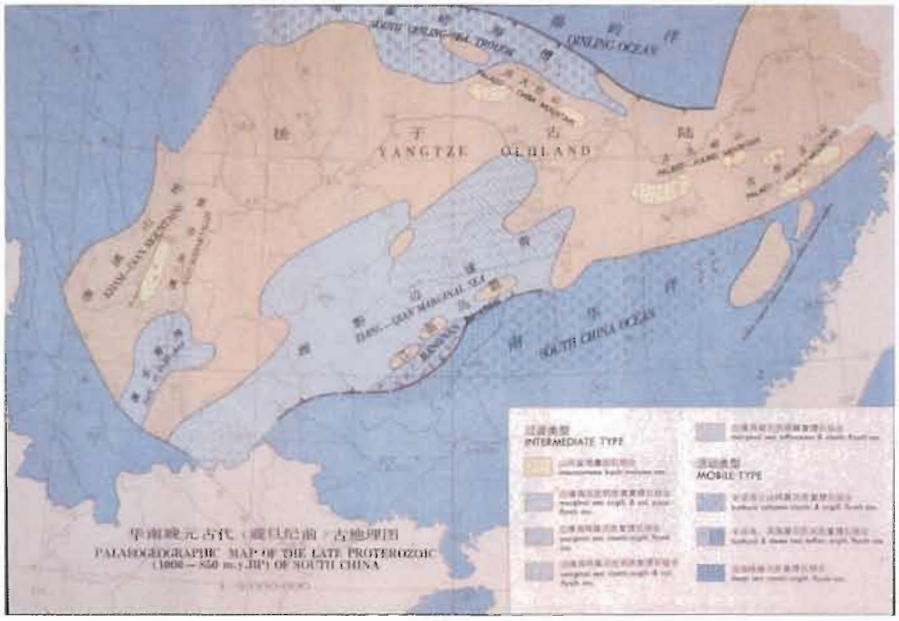
QINLING OCEAN
YANGTZE LAND
SOUTH CHINA OCEAN
INTERMEDIATE TYPE
MOBILE TYPE
华南晚元古代（震旦纪前）古地理图
PALAEOGEOGRAPHIC MAP OF THE LATE PROTEROZOIC
(1000 — 850 m.y.BP) OF SOUTH CHINA


中国中、晚元古代古构造图
（前震旦纪）
PALAEOTECTONIC MAP OF THE MIDDLE AND
LATE PROTEROZOIC (PRE－SINIAN) OF CHINA

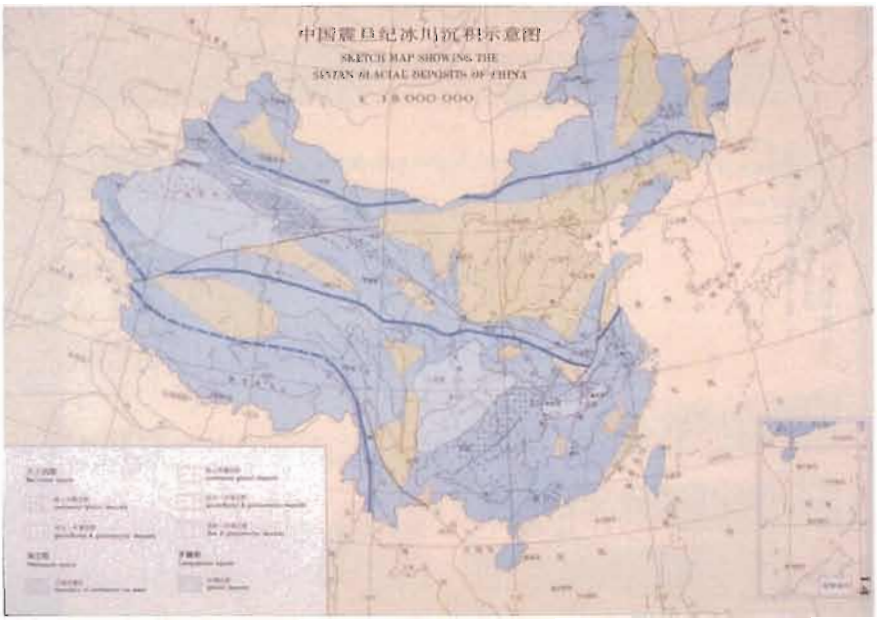
中国震旦纪冰川沉积示意图
SKETCH MAP SHOWING THE
SINIAN GLACIAL DEPOSITS OF CHINA


中国早寒武世古地理图
PALAEOGEOGRAPHIC MAP
OF THE EARLY SINIAN OF CHINA


中国晚寒武世古地理图
PALAEOGEOGRAPHIC MAP
OF THE LATE SINIAN OF CHINA

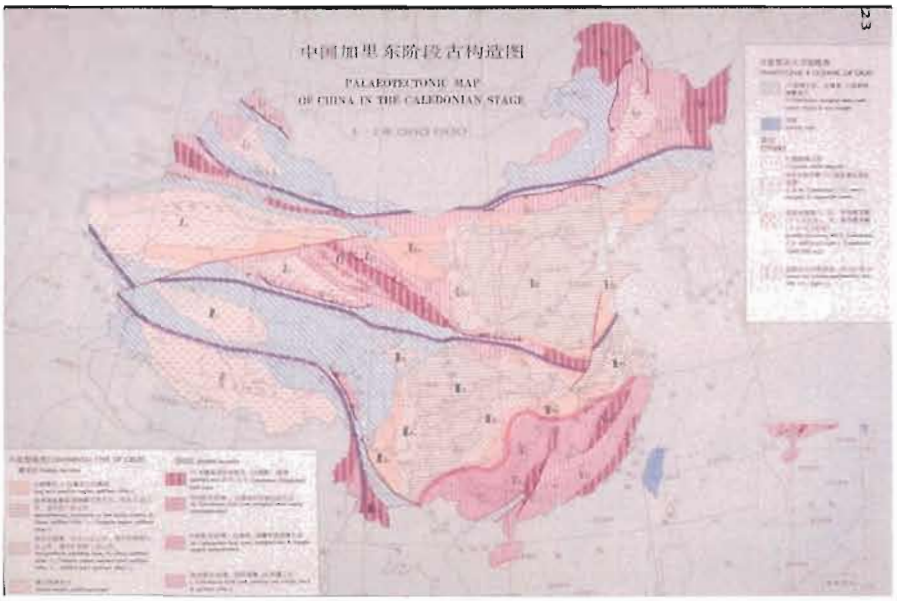
中国加里东阶段古构造图
PALAEOTECTONIC MAP
OF CHINA IN THE CALEDONIAN STAGE

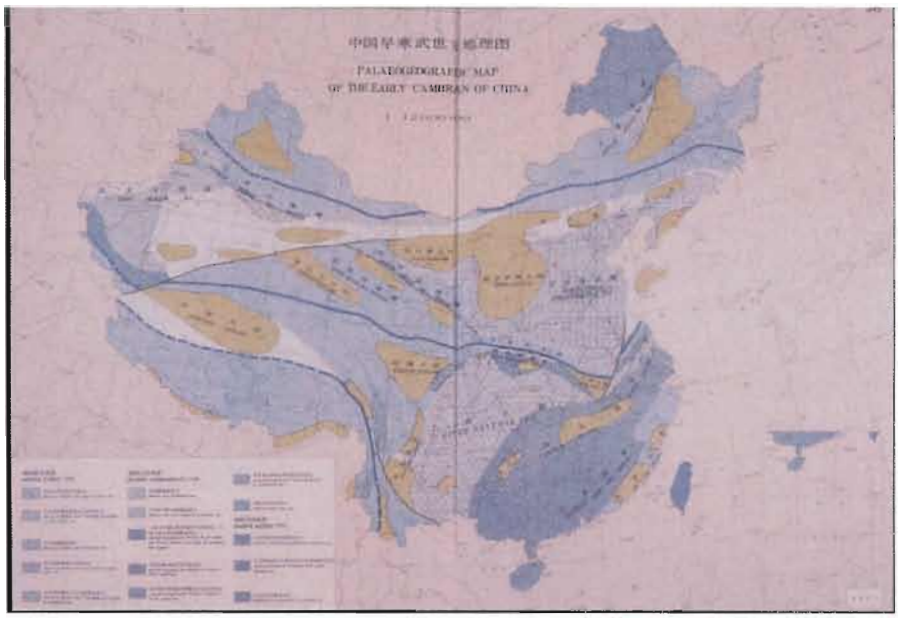
PALAEOGEOGRAPHIC MAP
OF THE EARLY CAMBRIAN OF CHINA

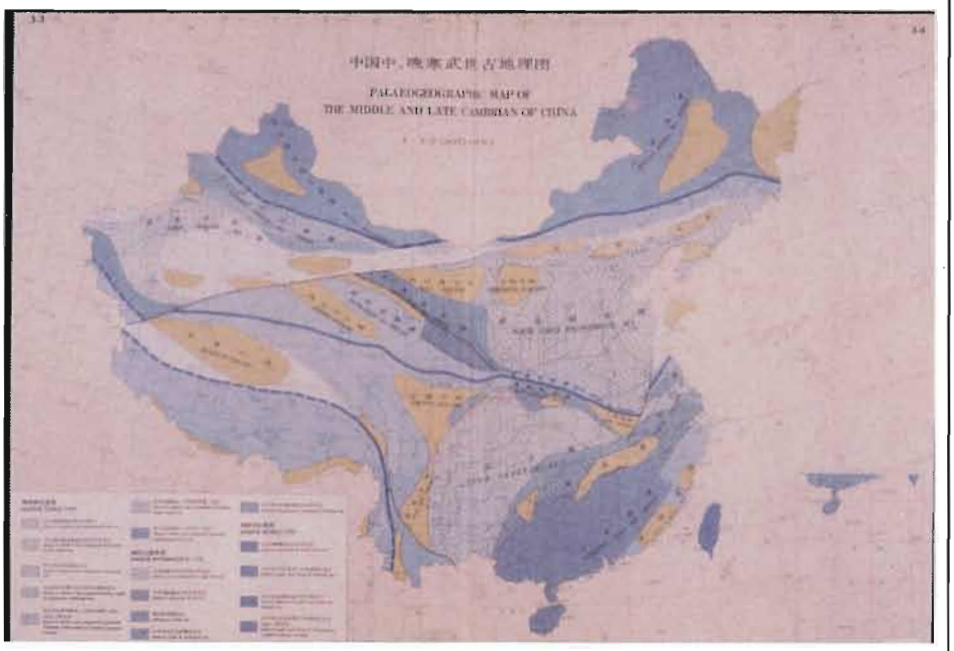
中国中、晚寒武世古地理图
PALAEOGEOGRAPHIC MAP OF
THE MIDDLE AND LATE CAMBRIAN OF CHINA

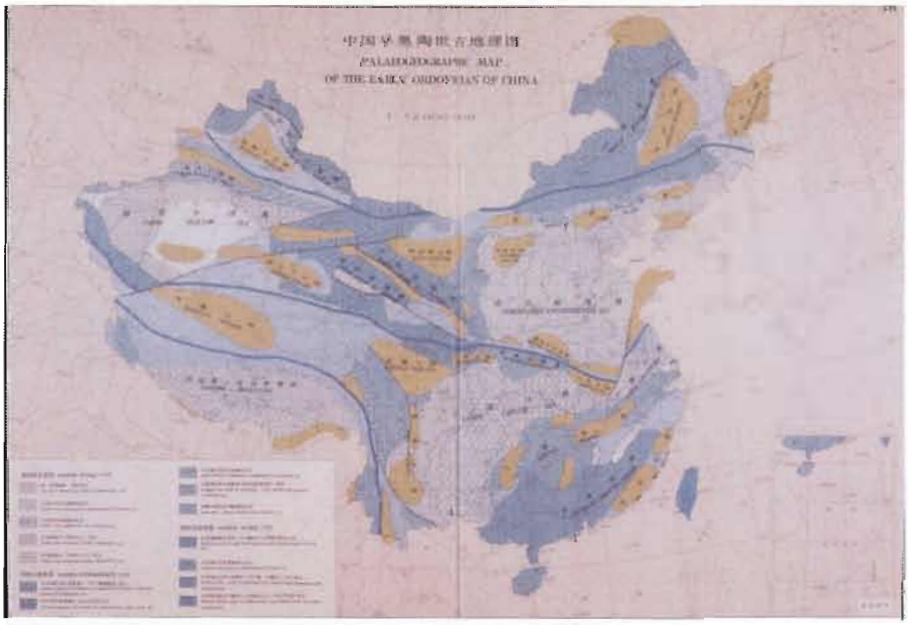
中国早奥陶世古地理图
PALAEOGEOGRAPHIC MAP
OF THE EARLY ORDOVICIAN OF CHINA

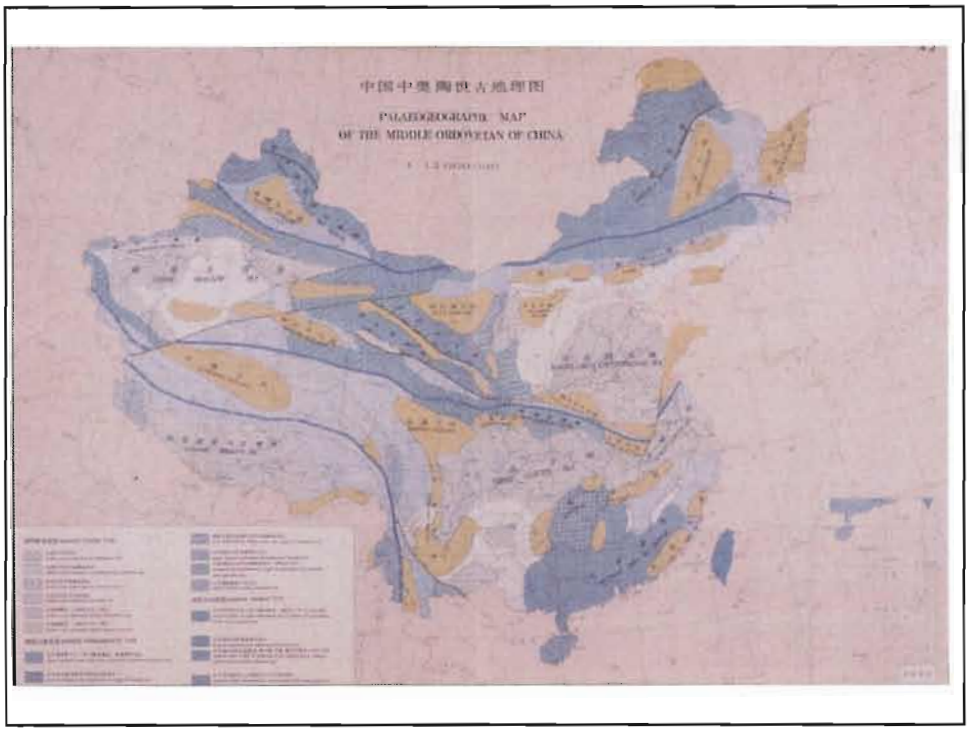
中国中奥陶世古地理图
PALAEOGEOGRAPHIC MAP
OF THE MIDDLE ORDOVICIAN OF CHINA

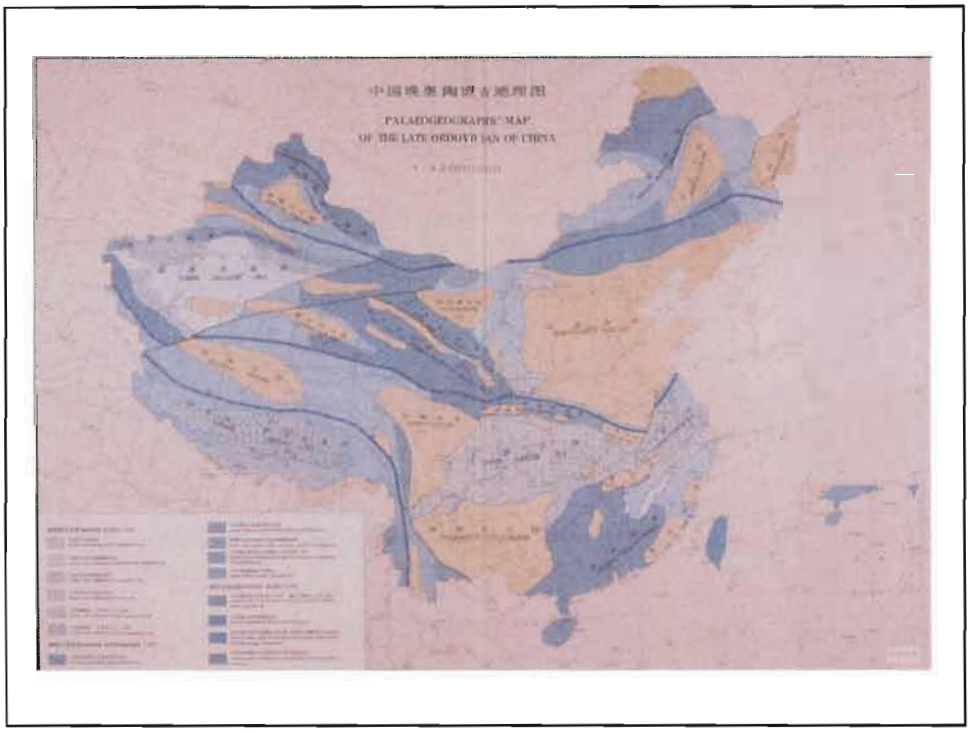
中国晚奥陶世古地理图
PALAEOGEOGRAPHIC MAP
OF THE LATE ORDOVICIAN OF CHINA

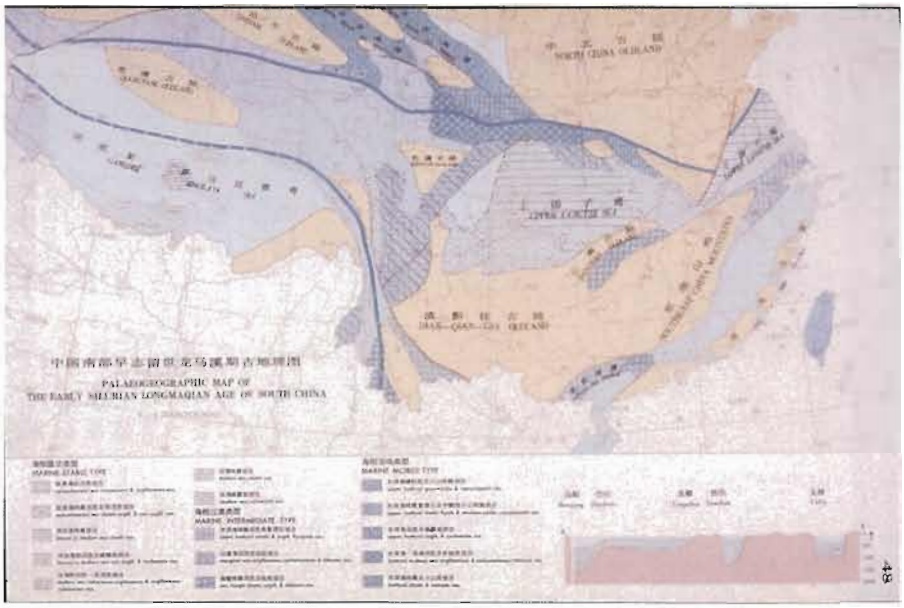
PALAEOGEOGRAPHIC MAP OF
THE EARLY SILURIAN LONGMAQIAN AGE OF SOUTH CHINA

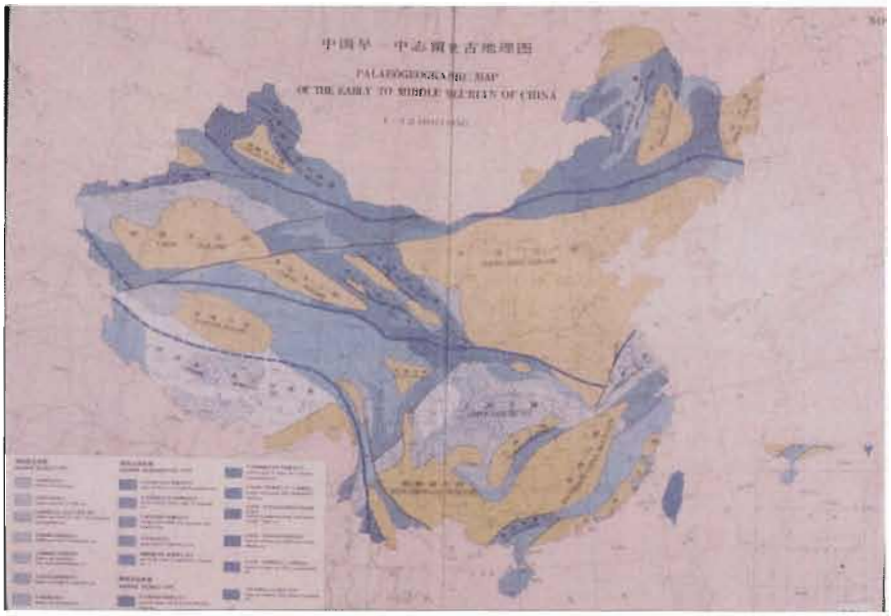
PALAEOGEOGRAPHIC MAP
OF THE EARLY TO MIDDLE SILURIAN OF CHINA

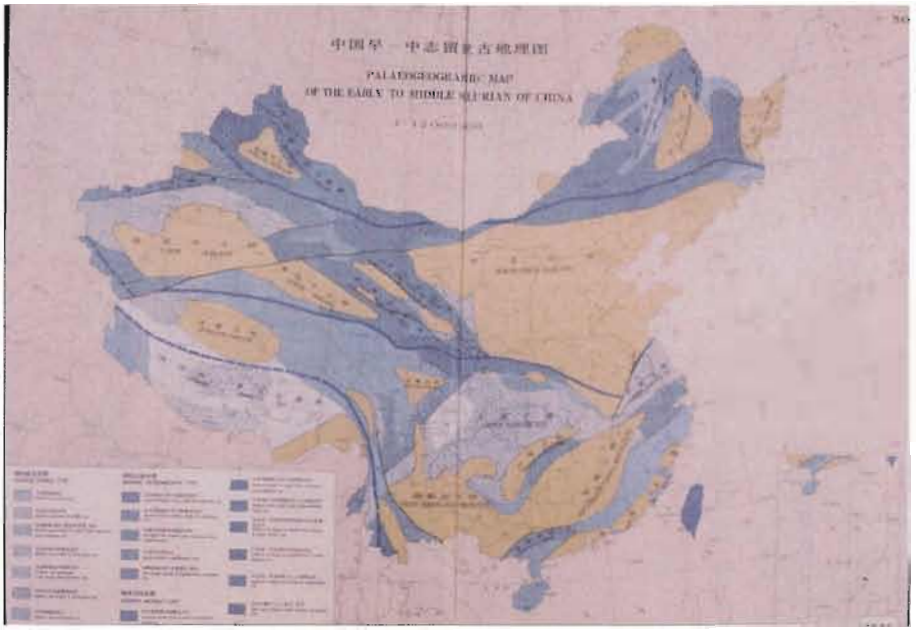
中国早—中志留世古地理图
PALAEOGEOGRAPHIC MAP
OF THE EARLY TO MIDDLE SILURIAN OF CHINA

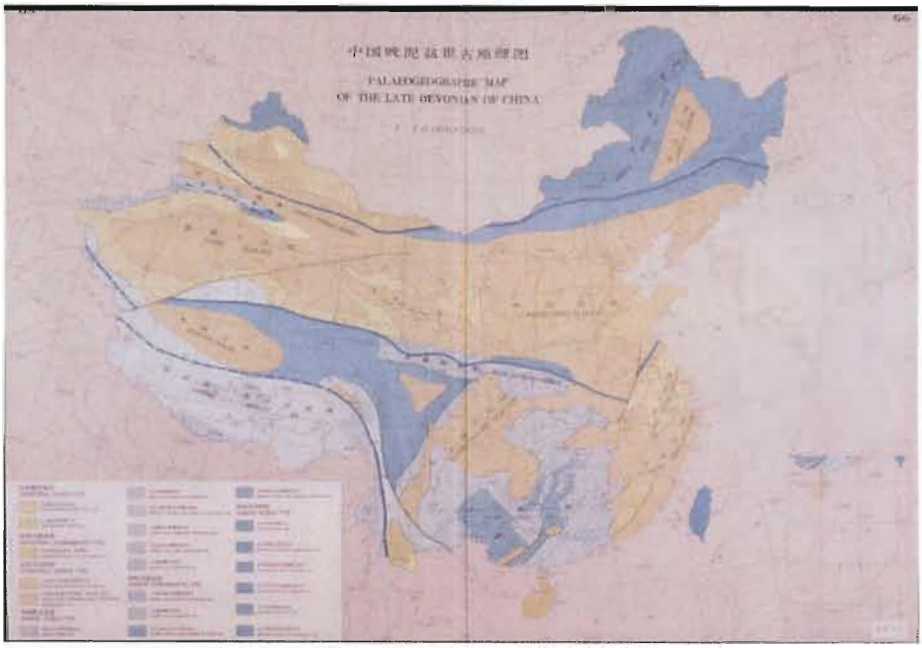
中国晚泥盆世古地理图
PALAEOGEOGRAPHIC MAP
OF THE LATE DEVONIAN OF CHINA

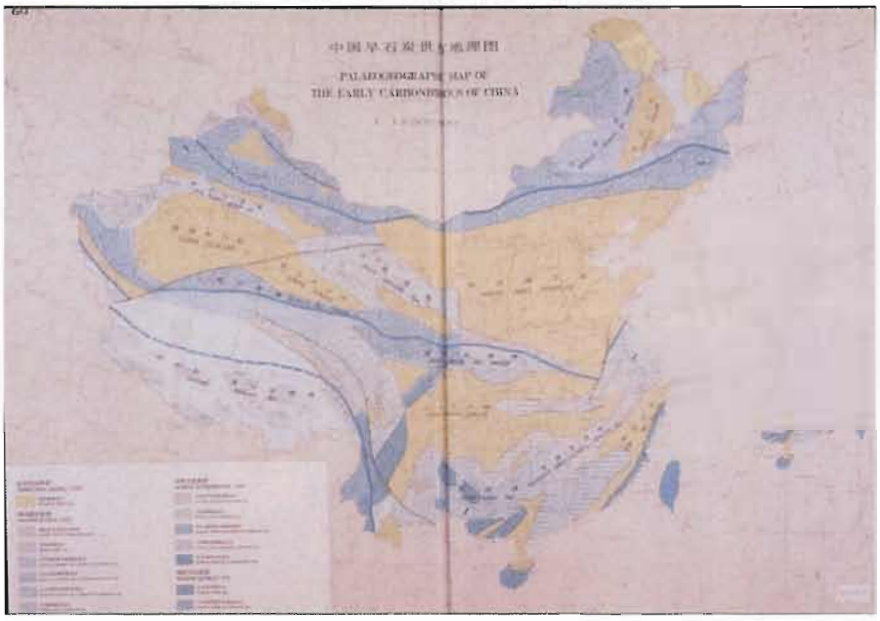
PALAEOGEOGRAPHIC MAP OF
THE EARLY CARBONIFEROUS OF CHINA

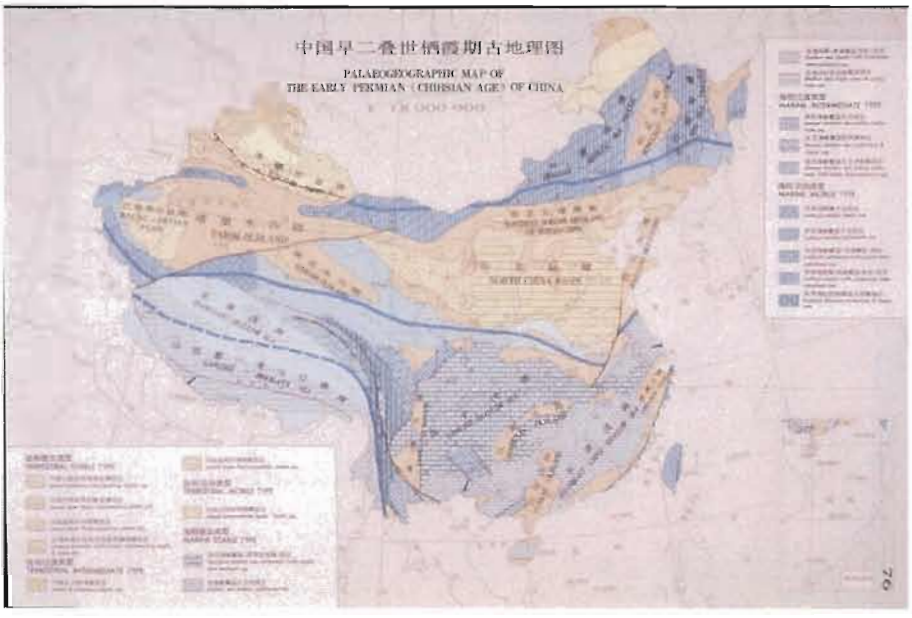
中国早二叠世栖霞期古地理图
PALAEOGEOGRAPHIC MAP OF
THE EARLY PERMIAN (CHIHSIAN AGE) OF CHINA
TARIM OLD LAND
NORTH CHINA BASIN


中国晚二叠世古地理图
PALAEOGEOGRAPHIC MAP
OF THE LATE PERMIAN OF CHINA

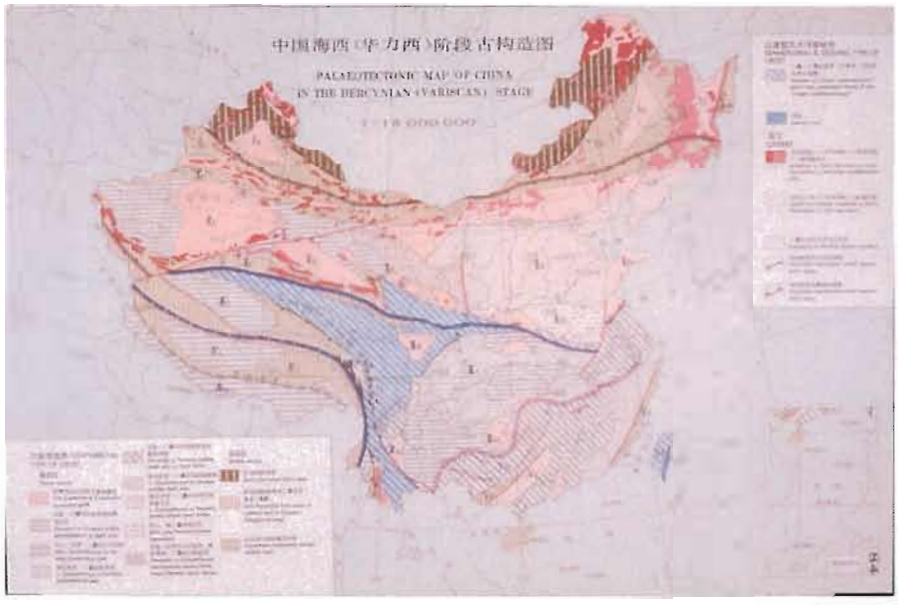
中国海西(华力西)阶段古构造图
PALAEOTECTONIC MAP OF CHINA
IN THE HERCYNIAN (VARISCAN) STAGE

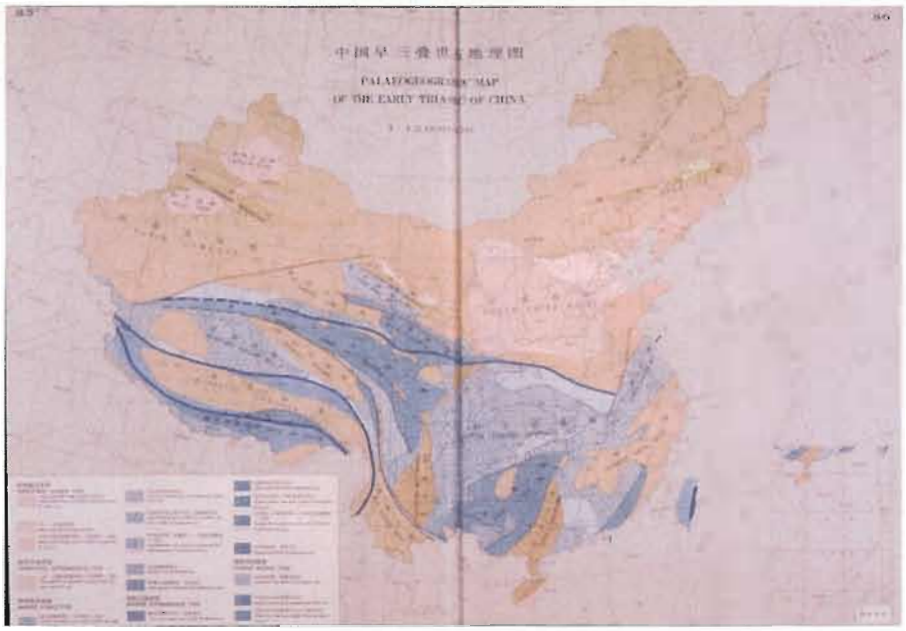
中国早三叠世古地理图
PALAEOGEOGRAPHIC MAP
OF THE EARLY TRIASSIC OF CHINA


中国中三叠世古地理图
PALAEOGEOGRAPHIC MAP
OF THE MIDDLE TRIASSIC OF CHINA


中国晚三叠世古地理图
PALAEOGEOGRAPHIC MAP
OF THE LATE TRIASSIC OF CHINA

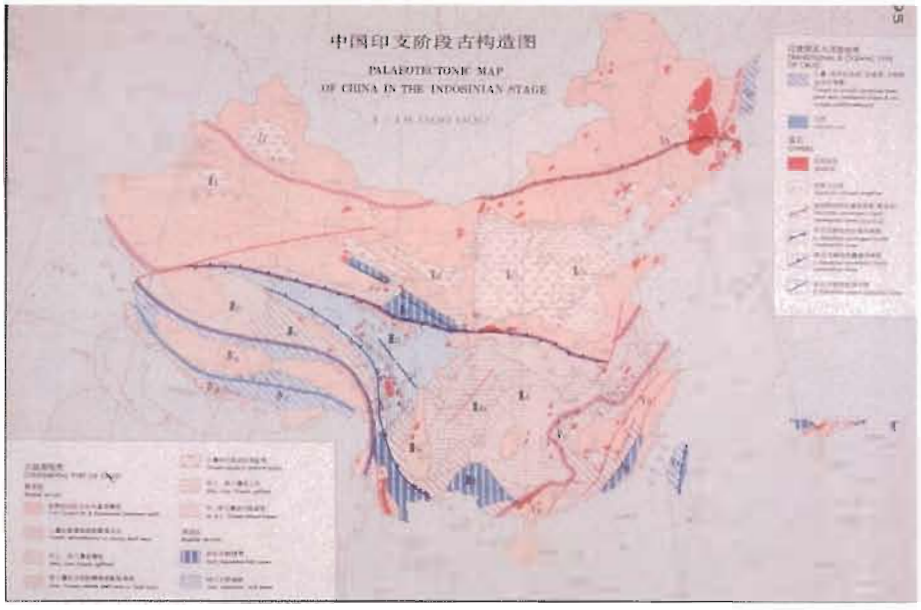
中国印支阶段古构造图
PALAEOTECTONIC MAP
OF CHINA IN THE INDOSINIAN STAGE


中国早侏罗世古地理图
PALAEOGEOGRAPHIC MAP
OF THE EARLY JURASSIC OF CHINA


中国中侏罗世古地理图
PALAEOGEOGRAPHIC MAP
OF THE MIDDLE JURASSIC OF CHINA

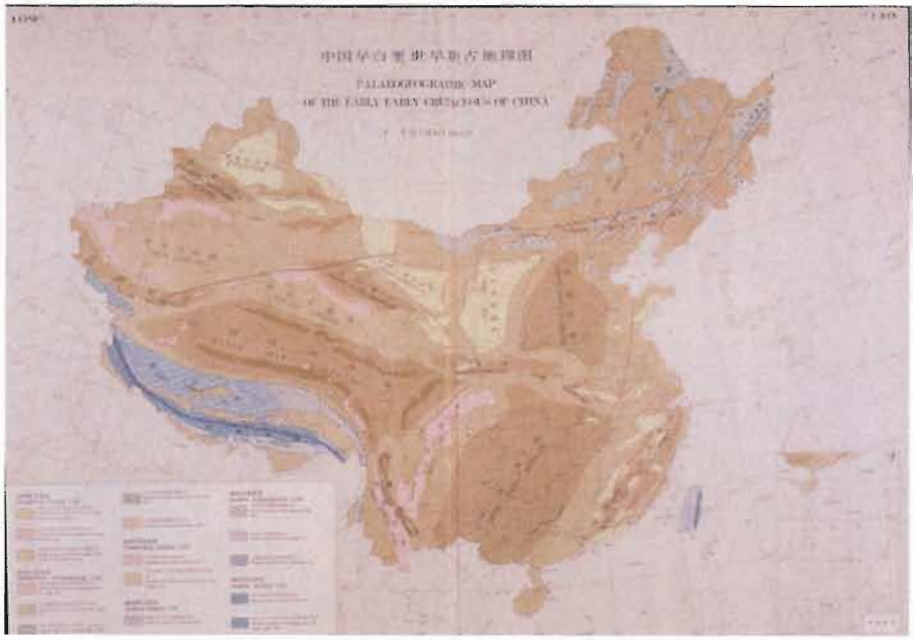
PALAEOGEOGRAPHIC MAP

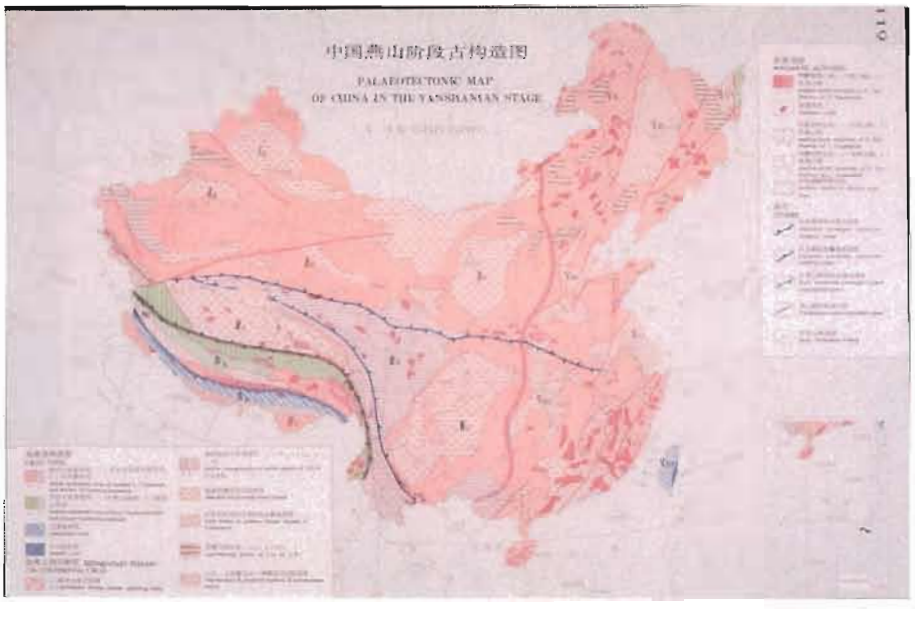
中国燕山阶段古构造图
PALAEOTECTONIC MAP
OF CHINA IN THE YANSHANIAN STAGE


地理图
MAP
OF CHINA

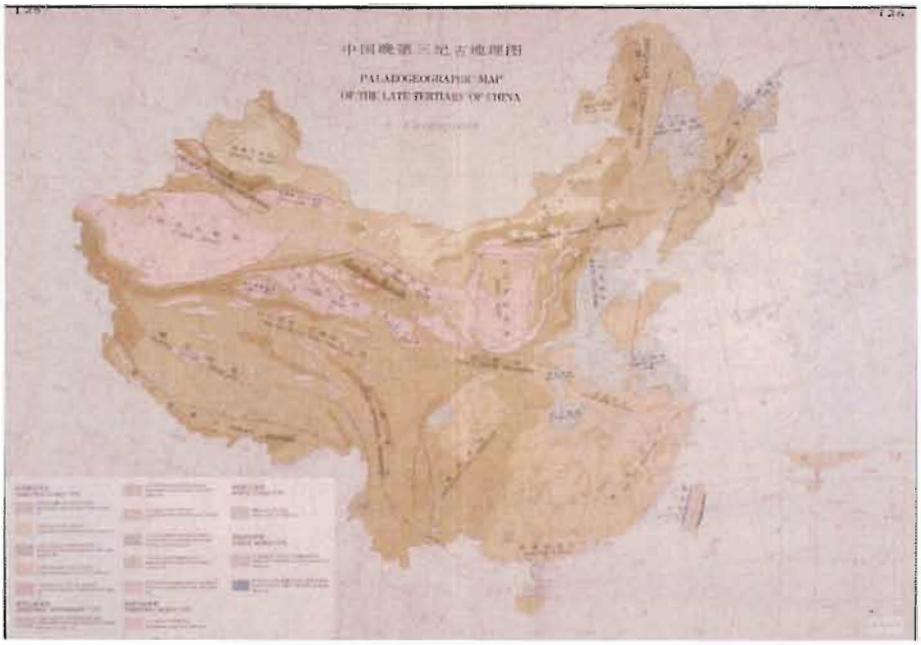
中国晚第三纪古地理图
PALAEOGEOGRAPHIC MAP
OF THE LATE TERTIARY OF CHINA

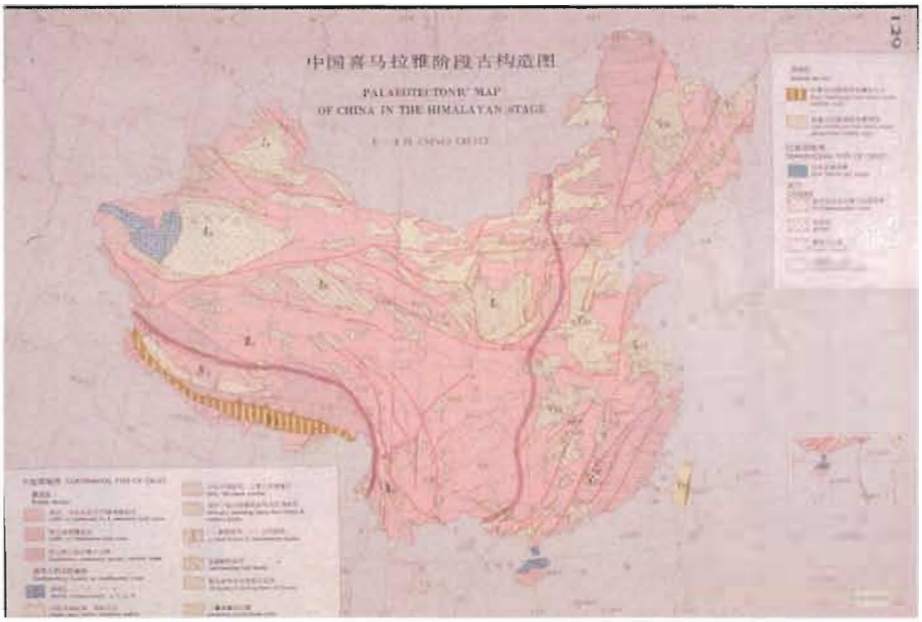
中国喜马拉雅阶段古构造图
PALAEOTECTONIC MAP
OF CHINA IN THE HIMALAYAN STAGE

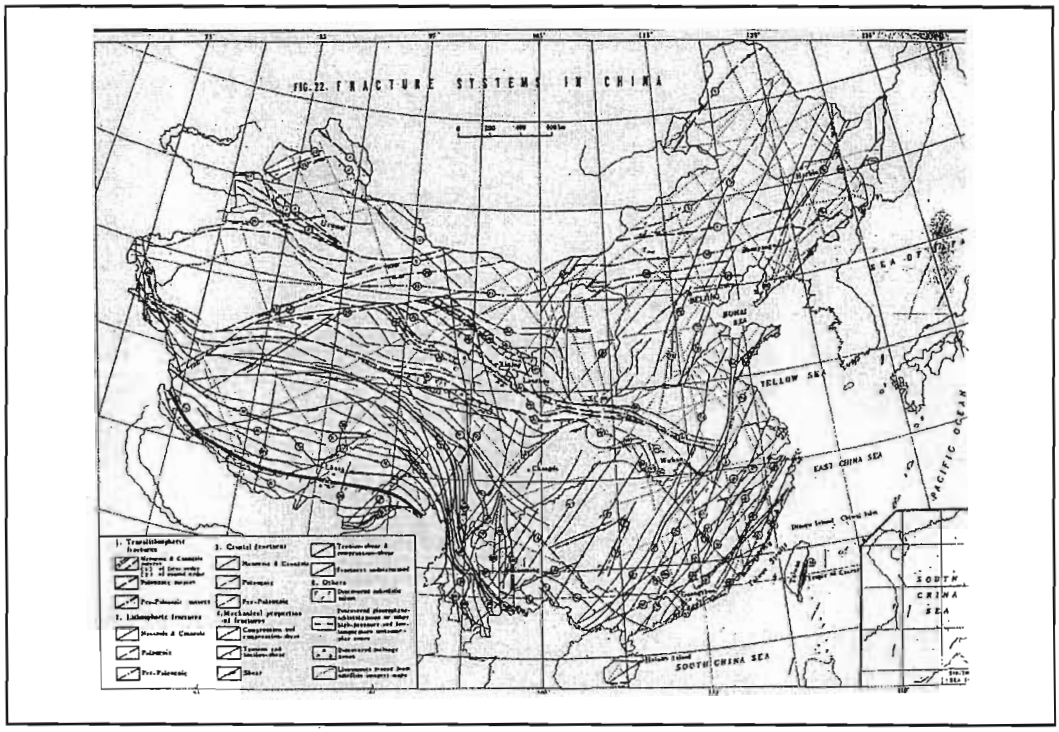
FIG. 22. FRACTURE SYSTEMS IN CHINA
YELLOW SEA
EAST CHINA SEA
PACIFIC OCEAN
SOUTH CHINA SEA
SEA OF JAPAN

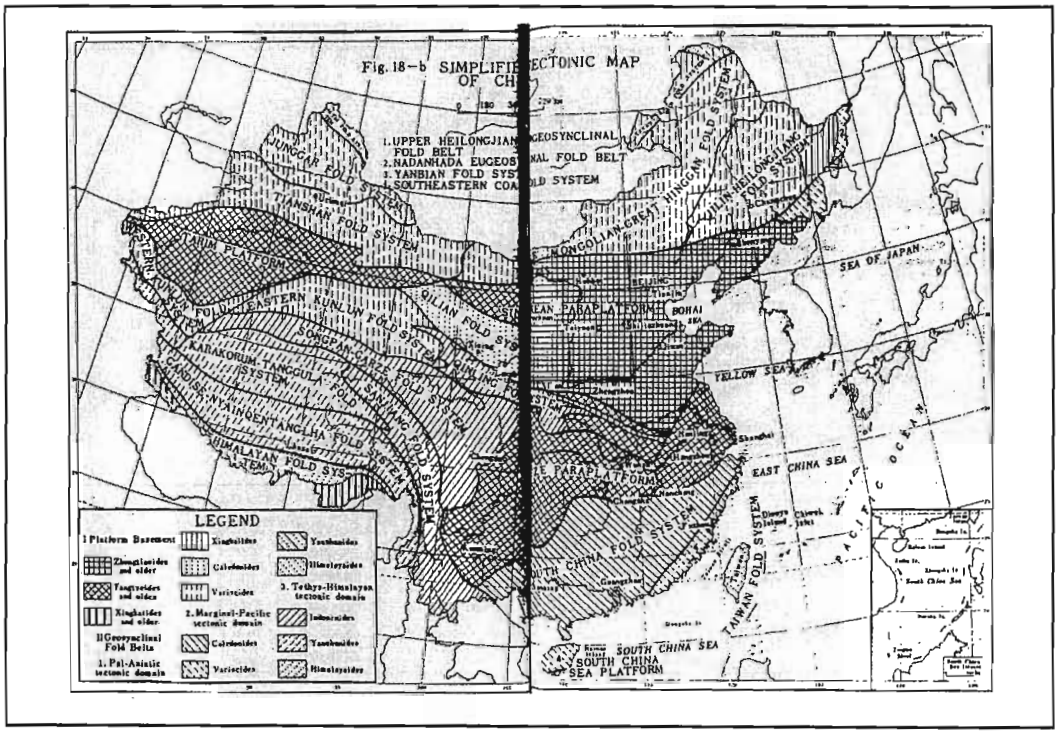
Fig. 18–b SIMPLIFIED TECTONIC MAP OF CHINA
1. UPPER HEILONGJIANG GEOSYNCLINAL FOLD BELT
2. NADANHADA EUGEOSYNCLINAL FOLD BELT
3. YANBIAN FOLD SYSTEM
4. SOUTHEASTERN COASTAL FOLD SYSTEM
TIANSHAN FOLD SYSTEM
TARIM PLATFORM
KUNLUN FOLD SYSTEM
QILIAN FOLD SYSTEM
SONGPAN-GARZE FOLD SYSTEM
KARAKORUM-TANGGULA FOLD SYSTEM
GANGDISE-NYAINGENTANGLHA FOLD SYSTEM
HIMALAYAN FOLD SYSTEM
SICHUAN BASIN PLATFORM
YANGTZE PARAPLATFORM
SOUTH CHINA FOLD SYSTEM
TAIWAN FOLD SYSTEM
SOUTH CHINA SEA PLATFORM
SEA OF JAPAN
YELLOW SEA
EAST CHINA SEA
PACIFIC OCEAN
SOUTH CHINA SEA
LEGEND
I Platform Basement
Zhongtiaoides and older
Tangtseides and olders
Xinghaides and older
II Geosynclinal Fold Belts
1. Pal-Asiatic tectonic domain
Xinghaiides
Caledonides
Variscides
2. Marginal-Pacific tectonic domain
Caledonides
Variscides
Yanshanides
Himalayides
3. Tethys-Himalayan tectonic domain
Indosinides
Yanshanides
Himalayides

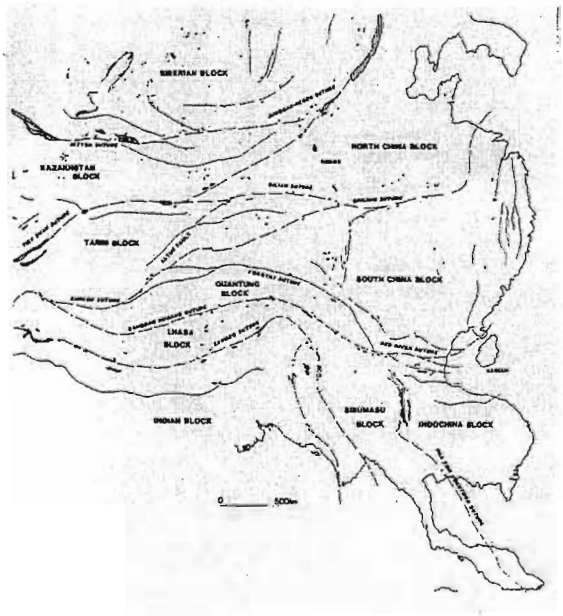
SIBERIAN BLOCK
NORTH CHINA BLOCK
KAZAKHSTAN BLOCK
TARIM BLOCK
QUANTUNG BLOCK
SOUTH CHINA BLOCK
LHASA BLOCK
INDIAN BLOCK
SIBUMASU BLOCK
INDOCHINA BLOCK

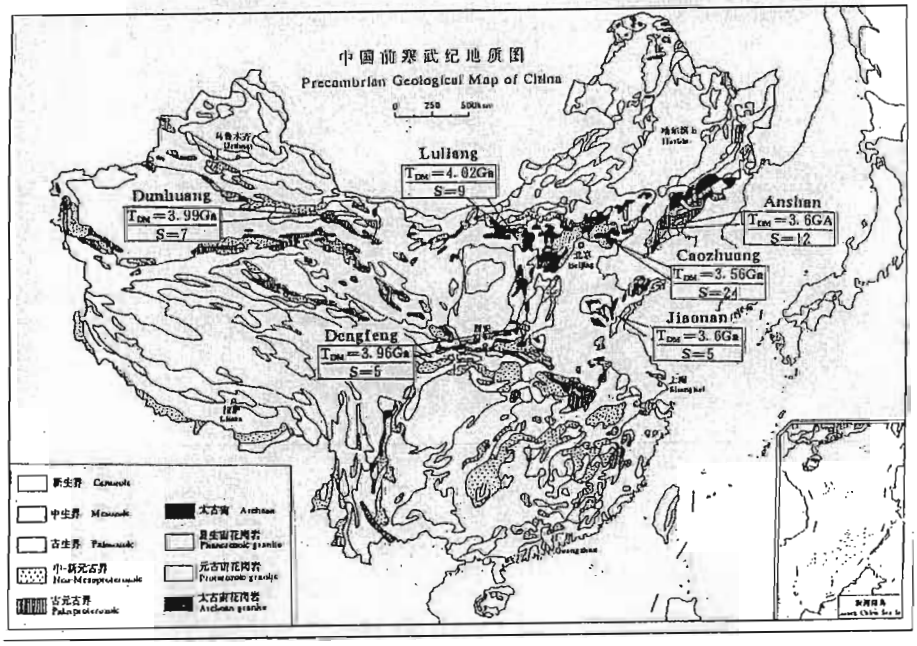
中国前寒武纪地质图
Precambrian Geological Map of China
Luliang
T_{DM}=4.02Ga
S=9
Dunhuang
T_{DM}=3.99Ga
S=7
Anshan
T_{DM}=3.6GA
S=12
Caozhuang
T_{DM}=3.56Ga
S=24
Jiaonan
T_{DM}=3.6Ga
S=5
Dengfeng
T_{DM}=3.96Ga
S=5
新生界 Cenozoic
中生界 Mesozoic
古生界 Paleozoic
太古宙 Archean
显生宙花岗岩 Phanerozoic granite
元古宙花岗岩 Proterozoic granite
太古宙花岗岩 Archean granite

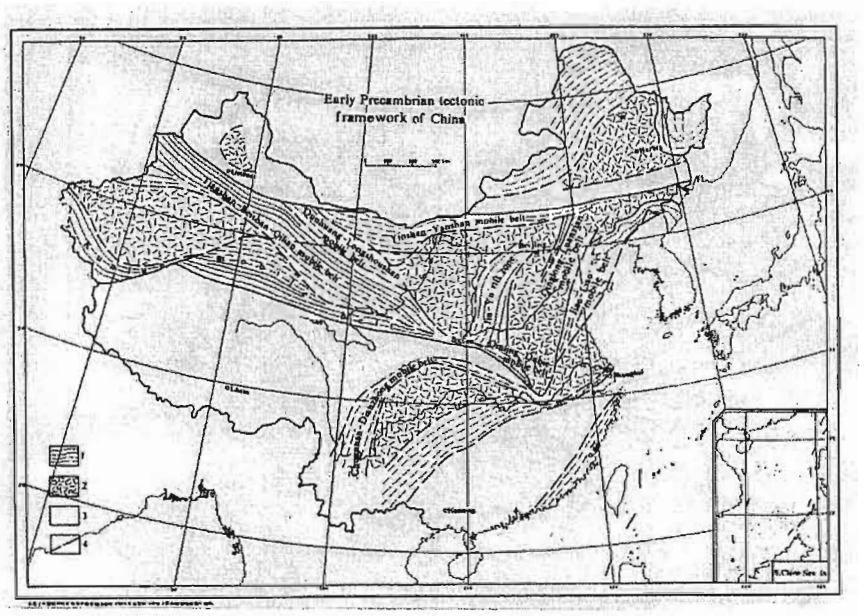
Early Precambrian tectonic framework of China

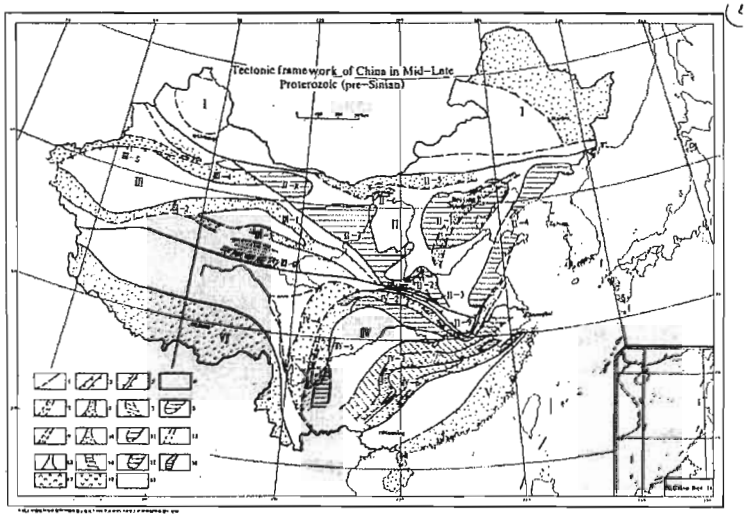
Tectonic framework of China in Mid-Late Proterozoic (pre-Sinian)

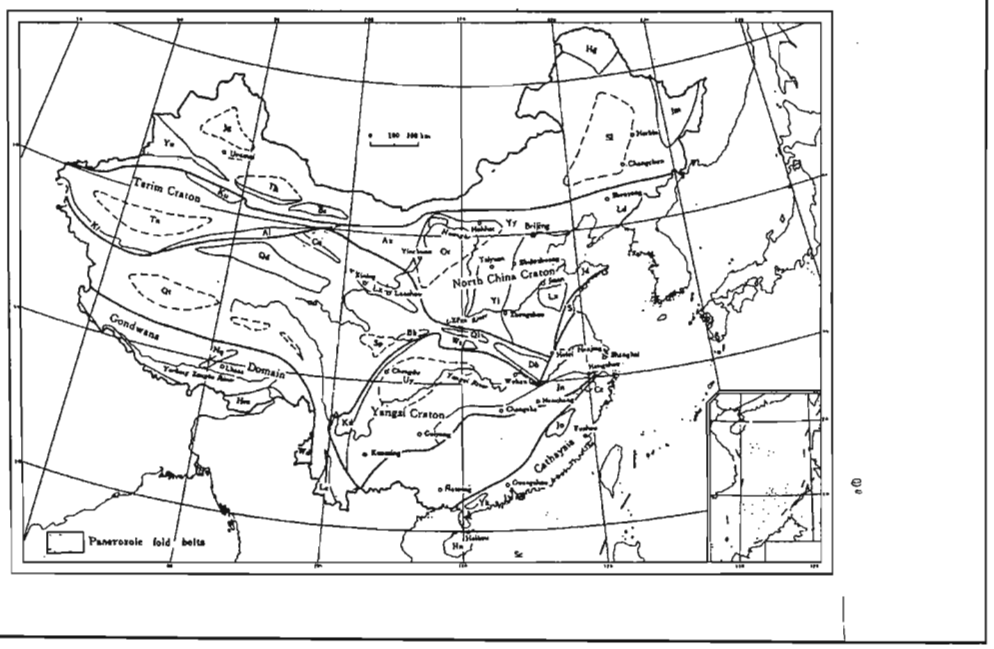
Tarim Craton
North China Craton
Yangzi Craton
Gondwana Domain
Cathaysia
Paleozoic fold belts

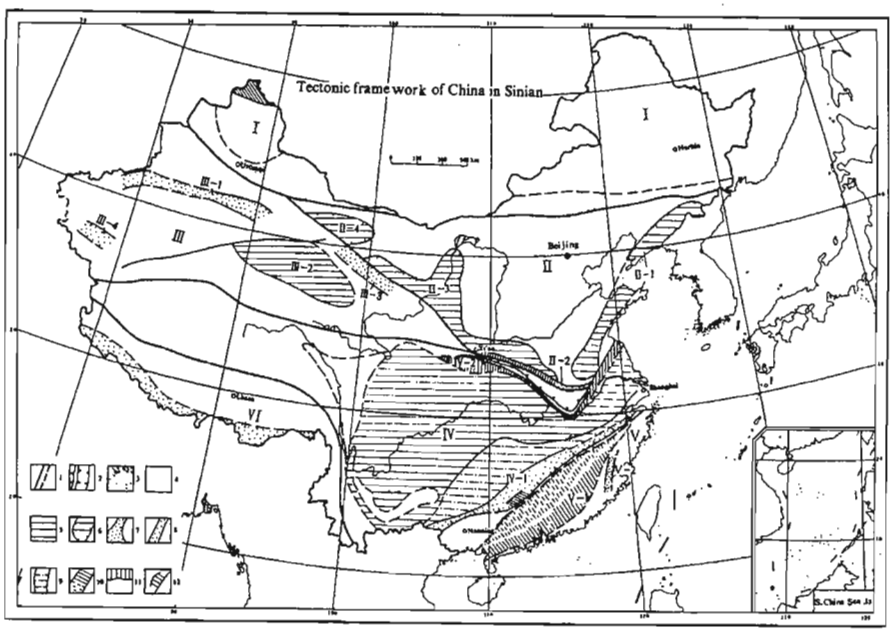
Tectonic framework of China in Sinian
Beijing
S.China Sea Is

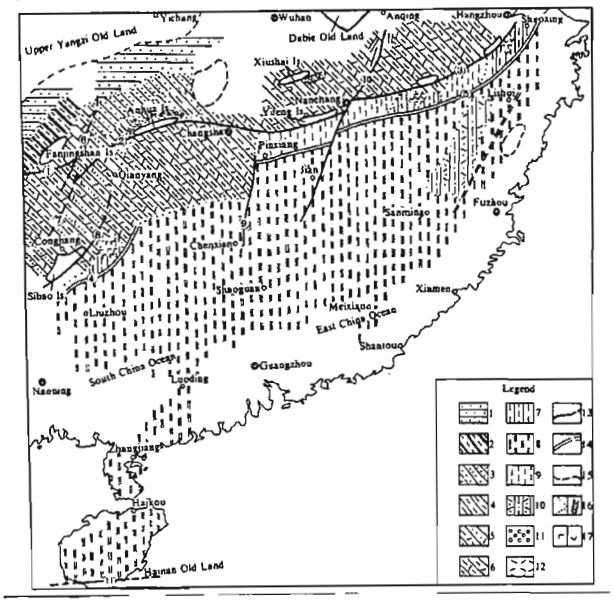
Upper Yangzi Old Land
Yichang
Wuhan
Anqing
Hangzhou
Shaoxing
Dabie Old Land
Xiushai
Nanchang
Yuan
Pingxiang
Changsha
Fanjingshan
Qianyang
Jian
Fuzhou
Sanming
Chenzhou
Shaoguan
Meixian
Xiamen
Sibao
Luzhou
East China Ocean
Shantou
South China Ocean
Guangzhou
Nanning
Leiding
Zhanjiang
Haikou
Hainan Old Land
Legend

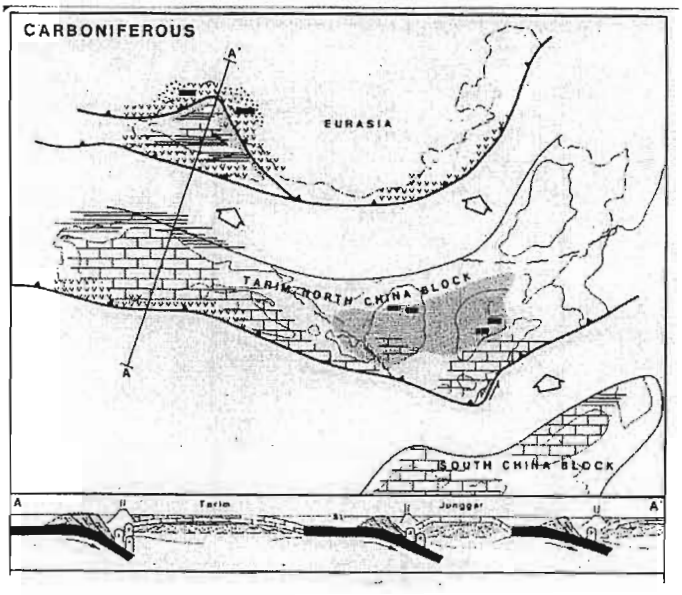
CARBONIFEROUS
A'
EURASIA
TARIM-NORTH CHINA BLOCK
A
SOUTH CHINA BLOCK
A
Tarim
Junggar
A'

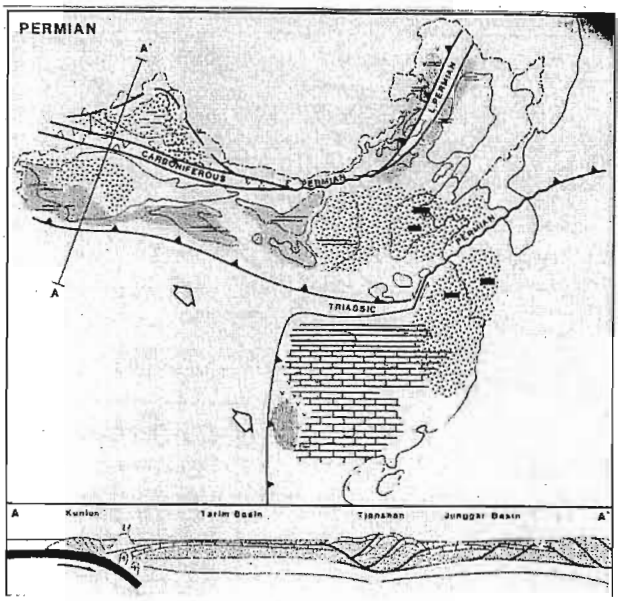
PERMIAN
A
A'
CARBONIFEROUS
PERMIAN
TRIASSIC
Kunlun
Tarim Basin
Tianshan
Junggar Basin

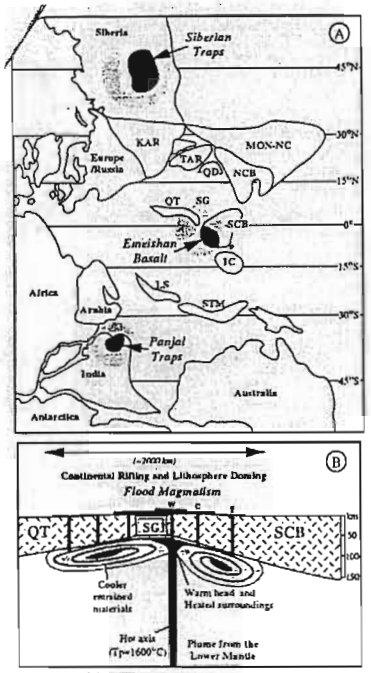
A
Siberia
Siberian Traps
45°N
30°N
15°N
0°
15°S
30°S
45°S
KAR
MON-NC
Europe /Russia
TAR
QD
NCB
QT
SG
SCB
Emeishan Basalt
EC
LS
STM
Africa
Arabia
Panjal Traps
India
Australia
Antarctica
B
Continental Rifting and Lithosphere Doming
Flood Magmatism
W
C
E
QT
SG
SCB
Cooler entrained materials
Warm head and Heated surroundings
Hot axis (Tp=1600°C)
Plume from the Lower Mantle

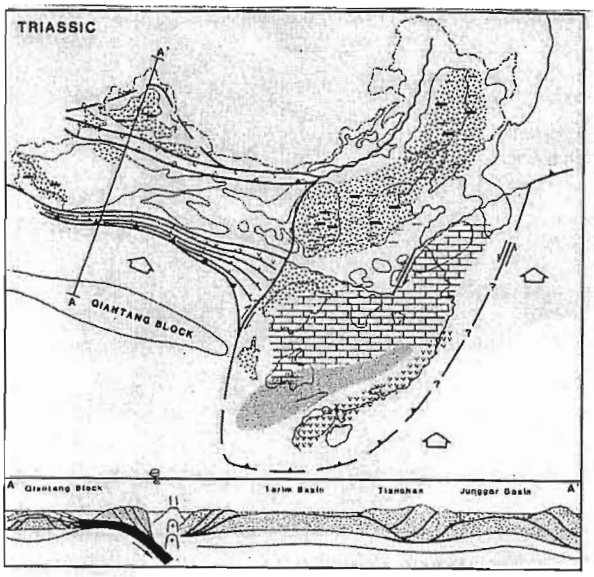
TRIASSIC
A
A'
QIANTANG BLOCK
A
Qiantang Block
Tarim Basin
Tianshan
Junggar Basin
A'

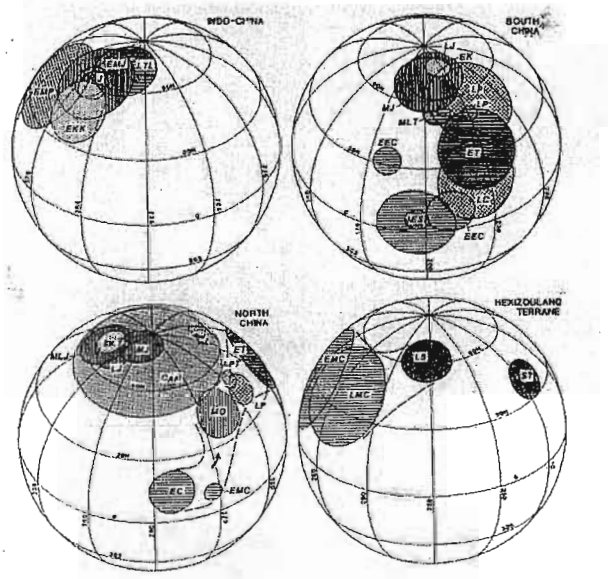
INDO-CHINA
SOUTH CHINA
NORTH CHINA
HEXI CORRIDOR TERRANE
EKK
MLT
EEC
EMC
LMC
LO
ET

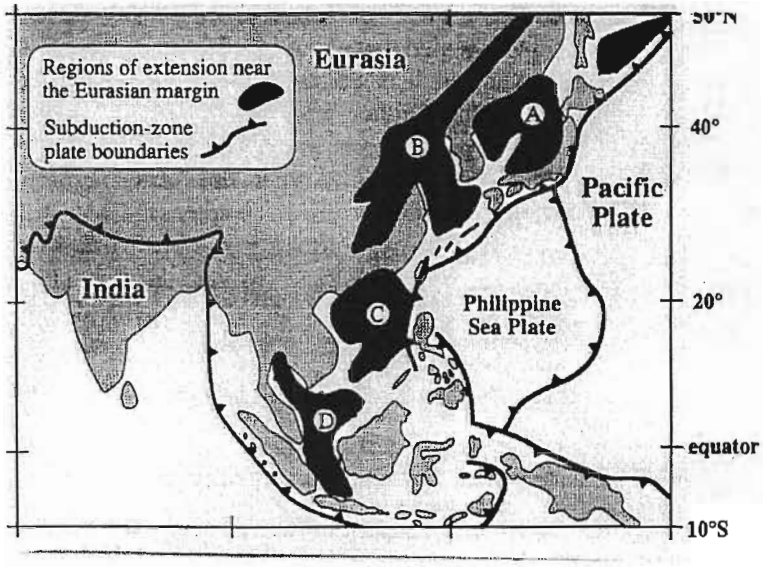
Regions of extension near the Eurasian margin
Subduction-zone plate boundaries
Eurasia
India
Pacific Plate
Philippine Sea Plate
A
B
C
D
40°
20°
equator
10°S

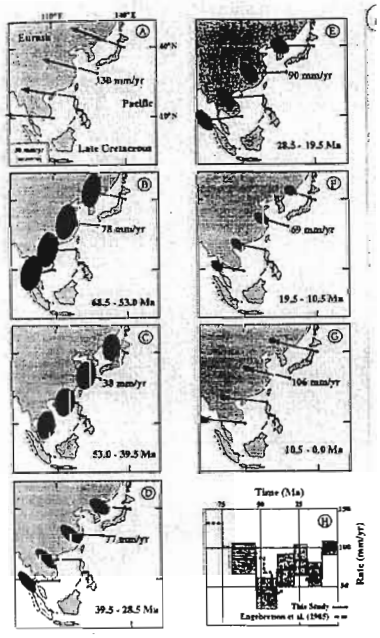
A
130 mm/yr
Late Cretaceous
B
78 mm/yr
68.5 - 53.0 Ma
C
38 mm/yr
53.0 - 39.5 Ma
D
77 mm/yr
39.5 - 28.5 Ma
E
90 mm/yr
28.5 - 19.5 Ma
F
69 mm/yr
19.5 - 10.5 Ma
G
106 mm/yr
10.5 - 0.0 Ma
H
Time (Ma)
Rate (mm/yr)

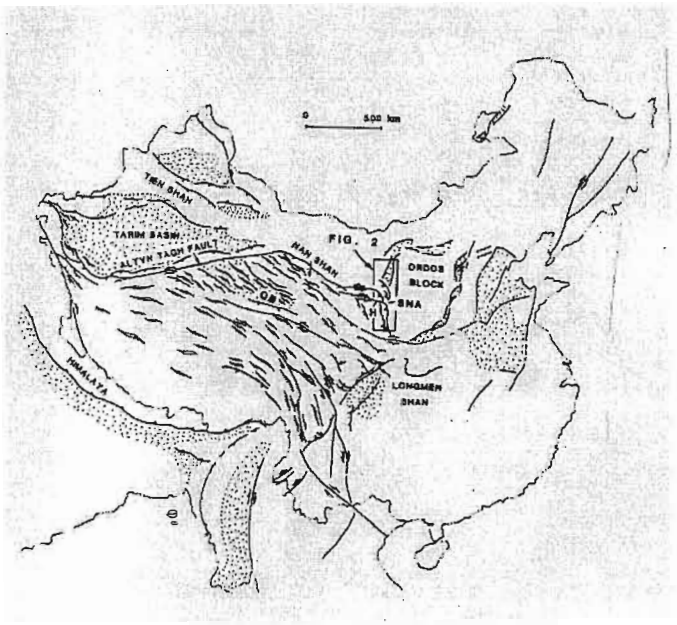
0 500 km
TIEN SHAN
TARIM BASIN
ALTYN TAGH FAULT
FIG. 2
NAN SHAN
ORDOS BLOCK
QB
SNA
HIMALAYA
LONGMEN SHAN

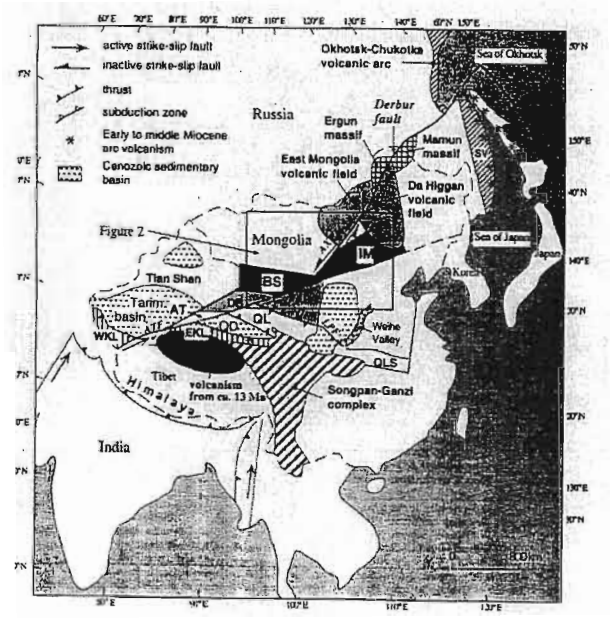
active strike-slip fault
inactive strike-slip fault
thrust
subduction zone
Early to middle Miocene arc volcanism
Cenozoic sedimentary basin
Okhotsk-Chukotka volcanic arc
Sea of Okhotsk
Russia
Derbur fault
Ergun massif
Mamun massif
East Mongolia volcanic field
Da Higgan volcanic field
Figure 2
Mongolia
Sea of Japan
Japan
Korea
Tian Shan
Tarim basin
Wehe Valley
Tibet
volcanism from ca. 13 Ma
Himalaya
Songpan-Ganzi complex
India

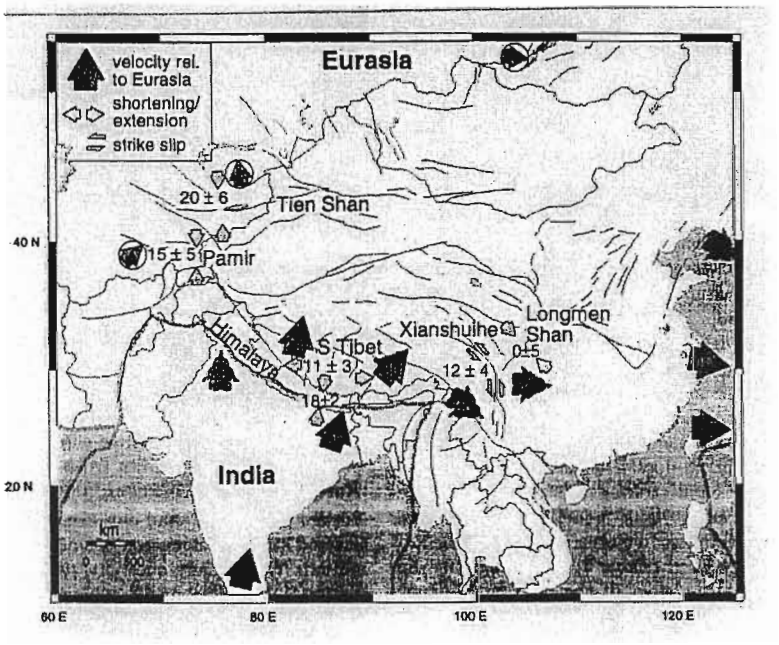
velocity rel. to Eurasia
shortening/ extension
strike slip
Eurasia
20 ± 6
Tien Shan
40 N
15 ± 5
Pamir
Himalaya
S Tibet
11 ± 3
18±2
Xianshuihe
Longmen Shan
0±5
12 ± 4
India
20 N
km
60 E
80 E
100 E
120 E

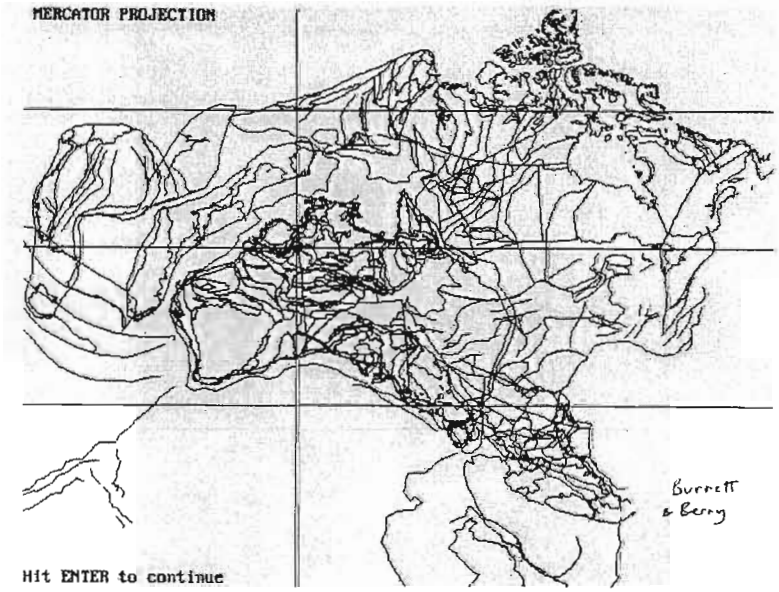
MERCATOR PROJECTION
Burnett & Berry
Hit ENTER to continue

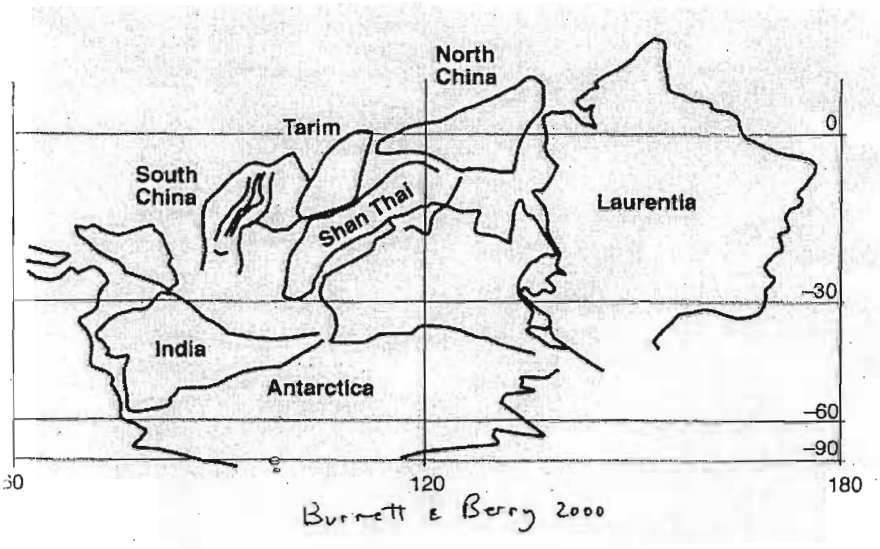
North China
Tarim
South China
Shan Thai
Laurentia
India
Antarctica
0
–30
–60
–90
120
180
Burnett & Berry 2000

Geological, Tectonic and Metallogenic Relations in South China (P603)

(Metallogenic Relations of China and Deposit Compilation)

Research Team:

Khin Zaw
Eleanor Bruce
Clive Burrett
Ron Berry
Ross Large

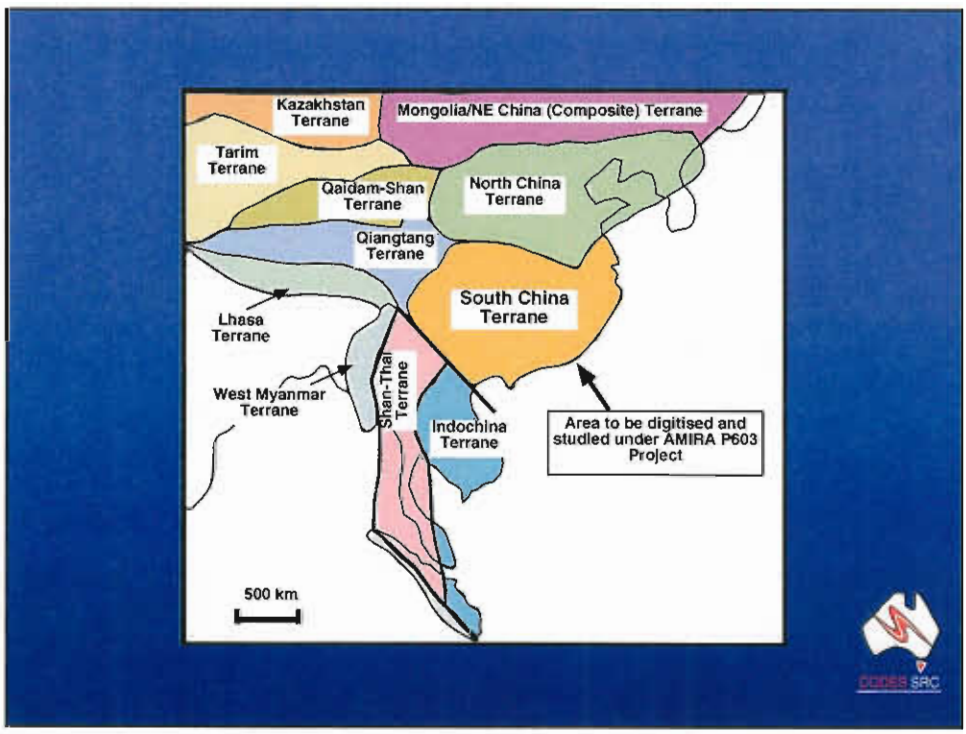

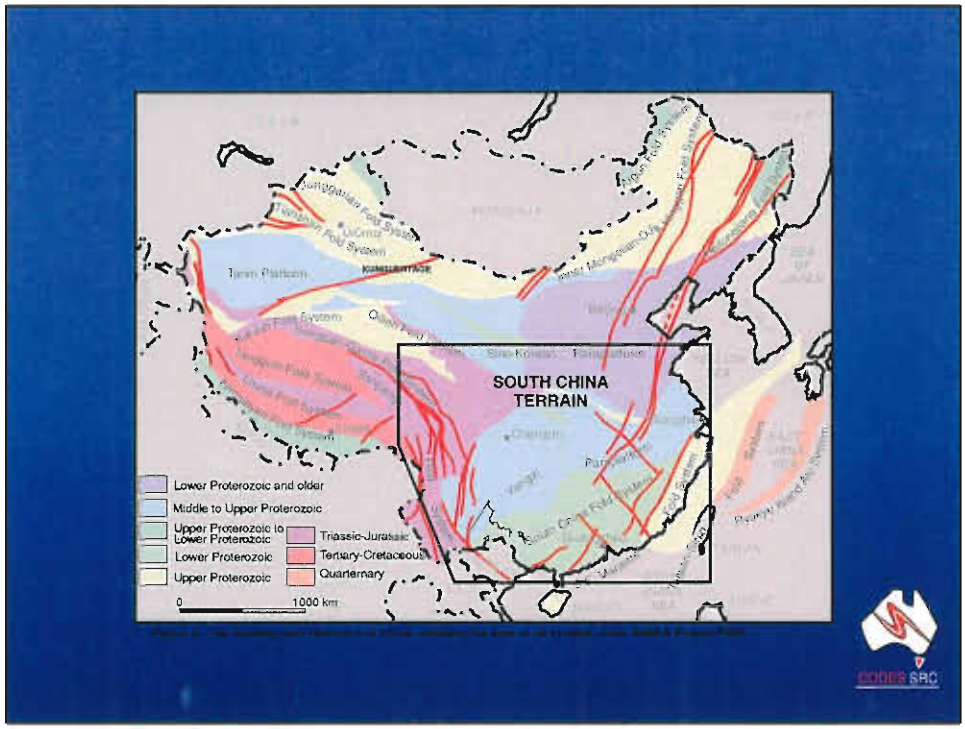
SOUTH CHINA
TERRAIN
Lower Proterozoic and older
Middle to Upper Proterozoic
Upper Proterozoic to Lower Proterozoic
Lower Proterozoic
Upper Proterozoic
Triassic-Jurassic
Tertiary-Cretaceous
Quaternary
0
1000 km
CODES SRC


Qinghai
Gansu
Shaanxi
Hennan
Shandong
Jiangsu
Anhui
Sichuan
Hubei
Hunnan
Jiangxi
Guizhou
Fujian
Yunnan
Guangxi
Guangdong
CODES SRC

China's Gold Production

1998 production: 160 t Au
70 major gold deposits
reserves >2000 t Au

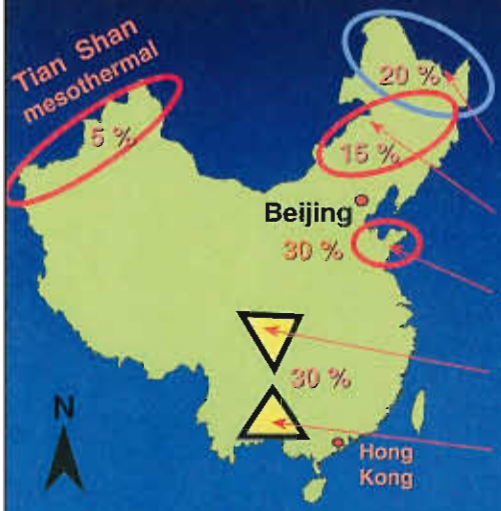

- Hei Long Jiang - placer
- North China - greenstone & - mesothermal
- East Shandong - mesothermal
- Quingling - Carlin-type & - mesothermal
- Southern China - Carlin-type

Compiled from Yang (1996), Zhou (1999) & Chromie and Khin Zaw (in prep.)

Regional Geological Setting of China's Gold Districts

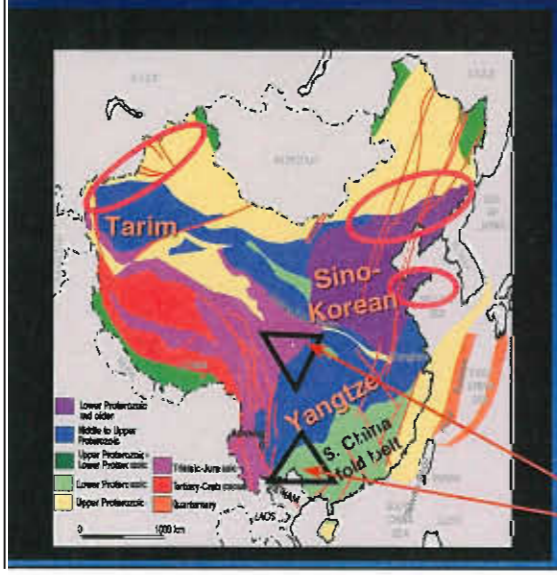

- China's gold deposits occur mostly within fold belts along the margins of 3 major cratons:
  - Sino-Korean (L - M Prot.)
  - Tarim (M - U Prot.)
  - Yangtze (M - U Prot.)
- Chinese Carlin-type gold deposits occur in two Palaeozoic - Mesozoic sedimentary basins along the margins of the Yangtze Craton:
  - (N Gold Triangle)
  - (S. Gold Triangle)

Southern China "Carlin-type" Deposits

(Nanpanjiang Basin - *Southern Golden Triangle: SGT*)

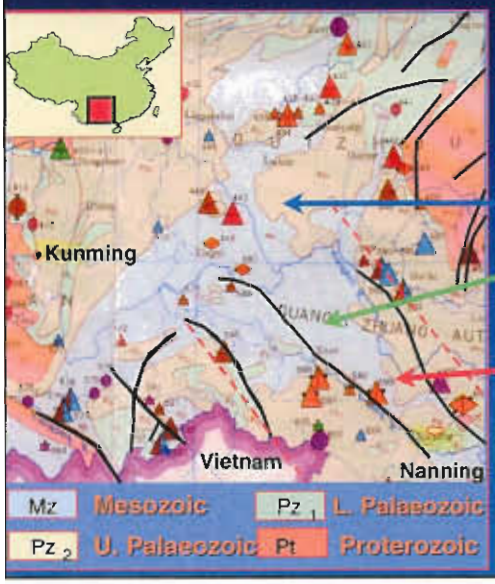

- *Cambrian - Tertiary* aged sedimentary sequences host "Carlin-type" gold within the Nanpanjian basin, along SW margin of the Yangtze Craton
- Basin - NW: platform sequence (Limestone & argillite)
- Basin - SW: deep basin (coeval) (Siliciclastics)
- Youjiang Rift formed during Indosinian (Triassic) to Yanshanian (Jurassic-Cret.)
- High angled NW-SE strike-slip faults cross-cut N-S thrust faults during the Upper Yanshanian

Southern China "Carlin-type" Gold Deposits

CODES SRC

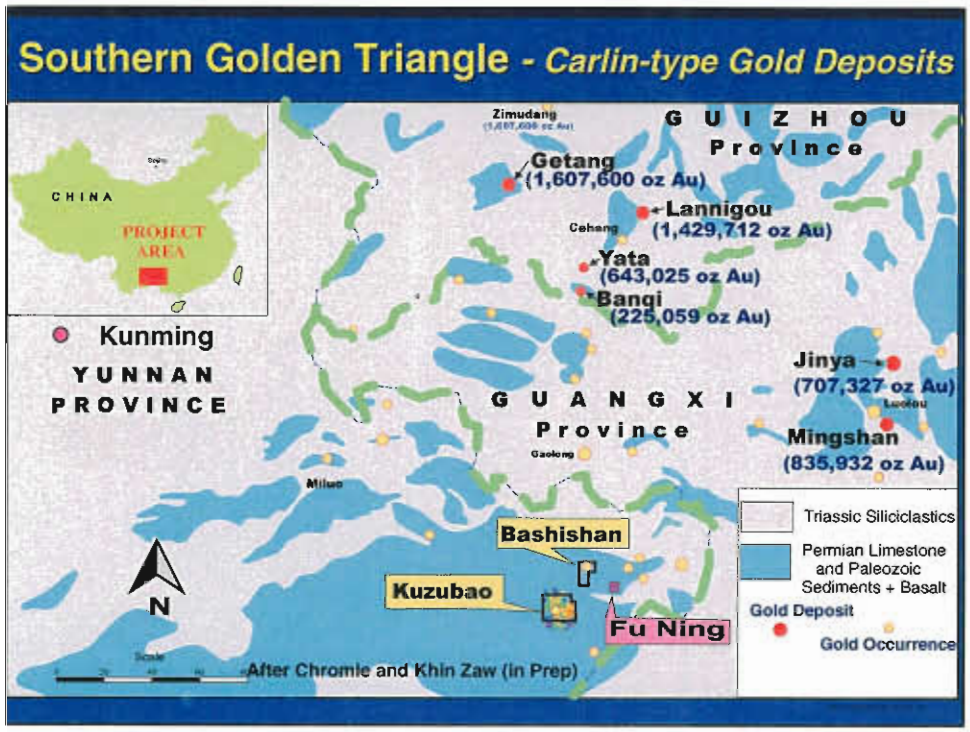
Southern Golden Triangle - Carlin-type Gold Deposits
CHINA
PROJECT AREA
Kunming
YUNNAN PROVINCE
Zimudang
GUIZHOU Province
Getang
(1,607,600 oz Au)
Lannigou
(1,429,712 oz Au)
Cehong
Yata
(643,025 oz Au)
Bangi
(225,059 oz Au)
Jinya
(707,327 oz Au)
Luolou
GUANGXI Province
Mingshan
(835,932 oz Au)
Gaolong
Miluo
Bashishan
Kuzubao
Fu Ning
N
Scale
After Chromie and Khin Zaw (in Prep)
Triassic Siliciclastics
Permian Limestone and Paleozoic Sediments + Basalt
Gold Deposit
Gold Occurrence

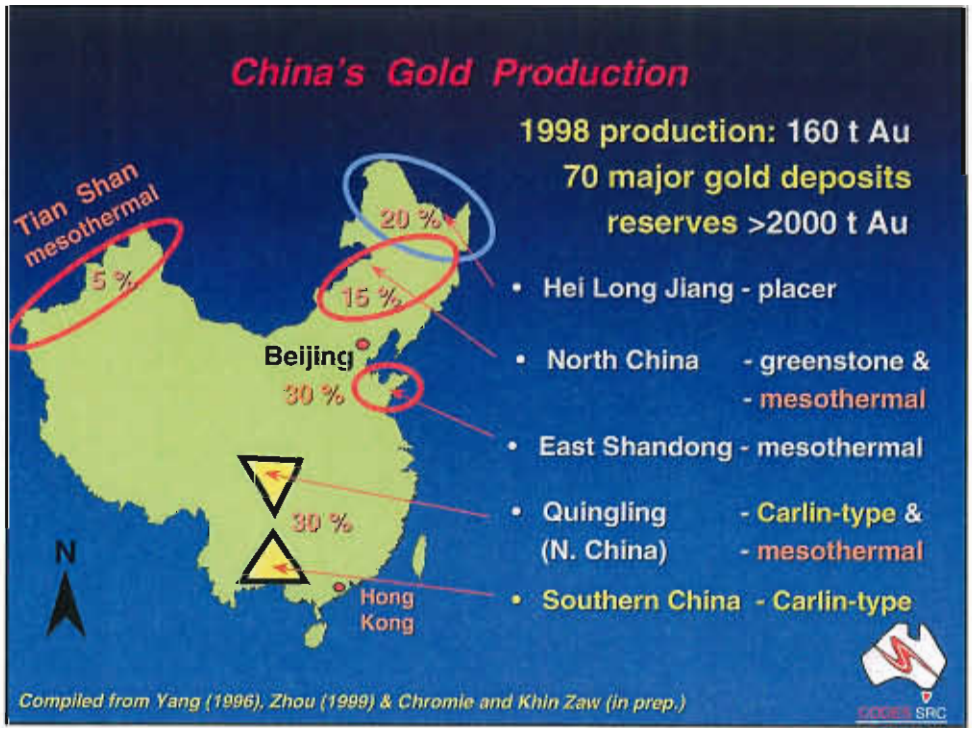
China's Gold Production
1998 production: 160 t Au
70 major gold deposits
reserves >2000 t Au
Tian Shan mesothermal
5 %
20 %
15 %
Beijing
30 %
30 %
N
Hong Kong
• Hei Long Jiang - placer
• North China - greenstone & - mesothermal
• East Shandong - mesothermal
• Quingling (N. China) - Carlin-type & - mesothermal
• Southern China - Carlin-type
Compiled from Yang (1996), Zhou (1999) & Chromie and Khin Zaw (in prep.)
CODES SRC

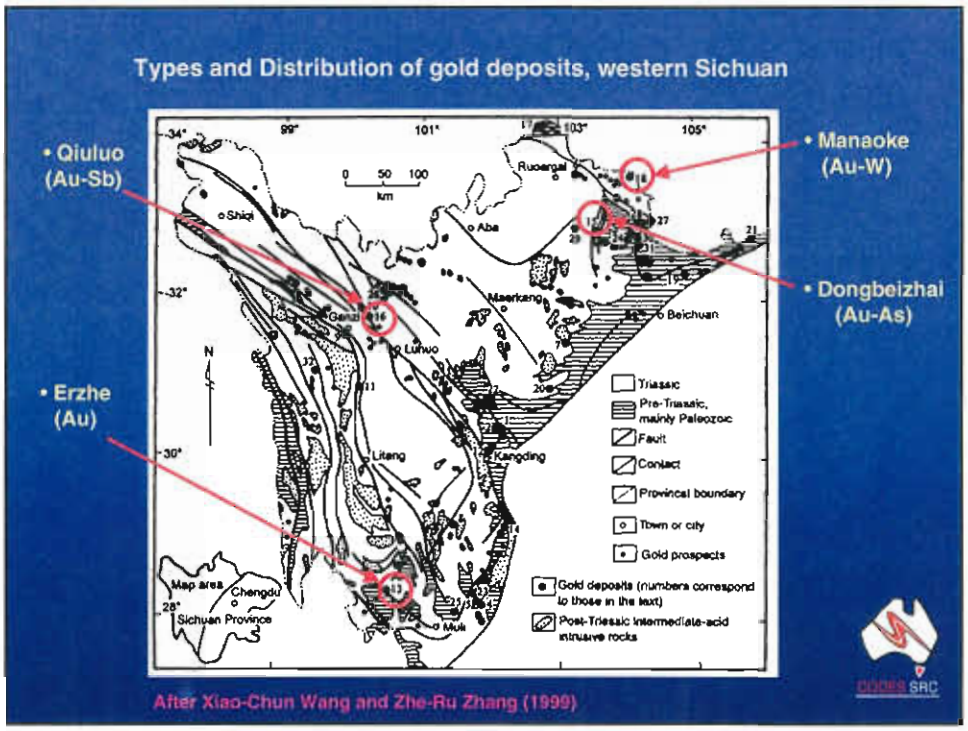
Types and Distribution of gold deposits, western Sichuan
• Qiuluo (Au-Sb)
• Manaoke (Au-W)
• Dongbeizhai (Au-As)
• Erzhe (Au)
Ruoergai
Shiqi
Aba
Maerkang
Beichuan
Ganzi
Luhuo
Litang
Kangding
Map area
Chengdu
Sichuan Province
Muli
Triassic
Pre-Triassic, mainly Paleozoic
Fault
Contact
Provincial boundary
Town or city
Gold prospects
Gold deposits (numbers correspond to those in the text)
Post-Triassic intermediate-acid intrusive rocks
After Xiao-Chun Wang and Zhe-Ru Zhang (1999)


China's Base Metal Deposits
• Ashele - VHMS (Devonian)
• East Jilin - VHMS (Ordovician)
• East Liaoning - VHMS (Proterozoic)
• Xiqiu - VHMS (Proterozoic)
• Eastern China - VHMS, SEDEX (Devonian-Carboniferous)
• West Sichuan - VHMS (Triassic) & MVT (Sinian)
• West Yunnan - VHMS & SEDEX (Proterozoic, Paleozoic to Tertiary)
Beijing
Qilian Mountain Belt
Baiyan (Paleozoic)
Xitieshan (Ordovician)
N
Compiled from Yang (1994) & Gu and Pei Ni (in press)

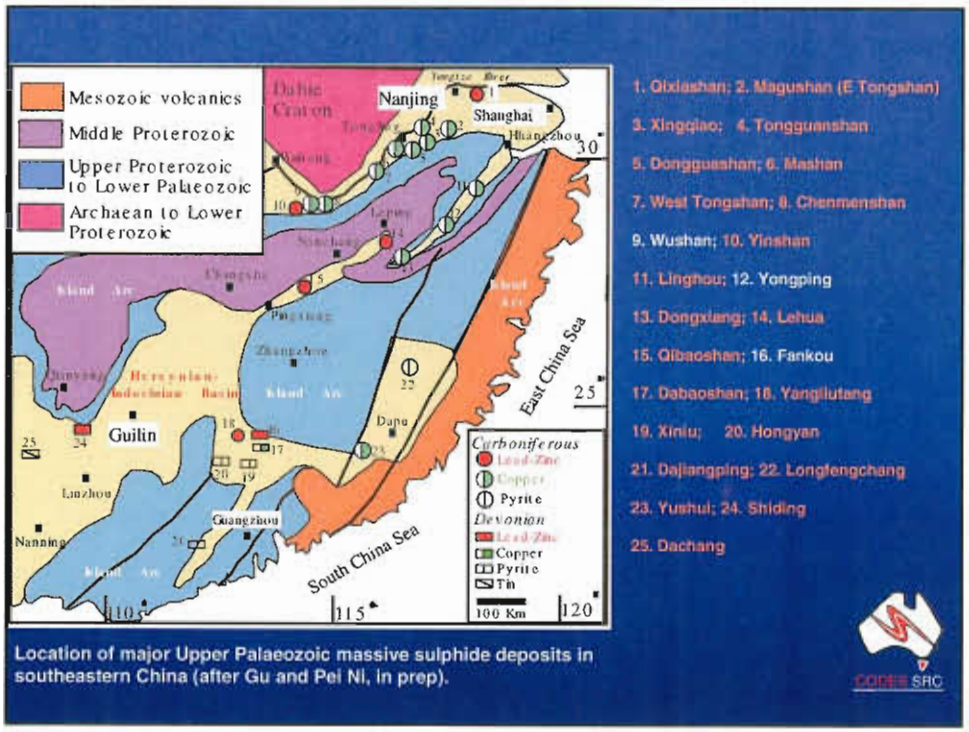

Location of major Upper Palaeozoic massive sulphide deposits in southeastern China (after Gu and Pei Ni, in prep).

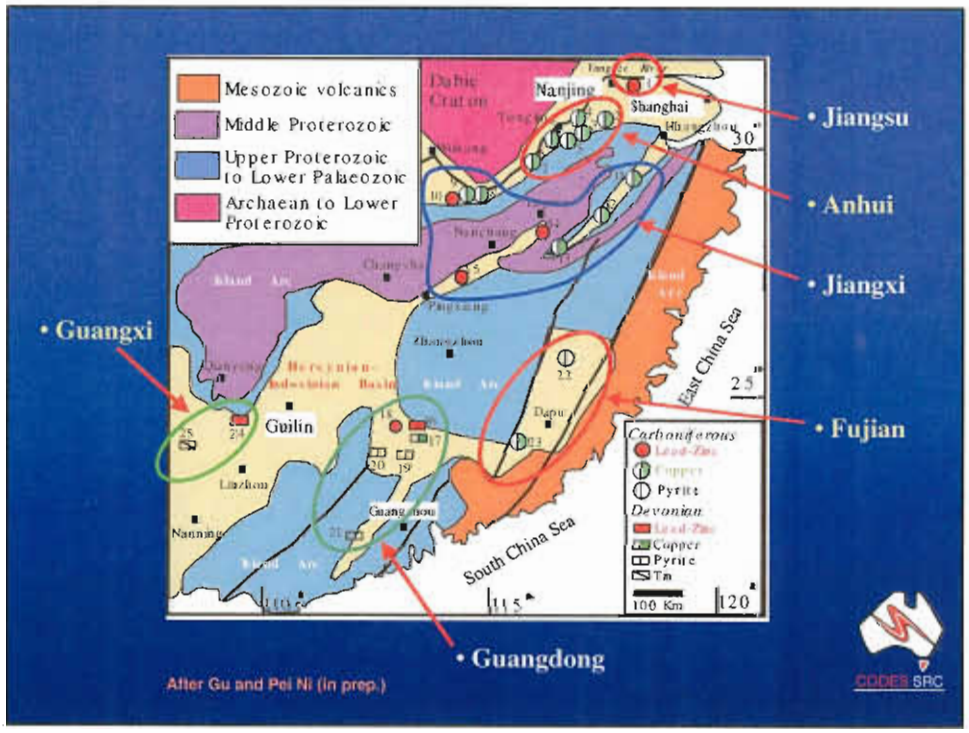

After Gu and Pei Ni (in prep.)

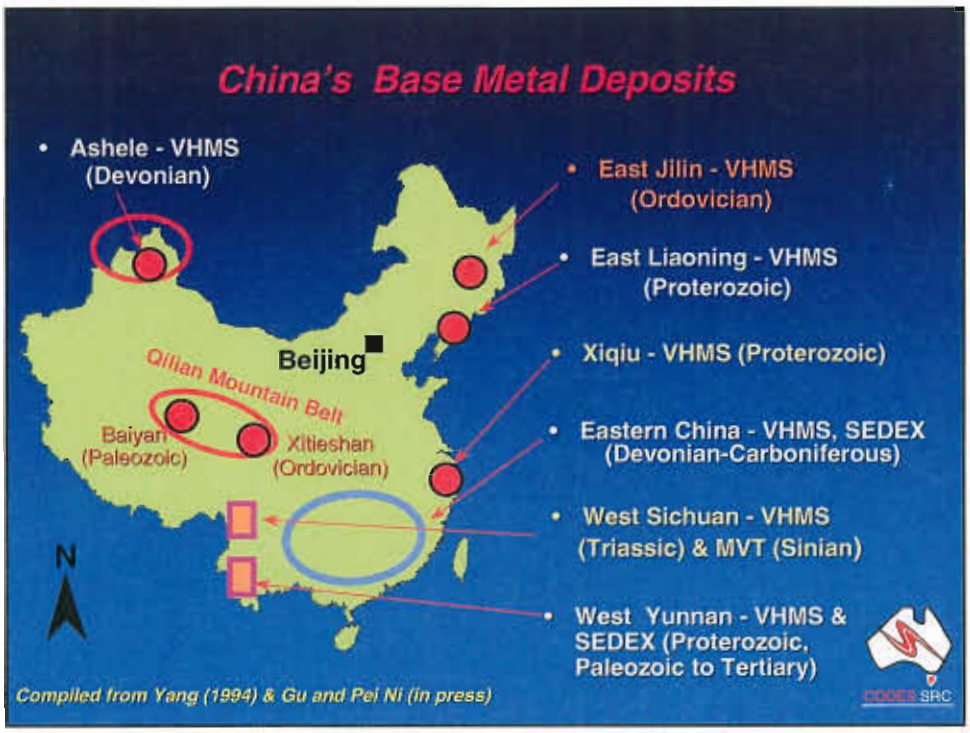
China's Base Metal Deposits
Ashele - VHMS (Devonian)
East Jilin - VHMS (Ordovician)
East Liaoning - VHMS (Proterozoic)
Beijing
Qilian Mountain Belt
Baiyan (Paleozoic)
Xitieshan (Ordovician)
Xiqiu - VHMS (Proterozoic)
Eastern China - VHMS, SEDEX (Devonian-Carboniferous)
West Sichuan - VHMS (Triassic) & MVT (Sinian)
West Yunnan - VHMS & SEDEX (Proterozoic, Paleozoic to Tertiary)
N
Compiled from Yang (1994) & Gu and Pei Ni (in press)
CODES SRC

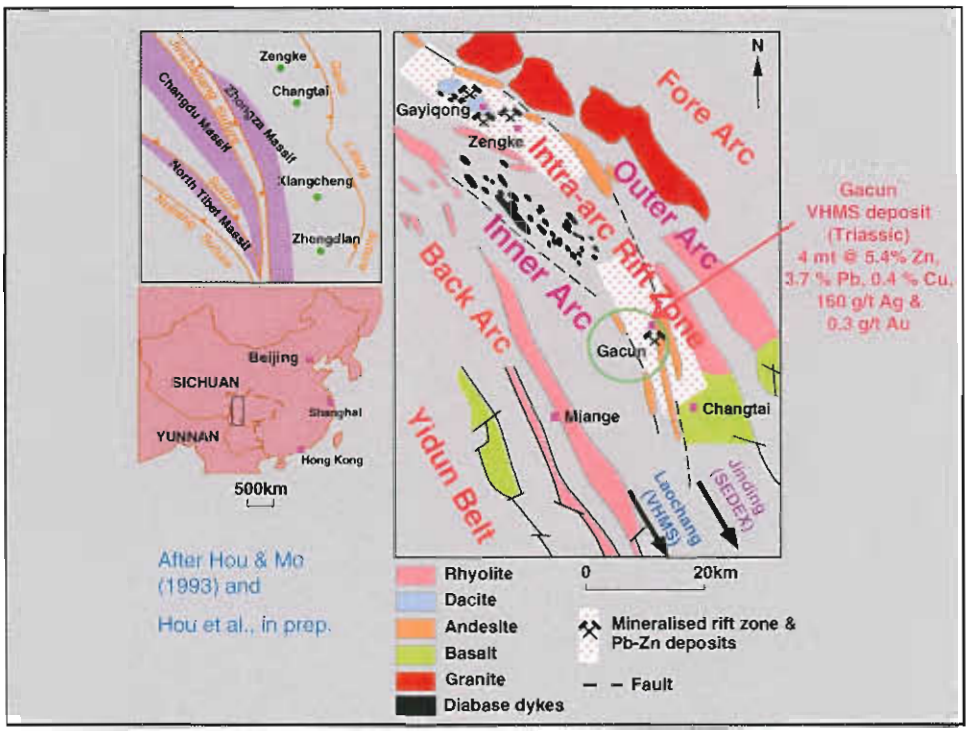
Zengke
Changtai
Chengdu Massif
Zhongza Massif
Xiangcheng
North Tibet Massif
Zhongdian
Beijing
SICHUAN
Shanghai
YUNNAN
Hong Kong
500km
After Hou & Mo (1993) and Hou et al., in prep.
N
Gayiqong
Zengke
Fore Arc
Intra-arc Rift Zone
Outer Arc
Inner Arc
Back Arc
Yidun Belt
Gacun
VHMS deposit (Triassic) 4 mt @ 5.4% Zn, 3.7 % Pb, 0.4 % Cu, 160 g/t Ag & 0.3 g/t Au
Gacun
Miange
Changtai
Laochang (VHMS)
Jinding (SEDEX)
0
20km
Rhyolite
Dacite
Andesite
Basalt
Granite
Diabase dykes
Mineralised rift zone & Pb-Zn deposits
Fault

Triassic Gacun VHMS deposit, Sichuan

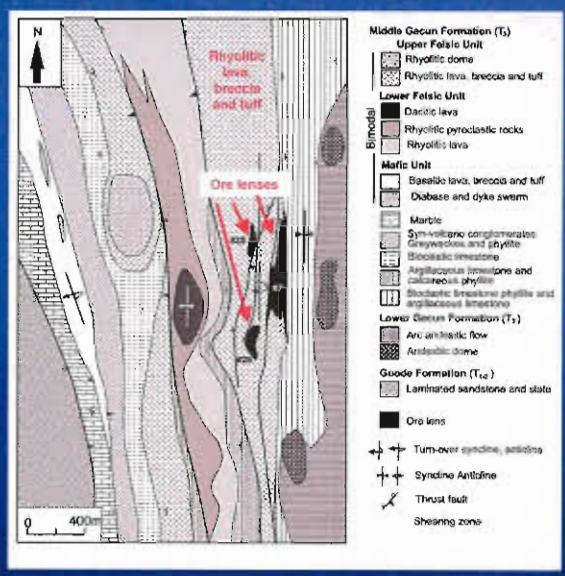

After Hou et al. (in prep)

CODES SRC

Triassic Gacun VHMS deposit, Sichuan

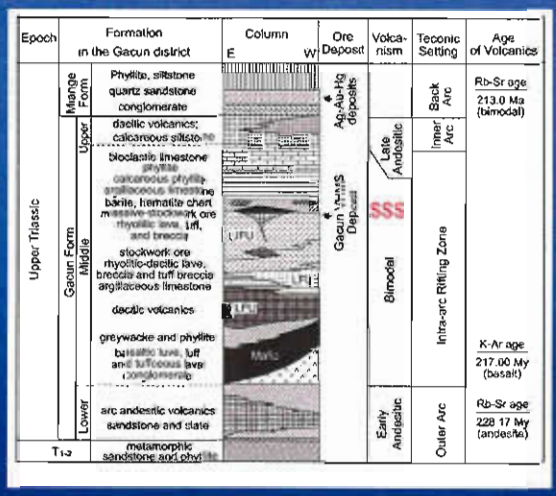

After Hou et al. (in prep)

CODES SRC

Triassic Gacun VHMS deposit, Sichuan

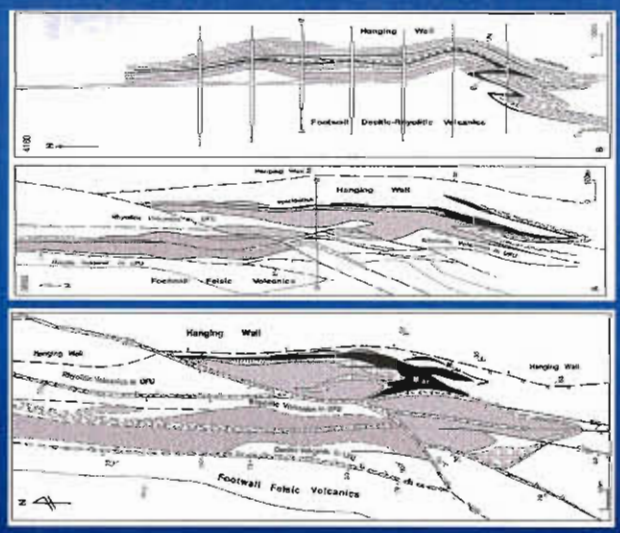

After Hou et al. (in prep)

Triassic Gacun VHMS deposit, Sichuan

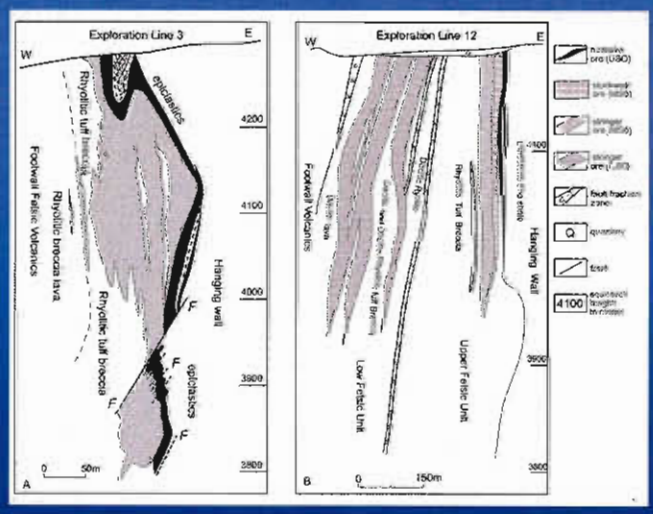

After Hou et al. (in prep)

Triassic Gacun VHMS deposit, Sichuan

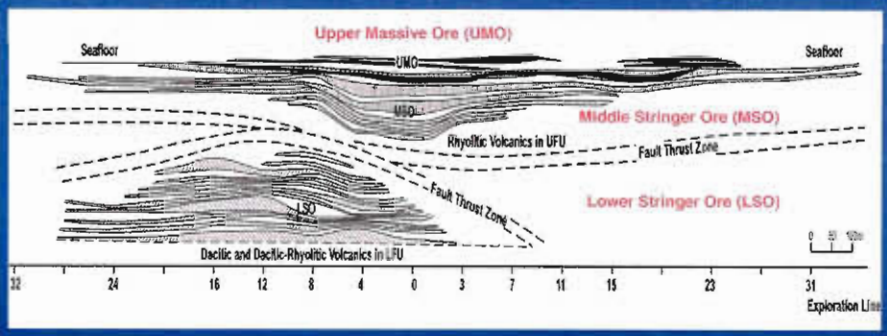

After Hou et al. (in prep)

CODES SRC

Triassic Gacun VHMS deposit, Sichuan

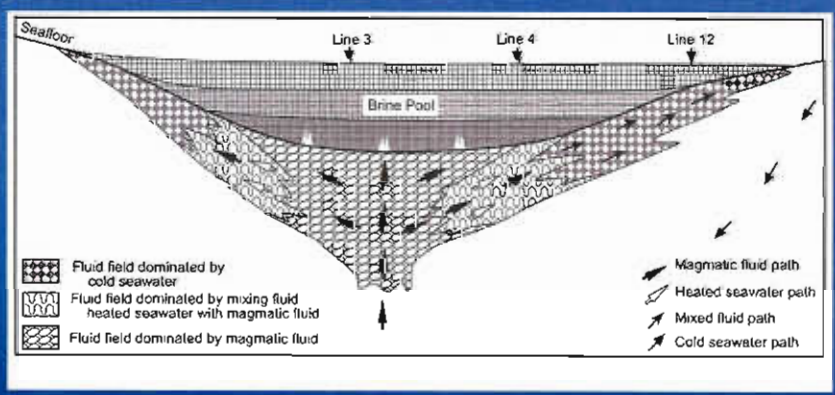

After Hou et al. (in prep)

CODES SRC

Deposit compilation
(Pb, Zn, Cu, Fe)
878 deposits
(Yunnan)

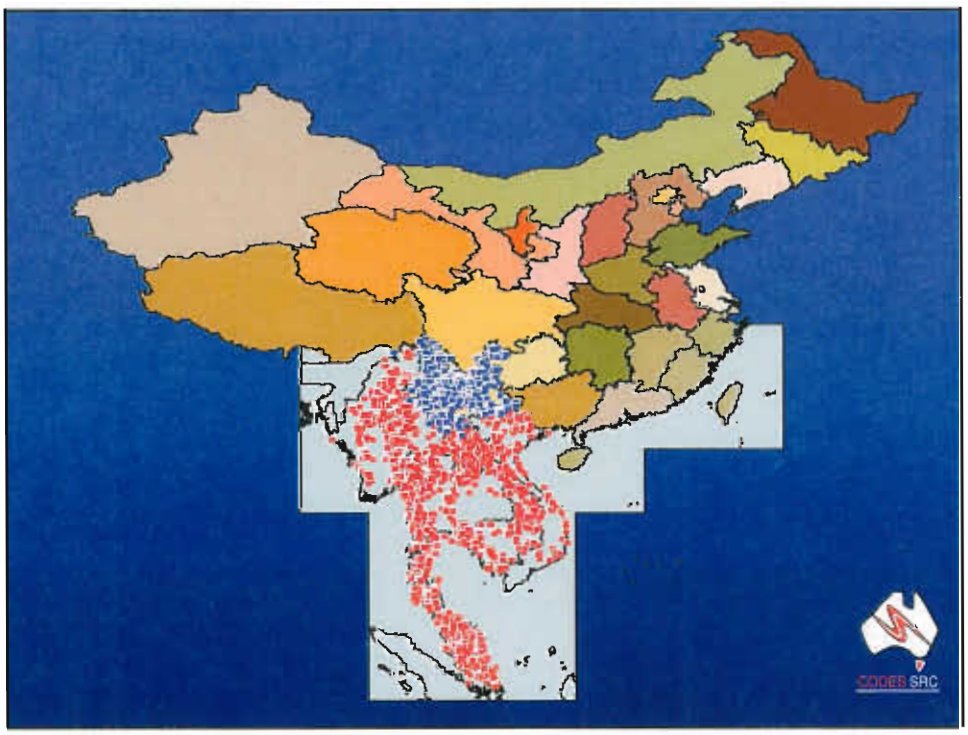

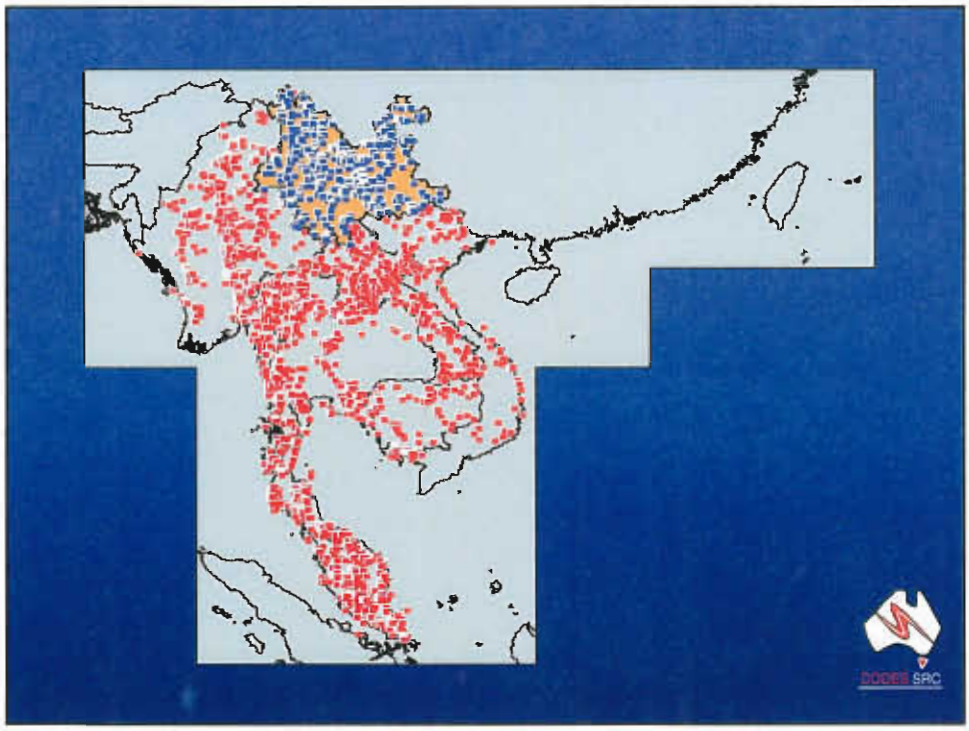

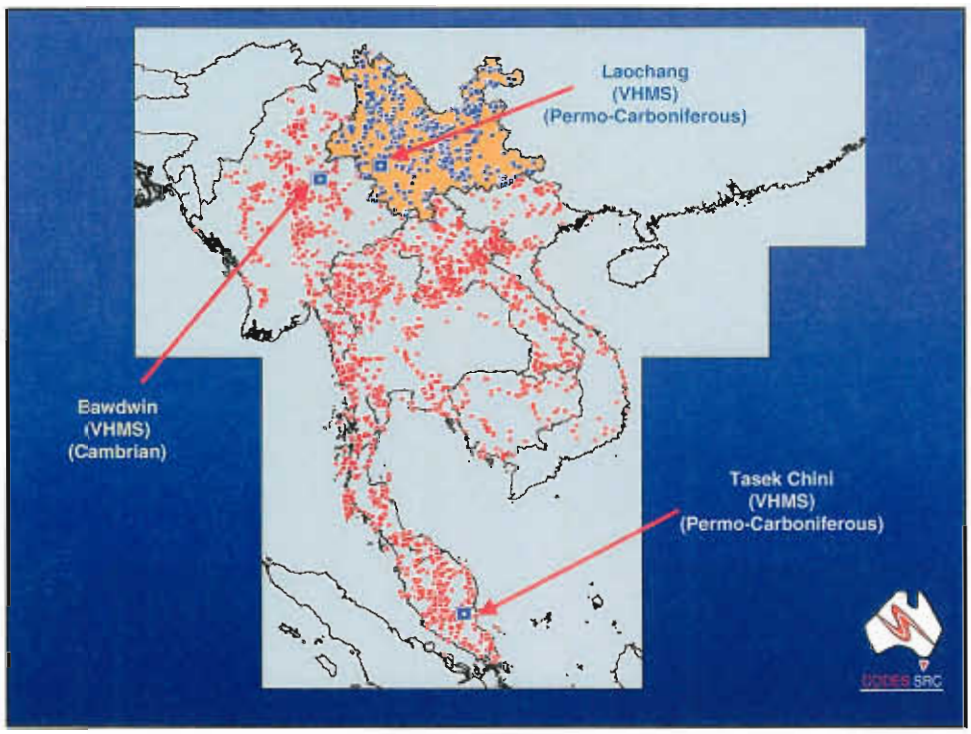
Laochang
(VHMS)
(Permo-Carboniferous)
Bawdwin
(VHMS)
(Cambrian)
Tasek Chini
(VHMS)
(Permo-Carboniferous)

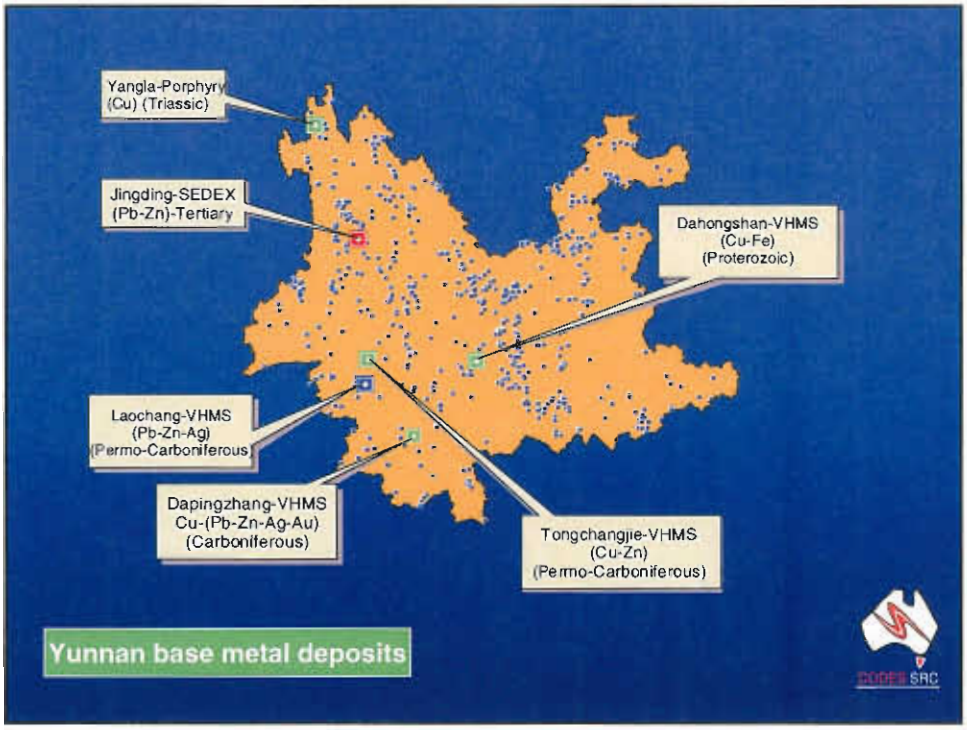
Yangla-Porphyry
(Cu) (Triassic)
Jingding-SEDEX
(Pb-Zn)-Tertiary
Dahongshan-VHMS
(Cu-Fe)
(Proterozoic)
Laochang-VHMS
(Pb-Zn-Ag)
(Permo-Carboniferous)
Dapingzhang-VHMS
Cu-(Pb-Zn-Ag-Au)
(Carboniferous)
Tongchangjie-VHMS
(Cu-Zn)
(Permo-Carboniferous)
Yunnan base metal deposits
CODES SRC

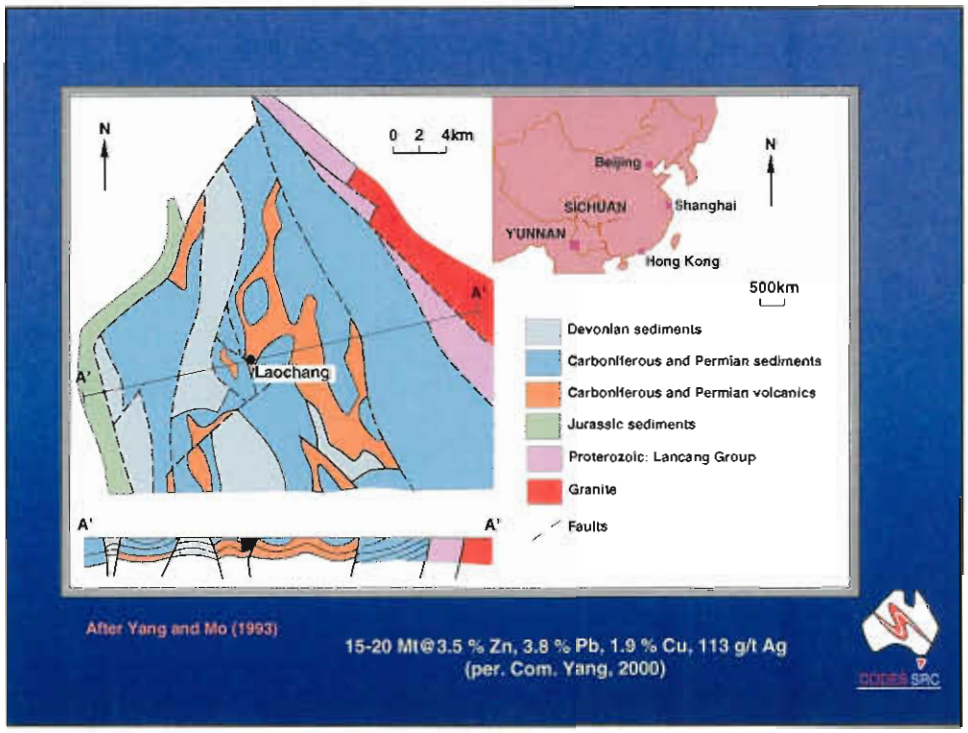
N
0 2 4km
A'
A'
Laochang
A'
A'
Beijing
SICHUAN
Shanghai
YUNNAN
Hong Kong
N
500km
Devonian sediments
Carboniferous and Permian sediments
Carboniferous and Permian volcanics
Jurassic sediments
Proterozoic: Lancang Group
Granite
Faults
After Yang and Mo (1993)
15-20 Mt@3.5 % Zn, 3.8 % Pb, 1.9 % Cu, 113 g/t Ag
(per. Com. Yang, 2000)
CODES SRC

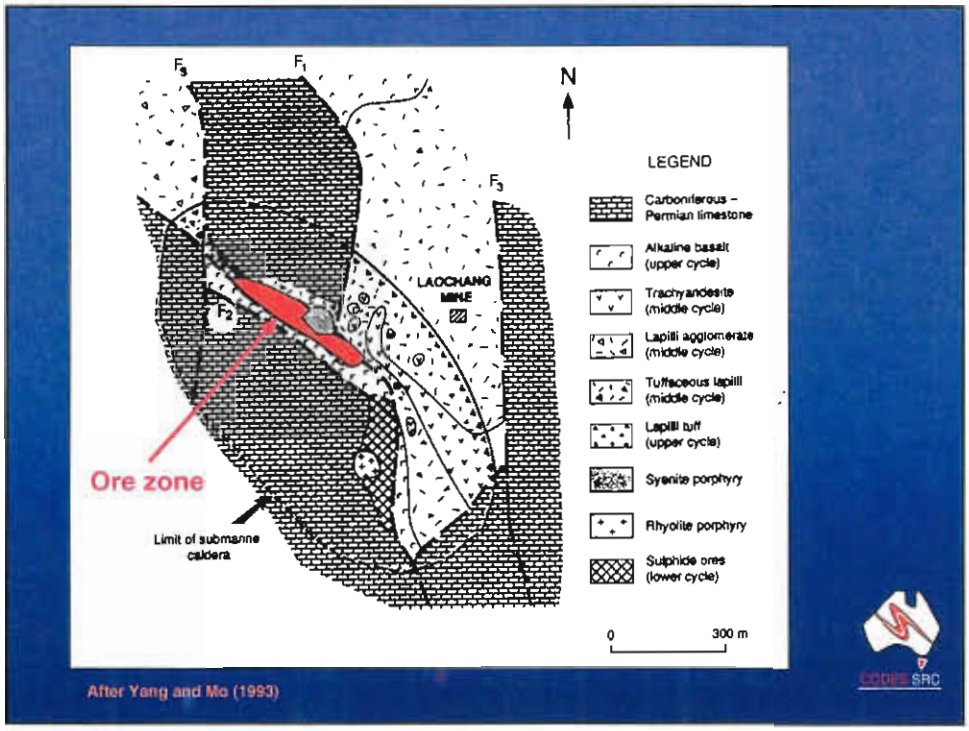
F3
F1
F2
F3
N
LAOCHANG MINE
Ore zone
Limit of submarine caldera
LEGEND
Carboniferous – Permian limestone
Alkaline basalt (upper cycle)
Trachyandesite (middle cycle)
Lapilli agglomerate (middle cycle)
Tuffaceous lapilli (middle cycle)
Lapilli tuff (upper cycle)
Syenite porphyry
Rhyolite porphyry
Sulphide ores (lower cycle)
0
300 m
After Yang and Mo (1993)
CODES SRC

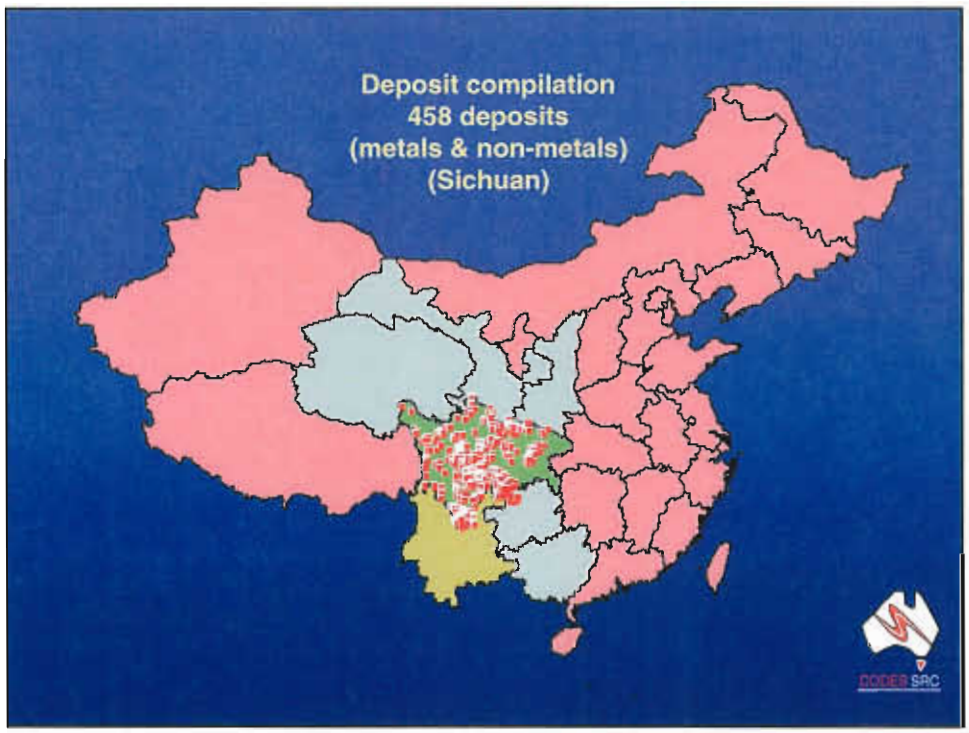
Deposit compilation
458 deposits
(metals & non-metals)
(Sichuan)
CODES SRC

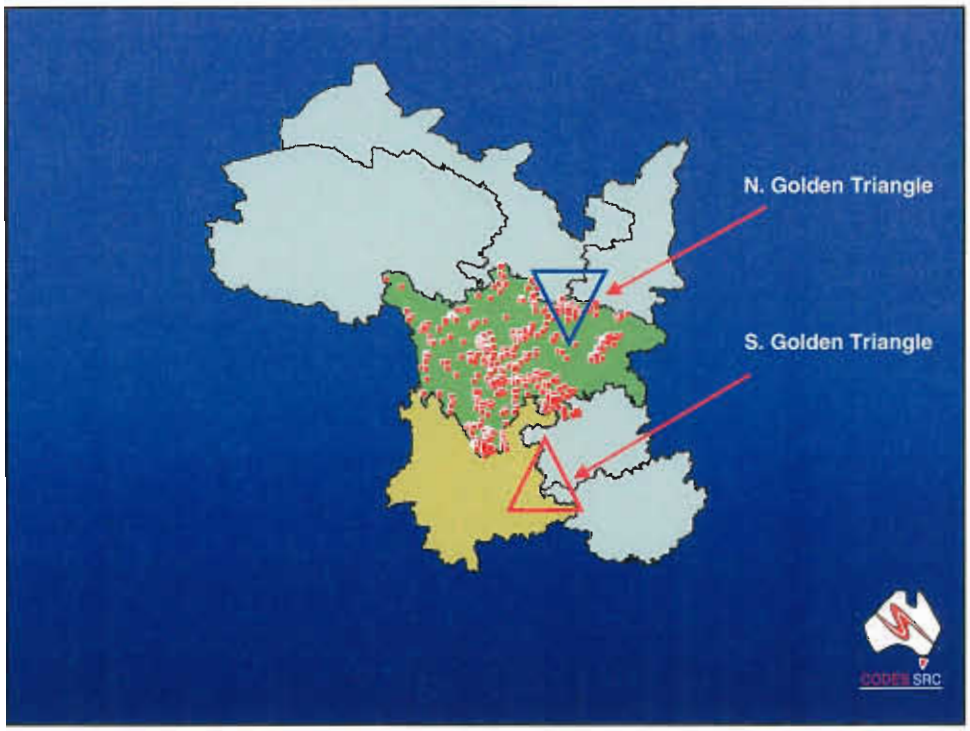

Progress Summary

- Preliminary contacts have been successfully made with various organisation, institute and individuals for mineral deposit data compilation and district to deposit scale ore deposit studies
- For example: Yunnan and Sichuan Bureau of Geology and Mineral Resources, SW Institute of Metallurgical and Mineral Resources Exploration & Development
- Institute of Mineral Deposits, Beijing and Nanjing University, Nanjing
- We need to undertake true "Collaboration" at a cost.

CODES SRC

GIS Database

South China P603
Progress Seminar15 June 2000

Eleanor Bruce
Centre for Spatial Information Science
School of Geography and Environmental Studies
University of Tasmania

GIS Database

- Digital capture of Geological mapsheets for Yunnan Province (1:1,000,000) completed
- Associated metadata and data dictionaries
- Deposit datasets
- Progress on Sichuan Province

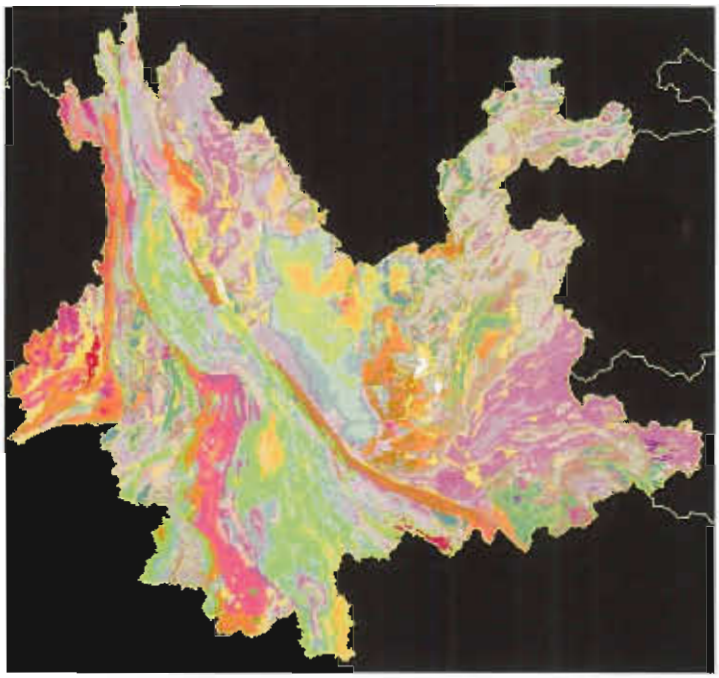

Geology of Yunnan Province

- Source data - Geological Map of Yunnan Province, 1990, Bureau of Geology and Mineral Resources of Yunnan Province, mapping series
- Scale 1:1 000 000
- Map Projection or Datum was not provided

Data Capture

- Images scanned and georeferenced
- "Heads-up" screen digitising
- Attribute labelling
- Automated error checking
- Error correction

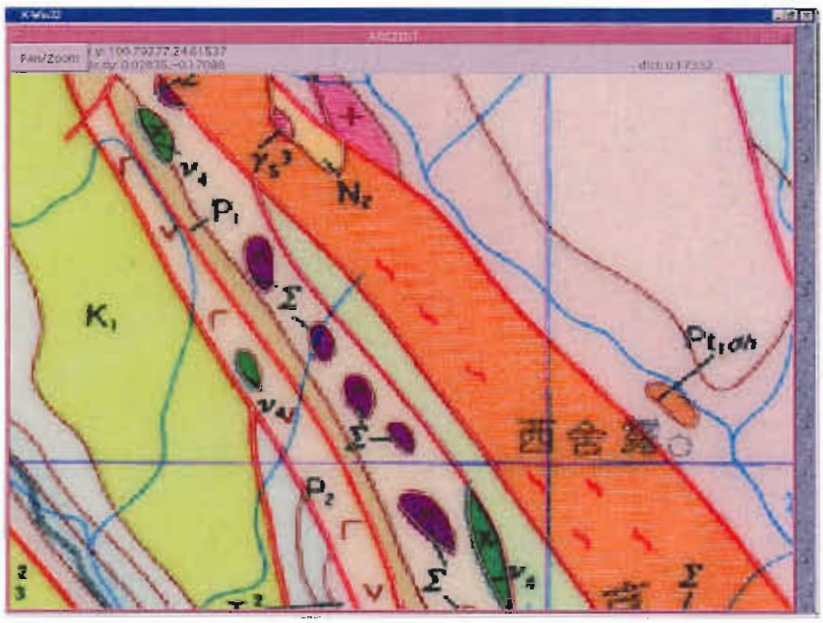

Edgematching

- 4 mapsheets were appended through 'Edgematching'

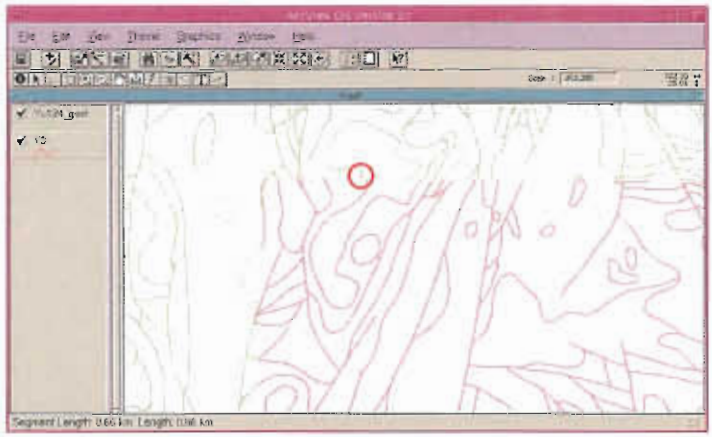

Spatial Adjustment

- Map Projection and Datum unknown
- Consistency with regional datasets
- China Administrative Regions GIS Data 1:1M
- Source: SEDAC, CIESIN 1990
- 4500 adjustment links

Adjust Process

Adjust Limit

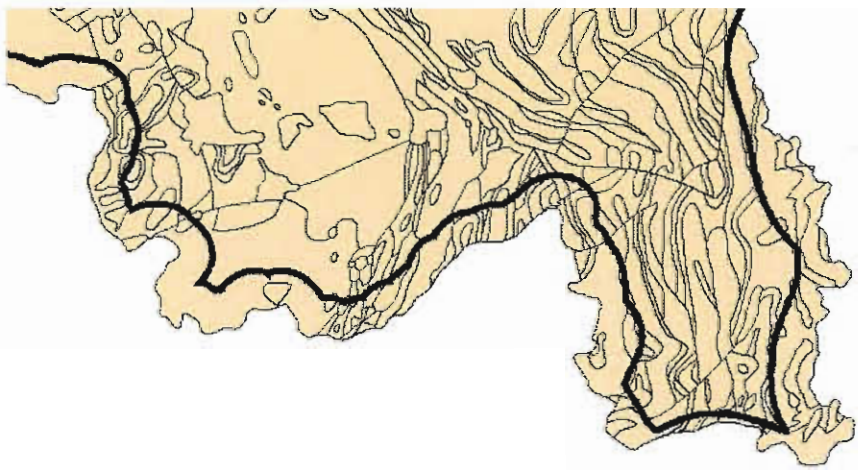

Comparison with DCW Data

Data Documentation

- Metadata - format based on the ANZLIC Metadata Standard.
- Data Dictionary - outlines contents of each GIS dataset and associated attribute fields

Geological GIS Data Progress

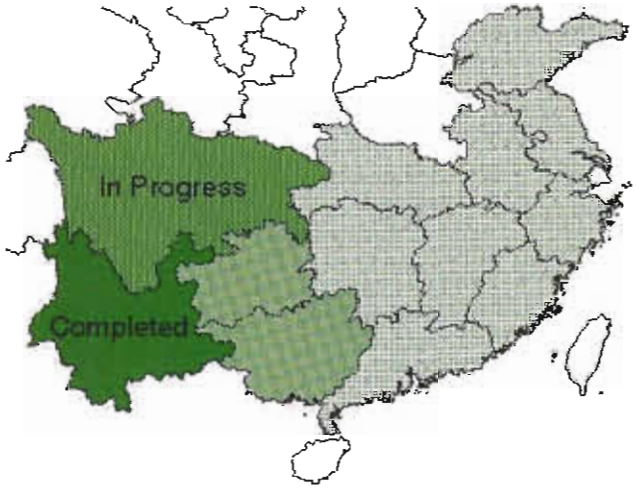

Deposit Data Progress

- Sichuan

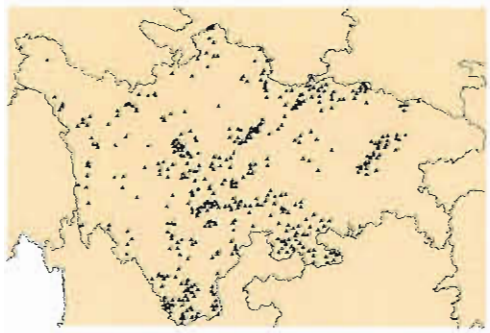

- Yunnan - in progress

Acknowledgments

Monica Jacobsen
Adrian Large
Mark Morffew
Chris Walsham
Sonya Huggins

International Geology Review, Vol. 36, 1994, pp. 293–300.

Volcanogenic Massive Sulfide Deposits in China

KAIHUI YANG

Department of Geology, University of Toronto, Canada M5S 3B1
and Institute of Geology, Chinese Academy of Geological Sciences,
Baiwanzhuang Rd. 26, Beijing 100037, P.R. China

Abstract

China has many volcanogenic massive sulfide (VMS) deposits, few of which are familiar to Western geologists. The economic importance of VMS deposits in China has been increasingly recognized, especially after progress has been made on exploration and research in major orogenic belts since the 1980s. VMS deposits of various types with ages ranging from Proterozoic to Mesozoic have been identified within a number of major metallogenic belts. The VMS deposits in northwestern China occur in Hercy-Caledonian orogenic belts (the Altaides [Altay] and Qilian); those in southwestern China appear in the Himalaya-Tethyan orogenic belt as well as at the margin of Yangtze continental plate; and those in eastern China are related to basemental sequences of Proterozoic to early Paleozoic ages. Most of the important VMS deposits in China appear to be associated with paleotectonic settings of convergent plate margins. Only a few deposits presently have been identified as economically important, but if VMS deposits occur in clusters within metallogenic belts, then the potential for discovering more deposits is considerable.

Northwestern China

THE MOST important VMS belts in northwestern China are the Ashele belt in the Altaides and the Baiyin and Xitieshan belts in the Qilian orogenic belt. Other VMS deposits occur in the Qinling orogenic belt (Shannxi Province), east of the Qilian belt (Fig. 1 and Table 1). The Ashele belt extends from NW to SE, straddling the boundary between northern Xinjiang Province in China and southeastern Russia in the Hercynian fold system of the northern Altaides. Tens of VMS deposits and occurrences appear in the Ashele belt, mostly within Russia. In China's northern Xinjiang the Ashele Zn-Cu deposit, discovered in 1984, is typical (Cheng, 1990). It is hosted in a Middle Devonian volcanic sequence (the Ashele formation) constituting part of an arc volcanic formation that includes lower dacitic-rhyolitic units and upper andesitic-basaltic units. Massive sulfides are localized within the lower rhyodacitic units, occurring close to synvolcanic dacitic intrusions, and are underlain by stringer zones with strong silicification and sericitization. The geological features of this deposit are similar to the Kuroko deposits of Japan.

Many VMS deposits occur in the Qilian orogenic belt, mostly in the Bayin and Xitieshan belts. The Baiyin belt in Gansu Province, including the Baiyin-Shiqingdong and Laohushan subbelts, is situated in the Caledonian fold system of the northern Qilian belt. It initially was explored in the late 1940s, and was the first VMS belt recognized in China (Song, 1949, 1954). In the Baiyin-Shiqingdong subbelt, the Cambrian-Ordovician volcanic sequence represents an arc volcanic formation possibly built on a continental margin. Numerous massive sulfide deposits and occurrences are associated with the felsic members (quartz-keratophiric formation) of a bimodal volcanic unit (Yan, 1983; Wu and Zhou, 1991). Six deposits have been discovered since the 1940s, which fall into two compositional groups—the Cu-Zn group, as illustrated by the well-known Baiyinchang deposit, and the Zn-Pb-Cu group, represented by the Xiaotieshan deposit—both of which show enrichments of Ag, Au, Se, As, and In and are anomalous in W, Mo, Sn, and Hg. Massive ores of these deposits occur close to felsic synvolcanic intrusions, and typically are underlain by stringer zones. Fe- and Mn-rich silica oxide formations and gypsum layers are extensively exposed as covers of the massive ores. These deposits generally are compared to Kuroko-type deposits (Wu and Zhou, 1991), but the differentiation of Cu, Pb, and Zn among the deposits in the Baiyin-

0020-6814/94/53/293-8 $10.00

TABLE 1. Summary of Geological Features of Selected VMS Metallogenic Belts in China

Metallogenic belt (Province)	Host rock lithology (ages)	Tectonic setting	Lithotectonic province or orogenic belt	VMS types	Metals	Major deposits (reserve/utility[1])	References
Northwest China							
1. Ashele (Xinjiang)	Rhyolitic, andesitic, and basaltic units (D2)	Volcanic arc	Hercynian fold system of the north Altaides	Kuroko-type (?)	Zn-Cu	Ashele (1)	Cheng (1990)
2. Baiyin (Gansu) 1) Baiyin-Shiqingdong subbelt	Felsic units of a bimodal sequence (C-O)	Volcanic arc	Caledonian fold system of the north Qilian orogenic belt	Kuroko-type	Zn-Pb-Cu, Zn-Cu	Baiyinchang (1/m), Xiaotieshan (2/m), Shigequan (2)	Wu and Zhou (1991)
2) Laohushan subbelt	Ophiolitic units (O)	Back-arc	Caledonian fold system of the north Qilian orogenic belt	Cyprus type	Cu	Yindonggou (3), Zhuzuiyaba (3)	Wu and Zhou (1991)
3. Xitieshan (Qinghai)	Intermediate-felsic sequence (O3)	Continental margin (volcanic arc?)	Caledonian fold system of the south Qilian belt	?	Pb-Zn	Xitieshan (1/m)	Wu (1985)
4. Others: Yangjiaping (Shannxi)	Spilitic keratophiric sequence (Pz1)	Continental margin (?)	Eastern extension of the Qilian belt	Cyprus-type (?)	Cu-Zn	Yangjiaping (2)	Shannxi Bureau of Geology and Mineral Resources (1990, unpub.)
Southwest China							
1. Deerni (Qinghai)	Ophiolitic suite (P-T)	Ocean floor (?)	Eastern Tethyan orogenic belt	Cyprus-type	Cu-Zn-Co	Deerni (1)	Zhang (1980)
2. Zengke-Xiangcheng (Sichun)	Felsic units of a bimodal sequence (T3)	Volcanic island arc	Eastern Tethyan orogenic belt	Kuroko-type	Zn-Pb-Cu, Zn-Cu	Gacun (1), Gayiqiong (2)	Hou and Mo (1991, 1993)
3. Lijiang (Yunnan)	Basaltic sequence (P)	Continental rift	Western margin of Yangtze platform	?	Cu	Lijiang (3), Yongsheng (3)	Yunnan Bureau of Geology and Mineral Resources (1981, unpub.)
4. Changning-Menglian (Yunnan)	Alkalic basaltic and tholeiitic sequences (C-P)	Continental rift transitional to initial oceanic spreading	Eastern Tethyan orogenic belt	Laochang-type Cyprus-type	Pb-Zn-Cu, Cu	Laochang (1/m), Tongchangjie (3)	Yang and Mo (1990a, 1990b, 1993), Yang et al. (1993)

TABLE 1 *(continued)*

Metallogenic belt (Province)	Host rock lithology (ages)	Tectonic setting	Lithotectonic province or orogenic belt	VMS types	Metals	Major deposits (reserve/utility[1])	References
5. Dahongshan (Yunnan)	Spilitic-keratophiric sequence (Pt2-3)	Convergent plate margin (volcanic arc ?)	Southwestern Yangtze platform	?	Cu-Fe	Dahongshan (1/m)	Cheng (1990)
6. Others 1) Pengxian (Sichun)	Metamafic volcanic sequence (C-P?)	Ocean floor (?)	Eastern Tethyan orogenic belt	Cyprus-type (?)	Cu	Pengxian (3/m)	Sichun Bureau of Geology and Mineral Resources (1981, unpub.)
2) Sandashan (Sichun)	Rhyodacitic tuffaceous units (P)	Volcanic arc	Eastern Tethyan orogenic belt	?	Cu	Sandashan (3/m)	Yunnan Bureau of Geology and Mineral Resources (1986, unpub.)
Eastern China							
1. Eastern Jilin (Jilin)	Felsic volcanic sequence (O3)	Volcanic arc (?)	Sino-Korean platform margin	Kuroko-type (?)	Zn-Pb-Cu	Fangniugou (2)	Jilin Bureau of Geology and Mineral Resources (1988, unpub.)
2. Eastern Liaoning (Liaoning)	Quartz-keratophiric (Pt3)	Rift (?)	Sino-Korean platform	?	Cu	Liaodong (2)	Liaoning Bureau of Geology and Mineral Resources (1989, unpub.)
3. Xiqiu (Zhejiang)	Spilitic-keratophiric sequence (Pt2-3)	Volcanic arc	Jiangnan massif margin	Kuroko-type (?)	Zn-Cu	Xiqiu (2)	Zhang (1986)
4. Others: Bainaimiao (Inner Mongolia)	Metavolcanic sequence (Pt)	Convergent plate margin (?)	Northern margin of the Sino-Korean platform	?	Cu(Mo)	Bainaimiao (2), Beiluwutu (2)	Inner Mongolia Bureau of Geology and Mineral Resources (1985, unpub.)

[1]Note: 1 = > 5 million tons; 2 = 0.5–5 million tons; 3 = < 0.5 million tons; /m = mining.

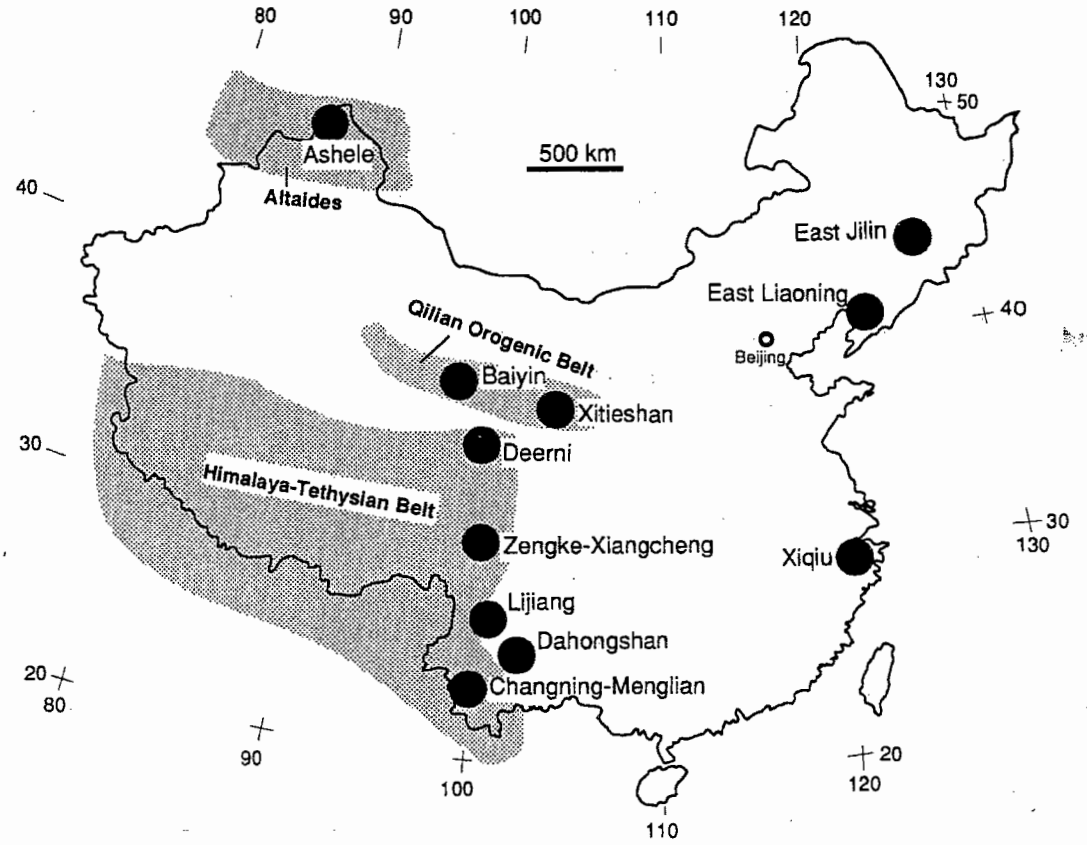

FIG. 1. Distribution of major VMS belts in China.

Shiqingdong belt requires further investigation. North of the Baiyin-Shiqingdong subbelt, the Laohushan subbelt is characterized by Cu massive sulfide deposits within an Ordovician ophiolitic belt, possibly representing a zone of back-arc spreading. The deposits and showings are hosted in a pillowed mafic volcanic sequence, showing similarities to Cyprus-type deposits. Two typical deposits are Yindonggou and Zhuzuiyaba, currently under exploration.

The Xitieshan belt in northern Qinghai Province is located in the southern Qilian orogenic belt, and is associated with an Upper Ordovician volcanic formation, possibly in a continental margin setting. The massive sulfide deposits, typified by the Xitieshan Mine—with compositions of Pb, Zn, and recoverable Au, Ag, Sn, Cd, Ga, In, and As—are hosted in an intermediate-felsic volcanic sequence (Wu, 1985). More than 100 economic massive sulfide orebodies have been identified within the units of tuffaceous slate, carbonate, and carbonaceous schists. Stringer zones rarely are observed beneath the massive layers, although veined and disseminated ores locally formed along the margins of the massive orebodies. It appears that the massive sulfide ores formed in basins distal to volcanic centers.

Southwestern China

At least five VMS metallogenic belts—i.e., the Deerni, Zengke-Xiangcheng, Lijiang, Changning-Menglian, and Dahongshan belts—have been explored in southwestern China since late the 1970s. The first four belts were associated with the Late Paleozoic to Mesozoic evolution of Tethyan tectonics, whereas the Dahongshan belt is associated with a Proterozoic volcanic belt. Other VMS deposits, such as the Sandashan in western Yunnan

Province and the Pengxian in western Sichun (Table 1), are not well documented yet.

The Deerni belt in southern Qinghai Province is situated east of the South Kunlun ophiolitic belt, which may represent the relics of a Tethyan ocean. The Deerni deposit, which includes Cu, Zn, Co, and recoverable Au and Ag, is typical of the belt (Zhang, 1981). It is hosted in a Permian-Triassic ophiolitic sequence that includes serpentinized cumulates (mostly olivine cumulates and pyroxenites) and basaltic units. The basaltic lavas, with high MgO content and LREE-depleted patterns, have chemical characteristics similar to mid-ocean ridge basalts (MORB). Massive sulfide orebodies are localized within basaltic pyroclastic units overlain by carbonaceous tuff and carbonate units. A stringer zone appears to underlie the massive ores. The geological features of the Deerni deposit are comparable to Cyprus-type deposits.

The Zengke-Xiangcheng belt in western Sichun Province occurs within the Triassic Yidun island arc terrane, and is characterized by Zn-Pb-Cu deposits (Hou and Mo, 1991, 1993; Mo et al., 1993). The massive sulfide deposits are associated with the Upper Triassic bimodal sequence of the Gacun Group. Massive ores are confined to several fault-bounded basins within the intra-arc rift of the Yidun paleo-island arc, and are localized in the felsic volcanic units in the vicinity of felsic synvolcanic intrusions around volcanic centers. Stringer zones are well developed beneath the massive ores, displaying strong sericitization and silicification zones. The development of the intra-arc rifting belt and associated massive sulfide deposits may be comparable to the Green Tuff Belt and the Kuroko deposits of Japan (Ho and Mo, 1993; Yang et al., 1992a, 1992b, 1993).

The Lijiang belt in western Yunnan Province is associated with a Permian volcanic belt that was related to a rift along the western continental shelf of the Yangtze Plate. The volcanic belt is dominated by basaltic flows with chemical affinities to continental basalts and associated pyroclastics. Tens of Cu massive sulfide deposits (Yunnan Bureau of Geology and Mineral Resources, unpub.), although each is small in tonnage, are associated with volcanoclastic units locally intercalated with coal-bearing formations. Massive orebodies typically are underlain by stringer zones that may represent fossil hydrothermal fluid conduits.

The Changning-Menglian belt in western Yunnan Province is characterized by the occurrences of Pb-Zn-Cu and Cu (Zn) massive sulfide deposits (Yang et al., 1992a, 1992b). It is related to a Permian-Carboniferous marginal rift belt that is expressed by dominant alkalic and minor tholeiitic volcanic units (Yang et al., 1994). The Pb-Zn-Cu deposits—as typified by the Laochang Mine possessing enriched Au, Ag, recoverable As, In, Ga, Tl, and anomalous Sb, W, and Mo (Yang and Mo, 1990a, 1993; Yang, K., unpublished)—are hosted in alkalic basaltic-andesitic sequences with intercalated limestones. This succession may represent an early phase of continental rifting. Massive ores are associated with coarse-grained volcanoclastic units, and are underlain by stringer zones that include an upper zone of sericite-quartz alteration and a lower zone of tremolite-diopside-garnet. The Cu(Zn) deposits, illustrated by the Tongchangjie Mine, with anomalous Au, As, In, and Co (Yang and Mo, 1990b; Yang et al., forthcoming), are associated with tholeiitic sequences that comprise part of a dismembered ophiolitic suite. These deposits may have formed in advanced rift basins with local emplacement of oceanic crust, and may be comparable to Cyprus-type deposits (Yang et al., 1993).

The Dahongshan belt in western Yunnan is situated at the western margin of the Yangtze continental plate. It is associated with a middle to late Proterozoic metavolcanic sequence that includes spilitic and quartz-keratophiric units, marbles, and greywacke, which probably originated in a convergent plate-margin setting. The Dahongshan deposit, typical of the belt, is composed of Cu massive sulfides and siderite layers within intermediate-felsic volcanic units and limestones; it therefore is called a Cu-Fe deposit (Qian and Shen, 1990). Although the deposit has experienced varied degrees of deformation and metamorphism, the relict features suggest that the massive ores formed in basins close to volcanic centers.

Eastern China

VMS deposits in eastern China are related to the Pre-Devonian basemental sequences of the

Asian plate. The representative deposits occur in three metallogenic belts: the eastern Jilin, eastern Liaoning, and the Xiqiu. In the eastern Jilin belt, the Fangniugou Zn-Pb-Cu deposit is typical (Jilin Bureau of Geology and Mineral Resources, unpub.). It is hosted in an upper Ordovician volcanic sequence that consists of intermediate-felsic flows, tuff, limestone, and siltstone. The tabular massive orebodies are associated with coarse-grained volcanoclastic units and are underlain by a stringer zone. Typical vertical zonation of ores includes an upper massive sulfide zone enriched in Mn, Fe, Zn, Pb, Ag, and Au, and a lower Cu-rich stringer zone enriched in Cu.

Several Cu massive sulfide deposits and occurrences recently have been observed to be related to an upper Proterozoic metavolcanic sequence in the east Liaoning belt (Liaoning Bureau of Geology and Mineral Resources, unpub.). The volcanic sequence consists of quartz-keratophiric lavas and tuff, as well as tuffaceous sandstone, siltstone, and dolomitic marble, possibly formed in a paleo-rift. Stratiform massive sulfide orebodies occur within the tuffaceous sandstone and siltstone, and locally are transitional into a layer of barite, gypsum, or magnetite. No stringer zone has been located under the massive ores, suggesting formation by exhalation of hydrothermal fluids distal to volcanic centers.

The Xiqiu belt in eastern Zhejiang Province is associated with a middle-upper Proterozoic metavolcanic sequence. The latter sequence is composed of spilitic-keratophiric flows and tuff with felsic synvolcanic intrusions, and exhibits the chemical characteristics of volcanic arcs. The arc is interpreted to have formed at a convergent plate margin along the Jiangnan massif. The Xiqiu Zn-Cu deposit, hosted in the lower felsic units of the volcanic sequence, is typical of the belt (Zhang, 1986). Stratiform orebodies are associated with quartz-keratophiric volcanoclastic rocks that are succeeded by greywacke, phyllite, and jasper layers. The massive ores, consisting of pyrite, sphalerite, chalcopyrite, gypsum, barite, and quartz, are underlain by a stringer zone that includes an upper sericite-quartz-rich zone and a lower chlorite-rich zone.

In addition to these belts, other polymetallic sulfide deposits have been identified in Inner Mongolia, northern China. They appear to be related to Proterozoic metavolcanics of the basemental sequences at the northern margin of the Sino-Korean platform, and may comprise a VMS belt (Pei and Nie, 1990).

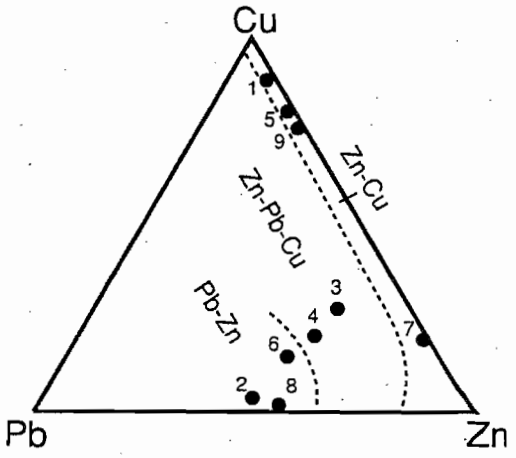

FIG. 2. Cu-Pb-Zn diagram showing the compositions of typical VMS deposits in China. The boundaries between different VMS groups are after Franklin et al. (1981). Legend: 1–2 = Changning-Menglian belt; 3–4 = Zengke-Xiangcheng belt; 5–7 = Baiyin belt; 8 = Xitieshan belt; 9 = Deerni belt.

Conclusions

Most of the important VMS deposits in China appear to be associated with paleotectonic settings of convergent plate margins. Some of these deposits are similar to Kuroko- or Cyprus-type deposits, but some, such as Laochang and Xitieshan, are not readily assigned to classic major VMS types (Hutchinson, 1973; Sawkins, 1976; Franklin et al., 1981). Perhaps certain new VMS deposit-types could be recognized from the deposits in China. Figure 2 indicates that the typical VMS deposits in China fall into Cu-Zn, Zn-Pb-Cu, and Pb-Zn groups. It is important to note that the Pb-rich (Pb-Zn or Pb-Zn-Cu) VMS deposits are numerous in the orogenic belts of western China in relation to the rest of the world. Moreover, different types of VMS deposits appear together within certain metallogenic belts, suggesting the effects of different phases of tectonic evolution. Geochemically, Chinese VMS deposits are always enriched in gold and silver (e.g., Song, 1991;

Wu et al., 1993). Some VMS deposits, in fact, can be mined as gold and/or silver deposits irrespective of major ore mineralization (such as Laochang, Gacun, and others). Tungsten, Mo, and Sn also are anomalous and recoverable in some deposits (such as Baiyin, etc.), implying that important roles are played by the crustal basement in mineralization processes.

It is still too early to assess the resources of VMS deposits in China in terms of quantifying reserves. Only the Baiyin-Shiqingdong VMS belt is relatively well known. In all other belts, only a few deposits presently have been identified as economically important, many occurrences require [initial] exploration, and many more need to be explored more thoroughly. Exploration and research of VMS deposits recently has received more attention in China. If VMS deposits in fact tend to occur in clusters within a metallogenic belt (Sangster and Scott, 1976; Scott, 1985; Franklin et al., 1981; Lydon, 1984), the potential to discover more such deposits in China is considerable. A particularly promising direction of future research would be a comparison of Chinese VMS metallogenic belts with (a) those belts in other parts of the world that are relatively well studied and (b) those located on the modern seafloor.

Acknowledgments

The author benefited from discussions with Professors Shuhe Song and Xuanxue Mo and Drs. Zengqian Hou and Jinglei Zhang. The author also is grateful to personnel at the Yunnan, Sichun, Shannxi, Inner Mongolian, Jilin, and Liaoning Bureaus of Geology and Mineral Resources, P.R. China, for access to their unpublished data and to Professor Steven D. Scott and Roger Moss, Department of Geology, University of Toronto, for support, encouragement, and assistance. In addition, Professor Brian J. Skinner, the editor of *Economic Geology*, is gratefully acknowledged for review comments on this manuscript.

REFERENCES

Cheng, Z., 1990, Characteristics of the Ashele massive sulfide Cu-Zn deposit: Bull. Nanjing Inst. Geol. M. R., Chinese Acad. Geol. Sci., v. 11, no. 1, p. 103–111 (in Chinese).

Franklin, J. M., Lydon, J. W., and Sangster, D. F., 1981, Volcanic-associated massive sulfide deposits: Econ. Geol., v. 76, p. 485–627.

Hou, Z., and Mo, X., 1991, The evolution of the Yidun island-arc and implications in the exploration of Kuroko-type volcanogenic massive sulfide deposits in Sanjiang area, China: Earth Sciences—Journal of China University of Geosciences, v. 16, p. 154–164 (in Chinese with English abstract).

————, 1993, Geology, geochemical and genetic aspects of the Kuroko-type massive sulfide deposits in Sanjiang region, southwestern China: Exploration and Mining Geology, v. 2, p. 17–30.

Hutchinson, R. W., 1973, Volcanogenic sulfide deposits and their metallogenic significance: Econ. Geol., v. 68, p. 1223–1246.

Lydon, J. W., 1984, Volcanogenic massive sulfide deposits. Part 1, A descriptive model: Geosci. Can., v. 11, p. 95–202.

Mo, X., Lu, F., Shen, S., Zhu, Q., Hou, Z., Yang, K., Deng, J., Liu, X., and He, C., 1993, Sanjiang Tethyan volcanism and related mineralization: Beijing, Geological Publishing House, 267 p. (in Chinese with detailed English abstract).

Pei, R., and Nie, F., 1990, Volcanism and metallogeny at ancient continental margin of central Inner Mongolia, P.R. China: Program with abstracts, 8th IAGOD Symposium A127–128, Ottawa, Canada, August 1990.

Qian, J., and Shen, Y., 1990, Dahongshan copper-iron ore deposit associated with volcanic rocks, Yunnan: Beijing, Geological Publishing House (in Chinese).

Sangster, D. F., and Scott, S. D., 1976, Precambrian strata-bound massive Cu-Zn-Pb sulfide ores of North America, *in* Wolf, K. H., ed., Handbook of strata-bound and stratiform ore deposits, v. 6, p. 129–222.

Sawkins, F. J., 1976, Massive sulfide deposits in relation to geotectonics, *in* Strong, D. F., ed., Metallogeny and plate tectonics: Geological Association of Canada, Spec. Paper 14, p. 221–240.

Scott, S. D., 1985, Seafloor polymetallic sulfide deposits: Modern and ancient: Marine Mining, v. 5, p. 191–212.

Song, S., 1949, The Baiyinchang pyrite-type deposit in Gaolan County, Gansu Province: Acta Geologica Sinica, v. 14, p. 31–40 (in Chinese).

————, 1954, Metallogeny and geological features of the pyrite-type copper deposits in Qilianshan: Acta Geologica Sinica, v. 32, p. 1–10 (in Chinese).

Song, X., 1991, Geochemical characteristics of volcanogenic massive sulfide deposits in China, *in* Pogel, M., and Leroy, J. L., eds., Source, transport and deposition of metals: Rotterdam/Brookfield, A. A. Balkema, p. 367–372.

Wu, C. Y., Bai, G., and Xu, L. M., 1993, Types and distribution of silver ore deposits in China: Mineral. Deposita, v. 28, p. 223–239.

Wu, J., 1985, Geological features of the Xitieshan massive sulfide deposit in Qinghai Province: Mineral Deposits (China), v. 4, no. 2 (in Chinese with English abstract).

Wu, J., and Zhou, S., 1991, Geological features and genetic model of the Baiyin exhalative volcanogenic massive sulfide deposit, China: International Symposium on Sulfide Deposits, Special Paper, Jinchang, Gansu, China, August 1991, p. 1–15.

Yan, J., 1983, Discussion on the genesis of the Baiyinchang pyrite-type deposit in Qilianshan: Mineral Deposits (China), v. 2, no. 3 (in Chinese).

Yang, K., and Mo, X., 1990a, A large Paleozoic volcanogenic massive Pb-Zn-Cu sulfide deposit: The Laochang Mine, Yunnan, southwest China: Program with Abstracts, 8th IAGOD Symposium A40–41, Ottawa, Canada, August, 1990.

———, 1990b, Geology and mineralogy of the Tongchangjie massive copper-zinc sulfide deposit, Yunnan, southwest China: Program with Abstracts, 8th IAGOD Symposium A41, Ottawa, Canada, August 1990.

———, 1993, Characteristics of the Laochang volcanogenic massive sulfide deposit, Yunnan, southwestern China: Exploration and Mining Geology, v. 2, p. 31–40.

Yang, K., Hou, Z., and Mo, X., 1992a, Volcanogenic massive sulfide deposits in Sanjiang region, southwest China: Geological features and main types: Mineral Deposits (China), v. 11, p. 35–44 (in Chinese with English abstract).

———, 1992b, Tectono-volcanic settings and metallogeny of the VMS deposits in the Sanjiang region, southwestern China, *in* Geological Society of China, Proceedings of the Meeting on Important Achievements of Geological Sciences during the Seventh Five Years (1986–1990): Beijing, Sciences and Technology Press, p. 455–459.

———, 1993, Volcanogenic massive sulfide deposits in southwestern China: Journal of Mineral Resource Geology, Spec. Issue, no. 17, p. 262–275.

Yang, K., Mo, X., and Zhu, Q., 1994, Late Paleozoic–early Mesozoic tectono-volcanic belts and regional evolution of southwestern Yunnan, China: Journal of Southeast Asia Earth Sciences (forthcoming).

Zhang, J., 1986, Lithological and ore petrographical features and genetic aspects of the Xiqiu copper deposit, Zhejiang Province: Unpubl. M. S. Thesis, 109 p. (in Chinese).

Zhang, W., 1981, Geology of the Deerni copper deposits: Beijing, Geological Publishing House (in Chinese).

Resource Geology Special Issue, No. 17, p. 263-276, 1993

Volcanogenic Massive Sulfide Deposits in Southwestern China

Kaihui YANG*, Zengqian HOU** and Xuanxue MO***

Abstract: Important progress has been made over the past years on the exploration and researches of massive sulfide deposits in the Sanjiang region, southwestern China. Most of the volcanogenic massive sulfide deposits and occurrences discovered hitherto are distributed in the Zengke-Xiangcheng and Changning-Menglian metallogenic belts, each distinct in tectonic settings and deposit types.

The massive sulfide deposits occurring in the Zengke-Xiangcheng belt in western Sichuan are characterized by Zn > Pb > Cu in composition, and are associated with particularly the Upper-Triassic bimodal sequence of the Gacun Group. The massive ores developed in three fault-bounded basins (i.e., the Gayiqiong, Gacun and Xiangcheng basins) within the intra-arc rift of the Yidun paleo-island arc, and are localized in the felsic volcanic units in vicinity of volcanic centres, and underlain by a disconcordant stringer zone. The development of the intra-arc rifting belt and associated massive sulfide mineralization might be compared with the Green Tuff zone and the Kuroko deposits of Japan, and the subtle differences between them are noted. Magmatic water mixing with seawater and connate water is suggested as the possible genesis of ore-forming fluid.

In the Changning-Menglian belt in western Yunnan, two types (Pb-Zn-Cu and Cu-Zn) of massive sulfide deposits have been recognized to be associated with the different phases of Late-Paleozoic rifting along the eastern margin of the Baoshan-Shanstate terrane. The Pb > Zn > Cu deposits produced in the initial Changning-Menglian basins, and are hosted in an alkalic basaltic-andesitic sequence, which was built on a sialic basement. The lead enrichment relative to Kuroko and other type deposits seems to be a feature inherited from the basemental rocks, as indicated by lead isotopes. Cu > Zn deposits and occurrences are hosted in the tholeiitic sequence with compositions close to T- or N-MORB, developed in the advanced rift basins with possible emplacement of oceanic crust. The metals of Cu > Zn deposits (Pb-poor) might have been supplied by magmatic water or selective leaching from the mafic volcanic sequence and (or) an ensialic basement.

The volcanogenic massive sulfide deposits in the Sanjiang region tend to occur in clusters in small basins near submarine volcanic centers and were formed during an extensional period of the volcanic arc or continental rifting. Three factors are emphasized in the massive sulfide metallogeny: 1) the basements which may indicate the evolution of regional lithosphere and may serve as a source of ore metals; 2) tectonic activity which initiated submarine volcanism and created channels and local depressions for the discharge of ore fluids; 3) magmatic systems which might have been a source of ore-froming fluids, and also provided heat to drive convective hydrothermal cells.

INTRODUCTION

Volcanogenic massive sulfide deposits are widely distributed in the main orogenic belts of China (Fig. 1), and have become important objectives of exploration and research projects since 1980s. Although few papers concerning the deposits of this category in China were published in international journals, investigation on this type deposits commenced in as early as the late part of 1940s, when Professor Shuhe SONG and his team carried out geologic survey on the Baiyin metallogenic belt. SONG (1949, 1954) firstly recognized the Baiyinchang deposit as a typical stratiform Cu-Zn pyrite-type deposit, and stressed its close association with the spilitic, quartz-keratophric sequences. Thereafter, much effort has been devoted to the exploration on this type of deposits over several districts in China.

Nevertheless, most of the volcanogenic massive sulfide deposits and metallogenic belts were discovered and explored only during the past decade. Perhaps, the most important progress on the exploration and research was made in the Sanjiang region (Fig. 2), southwestern China, a mountainous area of more than 500,000 sqare kilometers covering western Sichuan, western Yunnan, southern Qinghai and eastern Tibet. Many studies have been carried out on the tectonic framework, stratigraphic sequences and magmatic features, as well as associated ore deposits,

* Institute of Geology, Chinese Academy of Geological Sciences, Baiwanzhuang Rd. 26, Beijing 100037, China
** Institute of Mineral Deposits, Chinese Academy of Geological Sciences, Baiwanzhuang Rd. 26, Beijing 100037, China
*** China University of Geosciences, Xueyuan Rd. 29, Beijing 100083, China
Keywords: Polymetallic volcanogenic massive sulfide, Tectono-volcanic settings, Metallogenic model, Southwestern China

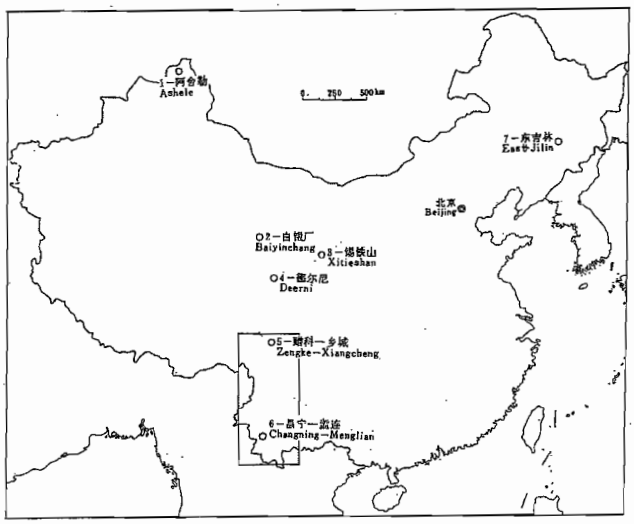

Fig. 1 Distribution of major volcanogenic massive sulfide metallogenic belts in China. The box area is the Sanjiang region studied.

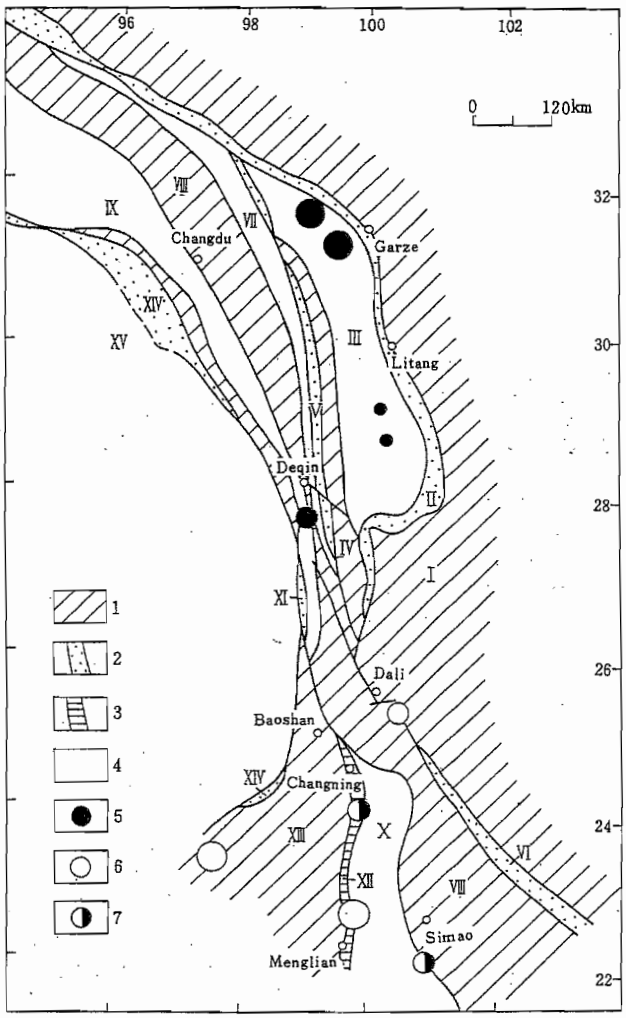

Fig. 2 Tectonic framework and distribution of volcanogenic massive sulfide deposits in Sanjiang region.
1, terrane or continent; 2, suture zone and ophiolitic belt; 3, rift-oceanic belt; 4, arc suite; 5, Zn–Pb–Cu deposit; 6, Pb–Zn–Cu deposit; 7, Cu (Zn) deposit. The large dots represent the large deposits; the middle dots, the small ones; and small dots, the prospects.
I, Yangtze plate; II, Garze-Litang suture zone (ophiolitic belt); III, Yidun island arc terrane; IV, Zhongza terrane; V, northern Jinshajiang suture zone (ophiolitic belt); VI, southern Jinshajiang suture zone (Ailaoshan ophiolitic belt); VII, Jiangda-Weixi arc terrane; VIII, Changdu-Simao terrane; IX, Tuoba-Yanjing-Nanzuo arc terrane; X, Lincang-Jinghong arc terrane; XI, Yinpan-Baijixun ophiolitic complex (Lancangjiang suture zone); XII, Changning-Menglian rift-oceanic belt; XIII, Baoshan-Shanstate terrane; XIV, Nujiang suture zone (Dingqing-Basu ophiolites); XV, Bomi-Tengchong epicontinental arc terrane, east of North Tibst terrace.

especially after a series of projects were performed over the last decade on main geological problems of the Sanjiang region and adjacent areas. Available data (e.g., YANG et al., 1992; HOU and YANG, 1993; CHEN et al., 1992) have shown the discoveries of tens of volcanogenic massive sulfide deposits and occurrences, most of which are distributed in the Zengke-Xiangcheng metallogenic belt in western Sichuan, and the Changning-Menglian belt in western Yunnan. Each of the belts is distinct from the other in tectonic and volcanic settings and related massive sulfide deposits.

This paper introduces the metallogeny of volcanogenic massive sulfide deposits in Sanjiang region, southwestern China, by reviewing the principal deposits and metallogenic belts. Emphasis is placed on the tectonic and volcanic evolution and their controls on massive sulfide deposits in the Zengke-Xiangcheng and Changning-Menglian belts. Preliminary tectonovolcanic models of the development of these metallogenic belts base on the authors' investigations since 1985, as well as on available literature.

REIONAL GEOLOGY

The Sanjiang Region constitutes the eastern portion of Tethyan orogenic belt and is considered as a crucial segment of the collision zones between Gondwana and Eurasian supercontinents (e.g., CHEN et al., 1987; CHEN et al., 1992). The eastern Tethyan belt comprises several terranes separated by the Late-Paleozoic to Mesozoic suture zones (Fig.2). Four terranes have been recognized on the basis of tectonostratigraphic successions as the Zhongza, Changdu-Simao, Baoshan-Shanstate and North Tibet terranes. Between them are four suture zones,

i.e., Nujiang, Lancangjiang, Jinshajiang and Ganzi-Litang suture zones. They are usually represented by dismembered ophiolites, tectonic melanges coeval with arc volcanic suites along the margins of terranes or continental plates, recording the birth, development and subsequent destruction of a series of Tethyan oceanic basins.

The Lancangjiang suture zone is expressed by Permo-Carboniferous dismembered ophiolites (e.g., Yinpan-Baijixun ophiolitic complex) juxtaposed by Permo-Middle Triassic arc volcanic suite. It is supposed to have recorded the widest Tethyan ocean (Lancangjiang ocean), separating the Gondwana and Eurasian supercontinents (e.g., CHEN et al., 1987). The arc volcanic suite developed along the western margin of Changdu-Simao terrane in the north (i.e. the Tuoba-Yanjing-Nanzuo arc terrane) and along the eastern margin of Baoshan-Shanstate terrane in the south (i.e. the Lincang-Jinghong arc terrane), suggesting that the oceanic crust might have subducted northeastward in the north and westward in the south. West to the Lancangjiang suture zone, the Baoshan-Shanstate and North Tibet terranes with sedimentary features of Gondwana facies are suggested to have been broken up from the Gondwanaland. The Nujiang suture zone contains Upper Triassic-Jurassic dismembered ophiolites (e.g., Dingqing-Basu ophiolitic belt), possibly representing the relics of a small oceanic basin developing between the South Tibet terrane and the North Tibet or Baoshan-Shanstate terranes. The oceanic crust might have subducted northeasterly, as indicated by the Tengchong arc terrane in western Yunnan. Within the Baoshan-Shanstate terrane, the Changning-Menglian volcanic belt reflects the development of an intra-cratonic basin being transitional from a continental to oceanic rift (YANG and MO, 1993b).

East to the Lancangjiang suture, the Changdu-Simao and Zhongza terranes encompass the stratigraphic and paleontological features similar to the South China facies over the Yangtze plate, and are supposed to be the blocks of the Eurasian supercontinent. The Jinshajiang suture zone is indicated by Carboniferous-Triassic dismembered ophiolites (e.g., Jinshajiang, Ailaoshan ophiolitic belts), possibly recording the history of the Jinshajiang ocean between the Changdu-Simao and the Zhongza terranes or the Yangtze plate. The related arc volcanic suite well developed in the Jiangda and Weixi area at the eastern margin of the Changdu-Simao terrane, suggesting west-dipping subduction of the oceanic crust. The Ganzi-Litang suture zone separates the Zhongza terrane from the Yangtze plate, and represents the relics of the Permo-Triassic Ganzi-Litang ocean, as recorded by ophiolitic suites and blueschists. The west-dipping subduction of the Ganzi-Litang oceanic crust toward the eastern margin of the Zhongza terrane, might have led to the development of the Late-Triassic Yidun island arc terrane (HOU and MO, 1991).

Volcanogenic massive sulfide deposits of various types has been recognized (Fig. 3) in most of the Carboniferous to Late-Triassic island arc or continental rift-related volcanic suites (YANG et al., 1992; HOU and YANG, 1993). Although massive sulfide occurrences have been discovered in most submarine volcanic domains in the Sanjiang region, the investigations were essentially focused on the Zengke-Xiangcheng and Changning-Menglian metallogenic belts. So far, available data permit us to discuss on the development of the two metallogenic belts. The contrasts in tectonic, volcanic setting are reflected in differences in the associated massive sulfide deposits of the two belts (Table 1).

GEOLOGY OF METALLOGENIC BELTS

Zengke-Xiangcheng Metallogenic belt

Volcanic Setting

The Zengke-Xiangcheng metallogenic belt is located within the volcanic domain of the Yidun paleo-island arc district in western Sichuan (Fig. 4). The Yidun arc terrane is defined by the Late-Triassic volcanic belt, which is 90 to 150 kilometers wide and extends about 500 kilometers from the north to the south (Figs. 2, 4). To the east, metamorphosed

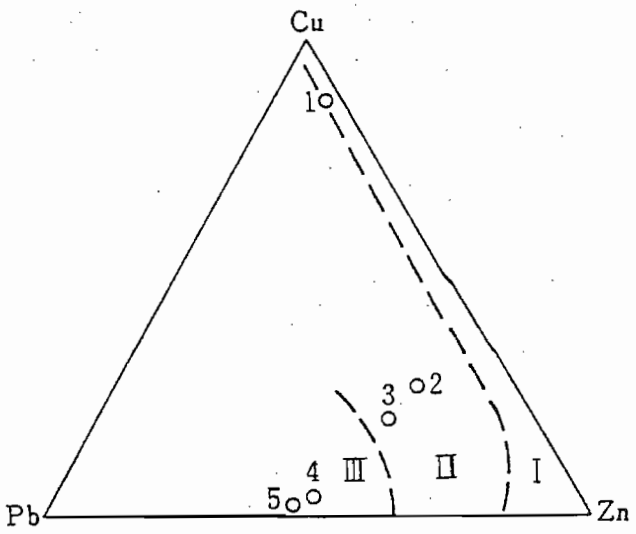

Fig. 3 Cu-Pb-Zn diagram of typical volcanogenic massive sulfide deposits in southwestern China
I, Cu-Zn group; II, Zn-Pb-Cu group; III, Pb-Zn (Cu) group (after FRANKLIN et al., 1981). 1, Tongchangjie; 2, Gayiqiong; 3, Gacun; 4, Laochang; 5, Bawdwin.

Table 1 Major features of two metallogenic belts in the Sanjiang region, southwestern China

	Zengke-Xiangcheng Belt	Changning-Menglian Belt
Regional Background	Passive continental margin of the Zhongza terrane	Intra-cratonic area of the Baoshan-Shanstate terrane
Tectonic Setting	Intra-arc rift within the Yidun island arc	Intra-continental rift transitional into intra-cratonic ocean
Ages of Mineralization	T3	C-P
Volcanic Assemblage	Bimodal suite	Dominant alkalic basalt and less tholeiite
Host Rocks	Felsic pyroclastic sequence	Trachybasaltic-andesitic or tholeiitic pyroclastic sequence
Metals of Massive Sulfide Accumulations	Zn > Pb > Cu	Pb > Zn > Cu or Cu (Zn)
Typical Deposits	Gacun, Gayiqong	Laochang (Pb > Zn > Cu) Tongchangjie (Cu > Zn)
Possible Analog	Green Tuff region of Japan	Red Sea (?)

flyshoid sequences of Middle-Late Triassic age occur with a large granitoid belt of mostly Indosinian cycles, possibly representing a fore arc of the Yidun arc system. Further easterly, a Permo-Triassic ophiolitic complex is well exposed, probably indicating the Garze-Litang suture zone. This petro-tectonic assemblage has been interpreted to have formed above a west-dipping subduction zone consuming Garze-Litang oceanic crust (HOU and MO, 1991; 1993).

The Late-Triassic volcanism on the Yidun island arc terrane can be sudivided into the Genlong, Gacun and Miange periods, which correspond to different phases of evolution of the arc. Volcanism in the Genlong period (the Genlong Group) commenced with the eruption of alkaline basalts, which is characterized by the enrichment of LREE and HFS elements with high Ti and relatively low MgO, similar to Emei flood basalt within the Yangtze plate. Progressively, volcanism became tholeiitic, similar to T-MORB in composition. HOU and MO (1991) suggested a setting of continental rifting to the volcanism in this period, on which the Yidun island arc was developed.

The Yidun island arc was developed in the Gacun period, and three cycles of the arc volcanic sequence (corresponding to the lower, middle and upper member of the Gacun Group) are recognized. The earliest cycle of volcanism produced andesites (i.e. the lower member) which constitute the east andesite belt of the outer-arc (Fig. 4). Volcanism in the middle cycle evolved into a bimodal suite (i.e. the middle member) occurring in the Zengke-Xiangcheng area. This volcanic suite is characterized by alternations of basaltic and rhyolitic rocks, indicating an intra-arc rifting zone behind the outer-arc. This was followed by another cycle of andesitic volcanism (i.e. the upper member) which formed the western andesite belt of the inner-arc. Two cycles of the andesitic volcanism are calc-alkaline, and andesites in the westrn belt seem to be higher in incompatible elements than those in the eastern belt at the same SiO_2 content of 60 wt% (HOU and MO, 1991). Basaltic members in the bimodal suite are low-K tholeiites (see HOU, 1993, this volume).

Volcanism recommenced in the Miange period predominantly with the eruption of dacite, rhyolite, and high-silica rhyolite, as well as shoshonitic rocks, all of which show highly enrichment of K and related elements. The volcanic sequences are dominantly distributed behind the west andesite belt in the north segment of the island arc terrane, and are considered to have formed possibly in a back-arc basin during the waning stage of the Yidun island arc development.

Massive Sulfide Deposits

Volcanogenic massive sulfide occurrences are distributed in the Zengke-Xiangcheng intra-arc rift zone of the Yidun island arc terrane, occurring as clusters in rift-controlled basins, i.e., the Zengke, Gacun and Xiangcheng basins. Most deposits and occurrences are polymetallic, with significant quantities of Zn, Pb, Cu and recoverable amounts of Ag, Au,

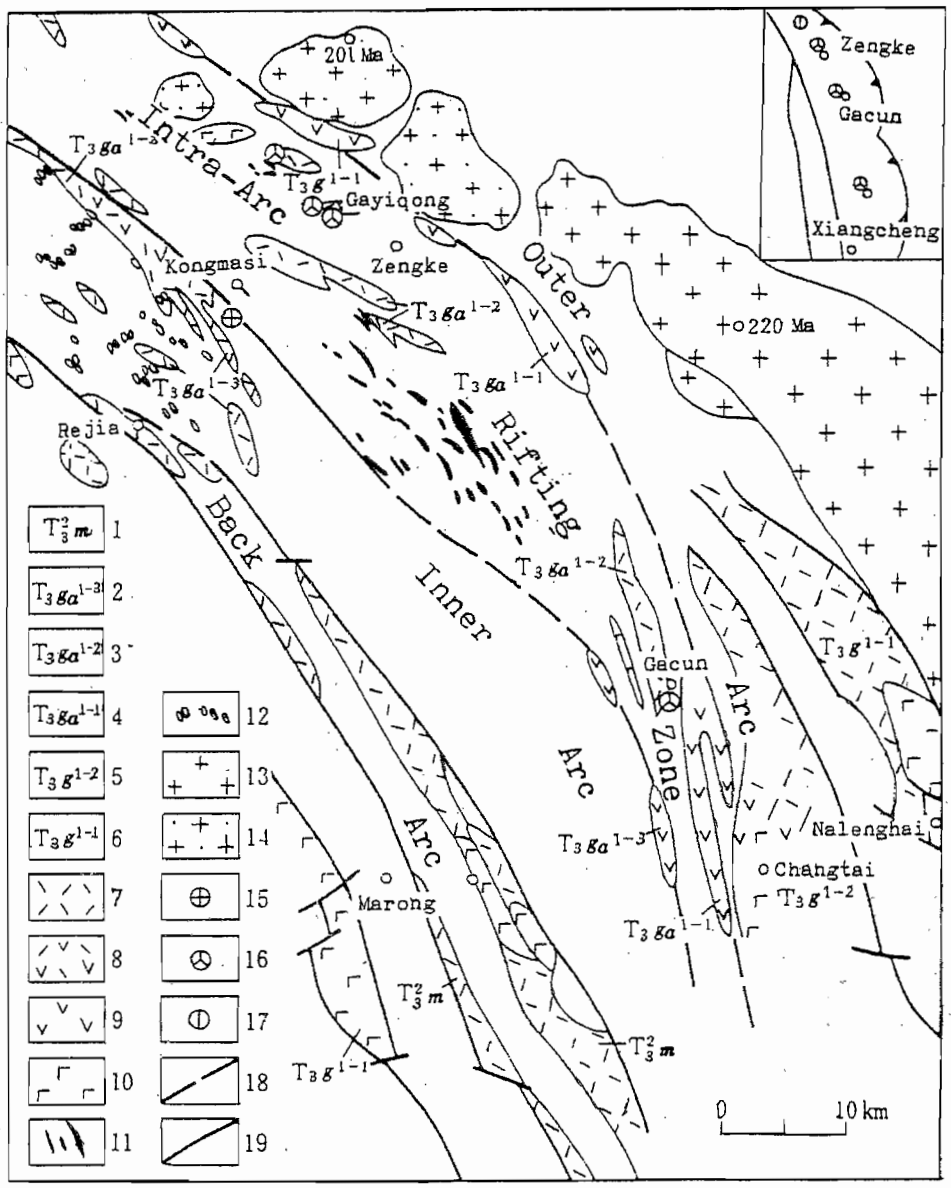

Fig. 4 Volcanic-tectonic sketch map of north Yidun island-arc.
1, Miange Group; 2, Upper member of Gacun Group; 3, Middle member of Gacun Group; 4, Lower member of Gacun Group; 5, Upper member of Genlong Group; 6, Lower member of Genlong Group; 7, Rhyolitic rocks; 8, Dacitic rocks; 9, Andesitic rocks; 10, Basaltic rocks; 11, Diabase dyke swarm; 12, Diorite; 13, Indosinian granites; 14, Yanshanian granites; 15, Hg deposit; 16, Kuroko-type deposits; 17, Cu deposit; 18, Supposed arc volcanic chain; 19, Fault.

and other metals, and are intimately associated with the felsic units of the bimodal sequence (Figs. 4, 5).

Zengke Area: Massive sulfide deposits occur in the middle-lower part of the Gacun Group, which consists of 500–800 m of felsic volcanic rocks overlain by 120–300 m of tuffaceous slate, limestone and sandstone with features of submarine debris flows. The strata have undergone a greenschist facies of metamorphism and been folded into a syncline with a general NNW-SSE strike. The stratigraphic successions of the Zengke area reflect a graben-like basin in the north of the intra-arc rift within the Yidun island arc area (Hou and Mo, 1991). Volcanic sub-basins were formed from the felsic eruptive and intrusive activity and associated cauldron subsidence. Massive sulfide deposits and occurrences are usually found as clusters on the top or flank of the dacitic domes emplaced around volcanic centers, and in the adjacent volcanic sequences suggestive of local depres-

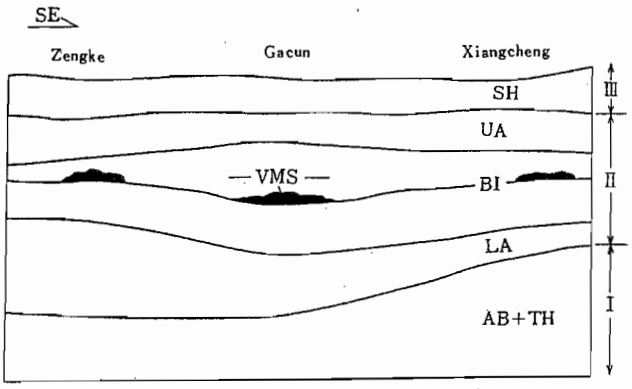

Fig. 5 Generalized stratigraphic section of the Zengke-Xiangcheng metallogenic belt.
I, Genlong cycle; II, Gacun cycle; III, Miange cycle; VMS, volcanogenic massive sulfide; AB, alkaline basalt; TH, tholeiitic basalt; LA, lower andesite; BI, bimodal suite; UA, upper andesite; SH, shoshonite and related rocks.

sions.

More than 10 deposits and prospects have been recognized in the Zengke district, such as the Shengmulong, Ronggong, Zeba, Gangsa, Gayiqong deposits. Among those, the Gayiqong deposit is typical. This deposit is believed to have developed in local depressions between the sysvolcanic domes which intruded within a submarine caldera (HOU, in preparation). Five massive sulfide lenses dip steeply west, and are localized conformably in dacitic tuffite units of the middle cycle of the Gacun Group and the overlying phyllite sequence, flanking the dacitic domes. They are composed of pyrite, sphalerite, galena with less amounts of chalcopyrite, pyrrhotite coeval with quartz, sericite, carbonates as well as volcanic detritus. A thin layer of Fe and Mn carbonates, locally with Si, Fe oxides, is usually observed overlying the massive sulfide bodies, and appears as an extensive unit throughtout the area.

Two stringer pipes directly underlying massive sulfide layers have been recognized within the dacitic domes and adjacent andesitic tuffites, each containing stockwork or disseminated pyrite, sphalerite, chalcopyrite within an alteration pipe which includes an upper sericite-carbonate zone and a lower quartz-sericite zone.

Gacun Area: The strata in the Gacun area formed a west-dipping anticline with the overall trend due north. Massive sulfide orebodies occur at the east limb of the anticline, and are associated with the middle-upper part of the Gacun Group, a 1,000–2,000 m thick bimodal volcanic sequence.

The volcanic units hosting massive sulfides in the Gacun area, comprise the felsic member of the bimodal sequence, and consist predominantly of rhyolitic and dacitic lapilli breccia, breccia lava and tuffite with intercalcated limestone and slate. Felsic volcanism in the Gacun area is more siliceous than that in the Gayiqong area, and evolved progressively from dacite to high-silica rhyolite. Synvolcanic intrusions are typically rhyolite or high-silica rhyolite, and occur as domes within submarine calderas. Surrounding a volcanic center, volcaniclastic rocks grade from volcanic breccia, lapilli tuff-breccia, to lapilli-tuff, tuffite, epiclastic tuffite, and change laterally and ascendingly into siltstone, slates and limestone. The patterns of the distribution and variation in thickness of volcaniclastic and sedimentary rocks reflect fault-bounded volcanic subsidence in the Gacun area (HOU and MO, 1991).

Numerous massive sulfide orebodies have been discovered in the Gacun area, among which the Gacun deposit is the largest. The Gacun deposit encompasses several massive sulfide layers or lenses and an underlying stringer zone. The volcanic units host to the massive sulfide deposits include three subcycles of eruption, each of which is rhyolitic. Massive sulfide ores are localized conformably in the upper layers of high-silica rhyolite and rhyolitic tuffite. Orebodies are predominantly composed of pyrite, sphalerite, galena and less chalcopyrite, and are closely associated with rhyolitic lapilli, lapilli tuff or siliceous, baritic breccia layers or lenses. Capping to the massive sulfide orebodies, a sulfidic barite-siliceous layer or jasper layer are extensively observed, which may be a marker layer corresponding to the Fe-, Mn-carbonate layer in the Zengke area. The volcanic sequence is succeeded ascendingly by a sedimentary sequence of limestone, siltstone, slate and phyllite.

The stringer zone underlying the massive sulfide orebodies developed within a rhyolitic dome, and exhibits stockwork and disseminated pyrite and chalcopyrite coeval with alteration zones. A siliceous core surrounded by sericite and chlorite zone occurs in the alteration pipe which probably served as a feeder zone for the overlying massive sulfides.

Xiangcheng Area: The geology of the Xiangcheng area indicates a fault-bounded basin within the intra-arc rift to the south, but as yet is not well documented. Available data show that the felsic volcanic units are similar to those in the Gacun area, within which a similar unit of barite, sulfides and carbonates can be traced extensively over the Xiangcheng area. Much effort is devoted to detailed investigation and exploration in this area.

Changning-Menglian Metallogenic Belt

Volcanic Setting

The Changning-Menglian metallogenic belt (Fig. 6) developed within a late Paleozoic volcanic belt in southwestern Yunnan, which is 20–60 km wide, and extends more than 250 km, from Changning in the north, through Tongchangjie, Laochang, to Menglian in the south in China, and further south into Burma. This volcanic belt is juxtaposed by a Permo-Triassic tectono-magmatic zone (the Lincang-Jinghong arc terrane, Fig. 2) including a metamorphic belt, a granitoid belt and an arc volcanic belt to the east, and may represent a continental extension zone behind a marginal volcanic arc related to west-dipping subduction of the Paleo-Lancangjiang oceanic crust (YANG et al., in preparation).

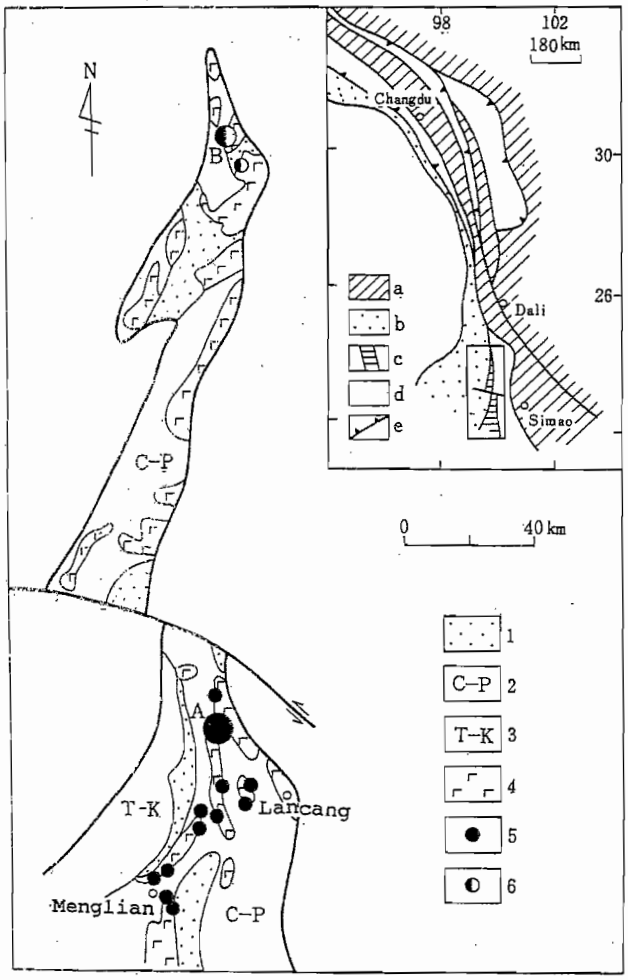

Fig. 6 Sketch map showing geology and distribution of massive sulfide deposits in the Changning-Menglian belt. 1, Devonian; 2, Permo-Carboniferous; 3, Triassic-Cretaceous; 4, volcanic sequence; 5, Pb-Zn-Cu deposit; 6, Cu (Zn) deposit. The large dots represent the large deposits; the middle dots, the small ones; and the small dots, the prospects. A, Laochang deposit; B, Tongchangjie deposit.
In the insert map: a, Eurasian continent; b, Gondwanaland; c, continental-oceanic rifting zone; c, volcanic arc; d, tectonic suture.

The volcanic rocks in the Changning-Menglian belt comprise the lower member of the Yiliu Group in the southern part of the Changning-Menglian rift, and the lower units of the Pengzhang Group in the northern part of the rift. In both of the groups, the volcanic units are succeeded by a sequence of limestone and clastic sedimentary rocks. The ages of the two groups are roughly constrained by the fossil evidence from Early-Carboniferous to Permian (CHEN et al., 1987). It has been recognized that the volcanic belt is dominated by alkaline basaltic rocks, with local tholeiitic rocks (YANG and MO, 1993b). Although a complete stratigraphic succession including both series of the volcanic rocks cannot be established yet, the fossils from the sedimentary interbeds within volcanic units, suggest that tholeiitic sequence might be younger than the alkaline volcanic sequence.

Alkaline volcanic rocks, characterized by the high enrichments of incompatible elements and undersatured in silica (YANG and MO, 1993b), are widespread in the Changning-Menglian belt. They are well exposed in the Laochang, Dadi and Yiliu areas. The volcanic sequence generally consists of alkaline basalt and less abundant andesite flows, pyroclastic and epiclastic rocks. They comprise at least three cycles of eruption, with the composition varying from trachybasalt, trachyandesite to picritic basalt in ascending stratigraphic succession. The alkaline volcanism might have occurred in submarine basins with variable topography controlled by considerable synvolcanic faulting. Volcaniclastic turbidites occur in the lower units of the volcanic sequence, while, in the upper units, volcanic layers are interbedded with limestone.

Tholeiitic volcanism was limited in the Tongchangjie area in the north, and in the Menglian area in the south. The volcanic units comprise basaltic flows and pyroclastic rocks, with compositions similar to N- or T-MORB (YANG and MO, 1993b). Within the volcanic sequence, a silty and siliceous shale unit is associated with radiolarian chert, suggesting a relatively deep marine environment. Isolated ultramafic blocks (serpentinized dunite) and mafic dikes (gabbro and diabase) are present as screens in the tholeiitic sequence. The assemblage, therefore, may constitute a dismembered ophilitic unit, indicating local emplacement of oceanic crust in the late phase of the Changning-Menglian rift.

Massive Sulfide Deposits

Two groups of massive sulfide deposits and showings have been recognized as a Pb>Zn>Cu group hosted in alkalic basaltic-andesitic sequences (e.g., Laochang area), and a Cu>Zn group in tholeiitic sequences as typified in Tongchangjie area (Fig. 6).

Laochang Area: At least three cycles of volcanism have been distinguished in the Laochang district (YANG, 1989). The early and middle cycles produced trachybasalt, trachyandesite lava and associated volcaniclastic units, as well as synvolcanic intrusions of syenite and rhyolite, and were followed by a period of accumulation of thick limestone units. The late cycle of volcanism recommenced with the eruption of picritic basaltic flows and pyroclastic rocks interbedded with limestone, siltstone. Massive sulfides are associated with the early and middle volcanic cycles.

The Laochang deposit, with Pb>Zn>Cu, is typical, which is hosted in a coarse-grained pyroclastic and epiclastic sequence with compositions varying from trachybasalt to trachyandesite. The host volcanic sequence is overlain by a thick unit of limestone, comprising the Laochang anticline which is cut by faults. Massive orebodies dip steeply west and strike variably from NW-SE to N-S, occurring in the west limb of the Laochang anticline. The phases of the volcaniclastic rocks over the area suggest a submarine cauldron (YANG, 1989).

The massive sulfide layers or lenses are dominated by pyrite, sphalerite and galena with less amounts of chalcopyrite, realgar and orpiment, localized within the units of sulfide-rich siliceous shale or sulfide-rich calcareous tuff, all of which developed from the exhalative activity during the waning stage of volcanism within a local depression. Textural features indicative of submarine detrital flows, such as graded beddings and chaotically emplaced blocks, are well preserved, indicating that the massive ores and host volcanic rocks have locally undergone slumping and displacement.

The massive sulfide zone is underlain by a stringer sulfide zone (stockwork ores), which developed in synvolcanic intrusions (altered syenite and rhyolite) and adjacent volcanic sequence. This zone has been traced for more than 400 m below the massive ores, and includes an upper zone of sericite, quartz, zeolites and carbonates, and a lower zone containing diopside, tremolite, actinolite, garnet and epidote. Stockwork or disseminated sulfides in the zone include mainly pyrrhotite, pyrite and chalcopyrite. Limestone intercalated in the volcanic sequence could have been responsible for the lower alteration assemblage.

Tongchangjie Area: Volcanism in the Tongchangjie district is tholeiitic, and includes 4 to 5 cycles of eruption, each with a mafic flow base and a pyroclastic or epiclastic breccia and tuff top (YANG, 1989). The sequence has undergone a greenschist facies metamorphism, and has been isoclinally folded, dipping moderately west and striking overall northeast. Ultramafic rocks and mafic dikes are coeval with the volcanic sequence, which may suggest a dismembered ophiolitic suite.

The Tongchangjie massive sulfide deposit, containing Cu with recoverable S, As, Se, Co, Pb, Zn and Au, is hosted in the lower units of the volcanic sequence (YANG, 1989; YANG and MO, 1990). Massive sulfide lenses are composed of dominantly layered pyrite, pyrrhotite and chalcopyrite with lesser amounts of magnetite and other minerals. They are associated with lapilli-tuff, tuffite, sulfide- or oxide-siliceous shales (locally jasper or chert units). A thin-layer of chlorites or ochre (2 cm- to 5 m- thick units of quartz, hematite, sericite etc.) occurs typically on top of massive ores, indicating that the sulfides might have undergone seafloor oxidation.

Within an orebody, the thin layers of sulfides are intercalated with lithic layers which are usually 2 mm to 10 cm thick, and are predominantly argillaceous, with varying amounts of sulfides and carbonates. Sulfide layers may grade laterally into sulfide- or oxide-siliceous shales with a decrease in sulfides. The shale units, locally rich in hematite and magnetite, serve as a marker unit for massive sulfides throughout the area.

The massive sulfide layers are underlain typically by stringer zones, which contain stockwork and disseminated pyrite and chalcopyrite, but are of little economic importance. Strong silification and carbonation occur in immediate contact with the overlying massive sulfides, and may change into a lower chlorite zone.

Other Massive Sulfide Deposits

Besides the above-stated metallogenic belts, numerous volcanogenic massive sulfide deposits and occurrences have also been documented in the southwestern China. The Sandashan cupriferous massive sulfide deposit in the eastern Lincang-Jinghong arc terrane is hosted in a unit of the Late Permian felsic tuffite and carbonaceous sericitic shale, which comprises the arc volcanic sequence at the eastern margin of the Baoshan-Shanstate terrane. Within the Baoshan-Shanstate terrane, the Bawdwin massive sulfide deposit is well-known in eastern Burma for its high contents of Pb (21.2%), Zn (15.8%), Ag (550 g/t) and recoveralbe Cu, Au, As, Gd, Bi (BRINCKMANN and HINZE, 1981). It is hosted in a late

Cambrian volcanic sequence, i.e. the Bawdwin felsic formation. The sulfide ores are closely associated with the coarse-grained pyroclastic or epiclastic rocks, and are assumed to have precipitated from exhalation of hydrothermal fluids during the waning stage of volcanic activity. Moreover, many volcanogenic massive sulfide deposits and occurrences have been recognized in Peng County in Sichuan Province and in the Dahongshan and Lijiang districts in western Yunnan Province (QIAN and SHEN, 1990; HOU and YANG, 1993), but many of which are still poorly documented.

TECTONO-VOLCANIC EVOLUTION OF THE METALLOGENIC BELTS

Development of the Yidun Island Arc Terrane and Massive Sulfide Metallogeny

The relationship of the Zengke-Xiangcheng metallogenic belt to the Yidun island arc system has been well documented by HOU and MO (1991, 1993). Based on patterns and styles of the volcanic rocks, a framework of the Yidun island arc system may be reconstructed as Figure 7. A stratigraphic succession of arc volcanic rocks is generalized in Figure 5. The setting of the Yidun island arc system may be a continental rift at the eastern margin of the Zhongza terrane, and the arc system might have been developed above a west-dipping subduction zone consuming Ganzi-Litang oceanic crust to the east. After the initial andesitic volcanism along the outer-arc, the Yidun arc experienced a period of intra-arc rifting, when the bimodal suite developed in the Zengke-Xiangcheng belt. This was succeeded by another cycle of andesitic volcanism along the inner-arc. Finally, shoshonitic and high-silica rhyolitic volcanism were associated with the post-arc extension behind the inner-arc in the northern Yidun island arc system.

Massive sulfide deposition was evidently related to the period of the Yidun intra-arc rifting, and hence confined within the Zengke-Xiancheng belt. Extension might have led to subsidence of crustal blocks in the rift zone, and created three major fault-bounded basins, i.e., the Gacun, Gayiqong and Xiangcheng basins. Within each basin, resurgent caldera and cauldron subsidence might have led to the local depressions with a complicated topography. Fracture zones which were reactive with volcanic eruptions and connected immediately to the depressions, might have served as conduits for hydrothermal fluids. Massive sulfides were accumulated during the waning stage of the felsic volcanism, and ore deposits occur in depressions in vicinity of volcanic centers typically associated with synvolcanic rhyolite or dacite domes.

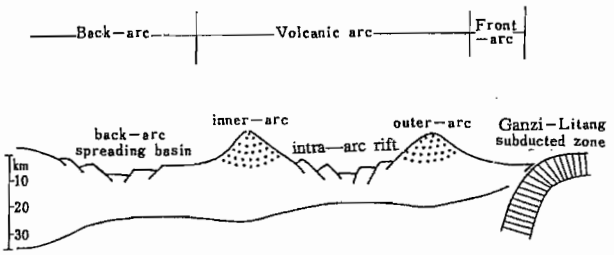

Fig. 7 Schematic cross section of the reconstructed Yidun island arc.

The Zengke-Xiangcheng belt has generally similarities to the Green Tuff belt in Japan. Both of them developed in a short geological interval when felsic volcanism was active within intra-arc rift basins with submarine Zn-Pb-Cu massive sulfide deposits (ISHIHARA, 1974; HOU and MO, 1991). The typical deposits in the Zengke-Xiangcheng belt, such as Gacun and Gayiqong, display classic metal zonation from elevated Cu-Fe in the lower and inner regions into enriched Pb-Zn in upper and outer parts, which is characteristic of the Kuroko deposits of the Green Tuff belt (SATO, 1974; SATO et al., 1974).

However, subtle differences between the typical deposits of the two belts are also apparent. It has been noted that gypsum and anhydrite occurring typically in the Kuroko deposits (LAMBERT and SATO, 1974), are absent in the Gacun and Gayiqong deposits. Instead, a layer of barite and siderite with lesser amounts of other carbonates and jasper occurs as a capping on the massive ores, or as a regional marker unit in the Zengke-Xiangcheng belt. Hanging wall alteration is rather weak in the Gacun and Gayiqong deposits, but strong in the Kuroko deposits. Further differences can be noted in the chemistry of ore-forming fluids. As indicated in Table 2, the salinity of the ore-fluids in the Gacun and Gayiqong deposits is much higher than that in the Kuroko deposits; the $\delta^{34}S$ values for sulfides are close to zero, much lower than those of the Kuroko deposits; and δD values are much lower, in spite of no clear distinction of $\delta^{18}O$ values between the two areas. Moreover, O and H isotopes values for the deposits in the Zengke-Xiangcheng belt are close to the field of magmatic water, distinctly different from the Kuroko deposits in which the data plot to the field of seawater (YE et al., 1991; HOU, in preparation).

The differences stated above may imply the differing hydrothermal processes and genesis of fluids. The enrichment of carbonates in the Gacun and Gayiqong deposits indicates that the ore-forming fluids might have been discharged into the basins relatively enriched in CO_2, in comparison with the Kuroko deposits.

Table 2 Variation in salinities and isotopic compositions of the ore-forming fluids for some typical deposits

	$\delta^{34}S$ (per mil)	δD (per mil)	$\delta^{18}O$ (per mil)	Salinity (wt% NaCl)
Laochang	−0.1 ~ +1.5	−98 ~ −54.3	−3.4 ~ +6.4	7.5–18.5
Gacun	−0.8 ~ +2.4	−135 ~ −68	−5.8 ~ +5.6	7.0–13.2
Gayiqong	−3.2 ~ +2.0	−140 ~ −107	−12 ~ +8	11–12
Kuroko	+2 ~ +8.0*	−30 ~ +15**	−6 ~ +4**	3.5–6**

* from OHMOTO et al. (1983)
** from PISUTHA-ARNOND and OHMOTO (1983)

The fluid compositions in the Gacun and Gayiqong deposits may suggest a dominant source of magmatic water, rather than a dominant source of recycled seawater which is considered typical of the Kuroko deposits (OHMOTO et al., 1983). This is further supported by lead isotopic studies. The lead isotope data for the Gacun and Gayiqong deposits and host volcanic rocks lie along a steep line that intersects the upper crustal and orogenic evolution lines defined by DOE and ZARTMAN (1979) (YE et al., 1991 Figs. 5-6b). These, together with the fact of close association between the massive ores and host volcanic rocks, indicate that the metallic components of the deposits might be derived from the felsic magmatic system with involvement of upper crustal materials.

Development of the Changning-Menglian Rift and Massive Sulfide Metallogeny

The Changning-Menglian volcanic suite records the evolution of Permo-Carboniferous intra-cratonic basins with the Baoshan-Shanstate terrane breakup being transitional from continental to oceanic rifting (Fig. 8) (YANG and MO, 1993b). This interpretation is supported by contrasting styles of volcanic sequences and associated massive sulfide deposits.

In the early stage of the Changning-Menglian rift (Fig. 8a), volcanism was initiated with extensive alkaline volcanic piles built on a sialic crust. The associated massive sulfide deposits and occurrences are rich in Pb with composition of Pb > Zn > Cu, which is suggested to be a distinct type of VMS deposit, different from the Kuroko-, Besshi- or Cyprus-type deposits (YANG and MO, 1993a). The initial rift basins controlled the accumulation of massive sulfides. The fault-bounded and graben-like basins limited by submarine calderas, are indicated as sites where mineralized fluids discharged (YANG, 1989). The paucity of oxides in the deposits suggests that the basins were relatively anoxic. In contrast, volcanic activity in late stage of the rift (Fig. 8b) occurred in a local area where an oceanic crust was formed. Based on the recent studies of the Tongchangjie area, the cupriferous massive sulfide deposits hosted in the

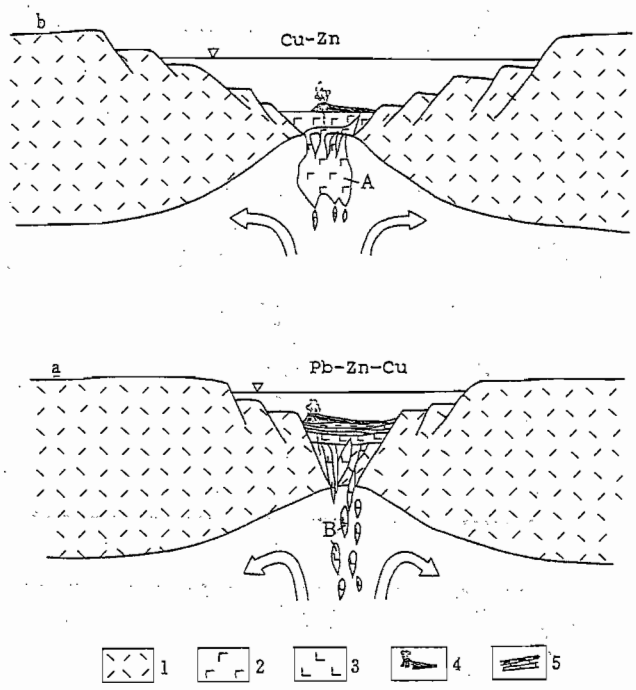

Fig. 8 Schematic model showing the development of the Changning-Menglian rift
1, sialic crust; 2, tholeiite; 3, alkaline basalt; 4, massive sulfides; 5, sedimentary sequence; A, tholeiitic melt produced in relatively shallow mantle; B, alkaline basaltic melt originated in relatively deep mantle.

tholeiitic sequence, are analogous to Cyprus-type instead of the Besshi-type deposits (YANG and MO, 1990). These massive sulfides probably accumulated in relatively open, and oxic basins, thereby becoming partially oxided.

The variation in composition of the massive sulfide deposits associated with the Changning-Menglian rift reflects different metallic sources. The metallic components might be controlled by 1) magmatic water and volcanic piles which fed the hyrothermal cell, and (or) 2) the basement crustal source. Both of the factors might have operated in

the early stage of the rift, when the volcanic sequence and associated Pb-rich massive sulfide deposits were produced on the sialic crust of the Baoshan-Shanstate terrane (Fig. 8a). This is indicated by lead isotope evidence, especially in the Laochang deposit (YANG, 1989). The lead isotope data of sulfides from the deposit and the host volcanic rocks define a steep line intersecting the upper mantle and upper crust lines, apparently suggesting the mixing between mantle lead and crustal lead (Fig. 9). Furthermore, the lead isotope data for the deposit is noted to overlap the trend of those for the granitoids in the terrane

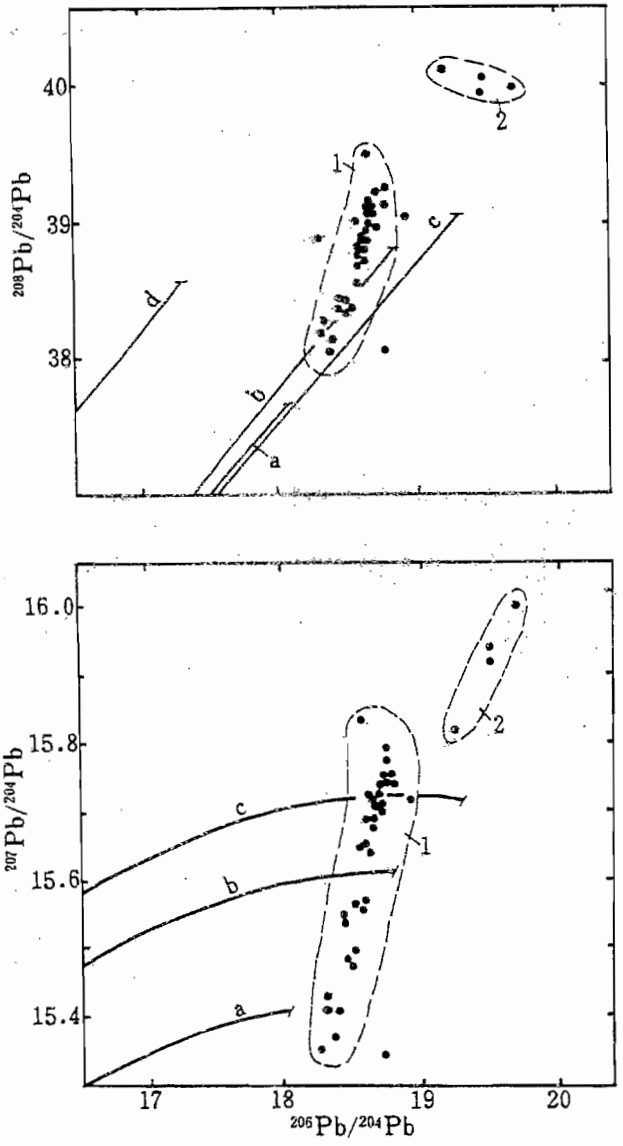

Fig. 9 Diagram of lead isotope data for the Laochang deposit, which is plotted after DOE and ZARTMAN (1979). The isotope evolution curves include: a, for the mantle; b, orogene; c, upper crust contributed to orogene; d, lower crust contributed to orogene.

(YANG, in preparation), evidently indicating that the lead for both might be a feature at least partially inherited from a similar basement. Besides, Pb and Zn enrichment in the basement of the Baoshan-Shanstate terrane is possibly suggested by the fact that numerous Pb, Zn deposits are hosted in the Lower Paleozoic volcanic sequence (e.g., Bawdwin) and in sedimentary sequence (e.g., Luzhiyuang, etc.). This basement, therefore, may be responsible for the anomalous high lead content of the deposits associated with initial rifting. On the other side, low $\delta^{34}S$ ratios (close to zero) for total sulfur in fluids and much negative δD values are noted in the deposit (Table 2). O and H isotope data for the fluids plot near the field of magmatic water, different from seawater (YE et al., 1991). These may be interpreted as the mixing of magmatic water with varying amounts of recycled seawater and (or) connate water. In contrast, in the late phase of the rift the tholeiitic sequences host massive sulfides (Fig. 8b). The preponderance of copper and paucity of lead and zinc in the deposits might be related to the sources of magmatic water and tholeiitic sequences which suggest the presence of oceanic crust instead of a sialic crustal source.

The geology of the Changning-Menglian belt may be analogous to the present-day situation in the Red Sea district (YANG and MO, 1993b), where widespread alkaline basaltic volcanism is succeeded by tholeiitic volcanism limited in the axial area of the rift. Both Cu-Zn and Pb-bearing massive sulfides occur on the floor of the Red Sea, with Cu-Zn sulfides accumulating in the central trough in immediate vicinity of the tholeiitic volcanic rocks, and Pb-bearing sulfides in the sediment-rich basins. Numerous Pb and Zn orebodies occur on the near shores of the rift (BLUM and PUTHELT, 1991, Fig. 1). These facts perhaps suggest that lead and zinc in massive ores on the Red Sea floor might be derived from the basement involved in the hydrothermal processes.

DISCUSSION ON GENERAL CONTROLS OF MASSIVE SULFIDE METALLOGENY IN SOUTHWESTERN CHINA

General controls on the volcanogenic massive sulfide deposits in southwestern China can be evaluated by the detailed analyses on the tectono-volcanic history of the area. Regional geologic setting, extensional tectonism and submarine volcanism are supposed to be the major constraints on the metallogeny of massive sulfide deposits of varying types.

Regional geologic setting is reflected by the development of basement, which could have controll-

ed the metal contents of the deposits. It has been known that most deposits overlying mafic volcanics are Cu and Zn rich, and Pb-rich massive sulfides are mostly localized in felsic volcanics and sedimentary sequence (SANGSTER and SCOTT, 1976; FRANKLIN et al., 1981). Stratigraphic successions below massive sulfide deposits are usually considered to be the metallic source through which hydrothermal fluids have circulated (FRANKLIN, 1986; LYDON, 1988). The studies of lead isotopes suggest that sialic source might supply Pb, and oceanic crustal source, Cu and Zn to the volcanogenic massive sulfide deposits (KLAU and LARGE, 1980; SWINDEN and THORPE, 1984). SANGSTER and SCOTT (1976) supposed that the paucity of Pb in the volcanogenic massive sulfide deposits in Canadian Shield (relative to Kuroku deposits in Japan) be related to the evolution of regional lithosphere. Apparently, the basement on which the deposits developed should be considered as an important source of metallic components. This is indicated by the isotopic data of the deposits in the Sanjiang region. As discussed above, the sialic crust of the Zhongza terrane on which the Yidun island arc was built, might be responsible for the Pb source of the massive sulfide deposits in the Zengke-Xiangcheng belt. Similarly, Pb-rich massive sulfide accumulations, such as the Laochang deposit, developing in the initial Changning-Menglian rift basins, might be inherent of the basemental geochemistry of the Baoshan-Shanstate terrane. Whereas, the Pb-poor massive sulfide deposits produced in the advanced Changning-Menglian rift basins, might reflect a feature of ensialic basement dominated by mafic volcanic sequence.

Extensional tectonism creates rift basins for massive sulfide accumulations, and associated faults and fractures on the flanks of rift basins serve as channels for submarine volcanism and hydrothermal exhalativity (OHMOTO, 1983; Cathles et al., 1983). This is also indicated by the present-day situations of massive sulfide accumulations on the seafloor, such as the Red Sea and the Gulf of California, etc. (SCOTT, 1985; FRANLIN, 1986). The rift-related volcanic basins dominate the distributions of massive sulfide deposits in both ancient and present situations. This is also true in southwestern China. In the Zengke-Xiancheng belt, most massive sulfide deposits developed in three major fault-bounded basins (i.e., the Gayiqong, Gacun and Xiangcheng basins) within an intra-arc rifting zone. In the Changning-Menglian belt, graben-like basins dominated the accumulation of massive sulfides of various types. Pb-rich massive sulfides deposited in the CO_2-rich, anoxic, limited environment of the initial rift basins, while Pb-poor massive sulfides accumulated in relatively oxic and opened basins associated with the advanced rifting (YANG, 1989). Within the rift basins, repetive volcanic eruption and resurgent cauldron might have created local depressions and an underlying permeable fracture system. The ore-forming fluids might have arisen through fracture zones to the surface of the depressions. Sulfides might have been discharged from the ore-fluids with the immediate changes of physiochemical conditions, and accumulated as massive sulfide orebodies. This is best illustrated in the Gacun, Gayiqong and Laochang areas. Rapid accumulation of volcanic detritus from the frequent eruption of submarine volcanoes (e.g., in the Laochang area) or rapid sedimentation of abundant epiclasts (e.g., in the Gacun area) might have been favourable for the formation and preservation of massive sulfides. Slumping and collapse of a resurgent cauldron frequently initiated detritus flows, which led to displacement, reworking and transportation of massive ores and host volcanic rocks, as is well displayed in the Laochang deposit (YANG and MO, 1993a).

Associated with rifting, massive sulfide formation is intimately related to submarine volcanism. In the southwestern China, massive sulfides, similar to elsewhere, occur as integral parts of volcanic sequences. Isotope data (meationed above and in Table 2) for the typical deposits suggest that ore-forming fluids might, at least in part, be derived from magmatic water, and that magmatic systems and their deriviatives might be responsible for dominant Cu and partial Zn source and less Pb source. On the other side, volcanism creates a domain of steep geothermal gradient which may drives the circulation of a hydrothermal cell (LYDON, 1984; FRANKLIN et al., 1981). Synvolcanic intrusions exposed in the submarine caldera of the rift-related volcanic belts, might have served as a generator for the convection of hydrothermal cells and might be the centers of hydrothermal activity. Hydrothermal exhalation was initiated at the intervals or waning stages of the submarine volcanic eruptions, and the associated massive sulfide ores were situated in vicinity of volcanic centers, commonly lying on the flanks or the tops of the synvolcanic intrusions.

Acknowledgments: This paper represents part of result of the program, "On the Main Volcanic Rocks and Related Mineralization in the Sanjiang Region, Southwest China", which was funded by the Ministry of Geology and Mineral Resources (86010-8) during 1985--1990. We thank the Geological Bureaus of Sichuan, Yunnan, Tibet Provinces for their effective cooperation. Special gratitude is due to Professors CHI, Jishang; SONG, Shuhe; WEN, Guang

and R.V. KIRKHAM for their encouragement and suggestion to our work and critical comments on preliminary drafts of the manuscript. Reviewing by Professor S. ISHIHARA is also gratefully acknowledged.

REFERENCES

BLUM, N. and PUCHELT, H. (1991): Sedimentary-hosted polymetallic massive sulfide deposits of the Kebrit and Shaban Deeps, Red Sea. Mineral Deposita, **26**, 217–227.

BRINCKMANN, J. and HINZE, C. (1981): On the geology of the Bawdwin lead-zinc mine, northern Shan State, Burma. Geol. Jahrb., Hanvber, **43**, 7–45.

CATHLES, L.M., GUBER, A.L., LENAGH, T.C. and DUDAS, F.O. (1983): Kuroko-type massive sulfide deposits of Japan: Products of an aborted island-arc rift. Econ. Geol., Mono. 5, 96–114.

CHEN, B., WANG, K., LIU, W., CAI, Z., ZHANG, Q., PENG, X., QIU, Y. and ZHENG, Y. (1987): Geotectonics of the Nujiang-Lancangjiang-Jinshajiang Region. Geological Publishing House, Beijing, 204p. (in Chinese).

CHEN, B., LI, Y., QU, J., WANG, K., AI, C. and ZHU, Z. (1992): On the main geotectonic problems in the Sanjiang Region and their relations to metallization. Geological Publishing House, Beijing. 110p. (in Chinese).

DOE, B.R. and ZARTMAN, R.E. (1979): Plumbotectonics: the phanerozoic. In: H.L. BARNES (ed.) Geochemistry of Hydrothermal Ore Deposits: New York, John Wiley and Sons, 22–70.

FRANKLIN, J.M. (1986): Volcanic-associated massive sulfide deposits—an update. In: C.J. ANDREW, R.W.A. CROWE, S. FINLAY, W.M. PENNEL and J.F. PYNE (ed.), Geology and Genesis of Mineral Deposits in Ireland, 49–69.

FRANKLIN, J.M., LYDON, J.W. and SANGSTER, D.F. (1981): Volcanic-associated massive sulfide deposits. Econ. Geol. 75th Ann. Vol., 485–627.

HOU, Z. and MO, X. (1991): The evolution of Yidun island-arc and implications in the exploration of Kuroko-type volcanogenic massive sulfide deposits in Sanjiang area, China. Earth Sciences—Journal of China University of Geosciences 16, 154–164 (in Chinese).

HOU, Z. and MO, X. (1993): Geology, geochemical and genetic aspects of the Kuroko-type massive sulfide deposits in Sanjiang region, southwestern China. Exploration and Mining Geology **2**, 17–30.

HOU, Z. and YANG, K. (1993): Metallogeny associated with volcanism in the Sanjiang region. In: X. MO and F. LU (ed.), The Tethys Volcanism and Relation to Metallogeny in Sanjiang Region, Southwestern China. Geological Publishing House, Beijing.

ISHIHARA, S. (1974): Magmatism of the Green Tuff tectonic belt, Northeast Japan: Soc. Mining Geologists Japan, Spec. Issue 6, 235–249.

KLAU, W. and LARGE, D.E. (1980): Submarine exhalative Cu–Pb–Zn deposits, a discussion of their classification and metallogenesis. Geol. Jahrb. **40**, 13–58.

LAMBERT, I.B. and SATO, T. (1974): The Kuroko and associated ore deposits of Japan: A review of their features and metallogenesis. Econ. Geol., **69**, 1215–1236.

LYDON, J.W. (1984): Volcanogenic masssive sulfide deposits. Part 1: A descriptive model. Geosci. Can., **11**, 195–202.

LYDON, J.W. (1988): Ore deposit models 14, Volcanogenic massive sulfide deposits. Part 2: Genetic models. Geosci. Can., **15**, 43–66.

OHMOTO, H. (1983): Geologic setting of Kuroko deposits, Japan. Part 1, Geologic history of the Green Tuff region. Econ. Geol., Mon. 5, 9–24.

OHMOTO, H., MIZUKAMI, M., DRUMMOND, S.E., ELDRIDGE, C.S., PISUTHA-ARNOND, V. and LENAGH, T.C. (1983): Chemical processes of Kuroko formation. Econ. Geol., Mon. 5, 570–604.

PISUTHA-ARNOND, V. and OHMOTO, H. (1983): Thermal history, and chemical and isotopic compositions of the ore-forming fluids responsible for the Kuroko massive sulfide deposits in the Hokuroku district of Japan. Econ. Geol., Mon. 5, 523–558.

QIAN, J. and SHEN, Y. (1990): Dahongshan Copper-iron ore deposit associated with paleovolcanic rocks, Yunnan. Geological Publishing House, Beijing (in Chinese).

SANGSTER, D.F. and SCOTT, S.D. (1976): Precambrian strata-bound massive Cu–Zn–Pb sulfide ores of North America. In: K.H. WOLF (ed.), Handbook of Strata-bound and Stratiform Ore Deposits, **6**, 129–222.

SATO, T. (1974): Distribution and geological setting of the Kuroko deposits. Soc. Mining Geologists Japan, Spec. Issue **6**, 1–9.

SATO, T., TANIMURA, S. and OHTAGAKI, T. (1974): Geology of Aizu metalliferous district, Northeast Japan. Soc. Mining Geologists Japan, Spec. Issue **6**, 11–19.

SCOTT, S.D. (1985): Seafloor polymetallic sulfide deposits: Modern and ancient. Marine Mining, **5**, 191–212.

SONG, S. (1949): The Baiyinchang pyrite-type deposit in Gaolan County, Gansu Province. Acta Geologica Sinica, **14**, 31–40 (in Chinese).

SONG, S. (1954): Metallogeny and geological features of the pyrite-type cupper deposits in Qilianshan belt. Acta Geologica Sinica, **32**, 1–10 (in Chinese).

SWINDEN, H.S. and THORPE, R.I. (1984): Variation in style of volcanism and massive sulfide deposition in Early to Middle Ordovician island-arc sequences of the Newfoundland Central Mobile Belt. Econ. Geol., **79**, 1596–1619.

YANG, K. (1989): Studies on the Paleozoic volcanic rocks and associated massive sulfide deposits of Sanjiang area, West Yunnan, China. Ph. D. thesis (Unpub.). 201p.

YANG, K. and MO, X. (1990): Geology and mineralogy of the Tongchangjie massive copper-zinc sulfide deposit, Yunnan, Southwest China. Program with Abstracts, 8th IAGOD Symposium, A41. (Ottawa, Canada, Aug. 1990).

YANG, K. and MO, X. (1993a): Characteristics of the Laochang volcanogenic massive sulfide deposit, Yunnan, southwestern China. Exploration and Mining Geology, **2**, 31–40.

YANG, K. and MO, X. (1993b): Late Paleozoic rifting-related volcanic rocks and tectonic evolution in southwestern Yunnan, China. Acta Petrologica et Mineralogica (in Chinese) (in press).

YANG, K., HOU, Z. and MO, X. (1992): Volcanogenic massive sulfide deposits in Sanjiang region, southwest China: Geological features and main types. Mineral Deposits, **11**, 35–44 (in Chinese).

YE, Q., SHI, G., YE, J. and YANG, C. (1991): Lead-zinc deposits in Nujiang-Lancangjiang-Jinshajiang region. Beijing Technological and Scientific Press, 164 p. (in Chinese).

This paper was presented at the 29th International Geological Congress (IGC), Symposium II-16-12: "Besshi and Kuroko type deposits in metamorphic terranes" on September 2, 1992

Best Wishes
Kaihui

Explor. Mining Geol., Vol. 2, No. 1, pp. 31-40, 1993
Printed in the U.S.A.

0964-1823/93 $6.00 + .00

Characteristics of the Laochang Volcanogenic Massive Sulfide Deposit, Southwestern Yunnan, China

KAIHUI YANG* and XUANXUE MO
China University of Geosciences, Xueyuan Road 29, Beijing 100083, China

Received May 6, 1992; accepted October 20, 1992.

Abstract — The Laochang mine, located in the Sanjiang area of southwestern Yunnan Province of China, is a volcanogenic massive Pb-Zn-Cu sulfide deposit. It is hosted by a pyroclastic sequence of Early Carboniferous age, namely the lower member of the Yiliu Group, which was intruded by syenite and rhyolite porphyry. The volcanic suite is basaltic or basaltic-andesitic in composition, has alkaline affinities, and is associated with the initial rifting along the margin of the Baoshan-Shanstate continental microplate (Yang, 1989). The ores are typically Pb>Zn>Cu in composition, averaging 3.82% Pb, 3.51% Zn, from 0.01% to 1.85% Cu (0.107% av.), a high average content of Ag (113 g/t) and recoverable amounts of Au, Tl, Gd, Ga, Ge, In. A massive sulfide zone, in which lenticular and stratiform orebodies are localized in a sulfide-carbonate-silica shale unit or sulfidic tuffite horizon that usually overlies coarse-grained pyroclastic rocks, is underlain by a stringer sulfide zone developed in a subvolcanic intrusion or volcanic sequence. The sulfide mineral assemblages, from the top to the bottom of the deposit, are: realgar + orpiment → galena + sphalerite + pyrite → chalcopyrite + pyrite + pyrrhotite + arsenopyrite. Oxide and sulfate minerals occur rarely in the massive ores. The massive ores are generally fine-grained and banded, but coarse-grained ore, colloform and framboidal texture, and growth-zoned pyrite and sphalerite are common. Sedimentary features such as graded bedding, brecciated and deformed ore clasts, and chaotically emplaced blocks, are well preserved, indicating that the massive orebodies have undergone slumping and displacement. Alteration is weak in the hanging-wall rocks, but strong in the stringer zone. Two distinctive alteration zones have been identified: the upper zone, characterized by an assemblage of quartz, carbonates, chlorite, albite, zeolite and sericite, and the lower zone containing diopside, tremolite, actinolite, garnet, clinozoisite, and epidote.

The general features of the Laochang deposit are in accord with the descriptive model of VMS deposits (Lydon, 1984). However, it falls into neither the Zn-Cu group nor the Zn-Pb-Cu group chemically (Franklin et al., 1981). The depositional setting of the Laochang deposit is quite different from Cyprus or Besshi-type massive sulfide deposits. Laochang is hosted by alkaline lavas that were erupted in a submarine continental rift. Although some features of the Laochang deposit are similar to those of Kuroko-type deposits, there are remarkable differences in the alteration mineral assemblage, the proportion of ore-forming elements (lead enriched) and the amounts of oxides and sulfates. These suggest corresponding differences in ore fluid composition and the associated ore-forming environment. Thus, the authors suggest that the Laochang deposit may be a distinct type of VMS deposit.

Introduction

In the past decade, important progress has been achieved in the investigation and exploration of massive sulfide deposits in the Sanjiang area, southwestern China. Two main belts of volcanogenic massive sulfide (VMS) deposits have been recognized: one is the Zengke-Xiangcheng belt of Kuroko-type deposits in western Sichuan, developed within the Yidun island-arc of upper Triassic age (Mo and Hou, 1988; Hou and Mo, 1990,1993); the other is the Changning-Menglian VMS belt of upper Paleozoic age, located in the western Yunnan (Yang, 1989). Within the latter belt, two types of VMS deposits (Cu>Zn and Pb>Zn>Cu) are associated with each other and can be related to the rifted margin of the Baoshan-Shanstate continental microplate (Yang, 1989; Yang and Mo, 1990 a, b). The Laochang deposit in Lancang County, western Yunnan (Fig. 1) is characteristic of the Changning-Menglian VMS belt. Broadly, the Laochang deposit is a composite body of several distinctive types of ore, but massive sulfides in the volcanic sequence form the major proportion of the deposit. In a narrow sense, the authors refer to the Laochang deposit as a volcanogenic massive sulfide deposit.

The recorded mining history of the deposit dates back to the Yongle Times of the Ming Dynasty, i.e., 1404 A.D. The prosperous mining activities of the old days left behind hundreds of relict sites and drifts. The relict drifts trend along the sulfide veins in limestone strata near the surface. From

*Present Address: Institute of Geology, Chinese Academy of Geological Sciences, Baiwanzhuang Road 26, Beijing 100037, China

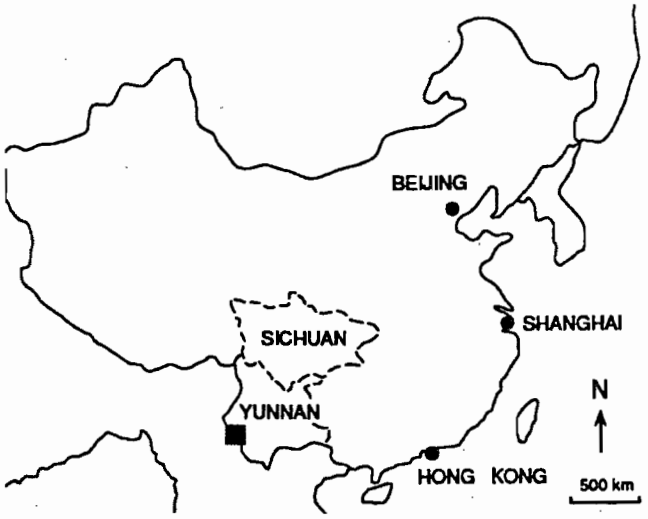

Fig. 1. Location of the Laochang deposit on the map of China published by Geological Publishing House, Beijing, 1990.

these drifts, Chinese ancestors exploited sulfide ores to extract silver and abandoned a large quantity of slag with high contents of lead and zinc, which is locally called "loudishi". It is the massive slag, the secondary oxide ores and the placer ores that have been exploited by the Lancang Lead and Zinc Refining Factory for nearly 40 years since its foundation in the 1950s.

For a long period of time, the Laochang deposit was considered to be composed only of numerous sulfide veins developed in the limestone strata. The massive sulfide orebodies hosted in the volcanic sequence stayed hidden until discovery by detailed exploration drilling, which has been conducted since the 1980s by the Nonferrous Metals Corporation of Southwestern China. It has been proved that Laochang is a large polymetallic deposit, in which the VMS ores are dominant.

The investigation of this deposit is conducted along two lines, namely, the systematical summarization of the geological characteristics and modelling of the genetic processes. Lydon (1984) discussed these two aspects in terms of the descriptive model and genetic model, and stressed that the former is the basis of the latter. The purpose of this paper is to describe the general features of the Laochang deposit and to compare it with the main types of VMS deposits in order to understand its significance. The ideas expressed in this paper arose from the authors' own observations together with a review of previous research achievements.

Geological Setting and Volcanic Host Rocks

The Laochang deposit was developed in the volcanic sequence which constitutes the lower member of the Yiliu Group of Early Carboniferous age. The sequence is a portion of the upper Paleozoic volcanic suite constituting the Changning-Menglian volcanic belt on the eastern margin of the Baoshan-Shanstate continental microplate (Yang, 1989). The underlying Devonian strata are mainly composed of clastic rocks and limestone with intercalated radiolarian siliceous

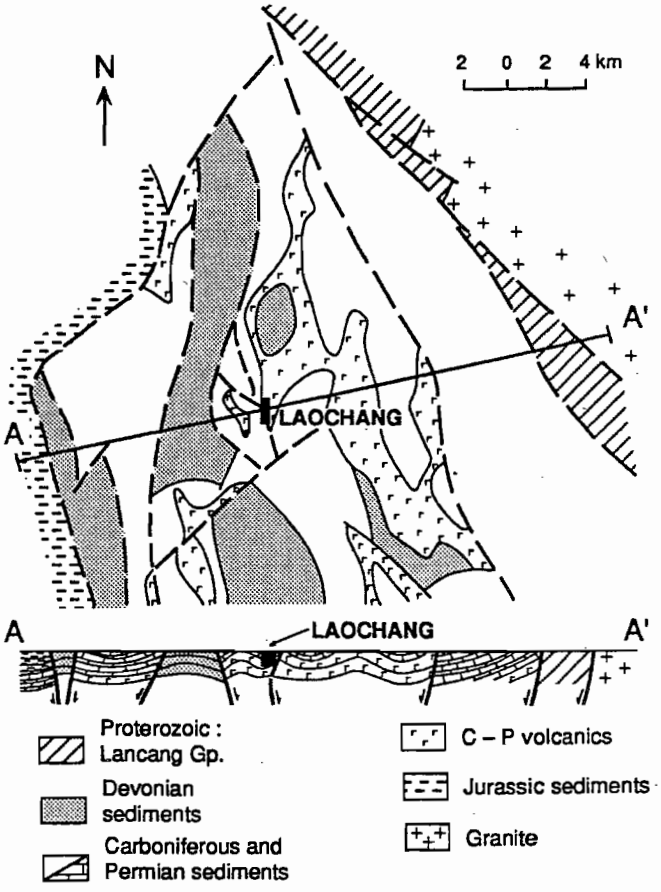

Fig. 2. Geological map of the Laochang district (modified from 1:200,000 Geological Map of Cangyuan Region).

shale. The oldest strata in the region discussed here are the Ximen Group and the Lancang Group, which are presumably Proterozoic in age. Figure 2 shows that the stratigraphic units are bounded by faults. The oldest units are distributed along both sides of the Changning-Menglian rift. Within the rift, the Devonian strata and lower Carboniferous Yiliu Group alternate, reflecting a framework composed of grabens and horsts. The Laochang deposit formed within a fault-bounded sub-basin, with accompanying submarine volcanic activity.

The volcanic sequence and the upper limestone of the Yiliu Group in the vicinity of the Laochang mine is shown in Figure 3. The volcanic rocks are in fault contact with limestone. Fs (Fig. 3) is the major fault in the Laochang district, dipping steeply westward with a strike of N-S in both north and south of the deposit, but changing to N-NW in the vicinity of the deposit. To a certain extent, this fault restrained the distribution of basaltic and andesitic lavas. It might have developed as a synvolcanic fracture and might have been active during the period of volcanism. F1 and F2 are upthrust faults dipping gently westward at depth, as indicated by drill core data. Although the slips of the faults are unknown, it is evident that the limestone unit is juxtaposed against the volcanic sequence along the fault surfaces.

The volcanic rocks in the Laochang district belong to an alkaline basalt series and are interpreted to be associated

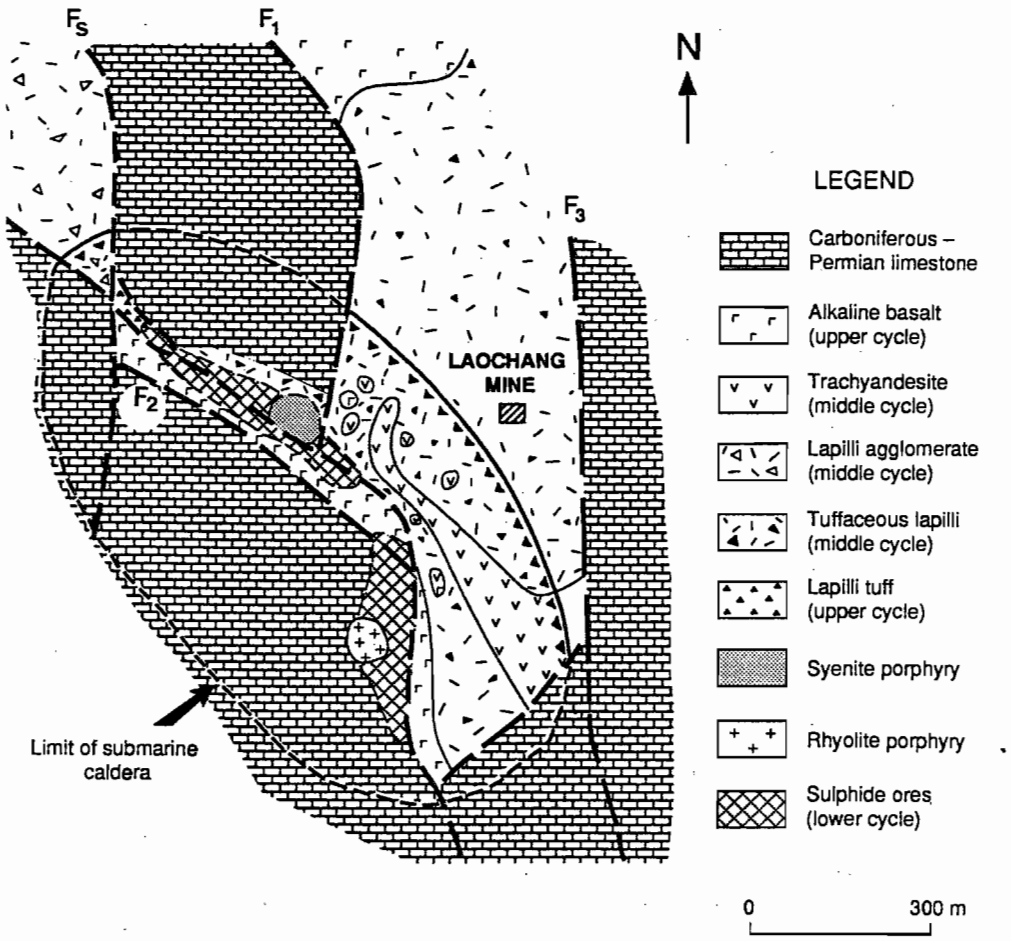

Fig. 3. Geological map of Laochang mine (modified from the 309 Geological Team, 1985, pers. comm.)

with initial rifting in the Changning-Menglian region (Yang, 1989). The sequence can be subdivided into three major cycles: the lower cycle consisting of trachybasalt, trachyandesite as well as corresponding pyroclastic rocks; the middle cycle containing basalt, amygdaloidal trachyandesite, corresponding pyroclastic rocks and volcano-sedimentary rocks; and the upper cycle mainly composed of alkaline picritic basalt and corresponding pyroclastic rocks.

The sulfide ores occur mainly in the middle and lower volcanic cycles. Based on observations from drill cores, as well as other available data, an idealized sequence of a host cycle may be established as follows, in descending stratigraphic succession:

1. banded fragmental exhalite limestone, calcareous siltstone and tuffite;
2. black sulfide (+ carbonates) - silica shale (exhalite);
3. black or dark gray sulfidic siltstone, tuffite and mudstone;
4. trachyandesitic-basaltic lapilli tuff with intercalated limestone lenses;
5. trachybasaltic-andesitic agglomerate-lapillistone;
6. pink or dark gray trachybasalt, trachyandesite.

This sequence, often changing rapidly in facies, repeats more than once and might form numerous cycles. The massive ores are localized in the upper part of a cycle, which is usually sulfide-silica shale or sulfidic tuffite horizons.

The subvolcanic intrusions present in the Laochang district include syenite and rhyolite porphyry. Drill core data indicate that syenite porphyry lies beneath the 1700 level in the north part of the Laochang deposit. The rock, fine-grained and microporphyritic, is predominantly composed of orthoclase, sodic plagioclase and quartz, and contains stringer or disseminated sulfides as well as alteration minerals, e.g., diopside, actinolite, and tremolite. Above the 1700 level, syenite porphyry is found only as breccia in the pyroclastic rocks.

Rhyolite porphyry fragments are found as detritus in the pyroclastic rocks, and the reason for its occurrence is still not clear. The rhyolite-porphyry contains the primary minerals quartz, potash feldspar and sodian plagioclase. Secondary minerals include sericite, chlorite and carbonates. The rock is veined and the microfissures cutting across the phenocrysts are filled with microcrystalline quartz, sericite and minor sulfides.

The subvolcanic intrusions were emplaced contemporaneously with the submarine volcanic eruptions, and before the formation of the massive sulfides. Additionally, several dykes, including diabase porphyrite and andesitic porphyrite, intrude and cut across every stratigraphic unit of the Laochang district; these dykes were formed long after the volcanic sequence and massive ores.

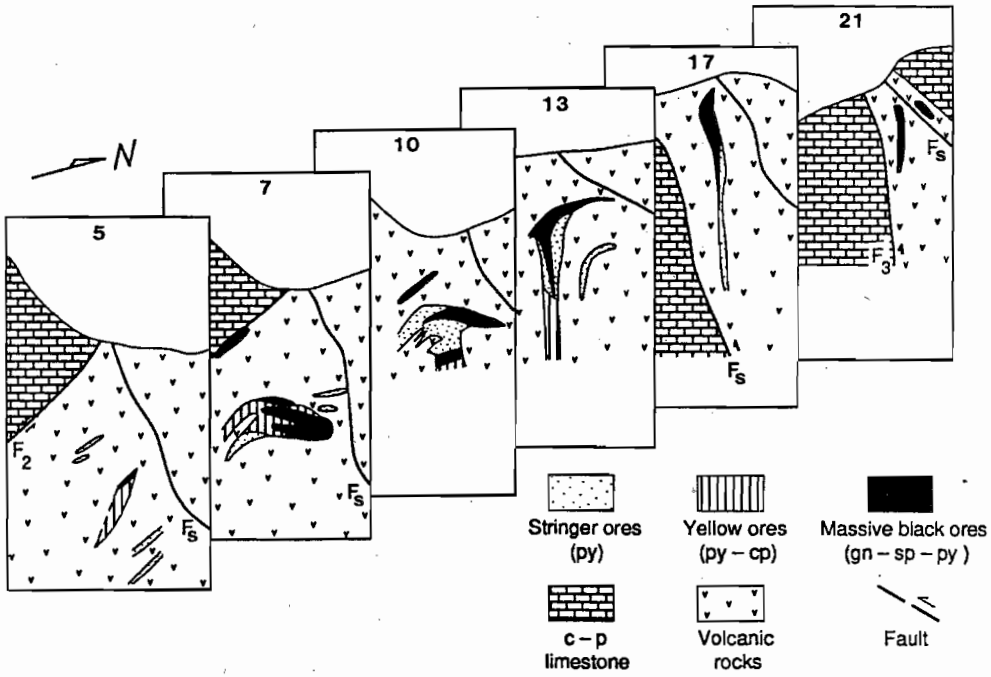

Fig. 4. Schematic diagram showing the forms of sulfide ores in several sections through the north part of Laochang mine (plotted on the data from the 309 Geological Team, 1985, pers. comm.).

General Features of Ore Deposit

Geometry of the Laochang Deposit

The north part of the Laochang deposit consists of a concordant massive orebody with an underlying disconcordant stringer sulfide zone (Fig. 5). As is shown in Figure 4, the ores grade from the top to the bottom of the deposit in the order: "black ores" (mainly massive Pb-Zn sulfide ores) → "yellow ores" (mainly massive Fe and Cu sulfide ores) → stringer ores (mainly Fe and Cu sulfides). The "black ores" and the "yellow ores" constitute the concordant massive orebodies which make up the massive sulfide zone.

In the south part of the Laochang deposit, the massive orebodies are multilayered, with alternating "black ores"and "yellow ores". Some drill core data have shown the existence of the underlying stringer zone in which copper mineralization seems promising, and exploration is under way to further locate the stringer zone at depth.

Geology and Petrology of Ores

Massive sulfide zone

The massive sulfide orebodies consist predominantly of massive, banded pyrite, galena, sphalerite, chalcopyrite and tetrahedrite. An individual orebody, stratiform or lenticular, from 1 m to 30 m in thickness (50 m maximum), usually has a clear-cut contact with the hanging-wall rocks, and is immediately underlain by the stringer zone.

Overlying the uppermost part of a massive orebody there is usually a black sulfide-silica (+ carbonate) shale layer (Fig. 5) in which realgar and orpiment commonly form a halo over the massive sulfide ores. With further enrichment by sulfides, this layer may change gradually into economic sulfide ore primarily composed of cryptocrystalline silica, mud, carbonates and sulfides, displaying fine-grained and laminated textures (Fig. 6a). The major part of an orebody is massive ore composed of sulfides (>90%) that are generally fine to coarse-grained, even pegmatitic, with the sizes of sulfide mineral grains usually larger than 3 mm, and with the largest galena crystal observed to date to be 12 cm in length. Mesoscopically, the massive ores are subdivided into "single" sulfide ores and "multi-" sulfide ores. The "single" sulfide ores consist of one sulfide species, and locally form unique sulfide layers, e.g., a pyrite-sphalerite or galena layer. Different sulfide layers may, alternate, within a massive orebody. The "multi-" sulfide ores consist mainly of pyrite, sphalerite and galena, with minor carbonates. Sphalerite (and galena) commonly occurs as small spheroids (0.2 cm to 2 cm) in the massive pyrite ore. With an increase in the content of the spheroids, the ores display a sponge-like texture. Locally, the sulfides occur as individual thin layers (each layer < 2 cm in thickness) that alternate in "rhythmic" patterns.

The massive sulfide zones have apparently undergone penecontemporaneous brecciation and slumping. The features reflecting such processes are readily observed from the underground workings developed in the north part of the Laochang deposit. Two distinctive types of transported ores have been recognized: (1) the fine-grained turbiditic sulfide matrix ores, laminated and commonly graded, in which sulfides together with silica and carbonates constitute the matrix, with lesser amounts of sulfidic or volcanic clasts and blocks (Fig. 6b); and (2) the coarse-grained debris flows that form conglomerate ores in which the fine-grained volcanic detri-

tus and mud dominate the matrix (Fig. 6c) and the sulfides occur either as clasts in the matrix or as blocks together with chaotically emplaced lithic blocks. Some large sulfide blocks were plastically deformed. These two types of transported ores may change gradually from one into another. Typically in the sulfide-bearing lapilli tuffaceous siltstone or sandstone (Fig. 6e), the sulfides occur as wispy discontinuous layers that are generally <1 mm thick, and rarely up to 2 cm thick. Turbidites with graded bedding, scoured surfaces, and Bouma sequences, usually consisting of *a* and *b* laminated members (Fig. 6d), are well preserved.

In the south part of the Laochang deposit, the massive sulfide orebody is in immediate contact with the upper limestone unit due to overthrust on the F2 fault. Some geologists (e.g., C. Fang, pers. comm.) postulated that the massive ores might have some direct relationship to the limestone or even the fault. According to our own investigation, the upper limestone formed long after the massive ores, and was overthrust from the west of the Laochang district. The limestone is thick-layered, with silty, muddy, and dolomitic laminae, distinct from the intercalated lenses or layers of fragmental limestone in the volcanic sequence. Furthermore, considerable amounts of volcanic clasts occur in the massive ores, and lapilli tuffite forms the immediate footwall of the massive orebodies. Besides, the variation in lead isotopes of the sulfides shows the same trend as that of the sulfides from the north part of the Laochang deposit (Yang, 1989). Therefore, the authors believe that these massive ores were also closely associated with submarine volcanic activity.

Stringer Zone

The Stringer Zone is primarily composed of vein, stockwork or disseminated pyrite and chalcopyrite. In the north part of Laochang deposit, the stringer zone (orebodies or mineralization zone) occurs in the volcanic rocks between or underneath the massive ores, as well as in the syenite porphyry intrusion. Due to the multistage activity of sulfide deposition, the early-formed massive ores may have been superimposed by later stringer-type ore. In general, the stringer zone seems to be mostly developed in the subvolcanic intrusion as well as its wallrocks. In the south part, drill core data indicate the existence of an extensively distributed stringer zone containing 0.1% to 1.86% Cu and extending for more than 100 m vertically beneath the massive ores.

Mineralogy

The mineral assemblage of the Laochang deposit is listed in Table 1. Pyrite is the predominant mineral in the deposit. Pyrite, galena, sphalerite and chalcopyrite constitute more than 95% of the massive ores. Two distinct textural types of pyrite are commonly observed. The first type is colloform or framboidal, xenomorphic fine-grained (<1 mm in size) pyrite (Fig. 6f); it usually forms wispy and discontinuous laminae in the sulfide-silica shale, sulfidic tuffite and tuffaceous sandstone, and siltstone. The second type is fine- to coarse-grained, euhedral or subhedral pyrite (1 mm to $>$ 20 mm), which is extensively distributed both in massive ores

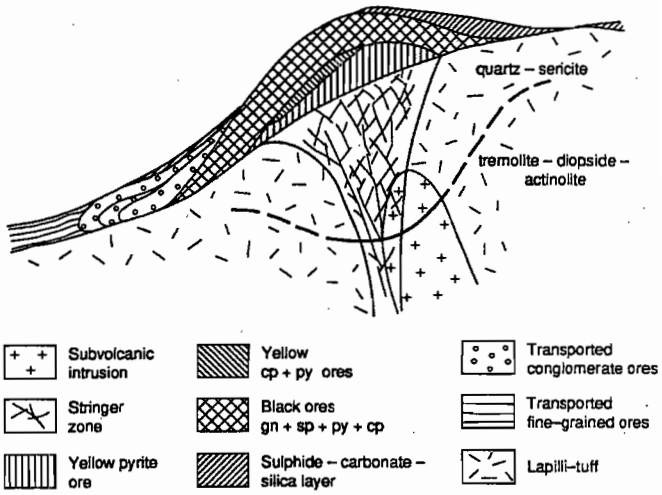

Fig. 5. Schematic diagram showing the idealized edifice of the Laochang deposit: distribution of sulfide ore types and alteration zones.

and stringer zone. Sphalerite is iron-rich (marmatite), usually dark brown or black and coeval with pyrite and galena. Some sphalerite crystals demonstrate growth zoning. Galena occurs as euhedral or subhedral columnar crystals, usually greater than 2 mm in size. Large galena crystals display growth striations; etched surfaces and minor vugs are well displayed. Cleavage planes deformed by strain are commonly observed. Small euhedral pyrite or calcite crystals are commonly included within large galena, sphalerite or pyrite crystals. Tetrahedrite and chalcopyrite are usually xenomorphic, fine-grained and interstitial to other sulfides. Cubanite occurs as inclusions in the pyrite and sphalerite. Acanthite also appears as inclusions in the tetrahedrite and galena. Realgar and orpiment are always found together in the sulfide-silica shale overlying the massive ores. Pyrrhotite and marcasite appear occasionally in the massive ores. The gangue minerals coeval with the sulfides include quartz, chalcedony, calcite, siderite, dolomite, sericite, chlorite as well as minor gypsum and barite.

In the stringer zone, pyrite, pyrrhotite and chalcopyrite are the dominant sulfides, with lesser amounts of galena, sphalerite and minor arsenopyrite. Those sulfides appear either as interlacing veins or dispersed, disseminated clusters in volcanic rocks or subvolcanic intrusions. They are usually xenomorphic and fine-grained, filling the interspace of other minerals or replacing gangue minerals pseudomorphically. The coeval gangue minerals include sericite, quartz, albite, diopside, tremolite, actinolite, clinozoisite, epidote, chlorite, dolomite, and garnet.

Alteration Zones

Alteration in the hanging wall of massive ores is rather weak and characterized by small amounts of quartz, chlorite, carbonates, talc, and zeolite minerals. Within the massive sulfide zone, conspicuous alteration occurring in the volcanic rocks between massive orebodies is linked with the underlying stringer zone (Fig. 5).

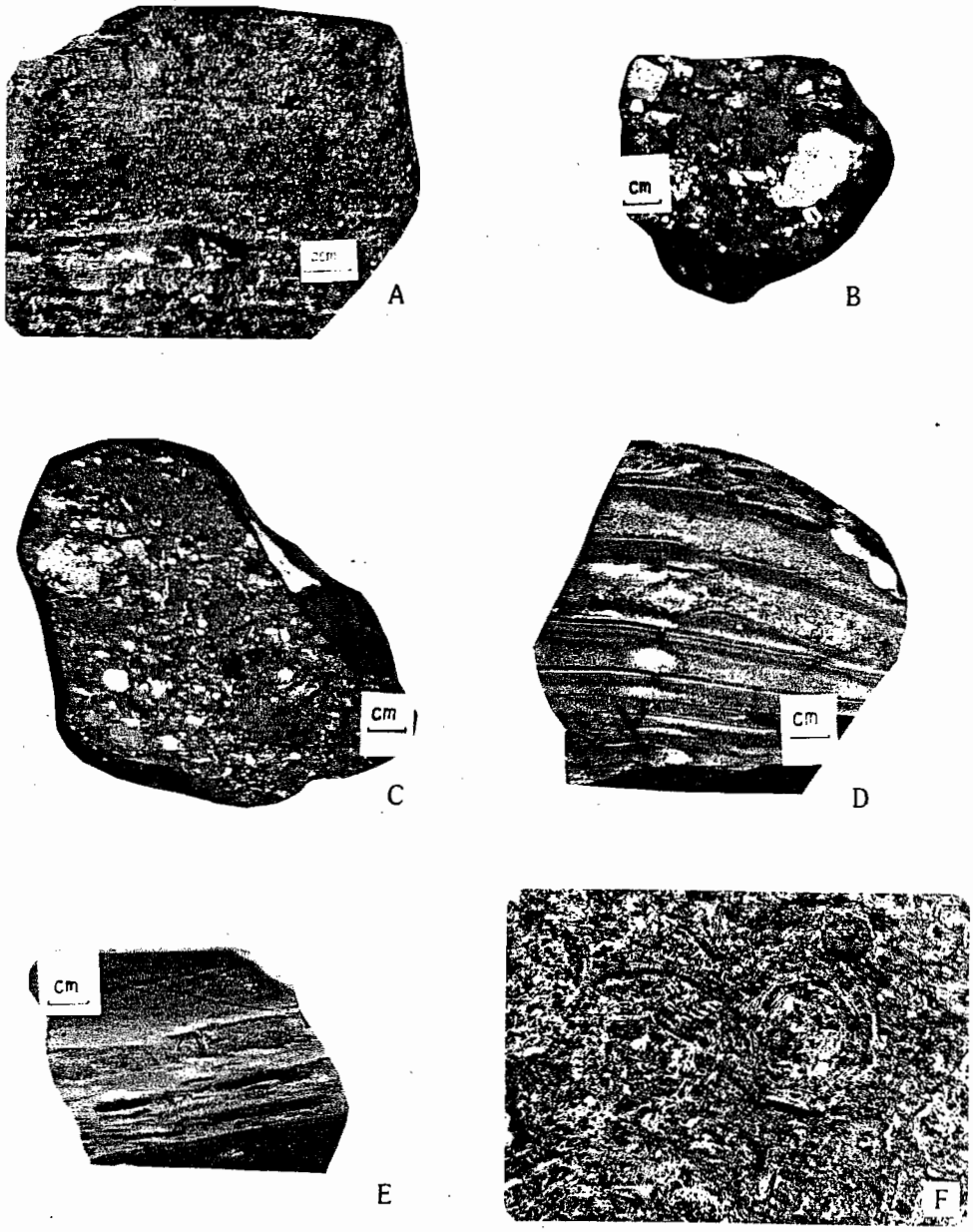

Fig. 6.
a. Banded sulfide ore mainly consisting of galena, sphalerite and pyrite form the upper massive ore layer.
b. Sulfide matrix ore with irregular pyroclastic detritus (dark gray) and galena, sphalerite fragments (bright).
c. Polylithic breccia conglomerate with lithic (pyroclastic) and sulfidic (galena, sphalerite and pyrite) fragments and tuffaceous matrix.
d. Graded bedding with *a* and *b* laminated members of a Bouma sequence. Each lamina consists of sulfide and tuffaceous detritus. The large fragment (bright) on the top right of the specimen is galena.
e. Sulfidic tuffite with fine-grained pyroclasts (gray) and cryptocrystalline sulfide (black or dark gray).
f. Colloform pyrite from banded massive ore. Reflected light. The field width is 2.8 mm.

In the stringer zone, two alteration sub-zones occur. The upper sub-zone, connected with the massive ores, is characterized by an assemblage of quartz, sericite, chlorite, sanidine, albite, zeolite, and talc, which occurs, as xenomorphic granular, acicular, foliated clusters or as veins or stockwork pervading volcanic rocks and the upper part of subvolcanic intrusions. In the lower sub-zone, diopside, tremolite, garnet and actinolite are the characteristic minerals. The upper zone is gradational into the lower zone. The latter overprinted the lower part of subvolcanic intrusions and wall rocks im-

Table 1. Mineral assemblages of the Laochang deposit

	Massive sulfide zone	Stringer zone
Metallic minerals	pyrite, galena, sphalerite, chalcopyrite, tetrahedrite, acanthite, realgar, orpiment, cubanite, marcasite, pyrrhotite	pyrite, chalcopyrite, pyrrhotite, acanthite, arsenopyrite
Non-metallic minerals	quartz, albite, sanidine, sericite, carbonates, chlorite, epidote, talc, zeolite, barite, gypsum	diopside, tremolite, actinolite, chlorite, pumpellyite, clinozoisite, sanidine, garnet

mediately adjacent to these intrusions. The early-formed minerals such as actinolite and diopside, are commonly replaced by the late-formed minerals epidote, chlorite, and pumpellyite; quartz, carbonates and sulfides replace all the other minerals.

The alteration sub-zones described above have been fully defined in the north part of the Laochang deposit. In the south part, however, only the upper sub-zone is observed at the present explored depth.

It should be noted that the alteration in the Laochang deposit was multistage. Besides the alteration types described above which are directly related to mineralization, seawater alteration (e.g., albite, epidote, chlorite) and late vein alterations (e.g., tremolite, calcite) arose during or after the volcanic activity and penetrated the entire volcanic sequence, and are not indicative of mineralization.

Chemistry

The available data indicate that the Laochang deposit is a large polymetallic deposit with a high content of Ag and recoverable amounts of Au, Ga, In, Gd, Sn, and Sb. The average content of Pb is 3.82%; Zn, 3.51%; Cu varies from 0.01% to 1.86%, 0.107% on average; Ag, 113.25 g/t on average and >1000 g/t locally; Au 0.02 to 0.39 g/t (av. 0.13 g/t), and 9.6 g/t locally (Pang, 1990).

The chemical zoning corresponds to the mineral zoning. Pb, Zn and As tend to be enriched in the upper part of the massive sulfide zone, and barren in the lower part as well as the underlying stringer zone. Cu is relatively enriched in the lower part of the massive sulfide zone as well as in the stringer zone. Moreover, the chemical zoning arising from the different alteration zones is also distinctive. The upper zone of the alteration pipe is predominantly of Si and K metasomatism, and the lower zone is characterized by Mg, Fe metasomatism.

Genetic Type of the Laochang Deposit

Comparison with the Typical Descriptive Model of a Classical VMS Deposit

Generally, a volcanogenic massive sulfide (VMS) deposit is a composite of massive sulfide ores and underlying stringer ores, which are hosted by a sequence of submarine volcanic rocks and are predominantly composed of Fe, Cu, Pb and Zn sulfides with minor amounts of Ag, Au, Se, Ga, In and Ge. Deposits of this type are extensively distributed in the major orogenic belts of the world, and have economic importance comparable to porphyry (copper) type deposits, and thus have received much attention. This is especially true in the Sanjiang area of China, the eastern segment of the well-known Tethyan, where numerous VMS deposits have been discovered.

Lydon (1984) proposed a descriptive model of VMS deposits. The main points of his model, with which the Laochang deposits are compared, are summarized below:

Geological Setting

VMS deposits typically occur in submarine volcanic sequences and are usually hosted by volcanic rocks. The massive orebodies tend to be localized within pyroclastic rocks, especially in a tuffite, exhalite or volcanic sedimentary unit, indicative of the waning stages of volcanic eruption. The Laochang deposit occurs within the sequence of submarine pyroclastic rocks of the Yiliu Group, and the massive sulfides are associated with the sulfide-silica unit or the sulfidic tuffite unit.

Characteristics of Ore Deposits

A VMS deposit usually consists of a concordant lens of massive sulfide underlain by a discordant stockwork or stringer zone. In accord with this point, the Laochang deposit is composed of several concordant layers or lenses of massive sulfide underlain by a stringer zone (Fig. 5).

The morphology of a sulfide orebody is related to the paleotopography and penetrative deformation, as well as the position of a hydrothermal feeder zone. Generally, an individual massive orebody may be stratiform, lenticular, tabular, sheet-like, cone-shaped or pencil-shaped, and the stringer zone may be pipe-like. In the Laochang deposit, the massive orebodies are lenticular or stratiform, and the stringer zone is pipe-like.

The most common sulfide mineral is pyrite. Pyrrhotite, chalcopyrite, sphalerite, galena and minor sulfosalts and bornite may be the subordinate sulfide species. Magnetite, hematite and cassiterite are the most common non-sulfide metallic minerals. The gangue minerals that may occur as co-precipitates with the sulfides are quartz, chlorite, barite, gypsum and carbonates. In the Laochang deposit, although the same sulfides as the above-mentioned ones dominate the ore, only minor gypsum and barite and no oxide minerals appear (Table 1). Ca-, Fe(Mn)- carbonates are relatively abundant. Moreover, there always exists a halo of realgar and orpiment over the massive sulfide ores.

The massive ore is dominantly fine-grained and banded, and the sulfide grains increase in coarseness with increasing metamorphic grade. The sedimentary features such as ripple, clastic, colloform and framboidal textures, brecciated, cross-laminated, graded bedding and others are well preserved. Most of these features are commonly observed in the Laochang deposit.

The zonation of VMS deposits is exhibited in the chemical composition and distribution of minerals, textures of the ores, and the metasomatic changes in the host rocks within the hydrothermal alteration pipe. The most obvious zonation pattern is the systematic decrease in Cu/Zn + Pb ratio (or chalcopyrite/galena + sphalerite ratio) upwards and outwards from the core of the alteration pipe and the base of the massive sulfide lens. Those features were thought to be most diagnostic of VMS deposits (Lydon, 1984; Sangster and Scott, 1976). The Laochang deposit demonstrates similar zonation patterns (Fig. 5).

A thin, bedded, pyritic or hematitic, siliceous exhalite or tuffite horizon is common over the massive orebodies. This sediment may have formed during the waning stages of hydrothermal activity, during volcanic quiescence. In the Laochang deposit, a sulfidic (not hematitic) siliceous unit occurs over the massive ores.

Hydrothermal Alteration

Strong alteration and its zonation are dominantly found within and surrounding the stockwork zone. Despite the considerable variations in wallrock alteration, there are two major zonation patterns: (i) a sericitic halo to a chlorite core, typical of the Precambrian deposits in North America; and (ii) a siliceous core surrounded successively by a sericitic zone and a zeolitic halo, characteristic of the Kuroko deposits in Japan. Contrasting with these patterns, the alteration pipe of the Laochang deposit is zoned with quartz-sericite at the upper part and tremolite-actinolite-diopside at the lower part (Fig. 5).

Other characteristics of VMS deposits include occurrences in spatial groups or clusters within certain favorable horizons, their compositions dominated by Fe, Cu, Pb, Zn sulfides with recoverable amounts of Ag and Au. These features also occur in the Changning-Menglian metallogenic belt (Yang, 1989).

In summary, the major features of the Laochang deposit are very similar to the classical descriptive model of VMS deposits. But some characteristics are peculiar to the Laochang deposit, including the paucity of sulfates and oxides, a halo of realgar and orpiment over the massive ores, and a distinctive alteration pattern i.e., a quartz-sericite zone over a tremolite-actinolite-diopside zone in the alteration pipe.

Comparison with the Main Types of VMS Deposits

General Considerations

Many proposals on the classification of VMS deposits have been put forward, most of which were based on the geotectonic setting and immediate footwall lithology of the deposits or on their main ore element composition. Each approach is distinct and relative to the other in spite of the emphasis on different aspects of VMS deposits. Based on ore element chemistry, Hutchinson (1973) and Solomon (1976) classified VMS deposits into three types, Cu, Cu-Zn, and Zn-Pb-Cu types. Using the data of massive sulfide deposits from the Canadian Shield, Scandinavian Caledonides, Green Tuff Belt in Japan, Bathurst in New Brunswick, Iberian pyrite belt, Fennoscandian Shield districts, and the principal sediment-hosted deposits, Franklin et al. (1981) and Franklin (1986) distinguished three groups of massive sulfide deposits, namely, Zn-Cu, Zn-Pb-Cu and Pb-Zn groups, of which the Pb-Zn group is sediment-hosted massive sulfide deposits and the Zn-Pb-Cu, Zn-Cu groups are mostly volcanogenic massive sulfide deposits. This proposal was further supported by Lydon (1984), who found that the bulk Zn/(Pb + Zn) ratios of the Zn-Pb-Cu deposits (between 0.7 to 0.8) are different from those of the Zn-Cu deposits (>0.95). Franklin (1986) noted that some deposits within the Precambrian Shield of Canada have a higher lead content than that which is typical of the Zn-Cu group,but do not fall in the Zn-Pb-Cu group defined by Lydon (1984), and therefore suggested that the Zn-Cu group should be subdivided into two subgroups, Zn-Cu group and Zn-Cu(-Pb) group.

In terms of metal proportions, the main groups of VMS deposits were defined by Franklin et al. (1981) and Franklin (1986; Fig. 1). On the diagram, the Laochang deposit falls into the Pb-Zn group, and is distinguished from the Zn-Cu or Zn-Pb-Cu group in bulk composition. Furthermore, the bulk Zn/(Pb + Zn) ratio of the Laochang deposit is 0.48, which is much lower than that of the Zn-Pb-Cu or Zn-Cu group. Clearly, the Laochang deposit, relatively enriched in Pb, falls outside the main groups of VMS deposits. In fact, the high enrichment of lead is characteristic of the deposits developed in the basemental sequence of the Baoshan-Shanstate district (Yang, 1989). West of this belt, the VMS deposits hosted by a felsic volcanic sequence in the Bawdwin district of Shanstate, Burma, are typically Pb-Zn-Cu in composition (Brinckman and Hinze, 1981). It has thus been suggested that the relative enrichment of lead in deposits might be related to its high geochemical background in the basement of the Baoshan-Shanstate continental microplate (Yang, 1989). It seems that this Pb-Zn-Cu type of VMS deposit is characteristic of the metallogeny of the area.

On the basis of tectonic setting and volcanic host rock lithology, numerous proposals on the classification of VMS deposits have been put forward (e.g., Sillitoe, 1973; Sangster and Scott, 1976; Hutchinson, 1980; Klau and Large, 1980; Sawkins, 1976). Sawkins (1976) recognized three main types of VMS deposits: (1) Kuroko-type, occurring in felsic, calc-alkaline volcanic sequences at sites of plate convergence in ocean areas; (2) Cyprus-type, occurring in low-potassium tholeiitic volcanic rocks in the ophiolitic sequences at sites of plate spreading; and (3) Besshi-type, occurring in tholeiitic volcanic-sedimentary sequences, which are believed to be formed at sites of backarc spreading or continental rifting (Scott et al., 1983; Slack, 1988; Maiden, 1988). Each of these three types possess specific characteristics and certain genetic processes distinct from the others.

Table 2 lists the important characteristics of the three main types of VMS deposit. Apparently, the Laochang deposit is distinguished from the Cyprus-type in the tectonic setting, and the composition of volcanic host rocks as well as the ore elements. Although the Besshi-type deposits may

Table 2. Main characteristics of Kuroko-, Besshi- and Cyprus-type VMS deposits and the Laochang deposit

	Tectonic setting	Volcanic suite	Host rocks	Main ore elements
Kuroko type	island arc	bimodal volcanism, calcalkaline, tholeiitic	rhyolitic pyroclastic, volcani-sedimentary rocks	Zn>Pb>Cu
Cyprus type	backarc or mid-ocean ridge	ophiolitic	pillowed tholeiitic lava and pyroclastic rocks	Cu>Zn
Besshi type	backarc or continental rift	tholeiitic	tholeiitic pyroclastic, volcani-sedimentary rocks	Zn>Cu
Laochang type	continental rift	alkaline basaltic	trachybasaltic and trachyandesitic pyroclastic rocks	Pb>Zn>Cu

be associated with continental rifting, the Laochang deposit differs from this type in volcanic host rocks and ore elements. The Laochang deposit may resemble the Kuroko deposits in composition of ore types in spite of the different proportions of Pb, Zn and Cu, remarkable differences exist in tectonic setting and volcanic host rocks.

Comparison with the Kuroko-type VMS Deposits

In order to further understand the genetic type of the Laochang deposit, comparison with the Japanese Kuroko-type deposits is made below, in view of the similarity in the main ore elements between them.

Detailed investigations of Japanese massive sulfide deposits have been carried out by many geologists (e.g., Ohmoto and Skinner, 1983; Scott, 1980). The well-known Kuroko deposits occur as clusters within the Tertiary green tuff zone which is characterized by bimodal volcanism associated with intra-arc rifting. Host rocks to the Kuroko deposits are felsic pyroclastic flows considered to have undergone slumping and displacement accompanying submarine eruption. Much of the Kuroko mineralization shows close spatial association with rhyolitic subvolcanic intrusions, and the massive ores are usually located within local depressions related to submarine calderas (Ohmoto and Skinner, 1983).

In comparison with the main characteristics of Kuroko-type deposits, it can be seen that the Laochang deposit possesses some features in common with the Kuroko-type, namely:

1. Both occur with submarine volcaniclastic rocks, and show a spatial correlation with subvolcanic intrusions.
2. Both show a tendency to occur in districts related to centres of volcanic activity. The orebodies in both cases tend to be localized in sub-basins or local depressions related to calderas, and underwent slumping and redistribution.
3. Both consist of two main ore types, massive ore and stringer ore. The massive ore in both instances is conformable with surrounding rocks, whereas stringer ore clearly cross-cuts strata.

There are, however, important differences between the Laochang deposit and the Kuroko deposits which impose constraints on the simple inclusion of the Laochang deposit into the Kuroko-type:

1. The Laochang deposit is hosted by a basaltic pyroclastic sequence with alkaline affinities, which was suggested to have been associated with initial rifting along the margin of a continental microplate (Yang,1989). But the Kuroko deposits occur in calc-alkaline felsic volcanic rocks which comprise the bimodal volcanic rocks associated with intra-arc rifting (Ohmoto and Skinner, 1983).
2. The barite and gypsum ore zones, characteristic of the Kuroko deposits, are absent in the Laochang deposit.
3. A sulfide-carbonate-silica shale unit commonly occurs over the massive ores of the Laochang deposit. This unit is quite different from the oxidic ferruginous quartz zone in the upper part of the Kuroko deposits.
4. A realgar and orpiment halo is commonly observed overlying the massive ores in the Laochang deposit, but is absent in the Kuroko deposits.
5. Compositionally, the Laochang deposit is characterized by Pb>Zn>Cu, whereas the Kuroko-type deposits are typically Zn>Pb>Cu.
6. The footwall alteration is zoned with quartz-sericite in the upper part and tremolite-actinolite-diopside in the lower part of the Laochang deposit, and no obvious alteration was found in the hanging-wall rocks. In contrast, the footwall alteration in the Kuroko-type deposits is predominantly siliceous and sericitic, and a broad zeolitic alteration is found in the hanging-wall rocks.

Although the Laochang deposit is similar to the Kuroko-type in some aspects, it possesses its own unique properties, which may indicate corresponding differences in ore fluid composition, ore-forming environment, and even the geological evolution of the regional lithosphere. These genetic aspects of the Laochang deposit will be discussed in another paper.

Conclusions

The Laochang deposit is a volcanogenic massive polymetallic sulfide deposit, hosted by an alkaline basic volcanic sequence associated with Changning-Menglian initial rifting along the margin of the Baoshan-Shanstate continental microplate. The relative enrichment of lead, the paucity of sulfates and oxides, as well as the alteration pattern of a quartz-sericite zone overlying a tremolite-actinolite-diopside zone, are distinctive features of the Laochang deposit in comparison with other VMS deposits.

The Laochang deposit is, therefore, different from the well-known types of VMS deposits, especially in terms of its tectonic setting in a continental rift and associated mafic alkali lavas. It is unusually Pb-rich and perhaps may be recognized as a separate type of VMS deposit (Table 2).

Acknowledgments

This investigation is a part of the project, "Main Volcanic Rocks and Associated Mineralization in the Sanjiang Area, Southwestern China", which is financed by the Ministry of Geology and Mineral Resources of the People's Republic of China (86010-2). The Nonferrous Metals Corporation of Southwestern China and its 309 Geological Team are thanked for permitting us access into the drifts of the Laochang mine, and offering the drill core data and allowing the use of some of their unpublished data. We are grateful to engineers Jiadi Pang and Zenghui Rao for their enthusiastic help during our investigation at the Laochang mine. We would like to express special thanks to Professors Jishang Chi, Shuhe Song, Guang Wen, Fengxiang Lu, Jinfu Deng, Shanping Sun, Conghe Zhao and Peying Lin for their kind help and advice in our work and for their critical comments on our manuscript. Drs. I.R. Jonasson, J.M. Franklin, R.A. Zierenberg and R.V. Kirkham are deeply thanked for their reviewing and critical comments and editing of our manuscript.

This paper was originally presented at the 8th IAGOD Symposium in Ottawa, Ontario, August 1990.

References

BRINCKMAN, J. and HINZE, C., 1981. On the geology of the Bawdwin lead-zinc mine, northern Shan State, Burma. Geologisches Jahrbuch, Hannover, D43: p. 7-45.

FRANKLIN, J.M., LYDON, J.W. and SANGSTER, D.F., 1981. Volcanic-associated massive sulfide deposits: Economic Geology, 75th Anniversary Volume, p. 485-627.

FRANKLIN, J.M., 1986. Volcanic-associated massive sulphide deposits — an update. *In* Geology and Genesis of Mineral Deposits in Ireland. *Edited by* C.J. Andrew, R.W.A. Crowe, S. Finlay, W.M. Pennell and J.F. Pyne, p. 49-69.

HOU, ZENGQIAN and MO, XUANXUE, 1990. Kuroko-type volcanogenic massive sulphide deposits and Yidun island arc in Sanjiang Area, Southwestern China (abstract) Programme with Abstracts, 8th IAGOD Symposium, p. A40 (Ottawa, Canada, Aug. 12-18).

HOU, ZENGQIAN and MO, XUANXUE, 1993. Geology, geochemistry and genetic aspects of Kuroko-type volcanogenic massive sulfide deposits in Sanjiang region, Southwestern China, Exploration and Mining Geology, this issue, p.17-29.

HUTCHINSON, R.W., 1973. Volcanogenic sulfide deposits and their metallogenic significance. Economic Geology, 68, p. 1223-1246.

HUTCHINSON, R.W., 1980. Massive base metal sulphide deposits as guides to tectonic deposits. *In* The Continental Crust and its Mineral Deposits, Geological Association of Canada Special Paper 20. *Edited by* D.W. Strangway, p. 323-339.

KLAU, W. and LARGE, D.E., 1980. Submarine exhalative Cu-Pb-Zn deposits — a discussion of their classification and metallogenesis. Geologisches Jahrbuch, 40, p. 13-58.

LYDON, J.W., 1984. Volcanogenic massive sulphide deposits Part 1: a descriptive model: Geoscience Canada, 11, p.195-202.

MAIDEN, K.J., 1988. Besshi-type Cu-Zn-Ag deposits. *In* Stratabound Copper Deposits, Workshop Notebook. *Edited by* R.V. Kirkham and W.D. Sinclair, IUGS/UNESCO Deposit Modeling Program, Taiyuan, Chiina, p. 454-456.

MO, XUANXUE, 1988, Characteristics and volcano-tectonic setting of Kuroko-type massive sulphide deposits in Sanjiang Region, Southwestern China. *In* Stratabound Copper Deposits, Workshop Notebook. *Edited by* R.V. Kirkham and W.D. Sinclair. IUGS/UNESCO Deposit Modeling Program, Taiyuan, China. p. 355-357.

OHMOTO, H. and SKINNER, B.J., 1983. Geologic setting of Kuroko deposits, Japan: Part 1, geologic history of the Green Tuff region. *In* The Kuroko and Related Volcanogenic Massive Sulfide Deposits. Economic Geology Monograph 5, *Edited by* H. Ohmoto and B.J. Skinner, p. 9-24.

PANG, JIADI, 1990. A discussion on the geological constraints on the mineralization of Laochang silver-lead deposit, Lancang, Yunnan. Ore Geology in Southwestern China (in Chinese), 4, No. 1, p. 29-35.

SANGSTER, D.F. and SCOTT, S.D., 1976. Precambrian stratabound massive Cu-Zn-Pb sulphide ores of North America. *In* Handbook of Stratabound and Stratiform Ore Deposits 6. *Edited by* K.H. Wolf, p. 129-222.

SAWKINS, F.J., 1976. Massive sulphide deposits in relation to geotectonics. *In* Metallogeny and Plate Tectonics. Geological Association of Canada, Special Paper 14. *Edited by* D.F. Strong, p. 221-240.

SCOTT, S.D., 1980. Geological and structural control of Kuroko-type massive sulphide deposits. *In* The Continental Crust and its Mineral Deposits. Geological Association of Canada, Special Paper 20. *Edited by* D.W. Strangway, p. 705-722.

SCOTT, S.D., EDMOND, J. and LONSDALE, P., 1983. Modern analogue of a Besshi-type massive sulphide deposit on the sea floor, Guaymas Basin, Gulf of California (abstract). American Institute of Mining, Engineering, Meeting, Atlanta, Program 84.

SILLITOE, R.H., 1973. Environments of formation of volcanogenic massive sulfide deposits. Economic Geology 68, p. 1321-1325.

SLACK, J.F., 1988. Besshi-type massive sulphide deposits: deposit model form. *In* Stratabound Copper Deposits, Workshop Notebook, *Edited by* R.V. Kirkham and W.D. Sinclair. IUGS/UNESCO Deposit Modeling Program, Taiyuan, China, p. 457-458.

SOLOMON, M., 1976. "Volcanic" massive sulphide deposits and their host rocks a review and explanation. *In* Handbook of Stratabound and Stratiform Ore Deposits, 6. *Edited by* K.H. Wolf, p. 21-54.

YANG, KAIHUI, 1989. Studies on the Paleozoic Volcanic Rocks and Associated Massive Sulphide Deposits of Sanjiang Area, West Yunnan, China (in Chinese with English abstract). Ph.D. Thesis of the China University of Geosciences. Unpublished.

YANG, KAIHUI and MO, XUANXUE, 1990a. A large Paleozoic massive Pb-Zn-Cu sulphide deposit: The Laochang mine, Yunnan, Southwest China (abstract). Program with Abstracts, 8th IAGOD Symposium, p. A40. (Ottawa, Canada, Aug. 12-18).

YANG, KAIHUI and MO, XUANXUE, 1990b. Geology and Mineralogy of the Tongchangjie massive copper-zinc sulphide deposit, Yunnan, Southwestern China. Program with Abstracts, 8th IAGOD Symposium, p. A41. (Ottawa, Canada, Aug. 12-18).

Explor. Mining Geol., Vol. 2, No. 1, pp. 17-29, 1993
Printed in the U.S.A.

0964-1823/93 $6.00 + .00

Geology, Geochemistry and Genetic Aspects of Kuroko-type Volcanogenic Massive Sulfide Deposits in Sanjiang Region, Southwestern China

ZENGQIAN HOU
Institute of Mineral Deposits, Chinese Academy of Geological Sciences, Baiwanzhuang Road 26, Beijing 100037, China

and

XUANXUE MO
China University of Geosciences, Xueyuan Road 29, Beijing 100083, China

Received May 6, 1992; accepted October 15, 1992.

Abstract — Yidun Island Arc in Sanjiang Region is one of the important Kuroko-type volcanogenic massive sulfide deposits (VMS) districts in southwestern China. Tectonically, the region is situated in the eastern portion of the Tethys orogenic belt, and is a late Triassic extensional island-arc. The island-arc underwent earlier arc construction, intra-arc rifting, later arc construction and back-arc spreading during its evolution and formed a complete trench-arc-basin system, i.e., the Ganzi-Litang suture zone, forearc basin, outer arc, intra-arc rifting zone, inner arc and back-arc basin from east to west across the island-arc.

Kuroko-type VMS deposits and occurrences discovered so far are limited to within the intra-arc rifting zone of the Yidun Island Arc and tend to occur in groups or clusters distributed in separate fault-bound basins; e.g., Zengke, Gacun and Xiangcheng basins, in which submarine volcanic rocks, especially bimodal volcanic suites, were extensively developed. The VMS deposits formed in the waning stages of volcanic eruption in the late Triassic and are hosted in the uppermost section of acidic volcanic rocks (rhyolitic-dacitic) within a bimodal suite. The orebodies are associated with these host rocks: rhyolitic-dacitic pyroclastic rocks and exhalites and chemical sedimentary rocks.

All VMS deposits in Sanjiang are of the Zn-Pb-Cu type. The architecture of the deposits is two-fold, consisting of concordant lenses and layers of massive sulfides and an underlying discordant stockwork. All deposits show metal zoning. The hydrothermal alteration related to mineralization is strong and asymmetrical, and is found dominantly within the stockwork zone and host rocks surrounding the ores. There are two alteration patterns: (1) chloritization → sericitization → silicification from outer sides to core of the alteration pipe; and (2) silicification + sericitization → silicification + carbonate from the lower to upper part of the alteration pipe.

The mineralization temperatures of ore-forming fluids vary in the range 200°C to 335°C. Thermal evolution of the fluids displays temperature profiles that first increase and then decrease with progression of mineralization processes. The majority of black-ore minerals (Groups I and II) formed during intensifying stages of hydrothermal activity, and the majority of semi-yellow-ore minerals (Group III) formed during a thermal maximum. There followed the formation of fine-grained black-ore minerals (Group IV), which interacted with barite layers during decreasing temperature phases.

Oxygen and hydrogen isotope studies show that the sources of ore-forming fluids for the Kuroko-type VMS deposits are two-fold: seawater and magmatic hydrothermal solutions, represented by the Kuroko deposits in Japan and Kuroko-type VMS deposits in Sanjiang, respectively. In the latter case the hydrothermal solutions reacted with host rocks and mixed with cold seawater percolating downward, and circulated through volcanic rocks resulting in development of alteration zones and formation of ore minerals in Kuroko-type VMS deposits.

Regional Geological Setting

The Sanjiang Region is situated tectonically in the eastern portion of the Tethys orogenic belt. The region is one of the more important Kuroko-type volcanogenic massive sulfide deposit (VMS) districts in China. Kuroko-type VMS deposits and occurrences discovered so far in the region are in the Changtai-Zengke-Xiangcheng areas (Fig. 1), which belong to the Triassic Yidun Island Arc. The island arc is located in the northwestern part of the Sanjiang Region, spanning Sichuan and Yunnan Provinces. The studies show that the formation of the VMS deposits seems to have a close relationship with the evolution of Yidun Island Arc, which is controlled by tectonic-volcanic evolution of the Paleo-Tethys Ocean.

Four ophiolite-arc volcanic rock belts have been recognized from east to west across the Sanjiang Region as follows (Hou and Mo, 1990): (1) Ganzi-Litang

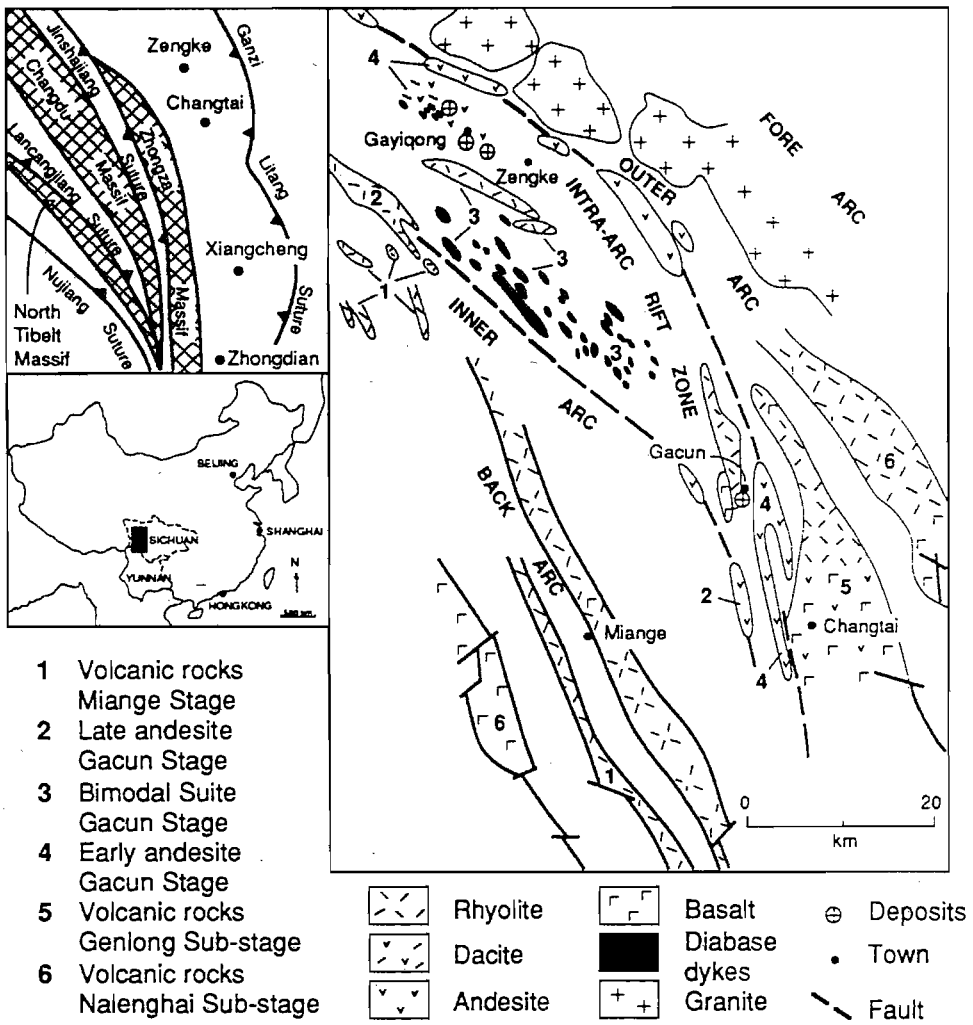

Fig. 1. Location of study area and a tectonic sketch map of the northern part of Yidun Island Arc.

ophiolite - Yidun arc volcanic rock belt, (2) Jinshajiang ophiolite - Jiangda arc volcanic rock belt, (3) Lancangjiang ophiolite - Nanzuo arc volcanic rock belt, and (4) Nujiang ophiolite - Zuogong arc volcanic rock belt (Fig. 1). Stratigraphic, paleontological, petrological and geochemical studies show that the Lancangjiang suture zone might be a fossil boundary line between Eurasia and Gondwana. Zhongza-Changdu Massifs and Baoshan - Northern Tibet Massifs, located on the eastern and western sides of the boundary line respectively, belong to Eurasia continent and Gondwanaland, respectively (Yang and Mo, 1992). The Lancangjiang and Jinshajiang Oceans, opening in the Carboniferous period, might represent the main part of Paleo-Tethys Ocean between the two continents. It is estimated by paleomagnetic data and rifting rates (Yang and Mo, 1992) that the two branches of the Paleo-Tethys Ocean, located on each side of Changdu Massif, were about 3000 km apart. The temporal and spatial distribution of four ophiolite-arc volcanic rocks belts show that the opening and closing of the Paleo-Tethys Ocean happened twice and shifted from the Lancangjiang-Jinshajiang Oceans to the margins of Gondwana and Eurasia, respectively. The closing and collision of the oceans and the opening of the Ganzi-Litang and Nujing Oceans, in Permian to Triassic time, happened at the same time or within a short period of time. It is suggested that the formation of the Lancangjiang-Jianshajiang Oceans in the Sanjiang region might have been related to asthenosphere upwelling around the Okavango upwelling center that formed in Carboniferous-Permian time (Irvine, 1989). On the other hand, the subduction beneath Changdu Massif of both oceanic plates in the Late Permian, and the opening of the Litang-Nujiang Oceans in the late Permian to late Triassic, were concerned with the Vietnam downwelling center that was active in the Mesozoicera (Irvine, 1989).

Yidun Island Arc, as a result of westward subduction of the Litang oceanic plate in the late Triassic, has a complicated history of alternate tension and compression. Its evolution is divided into three stages as follows:

Pre-arc Extensional Stage

Following subduction and collision of the Jianshajiang oceanic plate, the western margin of the Yangzi Platform (which belongs to Eurasia) became extensional and rifted to form the Panxi Rift dominated by large quantities of flood basalt, and the Litang Ocean characterized by MORB-type

basalts. Yidun area, as a part of Zhongza Massif, rifted from the margin of the Yangzi Platform and was the locus of intense basic volcanism and abyssal turbidite-facies sedimentation during Triassic time (Hu and Luo, 1989; Hou, 1988). The pre-arc volcanic rocks are well preserved in the northern part of Yidun area, e.g., the Changtai-Zengke volcano-sedimentary basins. The volcanic rocks of an early substage are distributed in the outer reaches of the basin, and are predominantly alkaline, high-TiO_2 basalts, similar to the Ermeishan basalts in Panxi Rift. The volcanic rocks of a middle substage occur in the central part of the basin, and consist mainly of transitional basalts, chemically. These facts show that a continental margin rifting system developed prior to the formation of the island arc in Yidun area. The volcanic rocks of a later substage, recently discovered, are distributed only in the southern part of Yidun area and consist of boninitic rocks and low-K_2O tholeiitic basalts. The development of these rock suites records the history of aborted continental rifting which led to the development of an island arc (Hou, 1988).

Main Arc-forming Stage

As a consequence of subduction of the Litang oceanic plate, an intense arc volcanism occurred. The arc volcanism included an earlier andesite substage, a bimodal volcanic rock substage, and a later andesite substage. The center of volcanism shifted westward with time and successively formed the eastern andesite belt, the bimodal suite belt, and the western andesite belt (Fig. 1).

Volcanic rocks of both the earlier and later substages belong to a calc-alkaline series and consist of andesite, and andesitic pyroclastic rocks with subordinate dacite, rhyolite and basaltic andesite. Arc volcanic rocks with relatively shallow-water deposits, formed during the earlier and later arc-constructional calc-alkaline volcanism, and constitute outer arc and inner arc, respectively.

Bimodal volcanism developed between earlier and later andesite substages, produced a co-existent rhyolitic (dacitic) rock - tholeiitic basalt bimodal suite. During the bimodal volcanism the arc crust split along the arc volcanic chain and subsequently formed several separate fault-bounded basins, e.g., the Gacun, Zengke and Changtai basins (Hou, 1988; Hou and Mo, 1990). The bimodal volcanic rocks and fault-bounded basins, as well as abyssal submarine sediments within the basins, constitute an intra-arc rifting zone.

Back-arc Stage

This stage is characterized by bimodal volcanism and development of fault-bounded basins, which occurred on the inner side of the inner arc. The bimodal suite consists of shoshonite and high-K_2O felsic lavas and ignimbrites. The basins are filled by turbidite-facies sediments.

In summary, the Yidun Island Arc formed on the base of a thinned continental crust (24 km ± 2 km), (Hou, 1988; Hou, 1990), which manifests a graben-horst system. It underwent two arc-constructional and two spreading events, and formed a complete trench-arc-basin system, i.e., suture zone - forearc - outer arc - intra arc - rifting zone, inner arc - back arc basin, from east to west across the island arc (Fig. 1). Intra-arc rifting and its associated bimodal volcanic suite are the most important features of the island arc geology and these are closely related to the formation of VMS deposits.

Geological Features of VMS Deposits

Temporal-spatial Distribution of VMS Deposits

Yidun Island Arc belt is not only a district of the most intense volcanism but is also a significant base and precious metals belt. The belt consists of hundreds of deposits and occurrences which extend over 450 km and laterally for 30 km to 50 km. There exist typical Kuroko-type VMS deposits and occurrences, sedex-type deposits (e.g., Qingda Pb-Zn deposit) and volcanogenic-type mercury deposits (e.g., Kongmasi Hg deposit), as well as porphyry-type deposits which occur at both ends of the island arc (e.g., Xuejiping and Changdagou Cu deposits). The Kuroko-type VMS deposits include the Gacun, Gayiqong, Shengmelong and Ronggong deposits. All these VMS deposits are located in the northern part of the island arc. Among them, the Ag- and Au-bearing Gacun Zn-Pb-Cu deposit is the biggest, and the Gayiqong Zn-Pb-Cu deposit, 50 km north of Gacun deposit, is next largest. The Kuroko-type VMS occurrences are mainly distributed in the southern part of the island arc, where geological data are limited; with increasing geological knowledge, these occurrences may be found to be larger than they are now thought to be. In general, the metallogenic belt in Sanjiang Region can be compared with the Green Tuff zone of Japan in geological and economic significance. Spatially, Kuroko-type VMS deposits are tightly restricted to within the intra-arc rifting zone on the island arc, tend to occur in groups or clusters, and are located in separate fault-bounded basins. For instance, the Gacun deposit cluster lies within Gacun's discrete graben basin; the Zengke deposit cluster is likewise confined. Individual deposits are situated in small isolated to semi-isolated submarine depressions. For example, the Gayiqong deposit and the Shengmelong deposit lie in small submarine basins, located on the eastern and western sides of a central submarine highland, respectively, within the fault-bounded basins. In contrast, the Gacun orebodies occur within an isolated basin surrounded by volcanic pyroclastic cones and submarine highlands (Hou, 1988). Temporally the deposits occupy a persistent horizon in the stratigraphic column, and occur in rhyolitic-dacitic pyroclastic rocks, which constitute the bimodal suite with thoeliitic basalts in the bimodal substage. It seems that the Kuroko-type VMS deposits, restricted to within the intra-arc rifting zone, formed during intra-arc rifting in an abyssal submarine environment, rather than during the arc-constructional stage.

Host Rocks, Exhalites, and the Age of Mineralization

As noted above, these Kuroko-type VMS deposits occur at a favorable stratigraphic horizon, i.e., the deposits and occurrences are situated within a narrow stratigraphic interval, and all are in the uppermost part of a rhyolite-dacite

series which constitutes the bimodal suite. The bimodal suite belongs to the middle member of the Gacun Formation, which is divided into three members (from the bottom to the top): the lower andesite member, the bimodal member, and the upper andesite member.

Host Rocks

Rhyolitic-dacitic volcanic rocks comprise the majority of the bimodal volcanic rocks in the island arc. Dacite and dacitic pyroclastic rocks are more abundant than acid volcanic rocks in Zengke district, whereas rhyolite and rhyolitic pyroclastic rocks are dominant in Gacun district and the Xiangcheng area. The acid volcanic rocks are characterized by multi-eruption of magmas to form several eruption cycles and a large quantity of pyroclastic rocks. In Gacun district, rhyolitic rocks include rhyolite, rhyolitic tuff, breccia and tuff-lava. The rock sequence can be subdivided into three eruptive cycles which are intercalated with abyssal turbidite sediments between two adjacent cycles. The sulfide ores mainly occur in rhyolitic pyroclastic rocks of the third cycle and are overlain by sediments (e.g., black calcareous silty and dolomitic limestone). In comparison with the Gacun district, dacitic volcanic rocks in the Gayiqong district are mainly dacitic tuff and tuff lava, with subordinate rhyolitic lava. The rock sequence can be subdivided into four eruptive cycles. The sulfide ores are situated within dacitic-rhyolitic rocks in the third cycle, whereas the scarce veined ores occur in dacitic rocks of the fourth cycle, which overlies the third cycle as lenses. The position of orebodies is also similar in the Xiangcheng area. These observations show that the degree of magma differentiation and thickness of host rocks bearing ore are closely analogous to mineralization of Kuroko-type VMS deposits, and that the deposits formed in quiescent intervals or in waning stages of volcanic eruption. The fact that orebodies mainly occur in rhyolitic-dacitic pyroclastic rocks indicates that the rocks might be an important facies controlling the distribution of orebodies, and possibly play a role in the formation of VMS deposits as a "porous barrier" (Lydon, 1988). The pyroclastic rocks occur not only as footwall rocks, but also in interlayers as lenses or thinner layers. This shows that the mineralization of the deposits was contemporaneous with volcanism.

Exhalites and Chemical Sedimentary Rocks

These rocks are thought to be products of the same hydrothermal venting activity on the sea floor which formed the ores, and commonly display a spatial and genetic association with VMS deposits. The rocks include chert, baritite, siderite and jaspilite-taconite. All these exhalites occur in the Gacun deposit, whereas only one exhalite, siderite rock, occurs in the Gayiqong deposit; and another, baritite, in the Xiangcheng area. In the Gacun deposit, the typical exhalite succession is chlorite-bearing siderite, jaspilite-taconite, baritite, from the top to the bottom. These special rocks are distributed near discharge vents of hydrothermal fluids, and are concordantly overlain by black calcareous slate. In the Gacun deposit, the exhalites overlie the lenses and layers of massive orebodies. In the Gayiqong deposit they lie on top of the pyroclastic rocks, in which stringer orebodies occur, rather than on the top of massive orebodies.

In summary, rhyolitic-dacitic host rocks, orebodies and exhalite-chemical sedimentary rocks in the three horizons constitute an intrinsic genetic association, which reflects the close relationship among them.

The Age of Mineralization

The favorable-horizon phenomenon of the VMS deposits and host rock, orebody, and exhalite association imply that the Kuroko-type deposits in the island arc formed during a rather short period of time. As mentioned above, after the westward subduction of the Litang oceanic plate, there were four important tectono-magmatic events which formed a trench - arc - basin system. The Rb-Sr age of andesites in the outer arc is 200.8 Ma (Hou, 1988). It was estimated that each of the four main events occurred during the upper Triassic (up to 195 ± 5 Ma), and could have happened within a period of 1 Ma to 2 Ma (Hou, 1988). This means that the age of rhyolitic-dacitic rocks in the bimodal suite might be about 199 Ma to 197 Ma. K-Ar age of rhyolitic rocks with the strongest alteration is 197 Ma (Yie et al., 1991), which is in accord with the Pb-isotopic model age (197.4 Ma) of the Gacun deposit (Duan, 1983). In contrast to 13 Ma during which the Kuroko deposits in Japan were formed (Ohmoto, 1983), the same type of VMS deposits in Sanjiang, China formed within a period of 1 Ma.

Architecture of VMS Deposits

The architecture of VMS deposits in the island arc is of two-fold configuration, consisting of concordant lenses and layers of massive sulfide orebodies and an underlying discordant stockwork or stringer zone. Spatially, the contact relationship between stockwork and massive orebodies is direct (Gacun deposit) or indirect (Gayiqong deposit). In the Gacun deposit, the stockwork zone consists of five stringers, veinlets and disseminated Pb-Zn orebodies (Fig. 2a). The orebodies occur mainly between exploration lines 24 to 15 and have greatest thickness near line 0. The massive orebodies directly overlie the stockwork zone (Fig. 2a). In Gayiqong deposit, the stockwork orebodies occur mainly at lines 4 and 7, and are overlain concordantly by siderite lenses rather than by massive orebodies which are situated near line 0. Drill core data indicate that subvolcanic rocks (dacitic) are developed below the 3600 m level along exploration lines 4 and 7. The fact that the stockwork orebodies were developed within subvolcanic rocks and overlying volcanic rocks, and disappeared below the subvolcanic rocks shows that the stockwork ore and associated subvolcanic rocks in drill cores of lines 7 and 4 might represent the feeder pipe of ore-forming fluids, whereas the positions of massive orebodies may have been controlled more by the topography of paleo-ocean basins.

The VMS deposits in the island arc show well-developed metal zoning. The Gacun deposit is the most typical. The

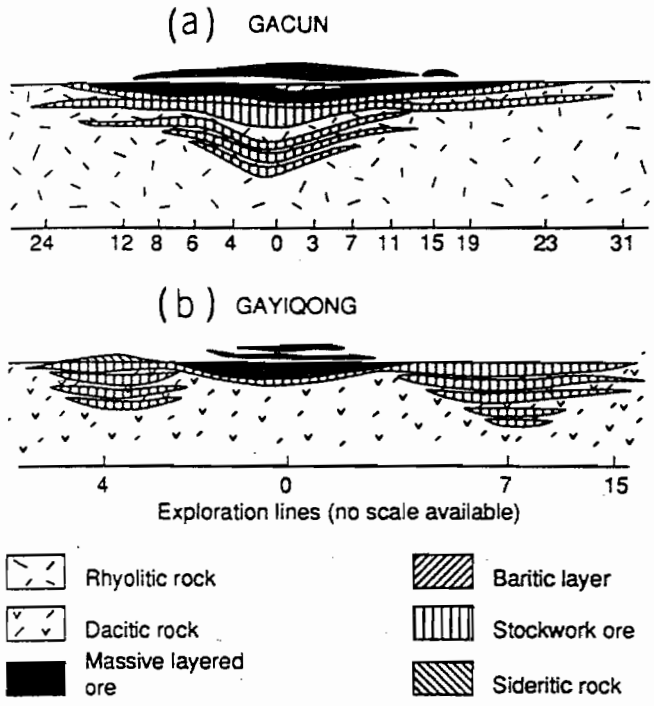

Fig. 2. Sketch of longitudinal section of orebodies. (a) Gacun deposit and (b) Gayiqong deposits (no scale available).

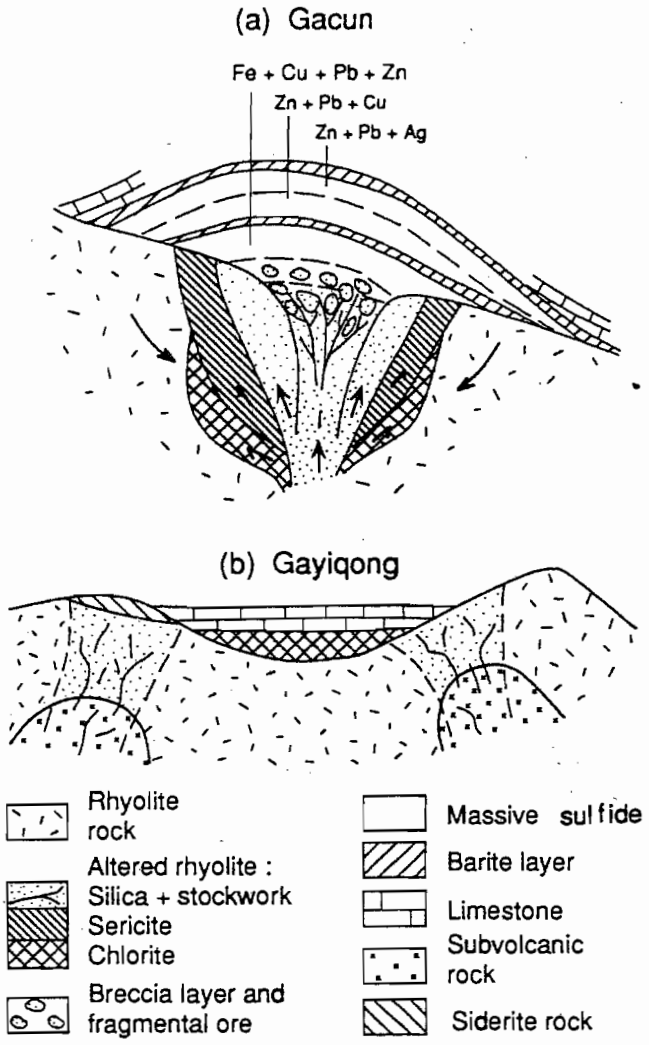

Fig. 3. Idealized profile and zoning of (a) Gacun deposit and (b) Gayiqong deposit.

stratigraphic sequence of the Gacun deposit from the top to the bottom is as follows (Figs. 3a, 5):

(6) a hangingwall that consists of calcareous slate and dolomitic limestone;

(5) the exhalite and chemical sedimentary rocks, i.e., barite layer etc., that concordantly overlie layered massive sulfide ores;

(4) layers and lenses of massive sulfide ore, which have the following sequence from the top to the bottom:

• black ore: laminated polymetallic layer overlain by the layers of alternate polymetallic massive sulfide and barite, with Cu 3.88 wt%, Pb 11.0 wt%, Zn 17.7 wt% and Ag 762 ppm on average;

• dark barite layer with intercalation of polymetallic massive ore, that is directly hosted in rhyolitic pyroclastic rocks and contains Cu 0.26 wt%, Pb 0.39 wt%, Zn 0.35 wt% and Ag 57 ppm, on average;

• semi-yellow-ore, that mainly consists of pyrite and is very massive in the uppermost portion and laminated in the middle, and contains fragments of rhyolite, barite and silicic breccia at the bottom. The metal contents in this layer are Cu 3.47 wt%, Pb 14.4 wt%, Zn 30.2 wt% and Ag 688 ppm on average;

(3) sulfide-matrix fragmental ore, gradually changing into layer (4) upwards and layer (2) downwards;

(2) stockwork ore zone, hosted in rhyolite, contains Cu 0.16 wt%, Pb 1.23 wt%, Zn 2.07 wt% and Ag 27.7 ppm on average. It shows clear metal zoning, i.e., Fe-Zn to Cu-Pb-Zn upwards and Cu-Pb-Zn to Pb-Zn outwards.

(1) a footwall, strongly altered rhyolite and rhyolitic pyroclastic rocks with Cu 141 ppm, Pb 176 ppm, Zn 207 ppm and Ag 14.5 ppm on average.

Figure 3 shows two models of the architecture for the VMS deposits developed on the basis of the above data, indicating an idealized profile, metal zoning and alteration zoning of these deposits.

Textures of VMS Deposits

Although stringers, veinlets and disseminated orebodies predominate over the stockwork zone, massive, laminated and layered orebodies are dominant in the massive sulfide zone. A variety of textures and structures shows that replacement processes are extensive in the stringer zones, whereas sedimentary textures and slump structures are dominant in the massive sulfides.

At the base of the massive orebodies, conglomerates and fragmental or clastic textures are commonly observed. There are two types of ores developed here: one is sulfide-matrix ore, in which sulfide constitutes the matrix with barite clasts and rhyolitic clasts; the other is fine-grained matrix ore, in which the matrix consists of the sulfides, and the clasts include pyrite, sphalerite and galena. These textures reflect the

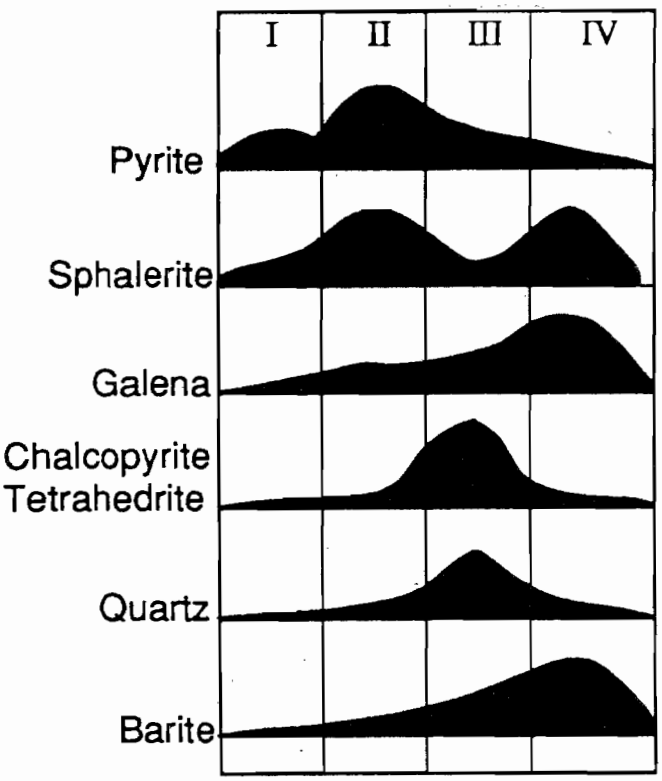

Fig. 4. Proportions of minerals in different stages of mineralization of the Gacun VMS deposit.

processes of slumping, brecciation and local transportation of the massive sulfides.

In the middle part of massive ores, laminated textures are very common. The small laminations may consist of single sulfide species or several sulfides with the same color. The laminations iterate in places into rhythmic patterns which are similar to those in the Kuroko deposits of Japan and the Laochang deposit of southern China (Yang and Mo, this issue 1992).

In the upper part of massive ores, the barite layer and sulfide layer alternate to form banded sulfide ores. The sulfides occur within the barite layer as lenses or as thin layers on the uppermost massive ores.

Finally, the massive ore itself also displays some sedimentary features such as graded bedding, lamination, colloidal texture and framboidal structure, which imply that the massive ores might be products of chemical precipitation of sulfide particles into isolated depressions on the seafloor.

Textures and Paragenetic Association

Although massive and stockwork ores are different in form and occurrence, they share similar characteristics in certain textures. For example, extensive replacement textures and crosscutting relations, as well as secondary overgrowth and recrystallization enlargement textures developed both in massive and stockwork ores. According to physical and chemical features of sulfides, and replacement and crosscut relations among the sulfide minerals in both zones, four paragenetic associations in VMS deposits have been recognized as follows (see Fig. 4):

Group I. Colloidal pyrite-sphalerite-galena association (Py > Sp > Ga > Cp) formed in the earliest stage of mineralization and developed in both massive and stockwork ores. It is characterized by colloidal texture and very fine grain size on recrystallization.

Group II. Granular pyrite-sphalerite-galena association (Py > Sp > Ga), extensively replaced and crosscut the minerals in Group I and were replaced by chalcopyrite of Group III. Pyrite developed secondary enlargement margins and growth zoning, and is characterized by euhedral crystals. Sphalerite has widespread chalcopyrite disease in a myrmekitic form.

Group III. Coarse-grained chalcopyrite-pyrite-quartz association (Cp > Py) in which copper minerals, galena and quartz are usually coeval, developed both in stockwork and massive ores. These minerals crosscut and intruded along cleavages and fissures of the minerals of Groups I and II.

Group IV. Fine-grained sphalerite-galena-barite association (Sp > Ga > other sulfide minerals) formed in the latest stage of mineralization. Sphalerite is light yellow-brown, and is distinct from dark brown sphalerite in Groups I, II and III. Galena is interstitial to the previously formed grains. Subordinate silver minerals have partly replaced or crosscut the minerals of the three earlier groups.

The four paragenetic associations, which are recognized only at the base of the Gacun deposit, are idealized. Other VMS deposits in the island arc might develop one or several of the four paragenetic associations. For example, the Gayiqong deposit displays only Groups I, II and III.

The paragenetic associations of Kuroko-type VMS deposits in Sanjiang Region are clearly similar to those of Kuroko deposits in Japan (Elderidge et al., 1983). The four paragenetic associations might be representative products of four corresponding stages or substages of mineralization. Pyrite and quartz precipitated over a long period, although pyrite mainly precipitated in stages II and III, and quartz in stage III. Copper minerals (chalcopyrite and tetrahedrite) mostly formed in stage III. Both sphalerite and galena have two generations, in stage II and IV. Most barite precipitated from hydrothermal solution in stage IV. Paragenesis stages are summarized in Figure 4.

Alteration Zoning

The alteration of the Gacun deposits (Fig. 5) is characterized by asymmetrical development. The alteration in the hanging-wall rocks is very weak or did not develop, whereas the alteration in footwall rocks and the stockwork zone is very strong.

In the stockwork zone and footwall rocks, the alteration related to VMS mineralization often is multistage and mainly includes silicification, sericitization, chloritization, carbonatization, barium-adularia alteration, and sideritization. There are different alteration types for different VMS deposits. In the Gacun deposit, alteration is divided into two stages: an earlier stage, in which the alteration includes silicification, sericitization and chloritization; and a later stage, in which the alteration includes silicification and barium-

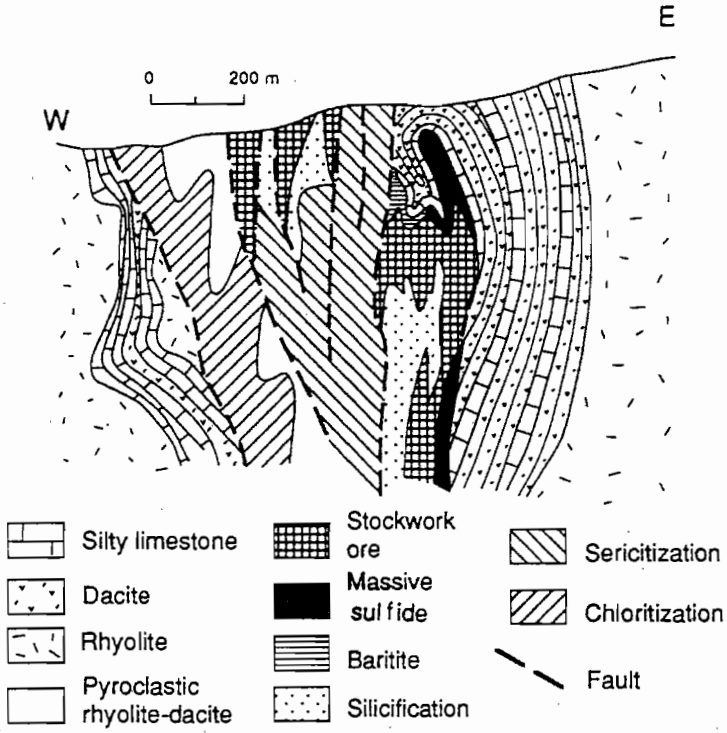

Fig. 5. Alteration zoning of Gacun VMS deposit.

adularia alteration, overprinted on the alteration zone of the earlier stage. In the earlier stage, silicification developed in the middle to upper portion of rhyolitic rocks enclosing stockwork ores (Fig. 2). Highly silicified rhyolites ($SiO_2 \geq$ 86 wt%) and even entirely silicified rocks formed in some areas. Quartz-sericite alteration occurs in the periphery of the silicification zone and formed as an assemblage of dominant sericite and quartz, plus a few grains of chalcopyrite. Sericite-chlorite alteration developed mainly in dacitic rocks and in the lower portion at the periphery of the silicification zone. A cross-section of the Gacun deposit shows the distribution of various types of alteration (Fig. 5).

In comparison with the Gacun deposit, carbonate alteration of the Gayiqong deposit is much more extensive. Carbonatization and silicification developed in the upper section of host rocks and within the stockwork zone, whereas sericitization and silicification prevailed in the lower section of host rocks containing veined ores. The longitudinal alteration zoning seems to be clear. The strong development of carbonate and lack of barium-adularia alteration are important characteristics of the Gayiqong deposit.

Figure 5 presents a model of alteration zoning for the VMS deposits, established on the basis of alteration in the Gacun deposit. The model shows the spatial distribution of the alteration zoning. These studies indicate that the sequence in which alteration zoning developed is chloritization to sericitization to silicification (Hou, 1991). The chloritization in the lower portion and outermost edges of the alteration pipe is the earliest product of mixing of discharging hydrothermal fluids with seawater penetrating downwards. The silicification, located in the inner zone or pipe core, represents the latest alteration product which overprinted previously formed sericitization and even parts of the chloritization zone.

Yie et al. (1991) determined the temperatures of alteration in the Gacun deposit, and pointed out that alteration temperatures increased from the margins to the core of the altered pipe, e.g., chloritization zone 190°C to 110°C, sericitization zone 250°C to 180°C, and silicification zone 310°C to 270°C (Fig. 6b). Evidently the variation of alteration temperatures with time is similar to the temperature profiles of mineralization, which will be discussed in detail later.

Physicochemical Conditions of Mineralization

Mineralization Temperature and Salinity

Homogenization temperature and freezing-point depressions for fluid inclusions were determined in samples containing several stages of mineralization, from the Gacun and Gayiqong deposits. The temperatures and salinities of fluid inclusions are listed in Table 1.

Temporal Variations

There are distinct differences in the filling temperatures and salinities of primary fluid inclusions. For the Gacun deposit, the filling temperatures in stage II vary from 180°C to 256°C, and from 99°C to 185°C in stage IV. Stage III primary fluid inclusions yield the highest filling temperatures recorded during ore deposition, and temperatures vary from 280°C to 320°C.

Contrasting with Kuroko deposits of Japan, in which the salinities of primary fluid inclusions remain fairly con-

Table 1. Mineralization temperatures (in °C) for Gacun VMS deposit

	Stage II				Stage III			Stage IV				
	SN	Sp	Sp-Salinity	Ba	SN	Qz	Qz-Salinity	SN	Sp	Sp-Salinity	Ba	Ba-Salinity
	BT4	250	7.9		BT4	294	15.8					
	BT5	246	7.9		BT5	295	17.1					
	BT6	251			BT6	304	17.7					
stockwork	BT8	228	9.3	196	BT8	281						
ore	BT19	251	5.7		BT19	302	19.9					
	BT20	259	7.0		BT21	311						
	BT1							BT1	149		114	
	BT2	247	9.3	217	BT2	279	15.1	BT9	138		110	
	BT3	231	8.6	215	BT3	279	16.4					
	BT17	209			BT17	279		BT17			114	
massive	BT18							BT18	116	13.2	110	5.7
Zn-Pb	BT23							BT23	180	10.4	110	6.4
ores	BT34	221	9.3					BT24	185	10.4	112	5.7
	BT36	258	5.7		BT36	310		BT27	139	14.5	101	6.4
	BT37	248	7.9		BT37	319	17.1	BT28	139	13.2	100	6.4
	BT39	213	11.5		BT38	298	14.5	BT29	160	10.4	100	7.9
	BT44	260			BT44	299		BT32	180	7.9	113	7.9
	BT45	258	5.1		BT45	299	21.3	BT37	181	9.3	114	5.7
	BT48	253			BT48	295		BT43	134	11.5	98	5.7
massive	BT10	223	7.9		BT10	285	18.4	BT9	138	11.5	110	7.9
Zn-Pb-Ag												
ores	BT13	240	7.9		BT13	301		BT16	140		104	7.0
								BT25	125	4.5	99	4.4
								BT26	122	13.2	100	5.1

SN: Specimen number; Qz — Quartz; Sp — Sphalerite; Ba — Barite.
Temperatures in Table 1 are homogenization temperature (in °C).
Salinity data are in wt. % equivalent NaCl.

stant at around 4.5 ± 1.5 equivalent weight percent NaCl during all stages of mineralization (Pisutha-Arnond and Ohmoto, 1983), the salinities of the primary fluid inclusions for the VMS deposits in Sanjiang Region vary from 4.5 to 21 equivalent weight percent NaCl, and show a changing trend of lower (5.1% to 11.5% NaCl) to higher (15.1% to 21.3% NaCl) to lower (4.4% to 14.5% NaCl) from stage II to III to IV, respectively (Table 1). For the Gayiqong deposit, the filling temperatures and salinities of primary fluid inclusions vary in the range 160°C to 226°C and 10% to 12% NaCl for stage II, and 280°C to 310°C and 12% to 15% NaCl for stage III, respectively. These data show that there is a general increase in filling temperatures and salinities from stage II to a maximum in stage III, followed by decreasing temperatures and salinities in stage IV, for each of these VMS deposits. Although different deposits display slightly different temperature profiles, they show similar patterns in overall temperatures versus time (Fig. 6a).

Spatial Variations

Different ore types have different filling temperatures and salinities of primary fluid inclusions in the same stage. The temperatures decreased upwards from stockwork ores to massive Pb-Zn ores and massive Ag-Pb-Zn ores in the same stage, although the three ores show very similar temperature trends with time (Fig. 6a). This implies that mineralization of massive ores and stockwork ores is related to a common integral hydrothermal solution system driven by a common thermal engine.

The true temperatures of mineralization formation may be obtained by correcting filling temperatures using mineralization pressure or seawater depth and the diagrams for pressure correction (Potter, 1977), using assumed average seawater depth for Kuroko-type VMS deposits in the island arc (ca. 1200 m). It was estimated that the magnitudes of temperature corrections vary from about 10°C to 15°C (Hou, 1988). Consequently, mineralization temperatures are about 275°C, 335°C, and 200°C in stages II, III and IV, respectively, for the Gacun deposit, and 235°C and 132°C in stages II and III, respectively, for the Gayiqong deposit.

The Evolution of Temperature of Ore-forming Fluids

Pisutha-Arnond and Ohmoto (1983) pointed out that the temperatures obtained from fluid inclusion studies represent only the thermal condition of fluids during the time of deposition of host minerals. They suggested that the temperature profiles reflect change with time in the temperature of the discharging fluids, i.e., filling temperature may be the true temperature of ore-forming fluids. It may be argued that the temperature of ore-forming fluids was much higher initially and that mineral precipitation was the result of subsequent cooling of the fluids down to saturation temperature. This means that the true temperature of ore-forming fluids could have remained constant throughout all stages of miner-

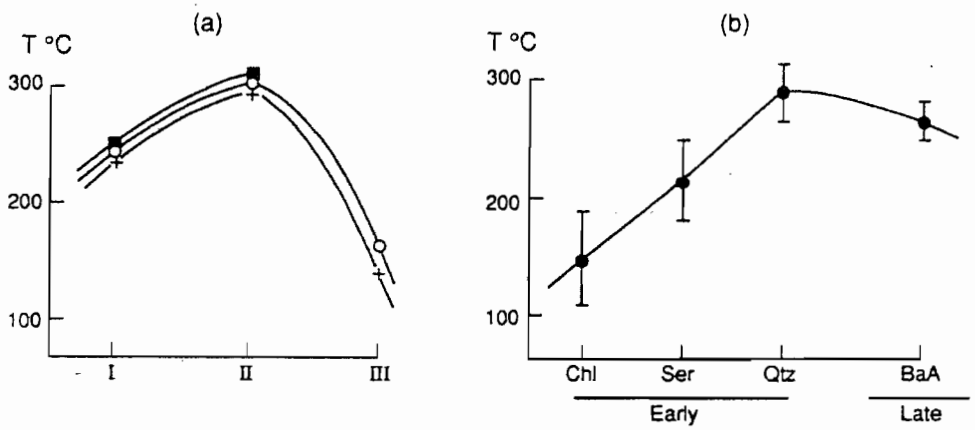

Fig. 6. (a) Temperature profile of ore-forming fluids during mineralization and (b) temperature trend during alteration for Gacun VMS deposit.
■ stockwork ore; 0 massive Zn-Pb ore; + massive Pb-Zn-Ag ore; Chl - chloritization; Ser - sericitization; Qtz - silicification; BaA - barium-adularia alteration

alization, and observed temperature profiles may simply reflect the degree of cooling (by processes such as mixing with cold seawater) necessary to reach saturation of the ore solution during the various stages of mineralization. This idea cannot explain the following data for the VMS deposits in Sanjiang Region: (1) the filling temperatures of fluid inclusions in sphalerites, first precipitated from hydrothermal fluids in stages II and IV, respectively, displayed distinct differences; (2) the salinities of ore-forming fluids in stage IV (T = 200°C) were much higher than those of ore-forming fluids in stage II (T = 275°C); and (3) the majority of quartz was deposited during the peak of ore-forming-fluid thermal history in stage III. It seems that the temperatures of fluid inclusions in various stages indeed represent the temperatures of ore-forming fluids. The rise in temperature of ore-forming fluids from stage II to stage III is responsible for extensive replacement of minerals formed in earlier stages (I and II) by minerals precipitated in a later stage (III). The temperature profiles of ore-forming fluids are in accord with changing trends of temperature with time during alteration (Fig. 6b). These facts show that mineralization of massive and stockwork ores, as well as wall-rock alteration, were all related to a common integrated hydrothermal solution system.

Mineralization Pressure

By determining that NaCl-H_2O fluid in inclusions had a constant filling volume and CO_2 density, pressures during deposition of the Kuroko-type VMS deposits have been estimated in the range of 50 bars to 200 bars (Hou, 1991). The pressure inferred for stockwork ore seems higher (up to 200 bars) than that for massive ores (50 bars to 130 bars). In view of the over-pressure of ore-forming fluids prior to venting on the seafloor, the values of pressure given above correspond to 500 m to 1300 m below sea level.

The existence or absence of evidence for fluid boiling plus *T*-NaCl data of fluid inclusions, coupled with a knowledge of *P-T-V* of solution, is widely used to place constraints on the depth of seawater (Pisutha-Arnond and Ohmoto, 1983). For VMS deposits in Sanjiang Region, no convincing evidence for fluid boiling has been observed. So, using a *P-T* projection of the NaCl-H_2O system (Haar, 1971), an assumed salinity (5% to 20% NaCl), and a temperature of 300°C to 320°C for the ore-forming fluids, a minimum depth of seawater has been estimated in the range 600 m to 1000 m, which is in accord with results estimated using the CO_2 density method. The depth range is shallower than that of formation for Kuroko deposits, Japan (Ohmoto, 1983).

As noted above, Yidun Island Arc developed an intra-arc rifting zone between inner arc and outer arc. The intra-arc rifting resulted in a deep-seawater environment in a narrow foundering zone on the arc. The sedimentary facies show that the thickness of the sediments in the intra-arc rifting zone is at most 1200 m, whereas the thickness is less than 400 m in the outer and inner arcs (Hu et al., 1989). The fitting of estimated minimum depth of seawater with the thickness of sediments in fault-bounded basins within intra-arc rifting zone implies that the deep-seawater environment is necessary to form Kuroko-type VMS deposits in Sanjiang Region. The deposits, however, occur within the intra-arc rifting zone, rather than in the inner arc or outer arc.

Isotope Geochemistry and Possible Ore-forming-fluid Models

Oxygen and Hydrogen Isotopes

Many investigators have discussed the origin of ore-forming fluids for Kuroko deposits based on salinity data, and oxygen, hydrogen, sulfur isotope data (Pisutha-Arnond and Ohmoto, 1983; Ohmoto and Rye, 1974). Sato (1977) and Urabe and Sato (1978) favored magmatic fluids as the sole source of the ore-forming fluids. Bryndzia (1983) strongly suggested the presence of magmatic fluids to explain the high salinity values in fluids for the Kuroko deposits. Ohmoto and Rye (1974), Hattori and Sakai (1979), and Pisutha-Arnond and Ohmoto (1983) emphasized the important role of seawater. Pisutha-Arnond and Ohmoto (1983) suggested

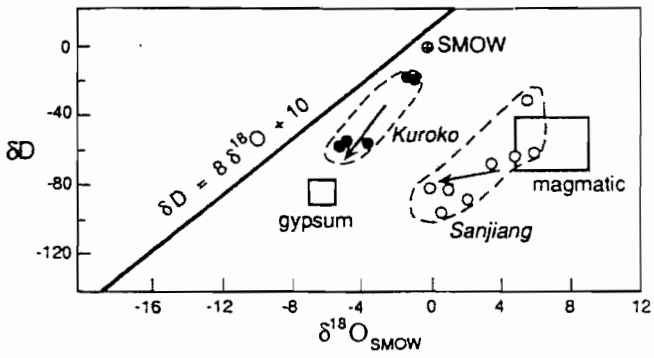

Fig. 7. δD versus $\delta^{18}O$ of ore-forming fluids for Kuroko-type VMS deposits in Sanjiang region.
Open Circles in the figure represent the isotopic composition of ore-forming fluid for Gacun deposit; solid circles for Kuroko deposits.

a model of continuous interactions, during the diagenetic through hydrothermal stages, between pore fluid (seawater) and host rocks to explain some deposit characteristics. This model has been adopted by most investigators. Our data indicate that Ohmoto's model overemphasizes the contribution of seawater in the formation of Kuroko deposits; ore-forming fluids could be mixtures of fluids of magmatic hydrothermal origin and seawater. Moreover, such mixing of the two fluids at different depositional sites in different mixing ratios was responsible for the observed oxygen and hydrogen isotopes and salinity values of the ore-forming fluids for the VMS deposits in Sanjiang Region.

Oxygen and hydrogen isotope compositions of ore-forming fluids have been obtained by two methods: (1) determining oxygen and hydrogen isotopic values of primary fluid inclusions in sulfate (barite) and sulfides, as well as hydrogen isotopic values of fluid inclusions, obtained from quartz by fluid-extraction procedures; (2) using available quartz - water fractionation factors and determining the formation temperatures to calculate oxygen isotopic values. The oxygen and hydrogen isotopic values of ore-forming fluids for the Gacun deposit are listed in Table 3. Oxygen isotopic values of the fluids vary in the range +7.1‰ to +7.5‰ for stockwork ores in Gacun deposit, and are in accord with oxygen isotopic values of the host-rock rhyolites. This shows that $\delta^{18}O$ of ore-forming fluids that formed the stockwork ores is near the zero-value range of the magmatic solution.

δD and $\delta^{18O}O$ values of fluid inclusions in chert lenses or thin layers are −86‰ and +1.2‰, respectively. These chert layers occur in limestone overlying exhalites and massive sulfide ore. They may have precipitated from heated seawater which had circulated through rhyolitic pyroclastic rocks, or from mixing of seawater with a lesser amount of hydrothermal fluids (i.e., exhalative fluids). Oxygen and hydrogen isotopic values of fluid inclusions in chert might represent those of heated seawater or seawater contaminated by exhalitic fluids. Oxygen and hydrogen isotopic values of fluid inclusions in barite, widely considered a typical exhalite that was directly precipitated from the seawater (Kusakabe and Chiba, 1983), are close to those in chert and support the above idea. The values of $\delta^{18}O$ and δD of fluid inclusions in sulfides from massive ores vary in the range +2.6‰ to 5.6‰ and −29‰ to −93.6‰, respectively, and vary between those of seawater and magmatic hydrothermal solution. Figure 7 records the trend of δD and $\delta^{18}O$ of ore-forming fluids in the Gacun deposit.

Using same methods, δD and $\delta^{18}O$ values of fluids that formed stockwork and massive ores in the Gayiqong deposit have been determined, and are −70‰ to −120‰ and +4.5‰ to +6.5‰, respectively. These values are similar to those of ore-forming fluids in the Gacun deposit.

Recent studies have shown that the δD and $\delta^{18}O$ values range from −51‰ to −5‰ for δD and −5.2‰ to −0.7‰ for $\delta^{18}O$ in Kuroko deposits; as well the ranges of both δD and $\delta^{18}O$ values are much larger than those reported from previous work (Pisutha-Arnond and Ohmoto, 1983). These data seem to constitute another trend, which shows decrease in δD and $\delta^{18}O$ values of inclusion fluids from stockwork to massive ores (Fig. 6). The δD and $\delta^{18}O$ values of ore-forming fluids vary between those of "Kuroko fluids" and inclusion fluids in anhydrite and gypsum (Fig. 7). Kusakabe and Chiba (1983) and Watanabe and Sakai (1983) studied $\delta^{18}O$, $\delta^{34}S$, and Sr^{87}/Sr^{86} ratios of anhydrite and gypsum, and suggested that anhydrite and gypsum may have precipitated either from a mixture of seawater and a hydrothermal fluid which was more diluted in ore metals, or from heated seawater which had circulated through volcanic rocks. The δD and $\delta^{18}O$ of fluid inclusions in anhydrite and gypsum may represent those of a mixed solution of seawater and hydrothermal fluid, or of seawater-changed isotope compositions. It seems that the two-stage model suggested by Pisutha-Arnond and Ohmoto (1983) is reasonable. According to the model, our calculation indicates that the model of continuous interaction between pore fluid (seawater) and volcanic host rocks during early diagenetic processes up through the stages of a thermally intensifying hydrothermal system cannot explain the isotope and salinity data of Kuroko-type VMS deposits in Sanjiang Region. This means that the changes in the $\delta^{18}O$ and δD values might be a result of mixing of magmatic hydrothermal solution with various proportions of seawater. The decrease of $\delta^{18}O$ and δD values of fluid inclusions in minerals from stockwork ore to massive ore reflect that seawater/magmatic hydrothermal solution ratios of ore-forming fluids increase from feeder pipe to seafloor. This explanation is not in conflict with *T*-NaCl data and chemical characteristics.

On the basis of these considerations, it is suggested that there are two sources of ore-forming fluids for Kuroko and related VMS deposits, viz., seawater and magmatic hydrothermal solution, which have reacted with host rocks and seawater during convection and discharge within the fractures and interstices of rhyolitic-dacitic pyroclastic rocks.

Sulfur Isotopes and Possible Sulfide Source

Sulfur isotope ratios of sulfate minerals such as barite, anhydrite and gypsum are one of the foundations for the view that there was a large contribution of seawater in the genesis of the Kuroko deposits. In order to estimate the contribution of seawater in the formation of VMS deposits in Sanjiang Region, sulfur isotopes were determined for barite

and sulfides from the Gacun deposit, Gayiqong deposit and Shengmelong deposit (Duan, 1983; Yie et al., 1991).

Sulfur isotope values of the only sulfate mineral present, barite, vary in the range 16‰ to 22‰ in the Sanjiang Kuroko-type deposits, and are comparable to those for barite from the Kuroko deposits, Japan (Kusakabe and Chiba, 1983; Watanabe and Sakai, 1983), and are close to Triassic seawater values. Sulfur isotope values of the sulfides vary in a narrow range and are lower than those from the Kuroko deposits, Japan. For instance, $\delta^{34}S$ values of sulfides vary in the range $-2.8‰$ to $+2.4‰$ for the Gacun deposit, whereas for the Gayiqong deposit, $\delta^{34}S$ values of these sulfides are nearer the zero value.

Watanabe and Sakai (1983) suggested ore-forming fluids in the Kuroko deposits were predominantly Miocene seawater, and that sulfates in the fluids were directly derived from Miocene seawater. Similarities of $\delta^{34}S$ values of barite from VMS deposits in Sanjiang with those of barite from Kuroko deposits in Japan imply a large contribution of seawater to ore-forming fluids and sulfur, whereas $\delta^{34}S$ values of the sulfides and $\delta^{34}S_{\Sigma S}$ values of ore-forming fluids reflect a large contribution of magmatic solution to the formation of sulfide ores in Kuroko-type deposits.

$\delta^{34}S_{\Sigma S}$ values of the ore-forming fluids have been estimated for the Gacun and Gayiqong deposits. These values range from $-0.2‰$ to $+0.5‰$ for stockwork ores, $+1.1‰$ to $4.5‰$ for massive black ores, and $+4.5‰$ to $+9.9‰$ for layered barite ores in the Gacun deposit (Yie et al., 1991; Hou, 1991), whereas the values for sulfide ores in the Gayiqong deposit vary from $-2‰$ to $+2‰$ (Hou, 1991). This indicates that sulfur and ore-forming fluids were derived predominantly from a magmatic hydrothermal solution in the feeder pipe. The exchange of sulfur isotopes between magmatic solution and seawater is in proportion to the amount of seawater in the mixture as mineralization progresses, as deduced by $M\Sigma SO_4^{-2}$ data (Hou, 1991). Sulfur isotope data support the idea that the sulfates in the ore-forming fluids were derived from seawater.

Possible Source of Metals

It has been suggested that the metal composition of VMS deposits shows a close relationship to rock type of the footwall from 1 km to 5 km below the ore horizon (Lydon, 1988; Franklin et al., 1981); Cu-Zn types are associated with basic volcanic rocks, whereas Zn-Pb-Cu types are related to felsic volcanic rocks. Kuroko-type deposits in Sanjiang discovered so far are all of the Zn-Pb-Cu type, consisting of dominant Zn, subordinate Pb and Cu and minor Ag and Au; this implies that the metal source was probably the underlying rhyolitic-dacitic rocks. This idea is supported by the following facts:

1. The felsic volcanic rocks in the districts and in host rocks have high abundance of metal elements, e.g., Cu 16 ppm to 36 ppm, Pb 160 ppm to 168 ppm, Zn 190 ppm to 260 ppm (Hou, 1988). The Cu/Pb, Zn/Pb, and Cu/Zn ratios are in accord with those of the orebodies themselves (Hou, 1988; Yang, 1990).

2. Rhyolitic rocks that occur within layered massive orebodies in thin layers have much less, e.g., Cu 0.02 ppm, Pb 0.1 ppm, Zn 0.32 ppm (Yang, 1990). The lower metal abundances may be related to leaching of the metals by circulating hydrothermal fluids or to strong partitioning of metals from magma into magmatic hydrothermal solution during a hydrothermal stage.

3. Pb isotope ratios of the sulfides in ores from Kuroko-type deposits in Sanjiang are in accord with corresponding ratios of host volcanic rocks, and volcanic rocks in the district (Hou, 1988; Yang, 1990).

Discussion of Genetic Aspects

A tectono-magmatic model proposes that the VMS belt in Sanjiang was controlled by the Yidun Island Arc and its intra-arc rifting zone, that the distribution of ore clusters was restricted to fault-bounded basins within the intra-arc rifting zone, and that the distribution of deposits and orebodies was localized by small, deep, isolated to semi-isolated, submarine sub-basins or depressions within a fault-bounded basin. The model shows that formation of VMS deposits is closely related to extensional or rifting activity. A deep subaqueous volcanic environment active during a period of foundering rather than during constructional calc-alkaline volcanism was necessary to form these VMS deposits. It was estimated that density of the ore-forming fluids varies in the range of 0.8 g/cm^3 to 1.1 g/cm^3. This means that the fluids discharging into seawater would be buoyant in seawater at higher temperatures, and that sulfides would precipitate from the cooling fluids. The development of deep subaqueous basins provided favorable deposition sites for precipitates from a confining pool of the ore-forming fluids for which density increased on mixing with cold seawater.

The host rock - ore - exhalite association is an important genetic aspect of VMS deposits. The fact that ore is associated with certain types of host rocks and exhalites shows that they constitute a sequence closely related to each other genetically during the period of hydrothermal activity and mineralization, and represent the products formed in different stages, i.e., from magmatic to hydrothermal mineralization stages. Recent studies of fluid inclusions indicate the presence of high-salinity fluid inclusions (with NaCl daughter crystals) in quartz from host-rock rhyolite in Gacun district. The measured salinity is 30 wt% to 40 wt% NaCl and homogenization temperature is higher than 350°C (Jin, pers. comm.). This implies the possibility of formation of magmatic hydrothermal solution during the latest period of magma activity. If the measured results are correct, the fluids could lie in the immiscible range in the H_2O-NaCl system up to 1000°C to 1500°C (Bodnar et al., 1985). In other words, the fluids may have generated two immiscible coexistent phases: (1) a high-salinity fluid containing metal components and moving downward; and (2) a low-salinity vapor moving upward. The existence of a majority of high-salinity fluid inclusions and lesser quantities of vapor inclusions in sulfides and quartz from VMS deposits in Sanjiang, and our own isotope data support the possibility of a magmatic hydrothermal solution fractionationing from the magma sys-

tem. It follows that the hydrothermal activity resulted in formation of orebodies and coeval exhalites.

During upward movement of the hydrothermal solution carrying metals, driven by a thermal engine-magmatic system, the solution might have mixed with cold seawater penetrating downwards, and then circulated within volcanic rocks from which more metals were leached to form a mixed fluid, i.e., the ore-forming fluid. During intensifying stages of hydrothermal activity, the hydrothermal solution reacted with volcanic rocks to form chloritization and sericitized zones near discharge centers and precipitated some black-ore minerals (Group I and II), probably by quenching of hot hydrothermal solution by trapped seawater. Metals and H_2S that remained in solution were transported to the sea floor and rapidly precipitated massive black-ore minerals by mixing of hot solution with cold seawater. A thermal maximum being achieved, the hydrothermal solution replaced host rocks to form the silicified zone in the core of the alteration pipe, and mixed with a lesser quantity of seawater to make an ore-forming fluid with higher salinity and elevated Cu content, which replaced and dissolved previously formed black-ore minerals and precipitated yellow or semi-yellow ore. As the temperature of fluids decreased, hydrothermal activity and alteration became weaker. These fluids reacted with volcanic rocks and resulted in further silicification and barium-adularia alteration, overprinted on previous alteration zones. Corresponding exhalative mineralization yielded fine-grained black-ore minerals (Group IV) and barite layers, which interacted with each other.

Rhyolitic-dacitic pyroclastic rocks in a bimodal suite are not just host rocks bearing ores and supplying some metals, but because of their high permeability they also constrained the location of orebodies as lithofacies controlling ores. It is possible that the pyroclastic rocks played a role in changing discharge pathways and in restricting the surface discharge rate of hydrothermal solutions by providing a porous dam (Lydon, 1988).

Acknowledgments

The research was financially supported by the Ministry of Geology and Mineral Resources of China under the research project, The Volcanic Rocks and Related Mineralization in Sanjiang Region. The authors thank Mr. L. Hou, Mr. S. Hu, Mr. Z. Luo, Mr. D. Fu, Mr. M.Xu, and Professor Q. Yie for helping with field work and providing some of the data. This paper was presented at the 8th IAGOD symposium, Ottawa, Canada, August 1990. I.R. Jonasson and J.M. Franklin (Geological Survey of Canada) provided constructive reviews and criticism, and assisted in editing of the final manuscript.

References

BODNAR, R.J., BURNHAM, C.W. and STERNER, S.M., 1985. Synthetic fluid inclusions in natural quartz. III. Determination of phase equilibrium properties in the system H_2O-NaCl to 1000°C and 1500 bars. Geochimica et Cosmochimica Acta, 49, p. 1861-1873.

BRYNDZIA, L.T., 1983. Mineralogy, geochemistry, and mineral chemistry of siliceous ore and alterated footwall rocks in the Uwamuki 2 and 4 deposits, Kosaka mine, Hokuroko District, Japan. Economic Geology Monograph, 5, p. 507-522.

DUAN, KEXUN, 1983. Geological characteristics of Gacun volcanogenic massive sulfide deposits, Sichuan. Contribution to the Geology of the Qinghai-Tibet, No. 13, p. 97-106 (in Chinese).

ELDERIDGE, C.S., BARTON, P.B. and OHMOTO, H., 1983. Mineral textures and their bearing on formation of the Kuroko orebodies. Economic Geology Monograph, 5, p. 241-281.

FRANKLIN, J.M., LYDON, J.W. and SANGSTER, D.F., 1981. Volcanic-associated massive sulfide deposits. Economic Geology 75th Anniversary Volume, p. 485-627.

HATTORI, K. and SAKAI, H., 1979. D/H ratios, origin, and evolution of the ore-forming fluids for the Neogene veins and Kuroko deposits of Japan. Economic Geology, 74, p. 535-555.

HOU, ZENGQIAN, 1988. Late Triassic volcanism and volcanogenic massive sulfide deposits in Yidun Island-Arc, southwestern China. Unpub. Ph.D. dissertation (in Chinese). China University of Geosciences.

HOU, ZENGQIAN, 1990. Magma density and its significance. Petrologica et Mineralogica Acta, 9, p. 309-319 (in Chinese).

HOU, ZENQIAN and MO, XUANXUE, 1990. The evolution of Yidun Island-Arc and implications in the exploration of Kuroko-type VMS deposits in Sanjiang, China. Earth Science, 16, p. 153-164 (in Chinese).

HOU, ZENGQIAN, 1991. Chemistry and thermal evolution of ore-forming fluids and chemical processes of Kuroko-type VMS deposits in Gacun, Western Sichuan. Mineral Deposits, 10, p. 411-423 (in Chinese).

HU, SHIHAU and LUO, ZAIWEN, 1989. Late Triassic volcanism-sedimentation and mineralization in Zengke-Xiangcheng districts, Sichuan. Unpub. research report (in Chinese).

IRVINE, T.N., 1989. A global convection framework: concepts of symmetry, stratification, and system in the Earths dynamic structure. Economic Geology, 84, p. 2059-2114.

KUSAKABE, M. and CHIBA, H., 1983. Oxygen and sulfur isotope composition of barite and anhydrite from the Fukazawa Deposits, Japan. Economic Geology Monograph, 5, p. 292-301.

LYDON, J.H., 1988. Ore deposit models-14. Volcanogenic massive sulfide deposits, part 2: genetic models. Geoscien.. Canada, 15, p. 43-66.

OHMOTO, H., 1983. Chemical processes of Kuroko formation. Economic Geology Monograph, 5, p. 570-604.

OHMOTO, H. and RYE, R.O., 1974. Hydrogen and oxygen isotopic compositions of fluid inclusions in the Kuroko deposits, Japan. Economic Geology, 69, p. 947-953.

PISUTHA-ARNOND, V. and OHMOTO, H., 1983, Thermal history, and chemical and isotope compositions of the ore-forming fluids responsible for the Kuroko massive sulfide deposits in the Hokuroko District of Japan. Economic Geology Monograph, 5, p. 523-558.

POTTER, R.W., II, 1977. Pressure corrections for fluid inclusion homogenization temperature based on the volumetric properties of the system NaCl-H_2O. U.S. Geological Survey Journal of Research, 5, p. 603-607.

SATO, T., 1977. Kuroko deposits: their geology, geochemistry and origin. *In* Volcanic Processes in Ore Genesis. London, Institution of Mining and Metallurgy, Geological Society of London, p. 153-161.

URABE, T. and SATO, T., 1978. Kuroko deposits of the Kosaka mine, Northeast Honshu, Japan products of submarine hot springs on Miocene sea floor. Economic Geology, 73, p. 161-179.

WATANABE, M. and SAKAI, H., 1983. Stable isotope geochemistry of sulfates from the Neogene ore deposits in the Green Tuff Region. Economic Geology Monograph, 5, p. 282-291.

YANG, CHONGQUI, 1990. Geochemistry of the ore-forming fluids in Gacun VMS deposit, Sichuan. Unpub. M.S. thesis (in Chinese).

YANG, KAIHUI and MO, XUANXUE, 1992. Characteristics of the Laochang volcanogenic massive sulfide deposit in Yunnan, southwestern China. Exploration and Mining Geology, 2, this issue, p. 31-40.

YIE, QINGTON, SHI, GUIHA, YIE, JINHUA and YANG, CHONGQIU, 1991. Geological characteristics and metallogenic series of lead-zinc deposits in Sanjiang Region. Beijing Scientific and Technical Publishing House.

Economic Geology
Vol. 86, 1991, pp. 831–846

Genesis of the Daliangzi Pb-Zn Deposit in Sichuan, China

MINGHUA ZHENG

Ore Deposit Section, Chengdu College of Geology, Chengdu, Sichuan, People's Republic of China

AND XIAOCHUN WANG

Southwest Institute of Metallurgical Geology, Chengdu, Sichuan, People's Republic of China

Abstract

Results are given of a detailed study of certain geologic features of the Pb-Zn deposit located at Daliangzi, Sichuan Province, China. The Daliangzi Pb-Zn deposit is strata bound in carbonate rocks. A systematic study of lead and sulfur isotopes, and a cluster and correlation analysis of trace elements (including rare earth elements) in the ores and the surrounding rocks, shows that mineralization was derived from several sources. A study of the hydrogen and oxygen isotopes of the fluid inclusions in sphalerite indicates that the ore-forming fluid belonged to a Ca^{+2}-Mg^{+2}-Cl^{-}-HCO_3^- type of weak acidic to near-neutral pH solution whose salinity was about 4 wt percent NaCl. The fluid had a meteoric source. The ore was formed at a depth of about 1 km at a temperature of about 150° to 200°C during the main stage of ore deposition.

From a comparison between the lead and sulfur isotopes and a study of the metallic complex solubilities, it appears that when hot solutions were passing through the mineralized area the metals and sulfur species were not transported in the same solution. The metals were moved as chloride complexes such as $PbCl_3^-$, $ZnCl_3^-$, and $ZnCl_2$. The metal-bearing solution moved along deep faults to low-pressure zones, where the metal ions reacted with reduced sulfur and were precipitated as sulfides. The textures of the minerals were controlled by the rate at which the reduced sulfur was supplied.

Geologic Features of the Ore District

IN THE Daliangzi ore district, the outcropping strata are the dolomitic ore-bearing Dengying Formation of the upper Sinian series, sandstone and shale formations of Lower Cambrian age, and Quaternary eluvium and alluvium. Sinian-age rocks underlie an uncomformity at the base of the Cambrian rocks.

The Dengying Formation (Fig. 1, Zbd) can be divided into three sections. In the Daliangzi area the lowest section is missing. The middle section (Zbd^2) may be separated into two strata: the first stratum (Zbd^{2-1}), which may be up to 361 m thick, consists mainly of gray algal-laminated dolostone (Fig. 2A and B) in which framboids are occasionally observed. The lead and zinc contents of this dolostone are 49 ppm Pb and 432 ppm Zn. The second stratum (Zbd^{2-2}), as much as 234 m thick, is thin-bedded silty dolostone whose color varies from gray-black to light gray. This dolostone is intercalated with quartz bands and thin-bedded muddy siltstone. Its background lead and zinc values are 49 ppm Pb and 297 ppm Zn. It is an ore-bearing stratum. The upper section (Zbd^3) is made up of thin-bedded to massive dolomite intercalated with gravel and sand, phosphorus-bearing dolostone, phosphate rock, and quartz-banded dolostone. This unit may be as much as 230.37 m thick. Its background lead and zinc concentrations are 229 ppm Pb and 54 ppm Zn. It is another ore-bearing stratum.

The ore district is located in a graben in which there is no folding, but there are many fissures and fractures. Faults F_1 and F_{15} are the largest. They are branches of a regional fault that is 15 to 20 km long and extends into the basement, which consists of metamorphosed rocks of the Huili Group (Pttn). The area to the south of F_1 and to the north of F_{15} is a fault block structure, where there are 40 more faults including two block fracture zones (R_1 and R_2 in Fig. 1). The orebodies are closely related to the fractures and block fracture zones.

No igneous rock crops out in the mine area. On the northwest outer margin of the district, however, the later Permian Emeishan basalts are found.

Mineralization Features

General description

The Daliangzi deposit consists of two orebodies which occur as veins cutting across the bedding. The ore composition is simple. The most abundant metallic minerals are sphalerite, followed by galena, pyrite and chalcopyrite, arsenopyrite, marcasite, freibergite, and pyrargyrite. The gangue minerals are calcite, quartz, and dolomite. The ore has a characteristically high zinc content; the Zn/(Zn + Pb) ratio is larger than 0.9.

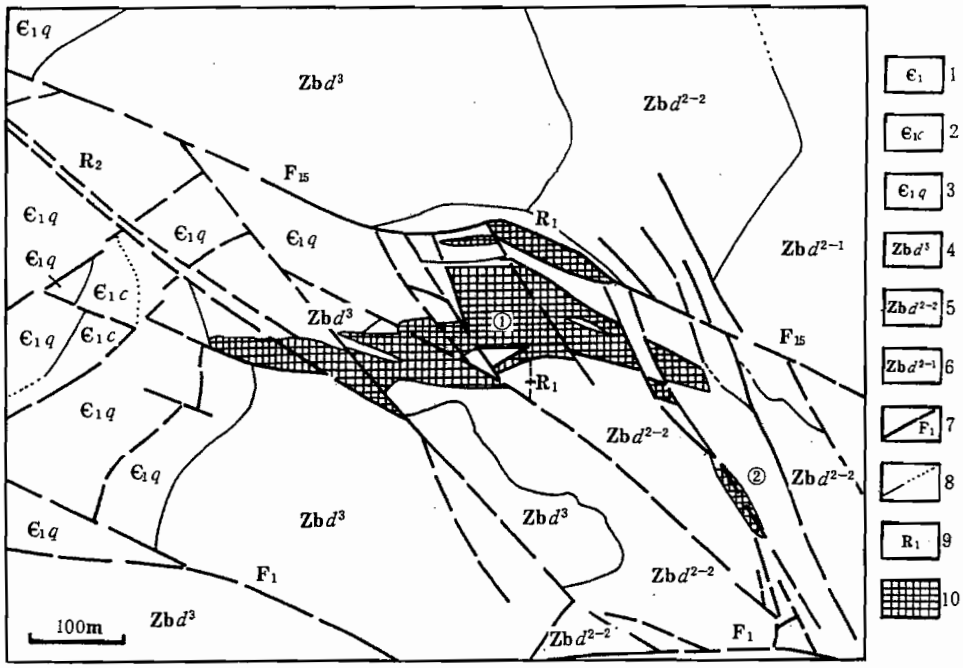

FIG. 1. Geologic plan sketch of the Daliangzi deposit. 1 = Longwangmioa Formation of the Lower Cambrian series; 2 = Canglangpu Formation of the Lower Cambrian series; 3 = Qiongzhusi Formation of the Lower Cambrian series; 4 = upper section of the Dengying Formation of the upper Sinian series; 5 = second stratum of the middle section of the Dengying Formation; 6 = first stratum of the middle section of the Dengying Formation; 7 = faults; 8 = geologic limits; 9 = block fracture zones; 10 = orebodies.

Chemical analysis and electron microprobe analysis of the main metallic minerals reveal that the sphalerite is lacking in iron but is rich in germanium; the Zn/Fe ratio is more than 20; the Ga/In and Ge/Ga ratios are larger than 1. This is analogous to ratios of sphalerite from reworked sedimentary Pb-Zn deposits in carbonate strata. The galena is rich in antimony and silver, and depleted in bismuth, forming an Sb-As association. The Co, Ni, As, and Se contents in the pyrite vary with the kinds of pyrite, but the Co/Ni ratios are all less than 1, indicating a nonmagmatic hydrothermal solution genesis.

The deposit was formed chiefly by open-space filling with replacement being of lesser importance. The main ore structures are brecciated, colloform, vein, and massive; in addition there are vugs (drusy) and disseminated structures. In brecciated structures the dolostone gravels are cemented by either sphalerite or pyrite or both (Fig. 2C). In other areas sphalerite gravels were shattered by later shear processes and subsequently cemented by calcite (Fig. 2D). The colloform structure results from the rapid precipitation of sphalerite during the main stage of ore formation. This rapid precipitation caused the growth of very small grained crystals which formed in concentric and banded grapelike aggregates (Fig. 2E and F). The surface of the ore material is often uneven, exhibiting contraction fissures that intersect the growth rings. The drusy structure is made up of minerals formed at a later stage. As a result of tectonic stresses and solutions, fissures and pores were formed in the early stages of lead and zinc ore formation. The ore-forming solutions filled the fissures and cavities. The minerals with higher idiomorphic values crystallized slowly, forming vugs (Fig. 3A and B) in which the precipitation sequence of minerals is, from first to last, calcite, quartz, sphalerite, galena, and pitchblende.

The textures of the ore can be classified into five groups with 13 varieties. The five groups are sedimentary, crystalline, metasomatic, strain, and inner texture. The sedimentary group typically has a framboidal texture. The microframboids are composed of micropyrite spheres (Fig. 3C), which are 0.025 to 0.075 mm in diameter, and each sphere is made up of numerous euhedral pyrite grains that are less than 1 μm in diameter. Often the framboids are homogenized due to simultaneous recrystallization, with the result that micrograins of sphalerite are found in between the pyrite grains (Fig. 3D). The crystalline texture is related to crystalline ability, time, and space. The minerals with higher crystalline ability such as arsenopyrite often occur as euhedral crystals.

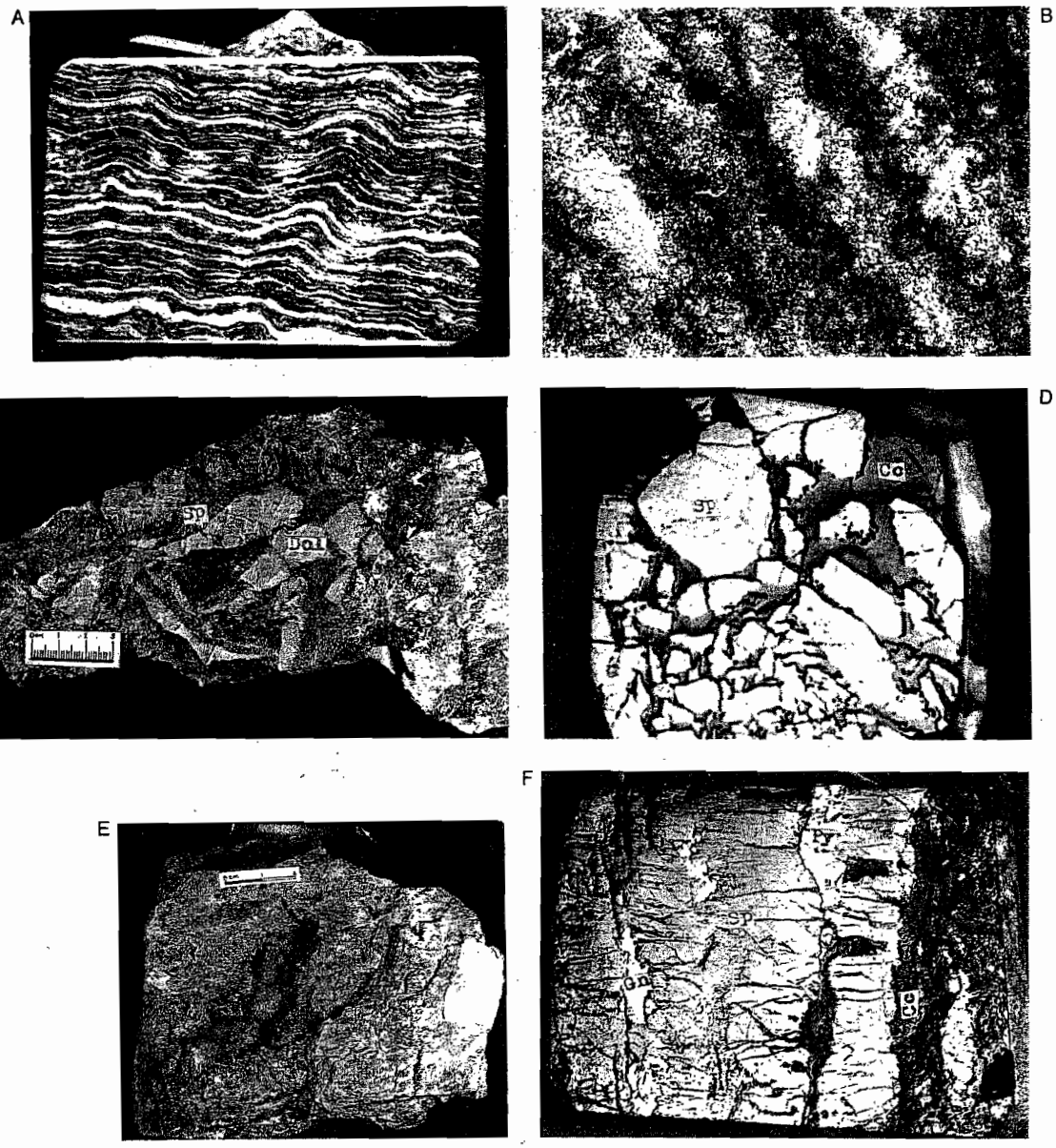

FIG. 2. A. Algal-laminated dolostone. Polished thin section. Size of sample = 4 × 2 cm. B. Algal-laminated dolostone. Polarized light, ×20. C. Brecciated ore composed of brown sphalerite (Sp) cementing dolostone breccia (Dol). D. Brecciated ore composed of calcite (Cc) and dark, fine-grained sphalerite (Sp). Polished thin section. Size of sample is 2.5 × 2.5 cm. E. Grape-form ore made up of dark, fine-grained sphalerite and some galena crystals. F. Banded ore consisting of sphalerite (Sp) in parallel bands and contracting fissures, galena (Gn), pyrite (Py), and calcite (Cc). Polished thin section. Size of sample is 3.5 × 3 cm.

Under certain growth conditions, the minerals with less crystalline ability such as sphalerite and quartz also occur as euhedral crystals (Fig. 3B). The metasomatic texture is mainly evidenced by galena or chalcopyrite or both replacing sphalerite.

The ores generally occur as cavity or fracture fillings in dolomitic wall rocks. The intensity of alteration and the variety of the alteration types is limited. Alteration varieties include recrystallization, silicification, carbonization, and pyritization, which are distributed narrowly in orebodies and wall rocks. The zonation of the alterations is not distinct.

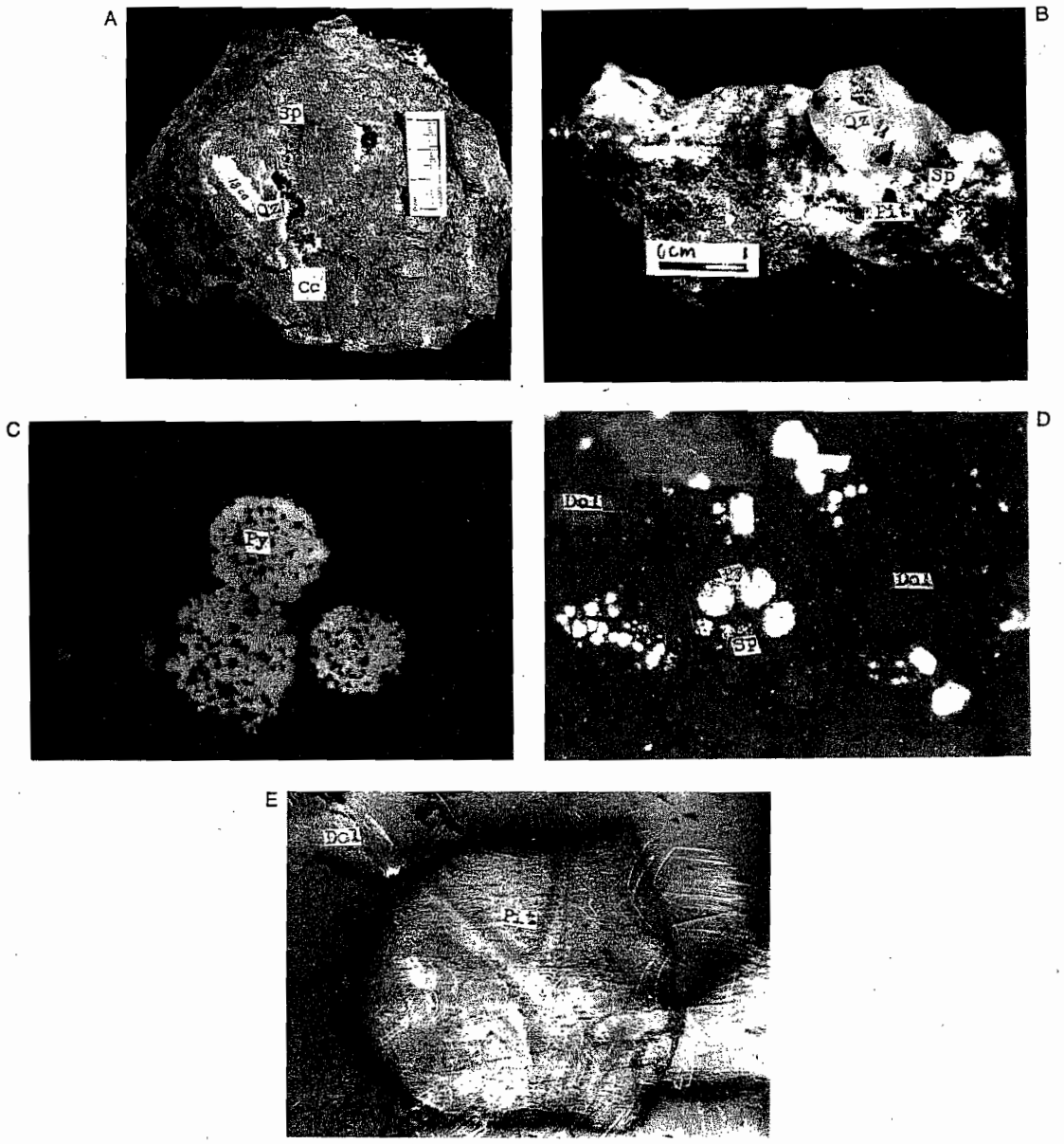

FIG. 3. A. Vugy ore structure composed of quartz (Qz), calcite (Cc), and orange sphalerite, mineral out of the vugs is main-stage sphalerite (Sp). B. Drusy ore consisting of quartz (Qz), orange sphalerite (Sp), and pitch (Pit), which grew along fissures of early mineral assemblages and wall rocks. C. Microframboidal texture of pyrite (Py), ×1,000. D. Microframboidal texture illustrating pyrite (Py) occurring as framboids in dolostone (Dol), among which microsphalerite crystals (Sp) are an infilling, ×1,000. E. Pitch (Pit) filling between dolomite crystals (Dol), ×50.

According to the ore-forming geologic and physicochemical conditions the evolution of the mineralization can be divided into three periods: sedimentary, hydrothermal, and weathering. Minerals formed during the sedimentary periods include mainly dolomite, lesser pyrite (chiefly as framboids), and rare sphalerite.

The hydrothermal period may be subdivided into three stages: pyrite-arsenopyrite, sphalerite-galena, and sphalerite-quartz. In the pyrite-arsenopyrite stage, the mineral association of pyrite + arsenopyrite + chalcopyrite + marcasite + quartz was formed and during the sphalerite-galena stage, the mineral association of sphalerite + galena + chalcopyrite + calcite

TABLE 1. Detailed Sequence of Mineral Formation

Mineral	Sedimentary epoch	Hydrothermal epoch[1] I	Hydrothermal epoch[1] II	Hydrothermal epoch[1] III	Weathering epoch
Dolomite	==========[2]		-----		
Pyrite	---------[3]	==========	-----		
Arsenopyrite		----------	-----		
Quartz		-------	-----	=====	
Sphalerite	-----		==========	=========	
Marcasite		----------	----		
Chalcopyrite		-------	-------		
Galena			=======	====	
Freibergite			------		
Pyrargyrite			------		
Calcite			----	-----	
Pitch	---			----	
Smithsonite					---------
Cerussite					---------
Greenockite					---------
Limonite					-------
Malachite					-------

[1] I, pyrite-arsenopyrite stage; II, sphalerite-galena stage; III, sphalerite-quartz stage
[2] Indicating the most abundant mineral
[3] Indicating the general mineral

+ quartz was formed. In this stage sphalerite has a dark black color and occurs in high-energy forms such as grape and band forms caused by rapid crystallization; chalcopyrite grains were also formed within sphalerite. Galena has inclusions of freibergite. The minerals of a higher idiomorphic degree which formed in the sphalerite-quartz stage include sphalerite, calcite, quartz, and galena. These occur in vugs where the sphalerite is coarse grained; there are no chalcopyrite grains within the sphalerite.

After the deposit formed, it weathered and formed a mineral association composed mainly of smithsonite and cerussite. The detailed sequence of mineral formation is shown in Table 1.

Ore-Forming Mechanism

The Daliangzi Pb-Zn deposit should be classified as Mississippi Valley type. It is analogous to Mississippi Valley-type deposits of North America such as those in southeast Missouri and the upper Mississippi Valley. The main metal ratios and the general geologic features of the Daliangzi ore district also resemble Mississippi Valley-type deposits in east Tennessee which belong to the platform zinc-rich subtype (Sangster,

TABLE 2. Trace Element Content of Ore and Rocks (ppm)

	Stratum[1]	Number of samples	Petrology	Cu	Co	Ni	Cd	Mn	W	Sn	Ag
1	Pttn	3	Phyllite, slate	36	15	31	26	550	21	8	1.09
2	Zbg	1	Muddy limestone	27	24	53	4	1,800	25	8	0.05
3	Zbd	1	Silty dolostone	120	14	12	10	230	21	5	0.35
4	Zbd	2	Laminated dolostone	33	14	12	16	230	21	4	1.65
5	Zbd	2	P-bearing dolostone	39	14	14	367	220	21	19	13.58
6	C1q	1	Silty sandstone	17	14	23	54	750	23	5	0.43
7	P2b	2	Basalt	140	37	81	4	1,500	24	12	
8	Orebody	5	Pb-Zn ore	230	14	21	2,840	290	24	6	115.95
9	Ore	1	Vein Pb-Zn ore	260	14	27	3,300	210	28	8	291.8
10	Ore	1	Massive Pb-Zn ore	380	14	13	6,400	99	21	5	187.57
11	Ore	1	Brecciated Zn ore	150	14	20	1,200	540	24	5	45.48
12	Ore	1	Brecciated Zn ore	130	14	28	1,600	440	22	5	31.55
13	Ore	1	Stockwork Zn ore	240	14	16	1,700	170	25	5	23.55

[1] Some abbreviations correspond to strata shown in Figure 1; P2b = Late Permian basalt; Pttn = Huili Group; Zbg = Doushantuo Formation of the upper Sinian series

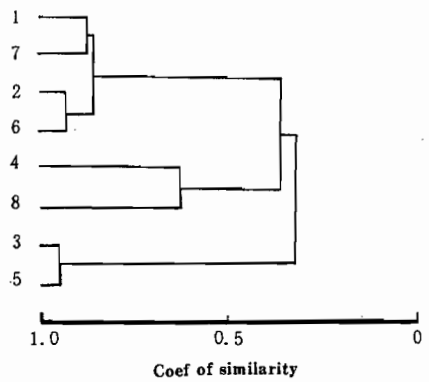

FIG. 4. Q-type cluster tree diagram of ore and rocks. Numbers correspond to those in Table 2.

1983). For a long time, the deposits were interpreted as being magmatic telethermal deposits, in which the ore-forming materials were derived from a deep hydrothermal solution. Since the 1950s when the strata-bound theory was proposed by Maucher (1954, 1965, 1972), many experiments and geologic observations have shown that these deposits formed from hot (saline) water and that the ore-forming materials were derived from the strata and rocks through which the saline solution circulated.

Sources of the Ore-Forming Materials

Metals

The results of Q-type cluster analysis of one orebody and seven wall-rock samples (see Table 2 and Fig. 4) show that the orebody resembles the laminated dolostone of the middle section of the Dengying Formation, but the correlation coefficient results (Table 3) show that the similar coefficients among the ores and rocks are next to one another, which indicates that the metals were not derived from a single stratum.

Rare earth elements are one group of elements whose characteristics are similar to each other and whose properties can be predicted. The authors analyzed the REE contents of ore and rocks at the periphery of the district (Table 4), because the shape of the REE model may indicate the sources of materials, solution chemistry, and water-rock reactions. The chondrite-standardized models are shown in Figure 5. From Table 4 and Figure 5, it can be seen that the ore is analogous to the dolostone of the Dengying Formation in regard to the REE patterns and element contents characteristics. This indicates that there is a certain relationship between them. When Ce/Y values are plotted against Eu/REE values (Fig. 6), it is seen that, except for the Huili Group (Pttn) and metamorphic rock and later Permian basalt (P_2b), the ore and other strata are located in the range of continental crust which is poor in Eu and rich in Ce. This indicates that there is a connection between the ore and continental crust strata.

Table 5 shows that the lead isotope composition of galena varies considerably. The projected points in the plot of the $^{206}Pb/^{204}Pb$ versus $^{207}Pb/^{204}Pb$ ratios (Fig. 7) are narrowly distributed, some are near the average lead evolution line of the orogenic belt and some are above the upper crystal lead line. In the diagram of $^{208}Pb/^{204}Pb$ versus $^{206}Pb/^{204}Pb$ ratios (Fig. 8), the points are also narrowly distributed but are essentially within the range of values characteristic of cratonic lead.

Using the constants: $\lambda_1 = 1.55125 \times 10^{-10}/yr^{-1}$, $\lambda_2 = 9.8485 \times 10^{-10}/yr^{-1}$, $\lambda_3 = 0.4948 \times 10^{-10}/yr^{-1}$ and $a_0 = 9.307$, $b_0 = 10.294$, $c_0 = 29.476$, and $t = 44.3 \times 10$ yr, and applying the single-stage model, the authors calculated the model ages and characteristic values of the source areas (see Table 5). The results indicate that the model ages are generally between 91 and 439 Ma, which coincides with the ages of the Paleozoic, the Sinian series, and the Huili Group although some are dated at 597 to 1050 Ma. The $u(^{238}U/^{204}Pb)$, $w(^{235}Th/^{204}Pb)$, and k(Th/U) values of the source area are high. These data indicate that the ore materials are related to these strata.

Analysis of the normal, unaltered rocks which are distant from the Pb-Zn deposits shows that the metal background values of strata in southwest Sichuan (Fig. 9) indicate that all strata in the area are rich in Pb and Zn and can provide the materials necessary for mineralization.

The Pb, Zn, and Fe in the deposit are derived from the upper crust. In particular, they are derived chiefly from the Paleozoic erathem, especially the upper Pa-

TABLE 3. Similarity Coefficients among Ores and Rocks

	1	2	3	4	5	6	7
9[1]	0.361	0.375	0.144	0.261	0.248	0.395	0.313
10	0.131	0.037	0.048	0.451	0.146	0.017	0.178
11	0.548	0.577	0.340	0.576	0.208	0.659	0.498
12	0.523	0.471	0.315	0.522	0.239	0.482	0.488
13	0.332	0.316	0.095	0.370	0.168	0.398	0.324

[1] Numbers correspond to those in Table 2

TABLE 4. Rare Earth Element Contents of Ore and Rocks (ppm)

	Stratum[1]	Petrology	La	Ce	Pr	Nd	Sm	Eu	Gd	Tb	Dy	Ho	Er	Tm	Yb	Lu	Y	Sc	La/Sm	Sm/Lu
1	Pttn	Phyllite	11	19	3.6	17	3.9	1.9	3.9	0.46	3.2	0.53	1.7	0.18	1.3	0.19	19	3.0	2.8	20.5
2	Zbg	Muddy limestone	17	24	4.7	16	3.2	0.68	2.9	0.48	2.8	0.45	1.7	0.19	1.3	0.18	13	2.8	5.3	17.8
3	Zbd	Dolostone	1.6	2.0	0.53	0.9	0.22	0.042	0.17	0.061	0.10	0.029	0.077	0.023	0.063	0.021	0.57	0.07	7.3	10.48
4	P_2b	Basalt	28	37	7.6	33	6.2	2.3	5.3	0.50	3.8	0.54	1.9	0.20	1.2	0.18	19	8.0	4.5	34.4
5	P_2b (1q	Sandstone	19	28	4.1	17	5.3	1.0	3.0	0.50	3.2	0.52	1.8	0.23	1.7	0.24	19	4.8	3.5	22.1
6	Ore	Zn ore	1.1	2.0	0.36	0.9	0.30	0.026	0.28	0.071	0.19	0.045	0.10	0.028	0.10	0.0074	0.9	0.08	3.7	40.54
7	Chondrite[2]		0.32	0.94	0.12	0.60	0.20	0.073	0.31	0.05	0.31	0.073	0.21	0.033	0.19	0.031	1.96			

[1] Some abbreviations correspond to strata shown in Figure 1; P2b = Late Permian basalt; Pttn = Huili Group; Zbg = Doushantuo Formation of the upper Sinian series
[2] The chondrite values are from Wedepohl (1970)

leozoic erathem, and secondly, from the ore-bearing strata (the Dengying Formation of Sinian system) and the underlying basement (the Huili Group). The late Permian Emeishan basalt may also provide some material.

Sulfur

The $\delta^{34}S$ values of sulfides in the deposit range from −6.5 to +15.1 per mil; the sulfur isotope compositions vary with the ore-forming stages (Table 6). The values of sedimentary pyrite vary considerably, which indicates the reduction of seawater sulfate by bacteria. The pyrite in the pyrite-arsenopyrite stage is rich in ^{34}S, with $\delta^{34}S$ values that correspond to that of seawater sulfate during Dengying time (about 20‰), indicating that seawater is the sulfate source of the sulfur.

The sulfur isotope composition of sulfides in the sphalerite-quartz stage is analogous to that of the sphalerite-galena stage, the $\delta^{34}S$ value ranges are narrow, indicating a near-equilibrium condition among the minerals. A study of sphalerite-galena pairs reveals that the $\delta^{34}S$ value of the ore-forming solution in the sphalerite-galena stage is 18.03 per mil which is close to that of seawater sulfate. During the sphalerite-galena stage, the temperature ranged from 200° to 150°C (see next section). Under such high temperature, the sulfur isotope composition cannot be explained by bacterial reduction of sulfate. The authors found pitch among carbonate crystals in the ore district (Fig. 3E). Pitch is generally regarded as resulting from decomposition of organic matter. At the same time, there was sedimentation of sulfates such as gypsum. Under the higher temperatures, the sulfate solution flowed through the carbonate rock layers and the sulfates were reduced by the organic matter to produce H_2S. In addition, sedimentary pyrite may also have provided some sulfur (biogenic sulfur).

In general the ultimate source of the sulfur in all stages is seawater sulfate, but the reducing mechanisms are different.

Carbon

In order to determine the source of the carbon, a study of rare earth elements was done. The analyzed ore samples in this paper are composed of Pb and Zn sulfide minerals, plus a few samples of calcite. Generally the amount of REE is very small in the sulfides. The REE content is very difficult to determine by modern analytic techniques, therefore, calcite was analyzed for REE (Table 4). The amount of Eu in calcite is also low (compared with chondrite), which is analogous to the condition in the second type of calcite in the lead-zinc veins of western Hartz, Germany (Moller et al., 1979), where the calcite (as well as the sulfides) was derived from heated wall rocks.

When the deposit was formed, the ore solution may

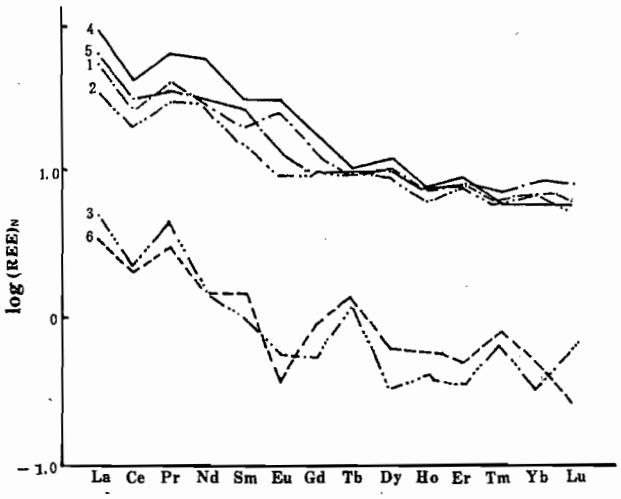

FIG. 5. The rare earth element distribution models of ore and rocks. Numbers correspond to those in Table 4.

have reacted with the host rock. If minerals in the host rocks were dissolved, their components may have been released into solution, forming a REE model similar to that of the host rocks, i.e., the ratio of La to Sm is 7.3, and that of Sm to Lu is 10.48. As a result of fractionation, the model of the carbonate minerals is different from that of the solution from which the carbonate minerals were precipitated. Compared to the fractionation experiment on calcite by J. L. Graf (1984), the La/Sm ratio in the ore calcite is 17 percent greater and the Sm/Lu ratio 35 percent less. Therefore, the ratios of La/Sm and Sm/Lu of the calcite precipitated from the host-rock solution should be 8.54 and 6.81, respectively, which is not in accord with the analytic results (Table 4). This indicates that the carbon was not derived from the host rocks. A study of the area geology and REE suggests that the carbon was derived from Paleozoic marine carbonate rocks.

Water

Through a determination of the oxygen isotope composition of quartz associated with sphalerite and of the hydrogen isotope composition of inclusion water in the quartz, the isotopic composition of the original solution can be projected in the plot of δD versus $\delta^{18}O$ (Fig. 10). The plotted point of the test sample is far from that of magmatic and metamorphic water but is close to that of geothermal water, including Salton Sea water. The water is likely to have been derived from a meteoric source.

Physico-Chemical Condition of Mineralization

Character of the ore-forming solution

Microscopic study reveals that there are a few of inclusions in the minerals and that the inclusions are small, generally less than 3 μm in diameter. Their vapor/liquid ratios range from 2 to 10 and there are no daughter mineral crystals. Selected under binocular microscope, the pure sphalerite particles were

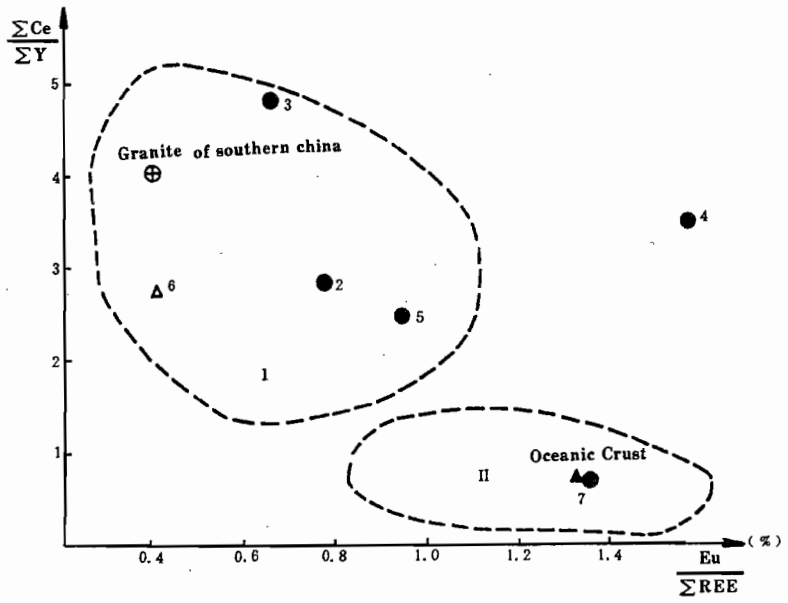

FIG. 6. Plot of the Ce/Y versus Eu/REE ratio of ore and rocks. I = continental crust type, II = oceanic crust type. Numbers correspond to those in Table 4 (from Wang et al., 1982).

TABLE 5. Lead Isotope Characteristics of Galena

	$\frac{^{206}Pb}{^{204}Pb}$	$\frac{^{207}Pb}{^{204}Pb}$	$\frac{^{208}Pb}{^{204}Pb}$	Source values u	w	k	Model age (Ma)	Reference
1	18.4855	15.7715	38.8305	9.774	40.736	4.033	309	This paper
2	18.6170	15.8815	39.2472	9.970	42.855	4.159	341	
3	18.9693	15.8534	39.5863	9.920	42.031	4.100	91	
4	18.667	15.693	38.994	9.634	39.696	3.987	106	
5	18.290	15.740	38.481	9.718	40.000	3.983	398	S. Yuexin (pers. commun.,
6	18.229	15.675	38.380	9.602	39.294	3.960	369	1988)
7	18.386	15.839	38.818	9.895	41.833	4.096	439	
8	18.1195	15.5612	38.2070	9.399	38.095	3.922	318	Team 603 of Southwestern
9	17.6868	15.2171	37.2740	8.786	33.096	3.667	218	Corporation of
10	18.0347	15.4624	37.7601	9.222	35.724	3.748	264	Metallurgy and Geology
11	18.3614	15.5596	38.2570	9.396	37.006	3.811	156	(unpub. data, 1981)
12	18.0072	15.4440	37.7473	9.190	35.651	3.754	261	
13	18.0932	15.5386	38.1441	9.358	35.758	3.904	310	
14	19.1472	16.4825	40.4438	11.043	51.000	4.469	597	Song and Qian (1985)
15	23.0718	19.8168	48.9273	16.993	101.641	5.788	1050	

cleaned by various methods. At a temperature of 300°C, the minerals decrepitate. The gaseous species in inclusions were analyzed immediately by a mass spectrometer, SC-8. The liquid species were extracted by means of the ultrasonic method and analyzed by a Hitachi 180-80 polarized Zeeman atomic adsorption spectrometer. The results (Table 7) reveal that the salinity of the inclusion solution is low (4.21 wt % NaCl), and its composition is of the Ca-Mg-Cl-HCO_3 type, which is similar to that of percolating water in carbonate rock areas but is different from Mississippi Valley-type ore-forming fluids. This is a distinct characteristic of the deposit.

Temperature

The temperatures of the ore-forming stages were determined by (1) a sulfur isotope thermometer of the sphalerite-galena pair, (2) the homogenization and decrepitation temperature measurement of inclusions in the minerals, (3) the Ge/Ga ratio thermometer of sphalerite (Moller, 1987), (4) the Na-K-Ca thermometer of geothermal water and inclusion water (Fournier, 1973), and (5) the trace element association characteristics of sphalerite and galena (see Table 8).

Fugacity of species

According to the mineral association, the sphalerite-galena stage has pyrite, arsenopyrite, and chalcopyrite and no magnetite, pyrrhotite, hematite, and bornite, so that the following reactions may be constructed:

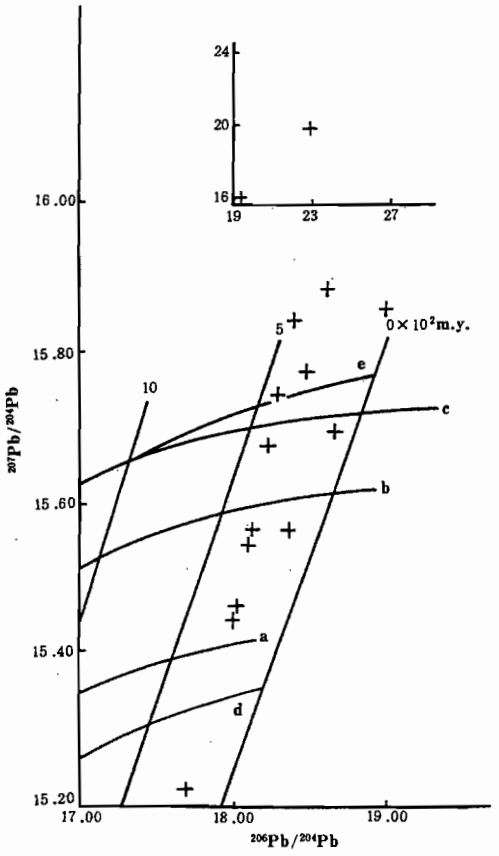

FIG. 7. Plot of the $^{207}Pb/^{204}Pb$ versus $^{206}Pb/^{204}Pb$ ratios of galena. a, b, c = average lead evolution lines of the mantle, orogenic belt, and upper crust, respectively (Doe, and Zartman, 1979); d and e = single-stage evolution lines; the μ values are 8.99 and 9.74, respectively.

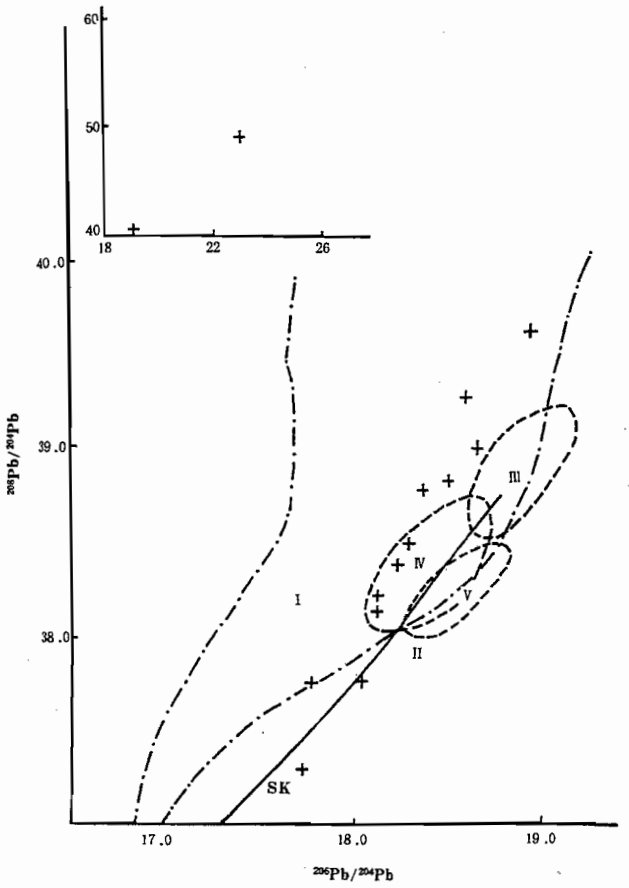

FIG. 8. Plot of the $^{208}Pb/^{204}Pb$ versus $^{206}Pb/^{204}Pb$ ratios of galena. I = cratonic crustal lead, II = oceanic volcanic lead, III = deep-sea sedimental lead, IV = mature island-arc lead, V = primary island-arc lead, VI = noncratonic crystal lead (Chen et al., 1980), SK = two-stage evolution line.

TABLE 6. The $\delta^{34}S$ Values of Sulfides in Ore-Forming Stages

Stage	Sulfide	$\delta^{34}S$ (‰)
Syngenetic-diagenetic	Pyrite (2)[1]	−6.5 to −15.1
Pyrite-arsenopyrite	Pyrite (1)	16.37
	Sphalerite (6) (D)[2]	+10.51 to −14.1[3]
		12.43
Sphalerite-galena	Sphalerite (1) (M)	12.48
	Galena (4)	+8.34 to −10.9
		10.8
Sphalerite-quartz	Sphalerite (3) (L)	+12.56 to −14.99
		13.62

[1] Number in parentheses is the number of samples
[2] D, M, and L indicate the color of sphalerite, i.e., deep, middle, and light, respectively
[3] Numerator and denominator indicate the range and average values, respectively

$$FeS_{(s)} + 0.5S_{2(s)} = FeS_{2(s)},$$

$$5CuFeS_{2(s)} + S_{2(g)} = Cu_5FeS_{4(s)} + 4FeS_{2(s)},$$

$$2FeS_{2(s)} + 1.5O_{2(g)} = Fe_2O_{3(s)} + 2S_{2(g)},$$

$$3FeS_{2(s)} + 2O_{2(g)} = Fe_3O_{4(s)} + 3S_{2(g)},$$

$$3FeS_{(s)} + 2O_{2(g)} = Fe_3O_{4(s)} + 1.5S_{2(g)},$$

$$Fe_{(s)} + 0.5S_{2(g)} = FeS_{(s)},$$

$$3Fe_{(s)} + 2O_{2(g)} = Fe_3O_{4(s)},$$

$$3Fe_2O_{3(s)} = Fe_3O_{4(s)} + 0.5O_{2(g)},$$

$$FeS_{2(s)} + As_{(s)} = FeAsS_{(s)} + 0.5S_{2(g)},$$

and

$$Fe_3O_{4(s)} + 3As_{(s)} + 1.5S_{2(g)} = 3FeAsS_{(s)} + 2O_{2(g)},$$

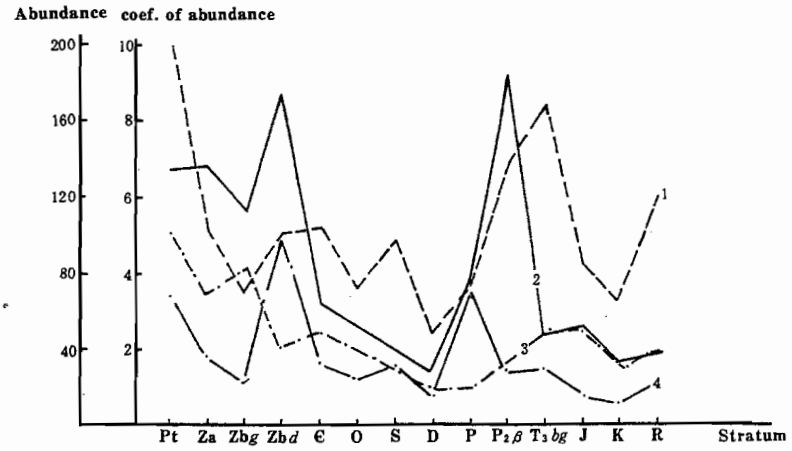

FIG. 9. The Pb and Zn background values of strata in the southwest of Sichuan province. 1 and 3 = the abundances of Zn and Pb; 2 and 4 = the abundance coefficients of Pb and Zn.

TABLE 7. Compositions of Inclusions in Dark Brown Sphalerite (in mg/10 g mineral samples)

Sample no.	K^+	Na^+	Mg^{+2}	F^-	Cl^-	HCO_3^-	H_2O	H_2	N_2	CO_2	CO	CH_4	Salinity (wt % NaCl)
T_{1-5}	0.043	0.049	0.387	0.07	0.750	0.592	47.0	Trace	0.054	Trace	0.011	0.138	4.21

Analyzed by the Analytical Center of Chengdu College of Geology, China

in which (s) and (g) and in later reactions, (l) and (aq), represent solid, gas, liquid, and aqueous components, respectively. From thermodynamic principles the changed value ($\Delta G^P_{T,R}$) of Gibbs free energy of a chemical reaction (R) at a given temperature (T) and pressure (P) can be calculated by the following formula:

$$\Delta G^P_{T,R} = \sum \Delta G^P_{T(\text{product})} - \sum \Delta G^P_{T(\text{reactant})}. \quad (1)$$

When the reaction reaches equilibrium,

$$\Delta G^P_{T,R} = -2.303RT \log K, \quad (2)$$

in which K is the equilibrium constant of the reaction. The Gibbs free energy of minerals may be found in Chuanxian Ling et al. (1985), and using equations (1) and (2), we can produce the diagram of log f_{S_2}-log f_{O_2} in the Fe-S(As)-O system during the sphalerite-galena stage (Fig. 11). It can be seen from the diagram that in the sphalerite-galena stage the range of log f_{S_2} is −16.42 to −18.60 and the mean value is −17.51.

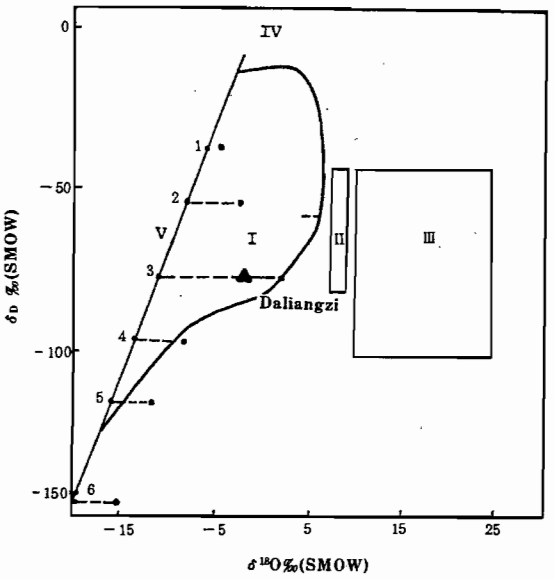

FIG. 10. Plot of $\delta^{18}O$ versus δD of various waters. I = geothermal water, II = magmatic water; III = metamorphic water; IV = marine water; V = meteoric water; modern geothermal areas: 1 = Wairakei, New Zealand; 2 = Larderello, Italy; 3 = Salton Sea; 4 = Lassen Park; 5 = Steamboat Springs; 6 = Yellowstone (from Borshchershiy, 1980); ▲ = ore-forming fluid.

Furthermore, it may be assumed that when captured in inclusions the gases were mixed ideal gases, which fit the Dalton partial pressure law. The fugacity coefficients of species may be obtained by the Newton graphic method (Fu et al., 1979). The fugacity of species such as CO_2, H_2, N_2, CO, and CH_4 in the sphalerite-galena stage may be calculated from the composition results of the inclusions (Tables 7 and 9). The f_{O_2} may be obtained from the following reaction:

$$CH_{4(g)} + 2O_{2(g)} = CO_{2(g)} + 2H_2O_{(l)}$$

so that

$$\log f_{O_2} \doteq 0.5\left(\log \frac{f_{CO_2}}{f_{CH_4}} + \frac{\Delta G_T}{0.0045T}\right).$$

pH

As mentioned above, quartz and calcite both occur in the sphalerite-galena stage. In general, quartz dissolves in alkaline solutions and precipitates in acids, which indicates that the pH values of solutions from which quartz precipitates are lower than the neutral

TABLE 8. Physico-Chemical Parameters of the Sphalerite-Galena Stage

Parameter unit	Sphalerite-galena stage
T, °C	200–150
P, atm	400
pH	5.73±
Eh, v	−0.254
f_{S_2}, atm	3.09×10^{-18}
f_{O_2}, atm	4.91×10^{-46}
f_{CO_2}, atm	5.00×10^{-3}
$a_{\Sigma S}$, mole	1.95×10^{-6}
$a_{\Sigma C}$, mole	5.01×10^{-6}
a_{Cl^-}, mole	0.2291
a_{F^-}, mole	0.0398

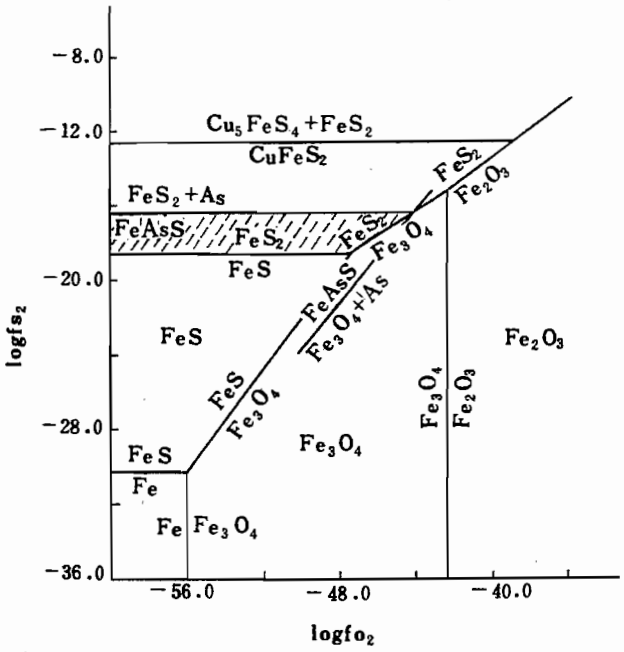

FIG. 11. Plot of log f_{S_2} − log f_{O_2} in the sphalerite-galena stage (T = 175°C).

pH value of water (H_2O) under the same conditions. On the other hand, the pH values of solutions from which calcite is precipitated are higher than the neutral pH value of water. Using the equilibrium constant of the decomposition of water at a temperature of 175°C, the pH value of the solution during the sphalerite-galena stage may be predicted as being above 5.73.

Activity of species

The activities of Cl^- and F^- may be computed directly from the composition of the fluid in inclusions (Table 7). The activities of sulfur atomic groups in the ore-forming solution can be calculated from the following reactions:

$$H_2S_{(aq)} + 0.5O_{2(g)} = H_2O_{(l)} + 0.5S_{2(g)},$$

$$K_1 = \frac{0.5 \log f_{S_2}}{a_{H_2S} \cdot 0.5 \log f_{O_2}},$$

$$H_2S_{(aq)} = H^+_{(aq)} + HS^-_{(aq)},$$

$$K_2 = a_{H^+} \cdot a_{HS^-}/a_{H_2S},$$

$$HS^-_{(aq)} = H^+_{(aq)} + S^{-2}_{(aq)},$$

$$K_3 = a_{H^+} \cdot a_{S^{-2}}/a_{HS^-},$$

$$0.5S_{2(g)} + 1.5O_{2(g)} + H_2O_{(l)} = HSO^-_{4(aq)} + H^+_{(aq)},$$

$$K_4 = a_{HSO_4^-} \cdot a_{H^+}/0.5 \log f_{O_2} \cdot 1.5 \log f_{O_2},$$

$$HSO^-_{4(aq)} = H^+_{(aq)} + SO^{-2}_{4(aq)},$$

and

$$K_5 = a_{H^+} \cdot a_{SO_4^{-2}}/a_{HSO_4^-}.$$

The total activity of sulfur species in the solution ($a_{\Sigma S}$) is given in the following reaction:

$$a_{\Sigma S} = a_{H_2S} + a_{HS^-} + a_{S^{-2}} + a_{HSO_4^-} + a_{SO_4^{-2}}.$$

In the same way the total activity of the carbon species in the ore-forming solution may also be calculated (see Table 8).

Eh

The value of Eh may be calculated from the following reactions:

$$CH_{4(g)} = H_2O_{(l)} = CO_{(g)} + OH^+_{(aq)} + 6e \quad (3)$$

and

$$CH_{4(g)} + 2H_2O_{(l)} = CO_{2(g)} + 8H^+_{(aq)} + 8e. \quad (4)$$

For reaction (3),

$$Eh_1 = E_{1,0} + 3.3 \times 10^{-5}T\left(\log \frac{f_{CO_2}}{f_{CH_4}} - \log a_{H_2O} - 6pH\right)$$

and for reaction (4),

$$Eh_2 = E_{2,0} + 2.48 \times 10^{-5}T\left(\log \frac{f_{CO_2}}{f_{CH_4}} - 2 \log a_{H_2O} - 8pH\right).$$

From the results (Table 8) it can be seen that the Eh value is low.

Migration and Precipitation of Ore Materials

The transport mechanism of Mississippi Valley-type ore has been disputed for a long time. Some investigators emphasize that the metals were transported as

TABLE 9. Fugacity of Species in the Sphalerite-Galena Stage (log f_i)

Species (i)	H_2	N_2	CO_2	CO	CH_4	O_2
log f_i	−0.7055	0.3715	−2.3013	−1.1255	0.1990	−45.4229

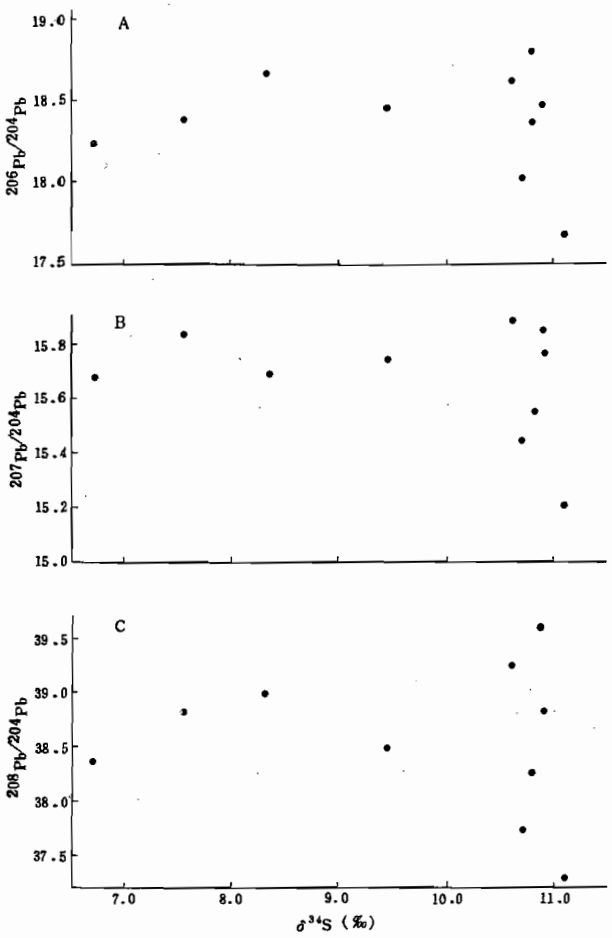

FIG. 12. Scatter diagrams for $^{206}Pb/^{204}Pb$ (A), $^{207}Pb/^{204}Pb$ (B), and $^{208}Pb/^{204}Pb$ (C) versus $\delta^{34}S$.

bisulfide complexes in alkalic solutions, while others such as Helgeson (1964, 1969) believe that lead and zinc migrated as chloride complexes in an acidic solution. There is also disagreement as to whether or not the metals and the sulfur were transported together, so it is necessary to discuss this problem in connection with the Daliangzi deposit.

Based on the obvious correlation between the radiogenic lead and the lighter sulfur in galena at the Buick mine in southeast Missouri, Sverjensky (1981) proposed that lead and sulfur moved in the same solution. The present authors made a similar comparison and found that the correlation coefficients between the $\delta^{34}S$ and $^{206}Pb/^{204}Pb$, $^{207}Pb/^{204}Pb$, and $^{208}Pb/^{204}Pb$ were 0.301, −0.292, and −0.139, respectively, all of which are less than the critical correlation coefficient (0.632) when the degree of confidence is 0.05 and the degree of freedom is 8 (see Fig. 12), indicating that there is no correlation between them. Therefore, it can be deduced that the lead and the sulfur were not transported in the same solution and that there was little reduced sulfur in the lead-bearing solution before mineralization.

It is known that there were anions such as Cl^-, F^-, HCO_3^-, CO_3^{-2}, HS^-, and $H_2S_{(aq)}$ in the ore-forming solution (Table 7), which may be complexed with cations of Pb^{+2} and Zn^{+2}. The solubilities of lead and zinc may be written as follows:

$$\sum M_{Pb} = M_{Pb^{+2}} + M_{PbCl^+} + M_{PbCl_2^0} + M_{PbF} + M_{PbF_2^0} + M_{PbF_3^-} + M_{Pb(HS)_2^0} + M_{Pb(HS)_3^-} + M_{PbHCO_3} + \cdots$$

and

$$\sum M_{Zn} = M_{Zn^{+2}} + M_{ZnCl^+} + M_{ZnCl_2^0} + M_{ZnCl_3^-} + M_{ZnF^+} + M_{ZnF_2^0} + M_{ZnF_3^-} + M_{Zn(HS)_2^0} + M_{Zn(HS)_3^-} + \cdots.$$

$M_{Zn^{+2}}$ can be determined by the following reaction:

$$M_{Zn_{+2}} = ZnS_{(s)} + 2H^+_{(aq)} + H_2S_{(aq)}$$

so that

$$\log M_{Zn^{+2}} = \log K - 2pH - \log a_{H_2S} - \log \gamma_{Zn^{+2}},$$

in which $\gamma_{Zn^{+2}}$ is the activity coefficient of the Zn^{+2} ion, which may be obtained from Table 10. K is the equilibrium constant of the reaction, which may be obtained from relative references. Using the data in Table 8, $M_{Zn^{+2}} = 2.8 \times 10^{-6} m$. The results of other species can be calculated in the same way and are listed in Tables 11 and 12.

It can be seen from the data in Tables 10 and 11 that the chloride complexes account for 99 percent of the total metal solubility, all the other complexes together are less than 1 percent. Assuming that at least 10 ppm Pb or Zn must be deposited as sulfide from the solution before an orebody can form, it can be seen that the complexes conforming to this condition are only chloride complexes such as $PbCl_3^-$,

TABLE 10. Activity Coefficients of Soluable Species (ion intensity = 0.5 and temperature = 175°C; Helgeson, 1964)

Species (i)	Pb^{+2}	Zn^{+2}	$PbCl^+$	$PbCl_3^-$	$PbCl_2^0$	Cl^-
Activity coefficient	−3.8	−2.4	−0.25	−0.24	−0.31	−0.28

The following are also assumed: $\gamma ZnCl^+ = \gamma PbCl^+$, $\gamma ZnCl_2^0 = \gamma PbCl_2^0$, $\gamma ZnCl_3^- = \gamma PbCl_3^-$, $\gamma F^- = \gamma Cl^-$, γ other species = 1

TABLE 11. Lead Complex Solubilities in the Sphalerite-Galena Stage

	Reaction	Species (i)	Molarity (m_i)	Percentage ($m_i/\epsilon m_i \times 100\%$)	Reference for K value
1	$PbS_{(s)} + 2H^{+}_{(aq)} = Pb^{+2}_{(aq)} + H_2S_{(aq)}$	Pb^{+2}	7.0×10^{-7}	1.8×10^{-3}	a
2	$Pb^{+2}_{(aq)} + Cl^{-}_{(aq)} = PbCl^{+}_{(aq)}$	$PbCl^{+}$	9.0×10^{-9}	2.3×10^{-4}	b
3	$PbCl^{+}_{(aq)} + Cl^{-}_{(aq)} = PbCl^{0}_{2(aq)}$	$PbCl^{0}_{2}$	9.7×10^{-6}	0.2419	b
4	$PbCl^{0}_{2(aq)} + Cl^{-}_{(aq)} = PbCl^{-}_{3(aq)}$	$PbCl^{-}_{3}$	4.0×10^{-3}	99.7390	b
5	$Pb^{+2}_{(aq)} + F^{-}_{(aq)} = PbF^{+}_{(aq)}$	PbF^{+}	8.0×11^{-11}	2.0×10^{-6}	a
6	$PbF^{+}_{(aq)} + F^{-}_{(aq)} = PbF^{0}_{2(aq)}$	PbF^{0}_{2}	6.0×10^{-10}	1.5×10^{-5}	a
7	$PbF^{0}_{2(aq)} + F^{-}_{(aq)} = PbF^{-}_{3(aq)}$	PbF^{-}_{3}	6.2×10^{-8}	1.5×10^{-3}	a
8	$Pb^{+2}_{(aq)} + 2H^{+}_{(aq)} + 2S^{-2}_{(aq)} = Pb(HS)^{0}_{2(aq)}$	$Pb(HS)^{0}_{2}$	9.8×10^{-15}	2.4×10^{-10}	c
9	$PbS_{(s)} + 2H_2S_{(aq)} = PbS(H_2S)^{0}_{2}$	$PbS(H_2S)^{0}_{2}$	8.7×10^{-17}	2.2×10^{-12}	d
10	$Pb^{+2}_{(aq)} + HCO^{-}_{3(aq)} = PbHCO^{+}_{3(aq)}$	$PbHCO^{+}_{3}$	1.5×10^{-12}	3.7×10^{-8}	e
11	$Pb(HS)^{0}_{2(aq)} + H^{+}_{(aq)} + S^{-2}_{(aq)} = Pb(HS)^{-}_{3(aq)}$	$Pb(HS)^{-}_{3}$	1.9×10^{-21}	4.7×10^{-17}	c

a = Naumov et al. (1974), b = Seward (1984), c = calculated from Rafal'sky, d = Barnes (1979), e = Leleu (1978)

$ZnCl^{-}_{3}$, and $ZnCl^{0}_{2}$. Therefore, the lead and sulfur were not transported in the same solution. The lead was moved as a chloride complex in a weak acidic to alkalic solution.

But how were the metals which were transferred as chloride complexes precipitated as sulfides? They must have been reduced by sulfur. As mentioned above, the ultimate source of sulfur is seawater sulfate, which can be classified as nonbiogenic sulfur resulting from sulfate reduced by methane (formed from the decomposition of organic matter) and as biogenic sulfur which occurs as framboidal pyrite. The reactions for the reduction of metal chlorite complexes can be written as (taking Pb as an example):

$$CaSO_{4(s)} + PbCl^{-}_{3(aq)} + CH_{4(g)} + H_2SiO^{-2}_{4(aq)}$$
$$= PbS_{(s)} + CaCO_{3(s)} + SiO_{2(s)} + 3H_2O_{(l)} + 3Cl^{-}_{(aq)}$$

and

$$FeS_{2(s)} + 2PbCl^{-}_{3(aq)} + 4e$$
$$= 2PbS_{(s)} + Fe^{+2}_{(aq)} + 6Cl^{-}_{(aq)}.$$

The values of Gibbs free energy of the two reactions in the sphalerite-galena stage at a temperature of 175°C are −633361 and −755449 Joules, respectively, which shows that the reactions are possible under the ore-forming conditions. Lead (zinc) ions may have reacted with the reduced sulfur to form galena (sphalerite); quartz and calcite may have been formed at the same time or nearly at the same time. After this, the concentration of the ferrous ions in solution increased relatively and redeposited as pyrite. This is in accord with the mineral association.

The textures of the precipitates are dependent upon the supply rates of reduced sulfur. A rapid mix-

TABLE 12. Zinc Complex Solubilities in the Sphalerite-Galena Stage

	Reaction	Species (i)	Molarity (m_i)	Percentage ($m_i/\epsilon m_i \times 100\%$)	Reference for K value
1	$ZnS_{(s)} + 2H^{+}_{(aq)} = Zn^{+2}_{(aq)} + H_2S_{(aq)}$	Zn^{+2}	2.8×10^{-6}	1.1×10^{-2}	a
2	$Zn^{+2}_{(aq)} + Cl^{-}_{(aq)} = ZnCl^{+}_{(aq)}$	$ZnCl^{+}$	5.1×10^{-7}	2.0×10^{-3}	b
3	$ZnCl^{+}_{(aq)} + Cl^{-}_{(aq)} = ZnCl^{0}_{2(aq)}$	$ZnCl^{0}_{2}$	4.0×10^{-4}	1.57	b
4	$ZnCl^{0}_{2(aq)} + Cl^{-}_{(aq)} = ZnCl^{-}_{3(aq)}$	$ZnCl^{-}_{3}$	2.5×10^{-2}	97.96	b
5	$Zn^{+2}_{(aq)} + F^{-}_{(aq)} = ZnF^{+}_{(aq)}$	ZnF^{+}	3.2×11^{-10}	1.3×10^{-6}	c
6	$ZnF^{+}_{(aq)} + F^{-}_{(aq)} = ZnF^{0}_{2(aq)}$	ZnF^{0}_{2}	2.4×10^{-9}	9.4×10^{-6}	c
7	$ZnF^{0}_{2(aq)} + F^{-}_{(aq)} = ZnF^{-}_{3(aq)}$	ZnF^{-}_{3}	2.5×10^{-7}	9.8×10^{-4}	c
8	$Zn^{+2}_{(aq)} + HS^{-}_{(aq)} + OH^{-}_{(aq)} = Zn(OH)(HS)^{0}_{(aq)}$	$Zn(OH)(HS)^{0}$	1.5×10^{-6}	3.9×10^{-3}	a
9	$ZnS^{+2}_{(aq)} + 2HS_{(aq)} = Zn(HS)^{0}_{2(aq)}$	$ZnS(HS)^{0}_{2}$	2.6×10^{-11}	1.0×10^{-7}	a
10	$Zn^{+2}_{(aq)} + 3HS^{-}_{(aq)} = Zn(HS)^{-}_{3(aq)}$	$Zn(HS)^{-}_{3}$	1.9×10^{-16}	7.4×10^{-13}	a
11	$Zn^{+2}_{2(aq)} + 4HS^{-}_{(aq)} = Zn(HS)^{-2}_{4(aq)}$	$Zn(HS)^{-2}_{4}$	4.2×10^{-24}	1.6×10^{-20}	a
12	$ZnS_{(s)} + 2H_2S_{(aq)} = ZnS(H_2S)^{0}_{2(aq)}$	$ZnS(H_2S)^{0}_{2}$	8.7×10^{-17}	3.4×10^{-13}	d
13	$Zn^{+2}_{(aq)} + HCO^{-}_{3(aq)} = ZnHCO^{+}_{3(aq)}$	$ZnHCO^{+}_{3}$	2.0×10^{-14}	7.8×10^{-11}	e

a = Bourcier and Barnes (1987), b = Ruaya and Seward (1986), c = Naumov et al. (1974), d = Barnes (1979), e = Ryan and Bauman (1978)

ing between the metal-bearing solution and reduced sulfur resulted in the formation of various high-energy products such as fine-grained, grape-shaped, and banded sphalerite minerals; a slow mixing resulted in the formation of idiomorphic coarse-grained minerals such as those in the sphalerite-quartz stage.

The Daliangzi deposit was formed during two periods: an initial enrichment period and a later period of mobilization, transport, and reenrichment.

The ore materials in this area were initially enriched during the sedimentary period. The Huili Group (Pttn) and the lower Sinian series are rich in zinc and lead and could have provided the ore materials. The close association of framboidal pyrite and sphalerite, the abundance of lead and zinc, and the primary stratiform zinc and lead mineralization in the regional Dengying Formation, all show that zinc and lead was concentrated initially during sedimentation.

During the Dengying period, there was orogenic activity in a vast area including the mine district and surrounding basin. The metals such as lead and zinc in the slightly metamorphosed Huili Group and in the lower Sinian rocks were transported into the basin by weathering or by underground brines. The metals were directly deposited in the carbonate mud of the tidal facies or they were absorbed and concentrated by microorganisms such as blue and blue-green algae and were then deposited in sediments. As the buried depth increased, the Eh value changed, the ferrous and zinc ions reacted with H_2S formed by algal reduction of seawater sulfates, and gradually precipitated the laminated and disseminated pyrite and sphalerite in a diagenetic state. Because the Dengying Formation is rich in organic matter, the minerals formed framboidal textures.

Generally, after initial enrichment of the ore materials, a deposit would not have formed, if there were no later mobilization, migration, and reenrichment by metals. It can be deduced from regional geologic data and data from the geology of the mine that the deposit was formed during the Hercynian and Indo-China orogeny. After the later Hercynian period, the Panxi rift entered its most active stage and changed into a normal geothermal area as a result of intensive magmatism. The heated meteoric water, after extracting ore materials such as lead and zinc from wall rocks during its circulation, became an ore-forming solution with low salinity. The Paleozoic erathem (Pz), the Sinian system (Z), and the basement Huili Group (Pttn) provided a source for some ore materials that were leached out by percolation of underground water along fractures and fissures. The metals migrated as chloride complexes in weakly acidic to alkalic ore solutions. The metal-bearing solution moved along deep faults into low-pressure zones such as fissures, brecciated zones, and unconformable surfaces,

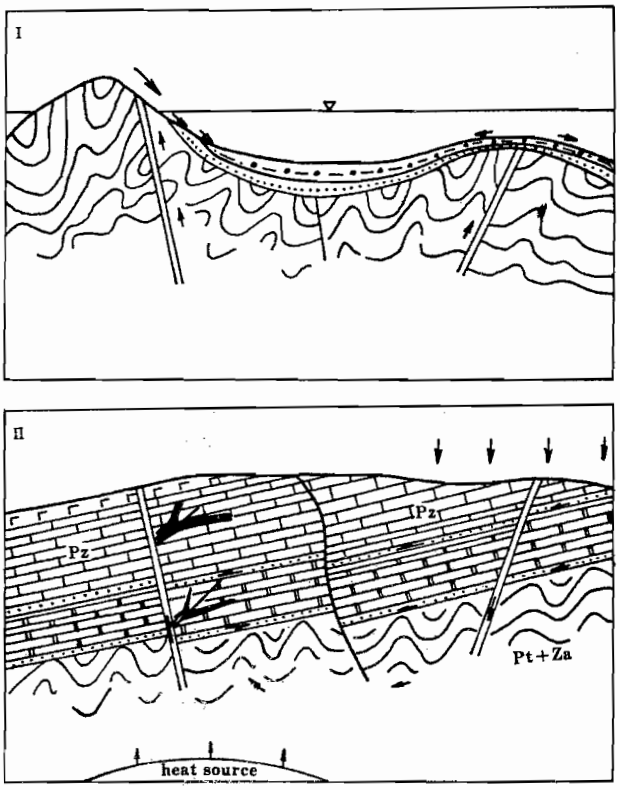

FIG. 13. Sketch diagram of the ore-forming process of the Daliangzi deposit. I = the initial enrichment stage of ore materials during sedimentation; II = the later stage of mobilization, migration, and reenrichment of ore materials.

where the metal ions reacted with reduced sulfur and were precipitated as sulfide minerals. The ore-forming process of the deposit is shown in Figure 13.

Conclusions

1. The Daliangzi Pb-Zn deposit belongs to the Mississippi Valley type and may have formed during two periods: an initial enrichment period and a later period of metal mobilization, transport, and reenrichment. In the second period three stages can be determined: a pyrite-arsenopyrite stage, a sphalerite-galena stage, and a sphalerite-quartz stage.

2. The mineralization materials were derived from several sources. The metals were derived chiefly from the Paleozoic erathem, especially from the upper Paleozoic erathem, and secondly from the Dengying Formation of the Sinian system, and from the underlying basement (the Huili Group). The sulfur was reduced from seawater sulfate by different mechanisms. The carbon may have come from Paleozoic marine carbonate rocks.

3. The ore-forming fluid belonged to a Ca^{+2}-Mg^{+2}-Cl^{-}-HCO_3^{-} type of weak acidic to near-neutral pH

solution whose solinity was about 4 wt percent NaCl. It had a meteoric source. The ore was formed at a depth of about 1 km at a temperature of about 150° to 200°C during the main stage of ore deposition.

4. The metals were transported as chloride complexes such as $PbCl_3^-$, $ZnCl_3^-$, and $ZnCl_2^0$. The metal-bearing solution moved along deep faults to low-pressure zones, where the metal ions reacted with reduced sulfur and were precipitated as sulfide minerals. The textures of the minerals formed were controlled by the rate at which reduced sulfur was supplied.

Acknowledgments

The authors would like to thank two *Economic Geology* reviewers for critically reviewing the manuscript and suggesting valuable improvements.

August 3, 1989; May 15, 1990

REFERENCES

Barnes, H. L., ed., 1979, Geochemistry of hydrothermal ore deposits, 2nd ed.: New York, Wiley-Intersci., 798 p.

Borshchershiy, Y. A., 1980, Oxygen and hydrogen isotope data on the nature of hydrothermal mineralizing fluids: Geochemistry Internat., v. 17, no. 6, p. 40–50.

Bourcier, W. L., and Barnes, H. L., 1987, Ore solution chemistry—VII. Stabilities or chloride and bisulfide complexes of zinc to 350°C: ECON. GEOL., v. 82, p. 1839–1863.

Chen, Y., Mao, C., and Zhu, B., 1980, Lead isotopic composition and genesis of phanerozoic metal deposits in China: Geochemistry, no. 3, p. 215–229 (in Chinese).

Doe, B. R., and Zartman, R. E., 1979, Lead structure in Phanerozoic time, *in* Barnes, H. L., ed, Geochemistry of hydrothermal ore deposits, 2nd ed.: New York, Wiley-Intersci., p. 22–70.

Fournier, R. O., 1973, An empirical Na-K-Ca geothermometer for natural water: Geochim. et Cosmochim. Acta, v. 37, p. 1255–1275.

Fu, X., and Chen, R., 1979, Physicochemistry: Beijing, Senior Educational Press.

Giordano, T. H., and Barnes, H. L., 1981, Lead transport in Mississippi Valley-type ore solutions: ECON. GEOL., v. 76, p. 2200–2211.

Graf, J. L., 1984, The effect of MVT mineralization on the REE model of carbonate rocks and minerals in Virburnum Trend, southeast Missouri: Geochemistry, 1986, no. 6, p. 1–10 (in Chinese).

Helgeson, H. L., 1964, Complexing and hydrothermal ore deposition: Oxford, Pergamon Press, 128 p.

——— 1969, Thermodynamics of hydrothermal systems at elevated temperatures and pressures: Am. Jour. Sci., v. 267, p. 729–804.

Leleu, M. G., 1978, L'Association sulfures-carbonates: Application au cas la galene en milieu hydrothermal: Chem. Geology, v. 22, p. 43–70.

Ling, C., Bai, Z., and Zhang, Z., 1985, Handbook of thermodynamic data of minerals and relative compounds: Beijing, Science Pub. House, p. 103–215.

Maucher, A., 1954, Zur alpinen Metallogeneses in den Bayrischen Kalkalpen zwischen Loisack und Salzack: Tschermaks Mineralog. Petrog. Mitt., ser. 3, v. 4, p. 454–463.

——— 1965, Die Sb-W-Hg Formation und ihre Beziehungen zu Magamatismus und Geotektonik: Freiburg. Forschungsh., Ser. C186, p. 173-188.

——— 1972, Time and strata-bound ore deposits and the evolution of the earth: Internat. Geol. Cong., 24th, Montreal, 1972, Proc., p. 83–87.

Moller, P., 1987, Correlation of homogenization temperatures of assessory minerals from sphalerite-bearing deposits and Ga/Ge model temperatures: Chem. Geology, v. 61, no. 1/4, p. 153–159.

Moller, P., Morteani, G., Hoefs, J., and Porekh, P. P., 1979, The origin of the ore-bearing solution in the Pb-Zn veins of the western Harz, Germany: As deduced from rare-earth element and isotope distribution in calcite: Chem. Geology, v. 26, p. 197–215.

Naumov, G. B., Ryzhenko, B. N., and Khodakosky, I. L., 1974, Handbook of thermodynamic data: U.S. Geol. Survey Natl. Tech. Inf. Service PB 226–722, 328 p.

Rafal'skiy, R. P., 1982, The solubilities of zinc and silver sulfides in hydrothermal solutions: Geochemistry Internat., v. 19, p. 152–159.

Ruaya, J. R., and Seward, T. M., 1986, The stability of chlorozinc (II) complexes in hydrothermal solutions up to 350°C: Geochim. et Cosmochim. Acta, v. 50, p. 651–661.

Ryan, M. P., and Bauman, J. E., Jr., 1978, Thermodynamics of zinc bicarbonate ion pair: Inorg. Chemistry, v. 17, p. 3329–3332.

Sangster, D. F., 1983, MVT deposit belongs to a kind of deposits whose characters are very different: Foreign Geol. Sci. Technology, 1985, no. 5, p. 22–36 (in Chinese).

Seward, T. M., 1984, The formation of lead (II) chloride complexes to 300°C: Geochim. et Cosmochim. Acta, v. 48, p. 121–134.

Song, X., and Qian, G., 1985, The geological features of S-Pb isotopes and the mechanism of mineralization of Pb-Zn deposits at the east margin of the middle section of Xikang-Yunnan axis: Yunnan Geology, v. 4, no. 2, p. 147–158 (in Chinese).

Sverjensky, D. A., 1981, The origin of a Mississippi Valley-type deposit in Viburnum Trend, southeast Missouri: ECON. GEOL., v. 76, p. 1848–1872.

Wang, X., Chen, Y., Lein, J., Wu, M., and Zhao, Y., 1982, On the rare-earth element geochemistry of sea-floor sediments in continental shelf of the east China sea: Geochemistry, no. 1, p. 56–65 (in Chinese).

Wedepohl, H., 1970, Handbook of geochemistry: Berlin, Springer-Verlag, v. II, pt. 5, chap. 39, p. 57–71, L1-3.

To: Mr. Khin Zaw

Xiaochun Wang

May 4, 2011

International Geology Review, Vol. 41, 1999, p. 1099–1113.

Types and Distribution of Endogenic Gold Deposits in Western Sichuan, China

XIAO-CHUN WANG[1] AND ZHE-RU ZHANG

Institute of Geochemistry, Chinese Academy of Sciences, Guiyang, Guizhou, 550002, People's Republic of China

Abstract

Endogenic gold deposits and prospects are widely distributed in western Sichuan, People's Republic of China. To the present time, 43 individual gold deposits and 2 associated gold deposits have been discovered, explored, and mined. All of these deposits belong to one of nine principal types, according to their host-rock series: (I) Archean high-grade metamorphic rock series–hosted; Phanerozoic intermediate-acid intrusive rock–hosted; (III) ophiolitic mélange rock series–hosted; (IV) carbonate rock series–hosted; (V) slightly metamorphic rock series–hosted; (VI) moderately metamorphic rock series–hosted; (VII) subvolcanic rock series–hosted; (VIII) slightly metamorphosed fine-grained clastic-subvolcanic rock series–hosted; and (IX) volcanic rock series–hosted. The tectonic setting, geological features, and temporal and spatial distribution of these different types of gold deposits and occurrences indicate that, to a great extent, gold mineralization reflects the evolution of tectonic environments in the western part of Sichuan Province throughout geological time.

Introduction

A GEOLOGIC SKETCH MAP of western Sichuan Province, People's Republic of China, is presented in Figure 1. Gold deposits and prospects are widely distributed in the area, and constitute one of the most important gold metallogenic regions and potential producers in China. The region continues to be the focus of intense exploration. The remains of several old smelters and ancient workings have been found in places such as Zhangla in Songpan County. Before the late 1970s, gold discoveries and targets in western Sichuan were mainly placers, and quartz-vein deposits in intrusive rocks and metamorphic rocks. No significant discoveries, however, had ever been made. During the late 1970s, however, the Dongbeizhai deposit was discovered as a result of a reinvestigation of old realgar shows. This discovery, coupled with the increase in gold prices in the 1980s, renewed interest in gold exploration in the district. Since then a number of new gold deposits and prospects have been discovered. Intensive efforts to attain a more comprehensive understanding of different types of gold mineralization have been undertaken over the last decade, and form the basis for the prospecting and assessment of gold reserves (Zheng, 1989, 1994; Lu and Wang, 1993; Wang, 1994a, 1994b; Jing and Wang, 1995; Luo, 1995; Gu, 1996; Wang et al., 1998).

This paper introduces the different types of gold deposits in this area and discusses their geological settings, main geological characteristics, and distribution in space and time. A preliminary genetic model for these gold deposits is also proposed.

Geological Background

The tectonic geology of western Sichuan has been described by Xu et al. (1992), Zhang et al. (1984), Huang and Chen (1987), Gao (1990), Burchfiel et al. (1995), and Gu (1996). Two major tectonic units, areally separated by the Longmenshan-Jinpingshan nappe zone, have been identified in the district (see Fig. 2)—the Yangtze craton and Kekexili-Bayankala massif.

The Yangtze craton

The basement of the Yangtze craton consists mainly of Late Archean and Early Proterozoic metamorphic complexes. Migmatites and intrusives are

[1]Also at Southwest Institute of Metallurgical Mineral Resources Exploration and Development, Chengdu, Sichuan, 610051, People's Republic of China.

0020-6814/99/430/1099-15 $10.00

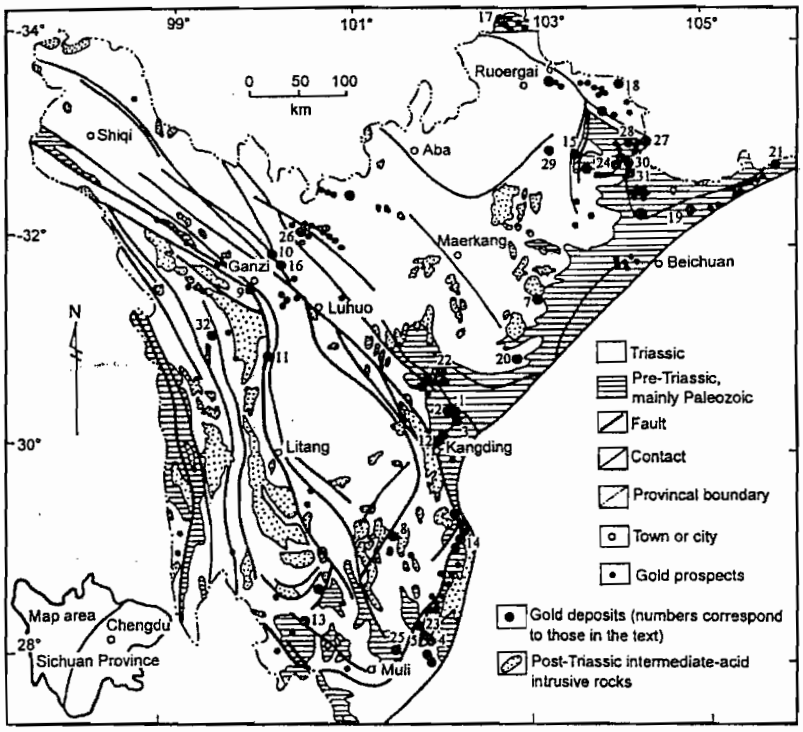

FIG. 1. Geological sketch map of Western Sichuan, PRC, showing the distribution of endogenic gold deposits and prospects. Numbers of deposits correspond to those in the tables.

isotopically dated at 2062 to 2957 Ma (Yuan, 1987). They are distributed in Kangding and Luding (the Kangding complex), Mianning (the Shaba complex), and Panzhihua (the Datian complex). Middle to Late Proterozoic metamorphic sequences dominated by various volcanic rocks such as schist, slate, and sandstone formations (the Hekou Group, the Huili Group, the Yanjing Group, the Tongmuliang Group, the Dengxiangyun Group, and the Huangshuihe Group) crop out in many locations. The Yangtze craton has undergone multiple deformations and metamorphic events since its consolidation in the Late Proterozoic. The influence of Phanerozoic orogenies was strong in the marginal parts of the craton. Tectonic reaction of the craton takes the form of deep-seated fracture systems, depression basins, and zones of magmatism. Two such reactivated units, the so-called Kangdian axis and the western marginal depression of the Yangtze craton, are featured in Figure 2. The sedimentary cover ranges from tillite, phosphorite, and black shales to various types of clastic and carbonate rocks, with ages from Sinian to Cenozoic (Huang et al., 1980; Wang and Mo, 1995).

Kekexili-Bayankala massif

Connected to the east with the Yangtze craton by the Longmenshan-Jinpingshan nappe zone, and to the southwest to other parts of the Tethyan-Himalayan tectonic domain (the Kalakunlun-Sanjiang fold belt) by the Jinshajing suture zone, the Kekexili-Bayankala massif consists of flysch, volcanics, and lesser amounts of carbonate units, mainly of Triassic age. The Triassic flysch sediments comprise a thickness of more than 5000 m and locally even 20,000 m. In Triassic time, it became the most important part of the Northern Tethys (Huang and Chen, 1987), forming the largest flysch basin in the world (Zhang et al., 1984). From west to east, subunits may be identified as the Dege-Zhongdian block (eugeosyncline), the Ganzi-Litang suture zone, the Kekexili-Yajiang block (miogeosyncline), and the western Qinling block, as shown in Figure 2.

The strongest tectonic disturbance in western Sichuan occurred in the Late Mesozoic Yanshanian and Cenozoic Himalayan orogenies. As a result, the fault-bounded Jurassic to Cretaceous basins are superimposed mainly on the Yangtze craton, and

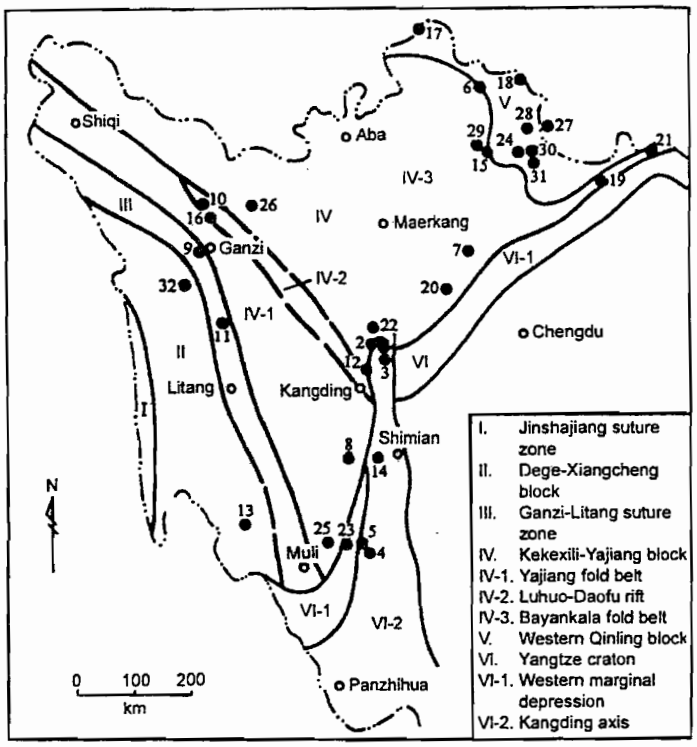

FIG. 2. Tectonic units of Western Sichuan, showing the distribution of major endogenic gold deposits. Numbers of deposits correspond to those listed in the tables.

accompanied intense intrusion of intermediate-acid magmatic rocks. These activities were important for gold mineralization in the study area. The Kekexili-Bayankala massif and Yangtze craton were finally sutured together during the Late Triassic.

Classification of Gold Deposits in Western Sichuan

The major endogenic gold deposits of western Sichuan are depicted in Figure 1. Their basic features, including tectonic setting, host rock series, mineralization pattern, mineral association, element association, and alteration, are presented in Table 1.

Different classification schemes of gold deposits may be obtained by employing different criteria (Boyle, 1979; Zheng, 1989; Wang, 1998b). The present authors believe that a reasonable classification should not only reflect the main geological features of gold deposits, but also be favorable to the investigation, exploration, and development of deposits. It should have clear criteria that may be easily grasped and put to use.

For the gold deposits of western Sichuan, we suggest a classification scheme based mainly on the gold-bearing rock series. These types and representative deposits are listed below; the deposit numbers correspond to those depicted in Figure 1 and listed in Table 1.

I. Archean high-grade metamorphic rock series–hosted type. Examples include the Huangjinping (1), Sandiao (2), and Beijintaizi (3) deposits.

II. Phanerozoic intermediate-acid intrusive rock–hosted type. These include the Jiqifang (4), Mianshawa (5), Baxi (6), Weiguangou (7), and Zhonggu (8) deposits.

III. Ophiolitic mélange rock series–hosted type. Typical deposits are the Gala (9), Pulongba (10), and Xionglongxi (11) deposits.

IV. Carbonate rock series–hosted type. Typical examples are the Picyanzi (12), Erzhe (13), and Jinjitai (14) deposits.

V. Slightly metamorphic fine-grained clastic rock series–hosted type. These include the Dongbeizhai (15), Qiuluo (16), Laerma (17), and Manaoke (18) deposits.

TABLE 1. Geological Features of the Main Western Sichuan Gold Deposits[1]

Deposit[2]	Tectonic setting	Host rocks (time)	Mineral-ization type	Intrusive	Metallic mineral	Gangue mineral	Defor-mation	Grade (g/T)/ reserves/ utility[3]	References
I. Archean high-grade metamorphic rock series–hosted type									
Huang-jinping (1)	Kangdian axis	Mig, pl-AMPB, Gr, GNSS (Ar)	qtz-vein-altered rock	Gr, DIBS	py, ep, gn, sp, po, bn, asp, ele	qtz, ser, dol, cal, chl	Strongly mylonitized	6–10/M/ Exp, Min	Chen et al., 1997
Sandiao (2)	Kangdian axis	AMPB, Gr, GNSS (Ar)	qtz-vein	Aplite, granoaplite dike	py, cp, ele, mag, po, bn, stb, gn, sp, asp	qtz, ser, dol, chl	Strongly mylonitized	6–11/M/ Exp	Chen et al., 1997
Beijintaizi (3)	Kangdian axis	Mig (Ar)	qtz-vein-altered rock	DIBS dike	py, cp, lm, ele, po, asp	qtz, ser, chl, cal	Strongly mylonitized	10/S/Exp	Chen et al., 1997
II. Phanerozoic intermediate-acid intrusive rocks–hosted type									
Jiqifang (4)	Kangdian axis	Ort, Gr (Mz)	qtz-vein	Gr batholith	py, sp, cp, gn, bn, ele	qtz, ser, cal	Strongly brecciated	5/S /Exp	Wang et al., 1998
Mianshawa (5)	Kangdian axis	Sch (D_2), Gr (Mz)	altered rock	Gr batholith	py, tet, cp, gn, ele, sp	qtz, ser, chl	Strongly mylonitized	5–7/S/Exp	Wang et al., 1999
Baxi (6)	Western Qinling block	Ss, Ls, Sl (T_2)	qtz-vein-altered rock	qtz-Di	py, asp, ele, stb, cp, sp, gn, mo, rar	qtz, cal	Strongly brecciated	4–10/M/ Exp	Luo et al., 1998
Weiguangou (7)	Bayankala fold belt	Ss, Sl (T_3)	qtz-vein-altered rock	Intermediate-acid rocks	py, asp, ele	qtz, ser	Strongly brecciated	10–15/M/ Exp	Wang et al., 1998
Zhonggu (8)	Yajiang fold belt	Ss, Sl (T_3)	qtz-vein-altered rock	Hln-monzonite	py, asp, cp, ele, sid	qtz, ser, tur, cal	Strongly mylonitized	1–5/S/Exp	Ni et al., 1996
III. Ophiolitic mélange rock series–hosted type									
Gala (9)	Ganzi-Litang suture	Opiolitic mélange (T_3)	qtz-vein-altered rock	Um, basic rocks	py, asp, stb, tet, ele, cp, sp, co	qtz, ser, cal, chl	Strongly mylonitized	3–5/L/Exp, Min	Zhang et al., 1998
Pulongba (10)	Luhuo-Daofu rift	Opiolitic mélange (T_3)	altered rock	Um, basic rocks	py, ars, ep, ele, bis, ted	qtz, chl, cal	Strongly brecciated	4–15/S/Exp	Wang, 1992
Xiong-longxi (11)	Ganzi-Litang suture	Opiolitic mélange (T_3)	qtz-vein-altered rock	Um, basic rocks	Py, ars, ele	qtz, ser, chl, cal	Strongly brecciated	3–6/M/Exp	Wang, 1994b
IV. Carbonate rock series–hosted type									
Pieyanzi (12)	Kangdian axis	Dols (Z_2)	qtz-vein-altered rock	DIBS dike	py, gn, bou, ele, cp, tet, tn	qtz, sel, ser, chl, cal, ms	Strongly brecciated	5–10/S/ Exp, Min	Zheng, 1989
Erzhe (13)	Ganzi-Litang suture	Mb, Phl, Sl (P_2)	qtz-vein	No	py, ars, cp, bn, tet, ele	qtz, sid, dol	Strongly brecciated	5–6/M/ Exp	Zheng, 1989
Jinjitai (14)	Kangdian axis	Dols, Mb (D_2)	altered rock	DIBS dike	py, tet, gn, cp, sp, bn, asp, ele	qtz, cal, ser, chl	Strongly brecciated	5–6/S/Exp	Wang and He, 1993

(continued)

TABLE 1. (*continued*)

Deposit[2]	Tectonic setting	Host rocks (time)	Mineral-ization type	Intrusive	Metallic mineral	Gangue mineral	Defor-mation	Grade (g/T)/ reserves/ utility[3]	References
V. Slightly metamorphic fine-grained clastic rock series–hosted type									
Dong-beizhai (15)	Bayanka-la fold belt	Phl, Sl, Ss, (T_3)	f. g. diss	DIBS dike	py, asp, rar, orp, cin, cp, tet, sp, lm	qtz, cal	Strongly phyl-lonitized	4–5/L/Exp	Zheng, 1989
Qiuluo (16)	Luhuo-Daofu rift	Ss, Sl, Sils (T_3)	f. g. diss	DIBS dike	py, stb, asp, ele, mar, tet, cin	qtz, ser, chl	Strongly brecciated	5–20/L/Exp	Wang, 1993
Laerma (17)	Western Qinling block	Che, Sl (Cam_1)	f. g. diss	DA Por	py, stb, mar, cin, sp, cp, gn, tet, ele, po, pit	qtz, ser, cal, dick, bar	Strongly brecciated	7/L/Exp	Zheng, 1994
Manaoke (18)	Western Qinling block	Ss, Sl, (T_3)	f. g. diss	No	py, wol, stb, rar, asp, ele	qtz, cal, ser, chl	Strongly brecciated	1–9/L/Exp, Min	Zheng, 1994
VI. Middle-slightly metamorphic rock series–hosted type									
Jinbao (19)	Bayanka-la fold belt	Ss, Sl (S)	qtz-vein	No	py, cp, gn, sp, asp, mar, ele, cin	qtz, ser, dol	Strongly brecciated	11–15/M/ Exp	Wu and Xia, 1996
Baliang-shan (20)	Bayanka-la fold belt	Ss, Sl (T_3)	qtz-vein	No	py, sp, ele, stb, gn, tet, cp	qtz, cal, ser, sid, chl	Less brecciated	2–4/S/Exp	Wang, 1994b
Mafangwo (21)	Bayanka-la fold belt	Ss, Sl (S)	qtz-vein	No	py, cp, gn, sp, mar, ele, cin	qtz, ser, dol	Strongly brecciated	5–12/S/ Exp, Min	Wang, 1994b
Dongjiagou (22)	Bayanka-la fold belt	Ss, Sl (T_3)	qtz-vein	No	py, cp, gn sp, mar, ele, cin	qtz, ser, dol	Strongly brecciated	3–17/S/ Exp, Min	Wang, 1994b
Chapuzi (23)	Western marginal depression	CS (T_2)	altered rock	Gr-Por	py, tet, gn, cp, mt, hem, ele, arg	dol, qtz, ser, chl	Mylonitized	4–6/M/Exp	Wang, 1994b
VII. Subvolcanic rock-series–hosted type									
Liangchahe (24)	Western Qinling block	Ss, Sl, Ls (D_2)	f. g. diss	Gr-Por	py, asp, rar, orp, stb, cin, cp, gn	qtz, cal, sid, ser, kln, chl, bar	Strongly brecciated	2–9/S/Exp	Wang, 1994b
Jinshan (25)	Yajiang fold belt	Gb-BIBS dike	qtz-vein-altered rock	Gb-BIBS dike	py, mag, po, cp, bn, ele	qtz, cal, chl	Brecciated	7/S/Exp	Wang, 1994b

(*continued*)

TABLE 1. (*continued*)

Deposit[2]	Tectonic setting	Host rocks (time)	Mineral-ization type	Intrusive	Metallic mineral	Gangue mineral	Defor-mation	Grade (g/T)/ reserves/ utility[3]	References
Shilong-zawo (26)	Bayanka-la fold belt	qtz-Di, Gb	qtz-vein-altered rock	qtz-Di, Gb	py, cp, tet, ele, asp, mag	ser, chl, qtz, al	Brecciated	4–10/S/ Exp, Min	Wang, 1994b
VIII. Slightly metamorphosed fine-grained clastic-subvolcanic rock series–hosted type									
Lianhecun (27)	Western Qinling block	Ls (D_2)	f. g. diss	Gr-Por	py, stb, asp, po, cin, rar, bn	qtz, sid, cal, ms, ser	Strongly brecciated	2–12/M/ Exp, Min	Wang, 1994b
Jiawuci (28)	Western Qinling block	Ss, Sl, Ls (D_2)	f. g. diss	Gr-Por	py, asp, rar, orp, stb, cin, cp, gn	qtz, cal, sid, ser, kln, chl, bar	Strongly brecciated	1–6/S/Exp	Wang, 1994b
Zeboshan (29)	Bayanka-la fold belt	Ss, Sl (T_3), qtz-Di-Por (Mz)	qtz-vein	qtz-Di Por	py, asp, sp, cp, ele, mo, gn, bn, cin	qtz, ser, bar	Strongly brecciated	3–4/S/Exp	Gu, 1996
Shuiniujia (30)	Western Qinling block	Sl, Ss (D_2)	f. g. diss	Gr-Por	py, po. asp, cin, rar, orp	qtz, ser, bar, kln	Strongly brecciated	4–6/S/Exp	Wang et al., 1998
Song-pangou (31)	Western Qinling block	Sl, Ss (D_2)	f. g. diss	Gr-Por	py, stb, asp, po, cin, rar	qtz, cal, ms, ser	Strongly brecciated	2–10/M/ Exp, Min	Wang et al., 1998
IX. Volcanic rock series–hosted type									
Gacun (32)	Degen-Zhongdian block	RH (T_3)	Associated gold	No	sp, gn, py, tet, cp, bn, arg, ele	qtz, adal, ser	Strongly brecciated	0.5–1/L/ Exp	Wang et al., 1998

[1]Abbreviations: adal = adularia; al = albite; AMPB = amphibolite; Ar = Archean; arg = argentite; asp = arsenopyrite; ba = barite; bis = bismuthine; bn=bornite; bou = bournonite; cal = calcite; cala = calaverite; Cam_1 = Early Cambrian; cp = chalcopyrite; che = chert; chl = chlorite; cin = cinnabar; co = calcocite; D =Devonian; Di = diorite; DIBS = diabase; dick= dickerite; dol = dolomite; Dols = dolostone; ele = electrum; f. g. diss = fine-grained and disseminated; Gb = gabbro; gn = galena; GNSS = granulite; Gr = granite; GS = greenschist; hem = hematite; hbl = hornblende; kln = kaolinite; kfs = K-feldspar; lm = limonite; Ls = limestone; mag = magnetite; mar = marcasite; Mb =marble; Mig = migmatite; mo = molybdenite; ms = muscovite; Mz =Mesozoic; orp = orpiment; Ort = orthoclase; Phl = phyllite; pit = pitchblende; pl = plagioclase; po = pyrrhotite; Por = porphyry; py = pyrite; pyr = pyrargyrite; Pz = Paleozoic; rar = realgar; RH = rhyolite; qtz = quartz; sel = sellaite; sep = serpentine; sch = scheelite; ser = sericite; sid = siderite; Sils = siltstone; Sl = slate; Ss = sandstone; stb = stibnite; T = Triassic; ted = tetradymite; tet = tetrahedrite; tn = tennatite; tr = tremolite; tur = tourmaline; UM = ultramafic rocks; wol = wolframite; Z = Sinian (late Proterozoic).

[2]Number in parentheses indicates location on Figures 1 and 2.

[3]L = large gold deposit with gold metal reserves more than 20 tons; M = medium-sized gold deposit with gold metal between 5 and 20 tons; S = small-sized gold deposit with gold metal less than 5 tons; Min = mined or under mining; Ex p = explored or under mineral exploration.

TABLE 2. Strata Distribution of Gold Deposits and Prospects, Western Sichuan

Stratum[1]	Ar	Pt_2	Z	Cam	S	D	C-P	T	Σ
Number of gold deposits and prospects	15	18	15	5	15	29	11	90	198
Percentage	7.6	9.1	7.6	2.5	7.6	14.6	5.6	45.4	100

[1]Ar = Archeozoic; Pt_2 = Middle Proterozoic; Z = Sinian (Upper Proterozoic); Cam = Cambrian; S = Silurian; D = Devonian; C–P = Carboniferous–Permian; T = Triassic.

VI. Moderately to slightly metamorphic rock series–hosted type. Representative gold deposits are the Jinbao (19), Baliangshan (20), Mafangwo (21), Dongjiagou (22), and Chapuzi (23) deposits.

VII. Subvolcanic rock series–hosted type. It is represented by the Liangehahe (24), Jinshan (25), and Shilongzawo (26) deposits.

VIII. Slightly metamorphosed, fine-grained clastic-subvolcanic rock series–hosted type. Typical gold deposits are the Lianhecun (27), Jiawuci (28), Zeboshan (29), Shuinuffia (30), and Songpangou (31) deposits.

IX. Volcanic rock series–hosted type. It is represented by the Gacun (32) deposits.

Discussion

Temporal distribution of gold deposits

It can be concluded from Table 2 and Figure 3 that endogenic gold deposits and prospects in western Sichuan occur in strata from the Archeozoic to Triassic, with 7.6% of the total occurring in Archaeozoic, 9.1% in Middle Proterozoic, 37.9% in Sinian to Permian strata, and 45.4% in Triassic units. Evidently gold mineralization increased in intensity with time.

Although the western Sichuan gold deposits occur in diverse strata of many ages, they were formed mainly during the Yanshanian and Himalayan periods (younger than Triassic), judging from isotopic dating (see Table 3 and Fig. 3). It is obvious that their formation was related to the geotectonic environment and tectonic evolution. The Indochina movement during Late Triassic time resulted in the closure and uplift of geosynclines in western Sichuan. Since the Jurassic period, the area experienced compression caused by the intense westward movement of the Pacific plate and northeastward movement of the Indian plate, as well as the impedance of the North China craton, and became part of a Yanshanian Himalayan intracontinental superposed compressive orogenic belt (Gao and Wang, 1992; Gao et al., 1996).

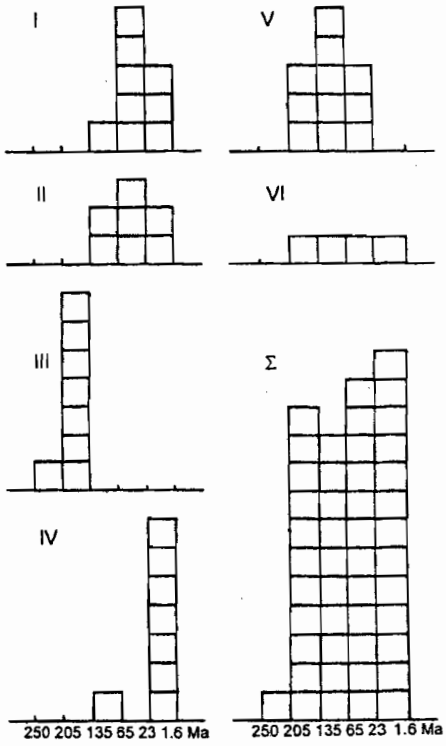

FIG. 3. Histogram of plot of metallogenic epochs for various types of endogenic gold deposits of western Sichuan. Roman numerals correspond to gold deposit types referred to in text.

Orogeny was accompanied by heating resulting from tectonic and magmatic activities. Thermal upgrading accompanied deformation, fracturing, and displacement of the rocks. Heating during deformation was manifested by a heat-sensitive carbon evolutionary trend (from amorphous kerogen, to

TABLE 3. Metallogenic Epochs of Major Endogenic Gold Deposits, Western Sichuan

No.	Deposit (type)	Petrology	Analyzed target	Analyzed method	Age, Ma	References
1	Huangjinping (I)	Gold ore	Muscovite	K-Ar	26.9	Luo, 1995
2	Sandiao (I)	Gold ore	Sericite	K-Ar	20.79	Liu et al., 1998
3	Sandiao (I)	Gold ore	Sericite	K-Ar	21.41	Liu et al., 1998
4	Xiasuozi (I)	Diabase vein	Whole rock	K-Ar	47.9	Liu et al., 1998
5	Xiasuozi (I)	Diabase vein	Whole rock	K-Ar	102.1	Liu et al., 1998
6	Wangjiaheba (I)	Mylonite	Hornblende	K-Ar	26.8	Liu et al., 1998
7	Wangjiaheba (I)	Mylonite	Hornblende	K-Ar	24.3	Luo, 1995
8	Yele (I)	Gold ore	Quartz	ESR	65	Yu, 1998
9	Yele (I)	Gold ore	Muscovite	K-Ar	15	Yu, 1998
10	Jiqifang (II)	Sericite-quartz-schist	Wholoe rock	K-Ar	38.2	Zhao, 1998
11	Jiqifang (II)	Lamprophyre	Whole rock	K-Ar	21	Zhao,1998
12	Mianshawa (II)	Sericite-quartz-phyllonite	Whole rock	K-Ar	28.9	Luo, 1995
13	Mofanggou (II)	Chlorite-sericite-phyllonite	Whole rock	K-Ar	13.3	Luo, 1995
14	Zhonggu (II)	Monzosyenite	Whole rock	Rb-Sr	126.5	Ni et al., 1996
15	Qingshuicun (II)	Au-bearing brecciated plagioclase-aplite	Whole rock	K-Ar	112.0	Zhao, 1998
16	Qingshuicun (II)	Au-bearing granitic mylonite	Whole rock	K-Ar	51.6	Zhao, 1998
17	Pulongba (III)	Olivine-diabase	Whole rock	K-Ar	154	Wang, 1992
18	Gala (III)	Gold ore	Whole rock	K-Ar	164	Zhang et al., 1998
19	Gala (III)	Gold ore	Whole rock	K-Ar	158	Zhang et al., 1998
20	Gala (III)	Gold ore	Whole rock	K-Ar	177	Zhang et al., 1998
21	Gala (III)	Altered rock	Whole rock	K-Ar	208	Zhang et al., 1998
22	Gala (III)	Altered rock	Whole rock	K-Ar	149	Zhang et al., 1998
23	Gala (III)	Gold ore	Whole rock	K-Ar	163	Zhang et al., 1998
24	Gala (III)	Gold ores, altered rocks	Whole rock	Rb-Sr	157	Zhang et al., 1998
25	Guangjinping (IV)	Quartz-scricite-phyllonite	Sericite	K-Ar	19.9	Wu et al., 1996
26	Guangjinping (IV)	Quartz-scricite-phyllonite	Sericite	K-Ar	21.2	Wu et al., 1996
27	Tianwan (IV)	Sericite-quartz- phyllonite	Sericite	K-Ar	15.4	Wu et al., 1996
28	Tianwan (IV)	Sericite-quartz- phyllonite	Quartz	ESR	17	Wu and Luo, 1998
29	Caizidi (IV)	Au-bearing diabase	Whole rock	K-Ar	21	Zhao, 1998
30	Caizidi (IV)	Diabase mylonite	Whole rock	K-Ar	22.6	Luo, 1995
31	Erzhe (IV	Gold ore	Quartz	Rb-Sr	118	Zheng, 1989
32	Pieyanzi (IV)	Gold ore	Quartz, siderite	K-Ar	9.5	Wang et al., 1998
33	Dongbeizhai (V)	Diabase	Whole rock	Ph	93.5	Zheng, 1989
34	Qiaoqiaoshang (V)	Granite-porphyry	Whole rock	K-Ar	172	Zheng, 1989
35	Qiaoqiaoshang (V)	Gold ore	Whole rock	Rb-Sr	167	Zheng, 1994
36	Laerma (V)	Gold ore	Quartz	$^{40}Ar/^{39}Ar$	49.5	Peng, 1992
37	Laerma (V)	Gold ore	Whole rock	U-Pb	79	Liu et al., 1996
38	Laerma (V)	Gold ore	Whole rock	U-Pb	117.1	Liu et al., 1996
39	Laerma (V)	Gold ore	Whole rock	U-Pb	73.1	Liu et al., 1996

(continued)

TABLE 3. (*continued*)

No.	Deposit (type)	Petrology	Analyzed target	Analyzed method	Age, Ma	References
40	Laerma (V)	Gold ore	Whole rock	U-Pb	66.4	Liu et al., 1996
41	Laerma (V)	Gold ore	Whole rock	K-Ar	57.1	Liu et al., 1996
42	Laerma (V)	Gold ore	Whole rock	K-Ar	127	Liu et al., 1996
43	Manaoke (V)	Gold ore	Quartz	Rb-Sr	46	Ji et al., 1999
44	Jinbao (VI)	Phyllonite	Sericite	K-Ar	146.5	Wu and Xia, 1996
45	Chapuzi (VI)	Granite-porphyry	Whole rock	K-Ar	20	Luo, 1995
46	Chapuzi (VI)	Granite-porphyry	Whole rock	K-Ar	70	Luo, 1995
47	Chapuzi (VI)	Granite-porphyry	Whole rock	K-Ar	31.9	Luo, 1995

fine-grained semicrystalline graphite, to crystalline graphite) and the gradual reduction of residual organic carbon in rocks in the trend (Zheng, 1989). Magmatic heat was supplied by intrusive igneous rocks, involving higher temperatures over a longer time interval; this effect was especially pronounced during the Yanshanian–Himalayan magmatism, reflecting unprecedented numbers and sizes of intrusives. The superimposition of tectonic and magmatic heat resulted in regional inhomogeneous geothermal anomalies in the region, which is supported by the paleo-geothermal gradient data from reflectance measurement of vitrinite (Wang, 1995a). Only regional geothermal anomalies can mobilize ore-forming materials over a wide region and concentrate ore elements to form gold deposits.

Spatial distribution of gold deposits and gold metallogenic belts

The main gold deposits of different types in western Sichuan are shown in Figures 1 and 4, with most being clustered in the western Qinling block and the western margin of the Yangtze craton. It is obvious that the distribution of these gold deposits, to some degree, is related to their tectonic setting. Based on geographic distribution, regional tectonic features, geologic setting, and mineralization type, 19 gold metallogenic belts (districts of gold concentration, possibly of great potential) have been identified (see Table 4, Fig. 4). It can be seen that in gold metallogenic belts of the mountainous region of the western margin of the Sichuan Basin, which are located in the Longmenshan-Jinpingshan nappe zone, the main deposits are types VI and IV, of which the mineralization is chiefly of the quartz-vein type of intermediate and higher grade and tonnage. In the Jinshajiang and Degen-Xiangcheng gold metallogenic belts, there is less evidence of gold mineralization. But type II and III gold deposits may be present in view of the geologic setting; this area deserves further study in the future. The most important metallogenic belts in the region are the Ganzi-Litang, Luhuo-Daofu, and Danba-Luding belts, as well as those in the northeast part of the region, including the northern Jiuzhaigou, Heye, Beima, Minjiang, Xueshan, and Huya belts.

Possible ore genesis

Type I deposits are located in Archean amphibolite, gneiss, and migmatite in the Kangdian axis. The mylonitic and fractured fabrics, intensive hydrothermal alteration, and high degrees of metamorphism of this category imply that their formation is related to the geological evolution of the Yangtze craton. Isotopic dating shows that the major gold enrichment occurred during the Cenozoic Himalayan orogeny (see Table 3 and Fig. 3). The deposits were formed by metamorphic waters, as demonstrated by hydrogen and oxygen isotopes of ore fluids, and pH values range from 6.72 to 7.44 (see Tables 5 and 6) (Chen et al., 1997, Zhang, 1998).

Type II deposits are mainly related to intermediate-acid intrusive rocks ranging from Yanshanian to Himalayan in age. Intrusive rocks are mainly syntectonic. The deposits occur in various tectonic units. The limited data obtained from the Mianshawa and Zhonggu deposits show that magmatic water and groundwater might be major components in the ore fluids (Table 5). Gold ores were formed in deeper environments, at pressures of ~9×10^7 Pa (Table 6).

TABLE 4. Characteristics of Metallogenic Belts for Endogenic Gold Deposits in Western Sichuan

Metallogenic belt	Ore-controlling fault, intrusive, and strata	Known deposit types[1]	Preferred deposit types
Northern Ruoergai (A)	Maxin-Yueyang fault, Yanshanian intermediate-acid rock, Cambrian chert, Triassic carbonate rock	V, II	V, II
Northern Jiuzhaigou (B)	Maxin-Yueyang and Xiangzai-Linjiang faults, Yanshanian intermediate-acid rock, Triassic fine-grained clastic rocks	V, VIII	V, VIII
Huoye (C)	Huoye, Longkang-Songbei-Liping faults, Yanshanian intermediate-acid rock; Triassic and Devonian fine-grained clastic rocks	V, VIII	VIII, V
Beima (D)	Jiawuchi and Beirria arc-type faults, Yanshanian intermediate-acid dike, Devonian fine-grained clastic rocks	V, VIII	V, VIII
Minjiang (E)	Kuaisiya fault, Triassic fine-grained clastic rocks	V	V
Xueshan (F)	Xueshan fault, Yanshanian intermediate-acid dike, Triassic and Devonian fine-grained clastic rocks	V, VII, VIII	V, VIII
Huya (G)	Huya fault, Triassic, Devonian–Carboniferous fine-grained clastic rocks and limestone	V, VI	V
Pinwu-Qinchuan (H)	Pinwu-Qinchuan fault, Triassic, Silurian, and Middle Proterozoic fine-grained clastic rocks	VI, IX	VI, V
Aba-Hongyuan (I)	Aba fault, Triassic, fine-grained clastic rocks		V
Rangtang-Heishui (J)	Rangtang-Maerkang-Heishui arc-type fault, Indochina-Yanshanian intermediate-acid dike, Triassic fine-grained clastic rocks	VIII	VIII, II
Back Longmenshan (K)	Beichuan-Yinxiu, Maowen faults, Indochina-Yanshanian intermediate-acid rocks, Triassic fine-grained elastic rocks, Silurian and Middle Proterozoic middle metamorphic clastic rocks	IV, II	II, V
Seda (L)	Seda-Yuke fault, Indochina-Yanshanian intermediate-acid dike, Triassic fine-grained clastic rocks	V, VII, VIII	VIII, VII
Luhuo-Daofu (M)	Luhuo-Daofu fault, Indochina (Triassic) ophiolitic mélange, fine-grained clastic rocks, Yanshanian intermediate-acid rocks	III, V, VI, II	III, V
Danba-Luding (N)	Aminghe, Xiaojin arc, Beichuan-Yinxiu, Maowen, and Xianshuihe faults, Himalayan intrusive rocks (dikes), Indochina ultrabasic rocks, Sinian-Paleozoic carbonate and fine-grained clastic rocks	I, IV, VI	I, IV
Shimian-Mianning (O)	Anninghe, Mopanshan, Jinhe-Qinhe, Xianjinhe, and Chenzhi faults, Yanshanian-Himalayan intermediate-acid rocks, Archeozoic migmatite, Sinian and Devonian dolostone, Triassic clastic rocks	I, II, IV, VI	IV, II
Ganzi-Litang (P)	Ganzi-Litang fault, Yanshanian intermediate-acid rocks, Triassic ophiolitic mélange	III	III
Muli (Q)	Ganzi-Litang and Muli arc fault belt, Indochina-Yanshanian intermediate-acid rocks, Sinian dolostone, Permian and Triassic volcanosedimentary rocks	IV, V, IX	IV, V
Degen-Xiangcheng (R)	Degen-Xiangcheng fault belt, Indochina basic-ultrabasic intrusive, Yanshanian intermediate-acid rocks, Triassic volcanosedimentary rocks	IX	II
Jinshajiang (S)	Jinshajiang fault belt, Hercynian basic-ultrabasic intrusive, Indochina-Yanshanian intermediate-acid rocks, Sinian-Triassic carbonate rocks, mélanges		III, II

[1]Deposit types correspond to those employed in the text.

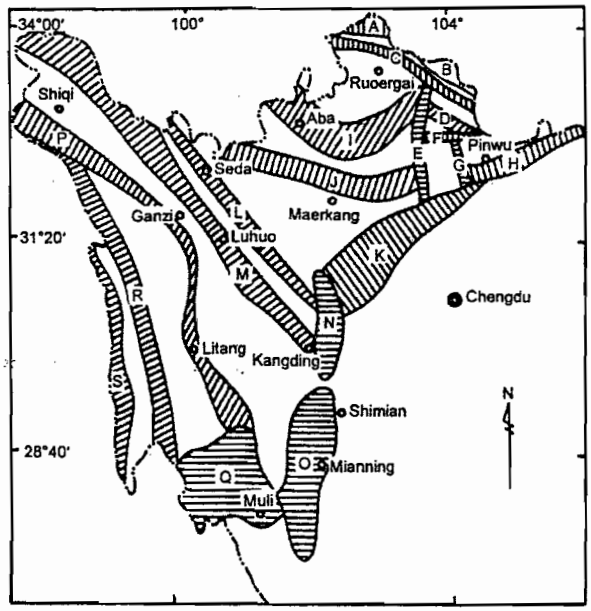

FIG. 4. Metallogenic belts of endogenic gold deposits in western Sichuan. Type codes correspond to those employed in text and Table 4.

TABLE 5. Hydrogen- and Oxygen-Isotopic Data of Ore Fluids in Western Sichuan Endogenic Gold Deposits[1]

Deposit (type)	Sample	*n*	$\delta^{18}O_{H_2O}$, ‰	δD, ‰	References
Huangjinping (I)	Quartz	4	5.3 to 6.3 (6.0)	–89.4 to –49.9 (–66.4)	Chen et al., 1997; Zhang, 1998
Mianshawa (II)	Quartz	2	–7.0 to –8.5 (–7.8)	–95.0 to –93.0 (–94.0)	Wang et al., 1999
Baxi (II)	Quartz	7	–1. 1 to 5.8 (1.5)	–118.0 to –55.0 (–97.1)	Luo et al., 1998
Gala (III)	Quartz	5	3.1 to 6.7 (4.6)	–109.0 to –77.0 (–91.0)	Zhang et al., 1998
Pulongba (III)	Quartz	2	0.7 to 6.8 (3.7)	–117.8 to –103.5 (–110.7)	Wang, 1992
Pieyanzi (IV)	Quartz	2	2.7 to 4.8 (3.8)	–61.2 to –59.6 (–60.4)	Zheng, 1989
Erzhe (IV)	Quartz, siderite	11	–12.3 to 9.5 (0.4)	–110.8 to –56.3 (–76.7)	Zheng, 1989
Jinjitai (IV)	Quartz	2	0.8 to 4.8 (2.8)	–90.0 to –80.0 (–85.0)	Wang and He, 1993
Dongbeizhai (V)	Calcite	5	12.3 to 16.2 (13.7)	–75.5 to –66.6 (–70.9)	Zheng, 1989
Qiaoqiaoshang (V)	Quartz, calcite	4	4.0 to 7.7 (5.8)	–92.0 to –50.4 (–68. 1)	Zheng, 1994
Laerma (V)	Quartz, barite	14	–11.1 to 13.2 (1.7)	–111.9 to –52.9 (–88.7)	Zheng, 1994
Manaoke (V)	Quartz	5	11.3 to 14.6 (13.0)	–78.1 to –62.3 (–70.3)	Zheng, 1994
Jinbao (VI)	Quartz, siderite, sericite	6	–8.3 to –2.1 (–4.6)	–82.6 to –38.9 (–66.2)	Wu and Xia, 1996

[1]Data in parentheses correspond to average.

TABLE 6. Ore-Forming Physicochemical Parameters For Various Types of Gold Deposits in Western Sichuan[1]

Deposit (type)	Stage	Temperature (°C)	Salinity (wt% NaCl)	Density (g/cm³)	Pressure[2] (×10⁵Pa)	pH	Eh (V)	References
Huangjinping (I)		100–390				6.7		Chen et al., 1997
Mianshawa (II)		185–255	10.3–14.6 (12.0)	0.93–0.95	900			Lu and Wang, 1993
Pulongba (III)		93–306 (169)	9.5–12.6	0.94–1.01	36–192	7.6–7.9	–.69 to –0.61	Wang, 1993
Jinjitai (IV)	I	220–300 (250)	21.0–19.0 (15.1)	0.86–0.97	275	7.6–8.0	–1.10 to –0.71	Wang and He, 1993
Jinjitai (IV)	II	80–210 (150)	6.0–11.0 (8.6)	0.86–0.97	100	8.0	–0.61	Wang and He, 1993
Erzhe (IV)	I	173–210 (180)	8.0	0.93	210			Zheng, 1989
Erzhe (IV)	II	156–184 (165)	0.7–1.2	0.90	150–164 (157)	8.5	–0.33	Zheng, 1989
Piyanzi (IV)	I	292–340 (314)	21.4–34.7	0.95–1.08		7.8	–0.49	Zheng, 1989
Piyanzi (IV)	II	220–280 (245)	8.6–23.6	0.90–1.02	26.9–7.6 (40.7)	7.2	–0.33	Zheng, 1989
Dongbeizhai (V)	I	170–220 (180)	5.09	1.01	205	5.7	–0.11	Wang et al., 1998
Dongbeizhai (V)	II	120–170 (150)	11.71	0.92	135	6.0	–0.11	Wang et al., 1998
Qiaqiaoshag (V)	I	175–220 (200)	8.8	0.93	137	5.8	–0.42	Wang et al., 1998
Qiaoqiaoshang (V)	II	70–150 (100)	10.7	1.02	100	5.54	–0.27	Wang et al., 1998
Qiuluo (V)		130–305 (243)	6.0–7.3 (6.8)	0.84–0.88 (0.85)	156–256 (193)	7.6–7.9	–0.69 to –0.61	Wang, 1993
Laerma (V)	I	250	7.5		100	4.8		Zheng,1994
Laerma (V)	II	200	8		70	4.5		Zheng,1994
Manaoke (V)	I	210–270 (240)	4.5	0.85	400	6.8	–0.28	Zheng,1994
Manaoke (V)	II	170–210 (190)	2.1	0.90	<400	7.0	–0.24	Zheng,1994
Chapuzi (VI)		98–310	2.22	0.81–0.96	380			Lu and Wang, 1993
Gacun (IX)		78–325	4.15–41.0	0.91–1.07	45.9–218.8	4.89–7.0	–0.57 to –0.17	Wang et al., 1998

[1]Averages are shown in parentheses.

[2]Calculated by means of lithostatic pressure gradient, except that Gacun's pressure was calculated by means of hydrostatic gradient.

Type III deposits occur chiefly along the Ganzi-Litang suture and Luhuo-Daofu rift. Study of the Pulongba and Gala deposits in the Luhuo-Daofu rift shows that this type of gold deposit was formed by ground water of lower to intermediate temperature and possessing a salinity ranging from 9.5 to 12.6 wt% NaCl under epithermal environmental conditions (see Tables 5 and 6). The ore-forming materials were derived mainly from a Triassic turbidite formation that itself originated from deep sources (volcanic rocks and ultrabasic intrusives) (Wang, 1992, 1993, 1994a, 1995a, 1995b; Zhang et al., 1998).

Type IV deposits occur mainly along the Longmenshan-Jinpingshan nappe zone. Investigation of the Jinjitai, Erzhe, and Pieyanzi deposits suggests that this type of deposit is of the saline-groundwater type (Table 5). The ore fluids are lower in temperature, pressure, and Eh values, and vary in salinity from 0.7 to 34.7 wt% NaCl (Table 6). The ore-forming materials are of multiple sources, in which Archeozoic strata may be important (Zheng, 1989; Wang and He, 1993; Wang, 1994b).

Type V deposits are widespread in the region; finely disseminated ore is characteristic of mineralization patterns. The ore fluids belonged mainly to the saline groundwater type, with salinity ranging from 2.1 to 11.71 wt% NaCl. Conditions involved a range of temperature from 150 to 250°C, and pressure from 70 to 400 x 10^5 Pa (Tables 5 and 6). Gold ores were formed in reducing environments, with Eh values from -0.69 to -0.11V (Zheng, 1989, 1994; Wang, 1993, 1995b, 1998a).

Ore-forming data for other types of gold deposits—including types VI, VII, VIII, and IX— are scarce. The limited data from the Jinbao deposit indicate that type VI deposits may be of the metamorphic hydrothermal type, controlled strictly by shear zones. Types VII and VIII might be similar to type VI in ore genesis. Type IX deposits are similar to seafloor massive sulfide deposits, which are related to seafloor volcanic exhalation (Wang, 1994b, 1998a, 1998b; Wang et al., 1998).

To summarize, the main endogenic gold deposits in western Sichuan were formed by various aqueous fluids, and located in different geological settings during the Yanshanian–Himalayan orogenies. The Yanshanian–Himalayan superimposed intracontinental orogenies facilitated the mobilization of ore materials from many sources (mainly gold-bearing formations) and their accumulation as ore deposits.

Conclusion

Gold deposits in western Sichuan are classified into nine contrasting groups in view of their host rock series. Multistage geologic activities resulted in some complexities, but the relations between gold mineralization and the evolution of tectonic settings through geologic time can be recognized.

Geographically, gold deposits and prospects are unevenly distributed, with most being clustered in the eastern and central portions of western Sichuan. The western part of the region also is rich in gold resources and has great potential. Gold deposits hosted by fine-grained clastic rock series have become the most important exploration target. Gold potential for deposits hosted by ophiolitic mélange also is evident. Current exploration activity focused on these deposit types is intense. If geologic exploration and research are expanded, gold resources of the area will grow substantially, and will be sufficient to meet the increased demand for gold production.

Acknowledgments

The first author wishes to acknowledge the Chinese Academy of Sciences (CAS) for funding his appointment as a senior visiting scholar at the Institute of Geochemistry, CAS. He also is grateful to the Southwest Institute of Metallurgical Mineral Resources Exploration and Development, for granting him a leave of absence. The study was financially supported by a pre-selection program of the Chinese National Climb Plan (Fundamental Research Concerning Exploration for Super-large Mineral Deposits) and a major program of the Chinese Academy of Sciences on Research on Gross Low-temperature Metallogenic Domains in Southwestern China.

REFERENCES

Boyle, R. W., 1979, The geochemistry of gold and its deposits: Geol. Surv. Can. Bull., 548 p.

Burchfiel, B. C., Chen, Z. L., Liu, Y. P., and Royden, L. H., 1995, Tectonics of the Longmenshan and adjacent regions, central China: INT. GEOL. REV., v. 37, p. 661–735.

Chen, Z. L., Liu, Y. P., Wei, S. Q., Li, J. Z., and Tang, W. Q., 1997, Study on ore-field structures of main gold mining areas along the Dadu River, Kangding, Sichuan, China: Beijing, Geol. Publ. House, 84 p. (in Chinese).

Gao, Y. L., 1990, Characteristics of the Pacific type paleocontinental margin of Qinghai-Tibet-Yunnan areas in Indosinian times: Acta Geol. Sinica, no. 3, p. 186–197.

Gao, Z. B., and Wang, X. C., 1992, The outstanding significance of the Yanshanian-Himalayan cycle in the formation of endogenic gold deposits and its reason: Mineral Deposits, v. 11, no. 2, p. 97–105 (in Chinese).

Gao, Z. B., Wang, X. C., and Rong, C. M., 1996, Ore-forming model for micro-disseminated type of gold deposits in China, *in* Liu, Y. K., et al., eds., Geology and mineral resources proceedings, MMI: Beijing, Int. Acad. Publ., p. 104–108.

Gu, X. X., 1996, Turbidity-hosted micro-disseminated gold deposits: Chengdu, Chengdu Univ. Sci. Technol., 240 p.

Huang, J. Q., and Chen, B. W., 1987, The evolution of the Tethys in China and adjacent regions: Beijing, Geological Publishing House, 109 p. (in Chinese).

Huang, J. Q., Ren, J. S., Jiang, C. F., and Zhang, Z. K., 1980, Tectonics of China and its evolution: Beijing, Sci. Press, 124 p. (in Chinese).

Ji, H. B., Wang, S. J., and Wen, J. M., 1999, The metallogenic chronology for the Manaoke gold deposit in northwestern Sichuan: Bull. Mineral., Petrol., Geochem., v. 18, no. 2, p. 95–98 (in Chinese).

Jing, C. G., and Wang, X. C., eds., 1995, On metallogenic condition and potential exploration targets for epithermal gold deposits in the Tethys domain of southwestern China: Tianjin, Unpubl. internal report, 149 p. (in Chinese).

Liu, J. J., Zheng, M. H., and Zhou, D. A., 1996, Metallogenic age analysis of gold and uranium deposits in the southern subzone of the western Qinling belt: Unpubl. conf. paper (in Chinese).

Liu, Y. P., Chen, Z. L., and Li, J. Z., 1998, Tectometallogenism in Kangding metamorphic core complex: Unpubl. conf. paper (in Chinese).

Lu, S. M., and Wang, X. C., eds., 1993, Metallogenic regularity and target prediction of gold deposits in the Shimian-Huili section of the Kangdian axis: Chengdu, Southwest Inst. Metallurg. Mineral Resources Explorat. Dvlpt., internal report, 233 p. (in Chinese).

Luo, Y. N., ed., 1995, Metallogenic condition and prospective prediction of nonferrous and precious metal deposits in the southwestern margin of Yangtze platform: Chengdu, Southwest Inst. Metallurg. Mineral Resources Explorat. Dvlpt., internal report, 233 p. (in Chinese).

Luo, M., He, H., and Wang, Y. W., 1998, Geologic features and genesis of Baxi gold deposit in Ruoergai, Sichuan: Mineral Deposits, v. 17 (suppl.), p. 377–380 (in Chinese).

Ni, P., Wang, J. M., Liu, Z. S., and Yao, P., 1996, Geology and geochemistry of Dingtianzhu granitoids and its genetic relation to the Zhonggu gold deposit, *in* Luo, Y. N., ed., Contributions to geology and mineral Resources in the Intracontinental Orogenic Belt: Chengdu, Sichuan Sci. Technol. Press, p. 112–119 (in Chinese).

Peng, D. Q., 1992, Preliminary analysis on distribution of gold, copper, and platinum group metals in northern Sichuan and southern Gansu gold (uranium) metallogenic belt: Geol. Acta Sichuan, v. 12 (suppl.), p. 43–46 (in Chinese).

Wang, H. Z., and Me, X. X., 1995, An outline of the tectonic evolution of China: Episodes, v. 18, p. 6–16.

Wang, X. C., 1992, On isotope geology of the Pulongba gold deposit: Contrib. Geol. Mineral Resources Res., v. 7, no. 2, p. 85–97 (in Chinese).

_____, 1993, On conditions of ore formation of fine disseminated–type gold deposits in the Qiuluo metallogenic belt, Ganzi: Mineralogy and Petrology, v. 13, no. 1, p. 68–75 (in Chinese).

_____, 1994a, On isotope geology of fine disseminated gold deposits in northwestern Sichuan: Jour. Shenyang Inst. Gold Technol., v. 13, no. 4, p. 309–316 (in Chinese).

_____, 1994b, Tectonic setting and metallogenic regions of gold deposits in Sichuan: Southwest Metallogenic Mineral Resources and Geology, no. 3, p. 8-17; no. 4, p. 10–29 (in Chinese).

_____, 1995a, Rifting and fine disseminated gold deposits: Example of the Luhuo rift, eastern Tethys: Unpubl. Ph.D. dissertation, Chengdu College of Technology, 88 p. (in Chinese).

_____, 1995b, On the ore-formation process of fine disseminated gold deposits in northwestern Sichuan: Acta Geol. Sichuan, v, 15, no. 1, p. 41–48 (in Chinese).

_____, 1998a, On migration and deposition mechanisms of ore-forming materials of sediment-hosted disseminated gold deposits in China: Contrib. Geol. Mineral Resources Res., v. 13, no. 1, p. 45–55 (in Chinese).

_____, 1998b, Classification system and dominant types of gold deposits in western Sichuan: Gold Sci. Technol., v. 6, nos. 5-6, p. 24–28 (in Chinese).

Wang, X. C., and He, G., 1993, On geology and geochemistry of the Jinjitai gold deposit in Sichuan: Mineral Resources and Geology, v. 8, no. 2, p. 74–82 (in Chinese).

Wang, X. C., Lu, S. M., Hu, J., and He, G., 1999, On geological and geochemical characteristics of the Mianshawa gold deposit in Sichuan: Bull. Mineral., Petrol. Geochem. (in Chinese, accepted).

Wang, X. C, Ye, S. P., and Xu, D. Z, 1998, The preferential selection of exploration targets for main types of gold deposits in western Sichuan: Chengdu, Southwest Inst. Metallurg. Mineral Resources Explorat. Dvlpt., internal report, 184 p. (in Chinese).

Wu, X. Y., Chen, J. P., Li, L. K., Li, H. W., Yang, Z. S., He, J. L., and Deng, T. X., 1996, Deformational features of the Moxi shear zone and its mechanism of formation, *in* Luo, Y. N., ed., Contributions to geology and mineral resources in the Intracontinental Orogenic Belt:

Chengdu, Sichuan Sci. Technol. Press, p. 74–82 (in Chinese).

Wu, X. Y., and Luo, Y. N., 1998, Deformation features and dynamic analyses of the Moxi shear zone in Tianwan, Shimian, Sichuan: Unpubl. conf. paper (in Chinese).

Wu, X. Y., and Xia, J. J., 1996, Genetic mechanism of shear zone type gold deposit in Jindonggou, Pingwu, Sichuan, *in* Luo, Y. N., ed., Contributions to geology and mineral resources in the Intra-continental orogenic belt: Chengdu, Sichuan Sci. Technol. Press, p. 181–189 (in Chinese).

Xu, Z. Q., Hou, L. W., and Wang, Z. X., 1992, Orogenic processes of the Songpan-Ganzi orogenic belt of China: Beijing, Geol. Publ. House, 190 p. (in Chinese).

Yu, A. G., 1998, Extentional structures in Shimian-Mianning, Sichuan: Unpubl. conf. paper (in Chinese).

Yuan, H. H., 1987, Preliminary outline for basement chronology of Kangdian axis: Contrib. to Panzhihua-Xichang Rift, China: Beijing, Geol. Publ. House, v. 2, p. 51–60 (in Chinese).

Zhang, J. K., 1998, Isotopic features and distribution of gold deposits from Kongyu to Huili gold belt, western Sichuan: Gold Geology, v. 4, no. 3, p. 27–29 (in Chinese).

Zhang, N. D., Cao, Y. W., Liao, Y. A., Zhao, Y., Zhang, H. J., Hu, D. Q., Zhang, G., and Wang, N. Z., 1998, Geology and metallogeny in Ganzi-Litang rift zone: Beijing, Geol. Publ. House, 119 p. (in Chinese).

Zhang, Z. M., Liou, J. G., and Coleman, R. G., 1984, An outline of the plate tectonics of China: Geol. Soc. Amer. Bull., v. 95, p. 295–312.

Zhao, J. X., 1998, Gold-bearing ductile shear zones in the Mianning and Muli areas: Unpubl. conf. paper (in Chinese).

Zheng, M. H., ed., 1989, An introduction to stratabound gold deposits: Chengdu, Chengdu Univ. Sci. Technol., 266 p. (in Chinese).

_____, ed., 1994, Stratabound gold deposits of the exhalation and turbidity types: Chengdu, Sichuan Sci. Technol. Press, 273 p. (in Chinese).

Geology of Sedimentary Rock-Hosted Disseminated Gold Deposits in Northwestern Sichuan, China

XIAO-CHUN WANG [†], AND ZHE-RU ZHANG

Institute of Geochemistry, Chinese Academy of Sciences, Guiyang, Guizhou, 550002 China

Abstract

Sixteen sedimentary rock-hosted disseminated gold deposits (such as Dongbeizhai, Qiuluo, Manaoke, Laerma, Gala and Lianhecun) and about fifty prospects have been discovered in northwestern Sichuan Province, China since the late 1970s. They are hosted in complex rock series including fine-grained clastic rock series, subvolcanic rock series and ophiolitic melange rock series of mainly Triassic age. They have a mineral association of pyrite, arsenopyrite, marcasite, realgar, orpiment, stibnite, cinnabar, quartz, calcite and barite, and an element association of gold, arsenic, antimony, mercury, thallium and barium. In addition, some minerals such as scheelite, uranite, and bismuth minerals are present in some deposits. Sub-micron-sized and micron-sized gold is disseminated within black, carbonaceous pelitic to sandy clastic and volcanoclastic rocks. Hydrothermal alteration phases are fine-grained silica, carbonate minerals (calcite, dolomite and siderite). Organic material is found in most clastic host rocks and ores. Ore bodies are obviously controlled by fractures. Fluid inclusion data show that the ores were formed at temperatures ranging mostly from 150 to 250°C, at pressures less than 400 bars, and from fluids with salinity from 3 to 14 Wt % NaCl and density from 0.82 to 1.00 g/cm^3. Isotopic data reveal that the ore-forming ages are from middle-late Mesozoic to Tertiary and that the ore fluids vary from -117.8 – -52.9 per mil (average -83.6 ± 16.5 ‰) in δD value and from -11.1 to 16.2 per mil (average 11.1 ± 9.2 ‰) in $\delta^{18}O$ value. Sulfur isotopes from epigenetic sulfide change from -25.6 to 7.8 per mil, mostly between -6.6 and -1.2 per mil. In view of the element associations, sedimentary rock-hosted disseminated gold deposits in northwestern Sichuan can be divided into six subtypes as follows: Au, Au-As, Au-Sb, Au-Hg, Au-W and Au-U.

These deposits have similar features to those in Nevada, U.S.A, including tectonic setting, mineral association, element association, gold occurrence, alteration (such as silicification and carbonatization), ore-forming temperature, metallogenic age as well as spatial relationship with igneous rock bodies. But there are some differences between them. Some minerals such as scheelite, uranite, and bismuth ones are present in some NW-Sichuan deposits. The high angle normal faults and regional oblique-slip (thrust) faults are emphasized for the localization of mineralization in Nevada deposits and NW-Sichuan deposits respectively. The NW-Sichuan deposits found to date are smaller than most U.S. deposits. In Nevada, the gold deposits occur mainly in impure carbonate rock series of Paleozoic age, but in NW-Sichuan, they are hosted in complex rock series of mainly Triassic age. In NW-Sichuan deposits, decarbonatization and shallow acid-leaching alterations are much weaker than those in Nevada deposits. Estimated pressures at NW-Sichuan deposits are smaller than those at Nevada deposits. The ore fluids in NW-Sichuan deposits have relatively higher salinities and slightly lower δD values than those in Nevada deposits.

The authors suggest a possible model for the NW-Sichuan deposits. Ore-forming materials were scavenged mainly from fine-grained clastic rocks by polygenetic fluids, which consisted of connate and meteoric water with moderate salinity. Regional geothermal anomalies resulted due to intensive tectonic and igneous activities during Yanshanian intra-continental superposed orogeny. Fracture zones acted not only as the percolating channels, but also as stress-releasing sites, where energy and pressure were released. The deep confined fluid, in which gold transported mainly as $Au(HS)^-_2$, flowed from the lateral subsidiary fractures and rose along deep fractures. When the fluid reached shallow depths, temperature and pressure decreased, and the fluid would become neutral in pH value accompanied by an increase in fO_2 and a decrease in total sulfur activity (and also the activity of reduced sulfur). The equilibrium of the fluid system would be destroyed causing decomposition of Au

[†] Also at Southwest Institute of Metallurgical Mineral Resources Exploration and Development, Chengdu, Sichuan, 610051 China . email: lhongjun@mail.sc.cninfo.net

transporting complexes and deposition of ore-forming materials. The successive cycling of ore-forming fluid and mineralizing was kept going by the constant supply of meteoric water.

Introduction

THE sedimentary rock-hosted disseminated gold deposits (or Carlin-type gold deposits) in the world are mainly distributed in two regions: the western United States (especially Nevada) and southwestern China. Over the last 20 years, great advances have been made in our understanding of the geology and mineralogy of sedimentary rock-hosted disseminated gold deposits as well as the chemistry of their ore-forming fluids (Radtke et al., 1980; Rye, 1985; Tooker, 1985; Hofstra et al., 1991; Kuehn and Rose, 1992; Arehart, 1996).

Since the late 1970's, a large number of sedimentary rock-hosted disseminated gold deposits and prospects have been discovered in the Indochina and in the Variscan fold belts along the periphery of the Yangtze craton. They constitute two triangular regions in Sichuan-Gansu-Shanxi and Yunnan-Guizhou-Guangxi (Fig.1). It was not until the middle 1980s, when sixteen sedimentary rock-hosted disseminated gold deposits and fifty-two prospects were discovered, that the northwestern part of Sichuan Province was acknowledged as one of the most important gold producing regions in China. The great potential of gold resources has been attracting worldwide attention and considerable exploration efforts have been devoted to this deposit type.

The deposits in NW-Sichuan not only share some common features with other sedimentary rock-hosted deposits elsewhere in the world, but also have their own unique characteristics. The aim of this paper is to present the geological setting, general characteristics, and suggest a possible genetic model for the gold deposits in this portion of China.

Geological Setting

The sedimentary rock-hosted disseminated gold deposits in northwestern Sichuan lie in the Kekexili-Bayankala massif. This is located between the Jinshajiang suture zone to the west and the Longmenshan nappe zone to the east. The basement of this massif belongs to the Yangtze craton. The Yangtze craton that is composed of crystalline rocks of Archean to Proterozoic age overlaid by shallow marine platform deposits ranging from Sinian (Late Proterozoic) through Triassic in age. The Kekexili-Bayankala massif may be divided into five units (Fig.2). The sedimentary rock-hosted disseminated gold deposits and prospects are located in the Ganzi-Litang suture (III), Luhuo-Daofu rift (IV-2), Bayankala-post Longmenshan fold belt (IV-3) and Western Qinling block (V) (Fig.3).

Rocks in the Kekexili-Bayankala massif are mostly Devonian through Triassic in age, varying from 5,000 to 20,000 meters in thickness, and are composed of fine-grained clastic sedimentary rocks. Volcanic and subvolcanic rocks are present in some areas such as rift, arc and suture. They increase in abundance from east to west and are accompanied by a subvolcanic lithology trend from acid to basic.

The rocks were folded during post-Triassic Indochina through Himalayan orogenies. North-northwest to northwest-trending and northeast-trending faults and folds are most common, but in some areas, east-trending or north-trending faults and folds are dominant. Gold distribution and mineralization was controlled by these faults on the deposit scale.

Variscan to Himalayan intrusive rocks are also present. Older intrusions are distributed in the eastern and western parts of the region whereas younger intrusions are generally restricted to the central portions.

Geological Characteristics of Sedimentary Rock-Hosted Disseminated Gold Deposits

NW-Sichuan is currently one of the largest potential producers of gold in China and continues to be the focus of intense exploration. A classification scheme based on element association and mining standard includes six subtypes as follows:

a. The Au dominant subtype in which only gold is of economic interest. Examples are the Lianghecun, Jiawuchi, Shuinuijia, Songpangou, Zeboshan, Xionglongxi, Pulongba, Bapengzi and Liangchahe deposits.

b. The Au-As subtype in which arsenic may be enriched to the degree where economically viable arsenic

deposits also exist. Usually, gold deposits of this subtype such as the Dongbeizhai and Qiaoqiaoshang were originally mined for arsenic ores.

c. The Au-Sb subtype, in which antimony mineralization (stibnite) is developed, was originally antimony occurrence. The Qiuluo and Gala deposits are examples of the subtype.

d. The Au-Hg subtype is accompanied by mercury mineralization (cinnabar) .An example is the Yinchang deposit that was discovered by virtue of mercury mineralization.

e. The Au-W subtype such as the Manaoke deposit.

f. The Au-U subtype gold deposits such as the Laerma deposit.

The gold deposits listed in Table 1 are noteworthy for their significant reserves and for their characteristic styles of mineralization.

Ore-bearing strata and ore bodies

Ore-bearing strata for the sediment-host disseminated gold deposits in northwestern Sichuan are mainly Triassic, followed by Middle Devonian and Lower Cambrian. For example, at the Dongbeizhai deposit (a on Fig.2 and Fig.3), ore bodies occur along NS-trending high angle reverse faults between Carboniferous limestone in the hanging wall and the slightly metamorphosed black fine-grained rocks (slate, and sandstone) of the Triassic Xingduqiao Formation in the footwall (Fig.4). The altered zones along N-trending faults at Dongbeizhai include thirteen major ore bodies and sixteen minor ore bodies in an area about 6000 m along the strike by about several tens to more than 100 meters across (using a grade cutoff of 1 ppm gold).

At the Qiuluo deposit (b on Fig.2 and Fig.3), gold mineralization occurs as layered and brecciated bodies in slightly metamorphosed basic volcanic and a fine grained clastic rock series of the Upper Triassic Runiange Formation (Fig. 5). In the ore district, the Runiange Formation may be divided into two units: (1) The first unit (T_3r^{2-1}) is composed of dark green basalt intercalated with limestone and sandstone; (2) The second unit (T_3r^{2-2}) consists of dark gray to black thin-bedded carbonaceous slate intercalated with sandstone, chert and pelitic limestone. Four ore bodies have been found in an area of 2500 × 800 m. The deposit has gold reserves of more than 10 metric tons based on recent shallow engineering, and has the potential to be a giant deposit.

The ore bodies at the Laerma deposit (c on Fig.2 and Fig.3) occur in the Lower Cambrian Laerma Formation, and are controlled by NWW-trending reverse faults. These ore bodies are localized in the juncture zone between the NEE-NE-trending faults and the NWW-trending faults. Nearly one hundred ore bodies have been delineated in an area of about 5600 × 350 m (Fig.6).

Seventeen layer-like or lens-like gold ore bodies conformable to the host layers have been discovered in the Manaoke deposit (d on Fig.2 and Fig.3). The ore bodies were hosted in Middle-Upper Triassic Zagunao Formation ($T_{2-3}z$) (Fig.7). The ore bodies vary from 80 to 1,100 m (average 350 m) in length, 1.19 to 6.12 m (average 3.08 m) in thickness, and 1.66 – 9.64 ppm (average 3.55 ppm) in grade. In addition, eight independent tungsten ore bodies (80 – 400 m in length, 0.7 – 3.0 m in thickness and 0.19 – 1.69 % in WO_3 grade) have been found in similar localized zones for gold ore bodies (Fig.7) (Zheng, 1994). Both gold and tungsten ore bodies are spatially related to the interlayer faults.

At the Yinchang deposit (e on Fig.2, Fig.3), gold ore bodies occur mainly in quartz graywackes intercalated with slates in the Middle to Upper Triassic Zagunao Formation, as well as Carboniferous and Permian carbonate rocks (Fig.8). Five gold ore bodies ranging from 30 to 720m in length have been found in the district. They may be divided into two types: stratiform and brecciated. The stratiform ore bodies such as No. II and No. III occur layer-like and lens-like within the strata, and range from 3.25 ~ 5.34 ppm Au with a maximum value of 19.61ppm. The brecciated ore bodies (such as No. I, No. IV and No. V) occur in the fractured belt, with average gold grades of about 10ppm. In addition, two mercury ore bodies from 83 – 402 m in length, 1.67 – 7.00 m in thickness, and containing 0.042 – 0.097 % mercury, occur in Permian carbonate rocks. Exploration of mercury-rich lenses revealed the gold deposit.

At the Pulongba gold deposit (f on Fig.2 and Fig.3), ore bodies occur as isolated phacoids in a sheared matrix in the Upper Section of the Upper Triassic Runiange Formation (T_3r^2) (Fig.9). This section can be divided into three

units: (1) The first unit is composed of basalt intercalated with carbonaceous silty slate and thin-bedded slightly metamorphosed sandstone; (2) The second unit consists of dark gray to black thin-bedded carbonaceous slate intercalated with sandstone, chert and pelitic limestone; (3) The third unit is made up of quartz graywack intercalated with thin-bedded silty slate, basalt and brecciated basaltic rocks.

In the Lianhecun deposit (g on Fig.2 and Fig.3), Devonian and Triassic sandstone and slate and Carboniferous carbonate rocks outcrop. More than thirteen gold ore bodies with grades over 3ppm occur as layer-like and lens-like forms along northeast- to nearly east-trending faults (Fig.10).

Igneous rocks

Igneous rocks do not exist in most Sichuan deposits such as Manaoke and Yichang. But they do outcrop in some deposits or nearby areas. For example, some dacite phophyritic and Early Yanshanian (Mesozoic) granite porphyry dykes outcrop at the Laerma and Lianhecun ore districts respectively. At the Qiuluo deposit, the Indochina orogeny age diabase dykes also outcrop in the mine. At the Pulongba deposit, basic-ultrabasic rocks such as pyrolite (which consists mainly of pyroxene and olivine) outcrop. Igneous rocks in the vicinity of the Dongbeizhai deposit are diabase dykes that were emplaced discontinuously along the N-S-trending fault in the form of isolated phacoids in a sheared matrix. They are slightly metamorphosed and tectonically cleaved and sheared. The cleavages of the isolated phacoids of igneous rocks are approximately parallel to those of the tectonites of the major fault. These were subsequently hydrothermally altered and locally mineralized.

Ore-host rocks

There are various rocks hosting gold mineralization in NW-Sichuan. Main rock types are slate, sandstone, and secondary types are chert, subvolcanic rocks, as well as basic-ultrabasic rocks. The fine-grained clastic rocks are carbonaceous, silty, Fe-bearing, dolomitic, debris-bearing quartz graywackes and slates, in which abundant organic material and diagenetic pyrite are present. Most gold deposits such as at Dongbeizhai, Qiuluo, Manaoke, Yichang occur in these rocks.

The host rocks are chert, slate and porphyritic dacite at Laerma, and are slates, tuffaceous slates, pyrolite (which consists mainly of pyroxene and olvine) and gabbro-diabase at Pulongba. The host rocks at Lianhecun are mainly sub-volcanic rocks (mainly granite porphyries), sandstone and slates.

All mineralized rocks are fault gouge, fault breccia and cataclastite, which are dynamic, metamorphosed products of host rocks.

Alteration phases

Hydrothermal alteration phases are mainly quartz, sericite, and carbonate minerals (calcite, dolomite, siderite). Quartz formed early in the paragenesis occurs as disseminated, veinlets and stockworks, and is accompanied by sericite, pyrite, arsenopyrite, which is spatially associated with gold mineralization. Veins or stockworks of carbonate minerals often crosscut the quartz veinlets, suggesting that they occurred later in the paragenesis. Some deposits such as Laerma and Dongbeizhai show certain degree of carbonate removal, which is accompanied with early-formed quartz.

The zinc-bearing sericite at Qiuluo formed later in the paragenesis is accompanied with stibnite, quartz and carbonate minerals (dolomite and calcite). At Laerma, there are also barite, and dickite. Barite formed later in the ore-forming stage, and was accompanied with quartz, dickite, stibnite and native gold. Scheelite and stibnite accompany the calcite veins at Manaoke. Chlorite is chiefly developed in the basic to ultrabasic rocks and tuffaceous rocks of the Pulongba deposit, in which mafic minerals and plagioclase were both replaced by chlorite. Kaolinite, fluorite, barite, anhydrite and jarosite are also common in host rocks at Lianhecun.

Metallic Mineral assemblage

The common metallic minerals are pyrite, arsenopyrite, stibnite, native gold, cinnabar, realgar, followed by marcasite, pyrrhotite, orpiment, sphalerite, arsenian tetrahedrite, chalcopyrite. The amounts of minerals in gold ores vary with the characteristics of host rocks and deposit subtypes. Vast amounts of scheelite occur at Manaoke. Certain amounts of uranite, bismuth minerals (native bismuth, bismuthine, and tetradymite) occur in the gold ores of Laerma and Pulongba respectively. Relatively abundant realgar and less arsenic occur in late veins of Dongbeizhai, together

with quartz and calcite. Stibnite occurs as veins, stockworks and disseminated forms in altered rocks and fissures. Arsenic contents of hydrothermal pyrite range from 0.48 to 2.46 %.

Native gold occurs mainly as sub-micron sized gold (< 0.2 μm) in pyrite, arsenopyrite and clay minerals (mainly sericite). Some native gold grains, with fineness from 822 to 995 and 2 – <100 μm in size, are found in arsenopyrite, pyrite (limonite) and sericite as well as in barite, quartz, stibnite and siderite in the oxidized and semi-oxidized ores. In addition to silver, native gold contains some iron, platinum, bismuth, palladium, copper, tellurium and arsenic at Pulongba (Table 2). The occurrence of bismuth minerals generally indicates the presence of high-grade gold ores at the Pulongba deposit.

Gold was accompanied by the deposition of pyrite, arsenopyrite and marcasite. Most antimony (as stibnite), mercury (as cinnabar), and even arsenic (as realgar and orpiment) was deposited later in paragenesis (see Fig. 11,Fig.12, Fig.13).

In addition, it is very interesting that certain amounts of cosmic dusts have been discovered in the ores at Manaoke (Zheng, 1994). The cosmic dusts occur mainly as black- and brown-colored spheroids, and vary from 25 to 183 μm in diameter. They have vesicular, impact crater, pelletoidal, vermiform, sheet-like, crustiform, and welded structures. The electrum probe analyses show that they are from 91.8 to 99.8 % iron in content, 0 to 8.2 % chromium, and 0 to 2.7 % silicon, suggesting the type of iron cosmic dust. The iron cosmic dust may have provided some material for the formation of source beds during Triassic.

Element association

The ubiquitous element association is gold, arsenic, antimony, mercury, barium and thallium (Table 3). In addition, gold ores at Laerma are also accompanied by selenium, uranium, and platinum group elements. Gold ores contain 18.0 – 57.5 ppm (average 28.8 ppm) selenium, 4.9 – 34.5 ppm (average 12.0 ppm) uranium, as well as 2 –103 ppb (average 17 ppb) platinum, 2 – 264 ppb (average 26 ppb) Palladium, and 2 – 22 ppb (average 4 ppb) Osmium.

Soil and stream sediment geochemical surveys in each district corroborate the association of arsenic, mercury, antimony and thallium with gold.

Arsenic mineralization has been proved to be a good indicator of gold mineralization in the area. There is a significantly positive Spearman rank correlation between gold and organic carbon at the Dongbeizhai deposit (Zheng, 1989), suggesting that the organic matter may have played some role in gold deposition.

Fluid inclusion feature

In most NW-Sichuan deposits, primary fluid inclusion types observed are liquid-rich and vapor-liquid inclusions (Table 4). They are irregular, from less than 3 to 30 μm in diameter, and 2 to 30 in vapor percentage. But in some deposits such as Laerma, vast amounts of fluid inclusions exist in quartz and barite. They are from 5 – 20 μm (maximum 60 μm) in diameter. Fluid inclusion types include vapor-liquid, pure vapor, pure liquid as well as three phase ones (with vapors of H_2O and CO_2 or CH_4 as well as liquid of H_2O). From the evidence that various types of primary inclusions in the same mineral, and same growth plane that occur as both fluid- and vapor-rich inclusions and that homogenize to the same temperature, it can be seen that local boiling existed during fluid evolution.

The temperatures are determined by homogenization and decrepitation measurements. The salinity is determined by ice melting temperature measurement. The temperature-density-salinity, and pressure-density-temperature relationship for NaCl-H_2O system respectively (Liu and Duan, 1987; Roedder, 1984) determine the density and pressure. On the basis of the equilibrium relationship of coexisting minerals, the assumption that the gases captured in inclusions are in ideal state, which are obeying the Dalton partial pressure law, various other physico-chemical parameters can be calculated and are listed in Table 4, in which the pH value be determined by the assumption that there is equilibrium relationship among calcite, HCO_3^-, H^+, Ca^{2+}, H_2O, and $CO_2(g)$ during ore-forming period. The results show that the ores were formed at temperatures ranging from 140 to 290 °C (mostly from 150 to 250°C), at pressure from 26 to 400 bars (average 193 Bars), and from fluids with salinity from 3 to 14 Wt % NaCl and density from 0.82 – 1.00 g/cm^3. Compared with the pH values of neutral fluids at corresponding temperatures, the ore fluids show the near neutral characteristics. The values of fO_2 and fS_2 were significantly low and dramatically decreased in the evolution of ore fluids.

Vitrinite geothermometry

Paleothermal gradients are based on virtrinite reflectance measurements of samples from the Luhuo-Daofu rift and yield vitrinite reflectance equivalent (VRE) values ranging from 3.07 to 5.88. These results indicate that organic material in unaltered rocks reached maturation levels equivalent to the anthracite/meta-anthracite boundary in coal. The temperature may be calculated by the condition that organic maturation be reached during post-Triassic Yanshanian and Himalayan periods (about 200 Ma). The minimum depth may be gained by the strata thickness overlaying the sample location. We interpret these results to be that the paleogeothermal gradient ranged from 51.3 to 153.9 °C/Km (averaging at 65.2 °C/Km) during Yanshanian and Himalayan periods (Wang, 1995a). Organic matter is distributed widely in both mineralized and unmineralized rocks. Quartz veinlets containing pyrite and arsenopyrite often crosscut organic matter such as pitch. These may show that the thermal event, caused by the combination of tectonic and igneous processes resulting in the maturation of organic matter, was apparently a regional event that preceded mineralization. Ore-forming hydrothermal activity occurred at some time later.

Isotopic geochemistry

The formation age of these deposits is controversial. Maximum ages in many cases are provided only by the Triassic of the youngest host rocks. At some deposits such as Pulongba, Laerma and Lianhecun, Middle-Late Mesozoic (Jurassic or Cretaceous) diabase dykes, granitic porphyries, and porphyritic dacite are hydrothermally altered and mineralized in varying degree, and are often crosscut by quartz veinlets, suggesting that gold mineralization occurred after the intrusion of these rocks. In addition, the direct dating of gold ores and minerals by K–Ar, U–Pb, Rb–Sr, and $^{40}Ar/^{39}Ar$ methods can give some constraints on the formation ages. It may be seen from the limited data in studies to date (Table 5) that the probable ages range between 208 and 46 Ma.

In order to determine the characteristics and origin of ore fluids, quartz, calcite, wallrocks, and rain, pit and spring waters have been sampled for the measurement of hydrogen and oxygen isotopes. The δD values of ore fluids may be directly determined by the measurement of inclusion water in quartz and calcite. The $\delta^{18}O$ values of ore fluids can be obtained by calculation based on the isotopic fractionation equations for quartz-H_2O and calcite-H_2O at corresponding temperatures (O' Neil et al., 1969; Clayton et al., 1972). The results (Table 6) show that the mineralized fluid may be interpreted as formation water recharged by meteoric water that an involved interaction with wallrocks occurred prior to the gold deposition.

A total of eighty-seven sulfide and two barite samples from major NW-Sichuan deposits have been analyzed for sulfur isotopes (Table 7). The pyrite can be classified into two types, diagenetic and hydrothermal pyrite. The diagenetic pyrites were separated from unaltered host rocks and hydrothermal pyrites were from altered, gold-bearing host rocks. Under the microscope, the diagenetic pyrites show framboidal texture, and the hydrothermal pyrites show metasomatic texture. The $\delta^{34}S$ values of Triassic diagenetic pyrites reveal a marine sulfide contribution by bacteria of reduction (Holser and Kaplan, 1966). The sulfur isotopic differences among hydrothermal sulfides in Triassic-hosted deposits are consistent with the differences of oxidation state of sulfur and the bond strength of iron pairs among them, suggesting their similar sulfur sources. As HS^- is the dominant dissolution species of sulfur in fluids, little isotopic fractionation between pyrite and HS^- takes place, the average $\delta^{34}S$ value of fluid may be represented by that of hydrothermal pyrites. The $\delta^{34}S$ values of hydrothermal pyrites are similar to the average value of diagenetic pyrites. These similarity reveals that the sulfur in gold ores was mainly contributed by the diagenetic pyrite in host sedimentary rocks. For the Lower Cambrian-hosted Laerma deposit, the varied isotopes of hydrothermal pyrite and marcasite may suggest the sulfur was mainly provided by diagenetic sulfides. The isotope differences between pyrite and stibnite also show their similar sulfur source. The sulfur isotopes of barite may have been resulted from the dissolution and oxidation of early-formed sulfides.

The $\delta^{13}C$ values of calcite and dolomite samples in the ores, limestone, and CO_2 in fluid inclusions of quartz from the Triassic-hosted deposits (Table 8) are in the range between those of marine limestone (ranging from -2.7 to 3.4 per mil, average 2.1 ‰) and marine organic carbon (from -27.2 to -25.1 ‰, average -22.0 ‰) in the Triassic system of southwestern China (Wang, 1996). These data, along with the $\delta^{13}C$ values of pitch samples in gold ores and CO_2 in fluid inclusions from a quartz sample in the Lower Cambrian-hosted Laerma deposit show that the carbon in the ores originated from host rocks and organic matter.

Lead isotope data of minerals, ores, and surrounding rocks from four deposits are listed in Table 9. The data of diagenetic pyrite, hydrothermal pyrite and stibnite, slate, sandstone, limestone, as well as diabase dykes from Dongbeizhai show that the ore lead originated from Triassic slate and diagenetic pyrite. At Laerma, the lead isotopic ratios of ore minerals vary significantly, showing the characteristics of anomalous lead. A positive relationship exists between $^{207}Pb/^{204}Pb$ and $^{206}Pb/^{204}Pb$, with the equation: $^{207}Pb/^{204}Pb = {}^{206}Pb/^{204}Pb \times 0.06096606 + 14.402$. By means of anomalous lead mixture modeling, with necessary t_1 as the model age of diagenetic pyrite, the ore-forming age of 113.5 Ma can be calculated. It is in the age range determined by other methods (49.5–127 Ma, see Table 5). Then, the lead in gold ores was likely to be from diagenetic sulfides and their surrounding rocks. At Manaoke, the isotopic range of ore lead represented by quartz and stibnite is very small, with single stage model ages from 906 to 994 Ma (average 947 Ma), which are older than their host rocks. Combined with geological setting, the lead may be supplied by the underlying basement (Bikou Group of Middle Proterozoic age). At Pulongba, the gold ores show a limited isotopic range, with single stage model ages varying between 188 and 243 Ma (average 211 Ma), which represent the ages of source rocks. By means of radiogenic decay equations, the lead isotopes of various rocks during the ore-forming period (154 Ma) can be calculated with their uranium, thorium, and lead contents. It may be shown from the lead isotopic comparison among ore and rocks during the ore-forming period (Fig. 14) that the ore lead was derived mainly from fine-grained clastic rocks or, to a lesser extent, from basic volcanic rocks in the strata. In summary, the lead in gold ores may be chiefly derived from host clastic rocks and diagenetic sulfides in them, and secondly from underlying strata.

At the Laerma deposit, the $\delta^{30}Si$ values change from 0.4 to 1.3 per mil (average 0.7 ‰) for five chert samples and from -0.7 to 0.2 per mil (average -0.2 ‰) for four samples of quartz in the major stage. The $\delta^{30}Si$ value of a quartz sample in early stage is 0.7 per mil (Zheng, 1994). These data show that the silicon in gold ores may have originated from chert and sandstone in ore-bearing strata.

Discussion

Comparison with sedimentary rock-hosted disseminated gold deposits of Nevada, U.S.A

The gold deposits in NW-Sichuan have similar features to those in Nevada, U.S.A, including tectonic setting, mineral association, element association, gold occurrence, alteration (such as silicification and carbonatization), ore-forming temperature, metallogenic age as well as spatial relationship with igneous rock bodies (see Table 10) (Radtke et al., 1972, 1980; Wells and Mullens, 1973; Radtke, 1985; Rye, 1985; Tooker, 1985; Fournier, 1985, 1986; Bagby, 1989; Cook and Chryssoulis, 1990; Nelson, 1990; Mao, 1991; Hofstra et al., 1991; Kuehn and Rose, 1992; Gao and Wang, 1992; Wang, 1992,1994, 1995a, 1996, 1998; Arehart et al., 1993; Jansma and Speed, 1993; Zheng, 1994; Drewes-Armitage et al., 1996; Arehart, 1996; Groff et al., 1997; Ilchik and Barton, 1997; Stenger et al., 1998). But there are some differences between them as follows.

The high angle normal faults are emphasized for the localization of mineralization in Nevada deposits, but in NW-Sichuan deposits, the main ore-controlling structures are regional oblique-slip (thrust) faults. Minerals such as scheelite, uranite and bismuth minerals are present in some NW-Sichuan deposits, but appeared to be rare or absent in the western US examples. Realgar and arsenian pyrite is the main arsenic mineral associated with gold mineralization in Nevada deposits (Ilchik et al., 1986), but in NW-Sichuan deposits, arsenopyrite and realgar are the chief arsenic minerals. Certain amounts of micron-sized native gold has been found in oxidized and semi-oxidized ores in some NW-Sichuan deposits.

There are differences in the age and rock series of ore-bearing strata between the two areas. In Nevada, USA, the gold deposits occur mainly in impure carbonate rock series of Paleozoic age, but in NW-Sichuan, they are hosted in complex rock series including a fine-grained clastic rock series, subvolcanic rock series, and ophiolitic melange rock series of mainly Triassic age. But at most NW-Sichuan deposits, decarbonatization and shallow acid-leaching alterations are much weaker than those in Nevada deposits (Radtke et al., 1980; Kuehn and Rose, 1992).

Estimated pressures at NW-Sichuan deposits (26 – 400 bars) are smaller than those at Nevada deposits (300 – 800 bars). Salinities of ore fluids in NW-Sichuan deposits (3 – 14 wt % NaCl) are relatively higher than those in Nevada deposits (< 5 wt % NaCl).

Hydrogen isotope data show that the ore fluids in Nevada deposits were slightly lighter ($\delta D < -100$ ‰) than those in NW-Sichuan deposits (-118 – -53 ‰). These suggest that the ore fluids in Nevada deposits were likely to be derived from meteoric water, and those in NW-Sichuan deposits may be a mixture of connate water and meteoric waters. Sulfur isotopes from epigenetic sulfides in NW-Sichuan deposits (-25.6 – 7.8 ‰, mostly -6.6 – -1.2 ‰) are lighter than those in Nevada deposits (5 – 25 ‰).

Under present circumstance, a quantitative comparison of grades and tonnages of the NW-Sichuan deposits with those in the model from Nevada (Mosier et al., 1992) provides a more realistic evaluation of the former deposits. Some of the NW-Sichuan deposits are above the median tonnage (5.5 Mt), and most of them are below the median tonnage. The median gold grade of the NW-Sichuan deposits (about 5.5 ppm) is higher than that of the Nevada (about 2.3ppm). However, some of the deposits in NW-Sichuan such as Qiuluo and Dongbeizhai may potentially be giant, because in the former, there are broad area of anomalous geochemistry in soils and rocks over an area of structurally prepared rocks but yet to be drilled. In the latter, the gold ore bodies do not thin out in depth, there are mineralization and geochemical anomalies in north, east, and south parts of the mine, and also to be drilled.

Possible genetic model for the NW-Sichuan deposits

Despite the economic importance and rather lengthy history of development, a consensus on the genesis of the sedimentary rock-hosted disseminated gold deposits has not been achieved. For the deposits in Nevada, USA, three contrasting genetic models draw parallels with better understood magmatic hydrothermal or metamorphic gold-bearing systems, or invoke alternative mechanisms to drive hydrothermal circulation. The first magmatic model suggests that these deposits are distal products of magmatic hydrothermal systems and proposes that magmas drive hydrothermal circulation and are the source for some fluid components and metals (Radtke et al., 1980; Sillitoe and Bonham, 1990; Arehart et al.,1993). The second hypothesis draws parallels with many models for mesothermal gold deposits and suggests that major fluid components and metals were derived during regional metamorphism of supercrustal rocks (Phillips and Powell,1993). A third model is that this type deposit develops in (meta)sedimentary rock-dominated terranes as a consequence of regional fluid circulation due to crustal extension. No link to magmatism or other heating events is necessary. Circulation of meteoric water is a response to extension-caused elevation of the geotherm and increases in permeability. Metals, sulfur, and silica are scavenged from sedimentary rocks at depth and are deposited in chemically favorably environments as the fluids ascend. Crustal extension is a net cooling process (Ilchik and Barton, 1997).

For the deposits in Northwestern Sichuan, the alteration phases, mineral assemblages, trace element suite, sulfide-silicate paragenesis, fluid inclusion, isotopic composition (hydrogen, oxygen, lead, carbon, sulfur, silicon), and the existence of igneous rocks reveal that the connate water and meteoric water did contribute to the ore fluids in the post-Triassic Yanshanian and Himalayan orogenies. The authors suggest a possible model for NW-Sichuan deposits as follows.

During the Variscan and Indochina orogenic periods, typical Au-bearing turbidites developed, that is, a black carbon-bearing pelitic and sandy rock series were formed in sedimentary basins through absorption of gold by bacteria and algae (Pashkova, et al., 1991; Titley, 1991). Ore elements were derived mainly from paleo-continental denudation and volcanic sediments. Gold in these formations was initially enriched as releasable species. The study of hydrogen and oxygen isotopes and fluid inclusion compositions show that ore-forming fluids were polygenetic, composed mainly of meteoric water and formation water, and enriched in the elements Cl, F, Na, and K. The Indosinian movement during the late-Triassic epoch resulted in the closing and uplifting of Variscan-Indosinian geosynclines in the Kekexili-Bayankala massif. Regional geothermal anomalies resulted due to intensive tectonic and igneous activities during the Yanshanian intra-continental superposed orogeny. Gold in the Au-bearing formations was mainly transported as $Au(HS)^-_2$ (Wang, 1995b, 1998). The increasing temperature would favor dissolution of gold and enlargement of volume and internal pressure for a low-density fluid. Thus these fluids would flow from relatively higher-pressure zones to lower pressure zones. In this case, fracture zones acted not only as the percolating channels, but also as stress-releasing sites, where energy and pressure are released. The deep confined fluid flowed from the lateral subsidiary fractures and rose along deep fractures. When the fluid reached shallow depths, temperature and pressure decreased, and the fluid would become neutral in pH accompanied by increase in fO_2 and decrease in total sulfur activity (and also the activity of reduced sulfur). The equilibrium of the fluid system

would be destroyed causing decomposition of Au transporting complexes and deposition of ore-forming materials. The successive cycling of ore-forming fluid and mineralizing was kept going by the constant supply of meteoric water.

Some considerations for future directions

As seen above, the sedimentary rock-hosted disseminated gold deposits in NW-Sichuan show many geological characteristics that are similar to those of deposits in the Great Basin, western United States. But NW-Sichuan gold deposits have their unique characteristics. The varied host rocks, specific elements and minerals determine the main differences from those deposits in the western United States. The structural dewatering model proposed is similar to traditional shear-zone related systems which occur in high-grade metamorphic rocks.

The model presented here, although consistent with the available evidence, points to a number of opportunities for future study:

1.The migration and deposition mechanism in the model is proposed mainly for gold and associated arsenic, antimony, and mercury. Uranium and tungsten may be migrated and deposited by other mechanisms, and deserves to be further researched.

2.Better constraints on timing of mineralization are critical to this, as well as to other alternative models.

3.Igneous rocks outcrop in some NW-Sichuan deposits. The available evidence shows that there is no direct relationship with gold mineralization. We think igneous rocks may supply some heat for gold mineralization, and that the similar tectonic environments resulted in their spatial association with gold mineralization. But are there any other roles of igneous rocks during the ore-forming period?

Acknowledgements

The first author wishes to acknowledge the Chinese Academy of Sciences (CAS) for funding for his appointment as a senior visiting scholar at Institute of Geochemistry, CAS. He also is grateful to Southwest Institute of Metallurgical Mineral Resources Exploration and Development, for granting him a leave of absence. The study is financially supported by a pre-selection program of the Chinese Climb Plan (Fundamental Research Concerning Exploration for Giant Mineral Deposits, No: 95-Yu-25) and a major program of the Chinese Academy of Sciences (Research on Gross Low-Temperature Metallogenic Domains in Southwestern China, No: KZ951-131-411). Comments by Dr. Andy Wilde, Marco T. Einaudi, William C. Bagby, Stephen G. Peters, and other two Economic Geology reviewers greatly improved the content and the style of the manuscript. The assistance provided by Mr. Chris Dieckmann and Prof. Wang Shengyuan in word processing the manuscript is appreciated. Thanks are also given to Mr. Jiang Guohao, Liu Ronggao and Zhang Chengbo, Liu Jiajun, Liu Xianfan, Gu Xuexiang, Yan Guihe, and Ms. Song Yunhong.

REFERENCES

Arehart, G.B., 1996, Characteristics and origin of sediment-hosted disseminated gold deposits: A review: Ore Geology Reviews, v. 11, p. 383 – 403.

Arehart, G.B., Foland, K.A., Naeser, C.W., and Kesler, S.E., 1993, $^{40}Ar/^{39}Ar$, K/Ar and fission track geochronology of sediment-hosted disseminated gold deposits at Post-Betze, Carlin trend, Northeastern Nevada: ECONOMIC GEOLOGY, v. 88, p. 622 – 646.

Bagby, W.C., 1989, Patterns of gold mineralization in Nevada and Utah: U.S. Geological Survey Bulletin, v. 1857-B, p. 11– 21.

Bagby, W.C., and Berger, B.R., 1985, Geological characteristics of sediment-hosted, disseminated precious-metal deposits in the western United States: Reviews in ECONOMIC GEOLOGY, v. 2, p. 169 – 202.

Clayton, R.N., O' Neil, J.R., and Mayeda, T.K.,1972, Oxygen isotope exchange between quartz and water: J.Geophys.Res., v. 77, p. 3057 – 3067.

Cook, N.J., and Chryssoulis, S.L., 1990, Concentrations of "invisible gold" in the common sulfides: Canadian Mineralogist, v. 28, p. 1 – 16.

Cox, D.P., and Singer, D.A., 1986, Mineral deposit models: U.S. Geology Survey Bulletin, v. 1693.
Drewes-Armitage, S.P., Romberger, S.B., and Whitney, C.G., 1996, Clay alteration and gold deposition in the Genesis and Blue Star deposits, Eureka County, Nevada: ECONOMIC GEOLOGY, v. 91, p. 1383 – 1393.
Fournier, R.M., 1985, Silica minerals as indicators of conditions during gold deposition: U.S. Geological Survey Bulletin, v. 1646, p. 15 – 26.
—1986, Carbonate transport and deposition in the epithermal environment: Reviews in ECONOMIC GEOLOGY, v. 2, p. 63 – 72.
Gao, Z.B., and Wang, X.C.,1992, The outstanding significance of Yanshanian-Himalayan cycle in the formation of endogenic gold deposits and its reason: Mineral Deposits, v. 11, no. 2, p. 97 – 105 (in Chinese).
Groff, J.A., Heizler, M.T., McIntoch, W.C., and Norman, O.L., 1997, $^{40}Ar/^{39}Ar$ dating and mineral paragenesis for Carlin-type gold deposits along the Getchell trend, Nevada: Evidence for Cretaceous and Tertiary gold mineralization: ECONOMIC GEOLOGY, v. 92, p. 601– 622.
Gu, X.X., 1996, Turbidite-hosted sediment-hosted gold deposits: Chengdu, Press of Chengdu University of Science and Technology, 240p.
Hofstra, A.H., Leventhal, J.S., Northrop, H.R., Landis, G.P., Rye, R.O., Birak, D.J., and Dahl, A.R., 1991, Genesis of sedimentary-hosted disseminated gold deposits by fluid mixing and sulfidation: Chemical-reaction-path modeling of ore-depositional processes documented in the Jerrit Canyon district, Nevada: Geology, v. 19, p. 36 – 40.
Holser, W.T., and Kaplan, I. R., 1966, Isotope geochemistry of sedimentary sulfates: Chem. Geol., (1): 93 – 135
Hu, J.P., 1991, Study on the Qiaoqiaoshang turbidite type gold deposit in Sichuan: Chengdu, Chengdu College of Geology, MSc. dissertation, 100p (in Chinese).
Illich, R.P., and Barton, M.D., 1997, An amagmatic origin of Carlin-type gold deposits: ECONOMIC GEOLOGY, v. 92, p. 269 – 288.
Jansma, P.E., and Speed, R.C., 1993, Deformation, dewatering, and decollement development in the Antler foreland basin during the Antler orogeny: Geology, v. 21, p. 1035 – 1038.
Ji, H.B., Wang, S.J., and Wen, J.M., 1999, The metallogenic chronology for the Manaoke gold deposit in the northwestern Sichuan: Bulletin of Mineralogy, Petrology and Geochemistry, v. 18, p. 95 – 98 (in Chinese).
Joralemon, P., 1951, The occurrence of gold at the Getchell mine, Nevada: ECONOMIC GEOLOGY, v. 46, p. 267 – 310.
Kuehn, C.A., and Rose, A.W., 1992, Geology and Geochemistry of wall-rock alteration at the Carlin gold deposit, Nevada: ECONOMIC GEOLOGY, v. 87, p. 1697 – 1721.
Liu, B., and Duan, G.X., 1987, Density formulae and isochore formulae of NaCl-H_2O solution inclusions and their application: Acta Mineralogica Sinica, v. 7, p. 345 – 352 (in Chinese).
Liu, J.J., Zheng, M.H., Zhou, D.A., 1996, Metallogenic age analysis of gold and uranium deposits in the south subzone of the western Qinling belt. Unpublished conference paper (in Chinese).
Mao, S.H., 1991, Occurrence and distribution of invisible gold in a Carlin-type gold deposit in China: American Mineralogist, v. 76, p. 1964 – 1972.
Mosier, D.L., Singer, D.A., Bagba, W.C., and Menzie, A.D., 1992, Grade and tonnage model of sediment-hosted Au, in, Bliss, J.D., ed., Developments in Mineral Deposit Modeling: U.S. Geological Survey Bulletin 2004, p. 26-28.
Nelson, C.E., 1990, Comparative geochemistry of jasperiods from Carlin-type gold deposits of the western United States: Journal of Geochemical Exploration, v. 36, p. 171 – 195.
O' Neil, J.R., Clayton, R.N., and Mayeda, T., 1969, Oxygen isotope fractionation in divalent metal carbonates: J. Chem. Phys., v. 51, p. 5547 – 5558.
Pashkova, Ye.A., Danilova, Ye.A., and Vasilevskaya, N.A., 1990, Humic acids and syngenetic gold in carbonaceous sediments: Geochem. Intern., v. 27, p. 26 – 32.
Peng, D.Q., 1992, Preliminary analysis on distribution of gold, copper, and platinum group in northern Sichuan and southern Ganshu gold (uranium) metallogenic belt. Geologica Acta of Sichuan, v. 12, supplement, p. 43 – 46 (in Chinese).
Phillips, G.N., and Powell, R., 1993, Link between gold provinces: ECONOMIC GEOLOGY, v. 88, p. 1084 – 1098.
Radtke, A.S., 1985, Geology of the Carlin gold deposit, Nevada: U.S. Geological Survey Professor Paper 1267, 124p.
Radtke, A.S., Heropoulos, C., Fabbi, B.P., Scheiner, B.J., and Essington, M., 1972, Data on major and minor elements in host rocks and ores, Carlin gold deposits, Nevada: ECONOMIC GEOLOGY, v. 67, p. 975 – 978.
Radtke, A.S., Rye, R.O., and Dickson, F.W., 1980, Geology and stable isotope studies of the Carlin gold deposit, Nevada: ECONOMIC GEOLOGY, v. 75, p. 641 – 672.
Raiswell, R., Bottrell, S.H., Al-Biatty, H.J., and Tan, M. M., 1993, The influence of bottom water oxygenation and reactive iron content on sulfur incorporation into bitumens from Jurassic marine shales: America Journal of Science, v. 293, p. 569 – 596.
Raiswell, R., Buckley, F., Bermer, R.A. and Anderson, T.F., 1988, Degree of pyritization of iron as paleoenvironmental indication of bottom-water oxygenation: Journal of Sedimentary Petrology, v. 58, p. 812 – 819.
Roedder, E., 1984, Fluid inclusions: Reviews in Mineralogy, v. 12, p. 41 – 48.

Rye, R.O., 1985, A model for the formation of Carbonate-hosted disseminated gold deposits based on the geologic, fluid-inclusion, geochemical, and stable-isotope studies of the Carlin and Cortez deposits, Nevada: U. S. Geological Survey Bulletin, v. 1646, p. 35 – 42.

Sillitoe,N.F., and Bonham, H.F.Jr., 1990, Sediment-hosted gold deposits: Distal products of magmatic hydrothermal systems: Geology, v. 18, p. 157 – 161.

Stenger, D.P., Kesler, S.E., Peltonen, D.R., and Tapper, C.T., 1998, Deposition of gold in Carlin-type deposits: The role of sulfidation and decarbonation at Twin Creeks, Nevada: ECONOMIC GEOLOGY, v. 93, p. 201 – 215.

Titley, S.R., 1991, Phanerozoic ocean cycles and sedimentary rock-hosted gold ores: Geology, v. 19, p. 645 – 648.

Tooker, E.W., 1985, Discussion of the disseminated-gold-ore-occurrence model: U.S.Geological Survey Bulletin, v. 1646, p. 107 – 150.

Wang, X.C., 1992, Indicator significance of As, Sb, Hg, Tl and Ba for the fine disseminated type of gold deposits: Mineral Resources and Geology, v. 6, no. 4, p. 307 – 312 (in Chinese).

—1994, On isotope geology of sediment-hosted disseminated gold deposits in northwestern Sichuan: J. of Shenyang Institute of Gold Technology, v. 13, no. 4, p. 309 – 316 (in Chinese).

—1995a, Rifting and sediment-hosted disseminated gold deposits, as exampled by the Luhuo rift, eastern Tethy: Unpublished Ph.D. thesis, Chengdu, Sichuan, China, Chengdu College of Technology, 88p (in Chinese).

—1995b, On ore-forming process of fine disseminated type of gold deposits in northwestern Sichuan: Acta Geologica Sichuan, v. 15, no. 1, p. 41 – 48 (in Chinese).

—1996, On isotope geology of fine disseminated type of gold deposits in China: in Liu, Y. et al. Eds., Geology and Mineral Resources Proceedings of Ministry of Metallurgical Industry: Beijing, International Academic Publishers, p. 109 – 113.

—1998, On migration and deposition mechanisms of ore-forming materials of sediment-hosted disseminated gold deposits in China: Contributions to Geology and Mineral Resources Research, v. 13, no.1, p. 45 – 55 (in Chinese).

Wells, J.D., and Mullens, T.E., 1973, Gold-Bearing arsenian pyrite determined by microprobe analysis, Cortez and Carlin gold mines, Nevada: ECONOMIC GEOLOGY, v. 68, p. 187 – 201.

Zhang, N.D., Cao, Y.W., Liao, Y.A., Zhao, Y., Zhang, H.J., Hu, D.Q., Zhang, G., and Wang, N.Z., 1998, Geology and metallogeny in Ganzxi-Litang rift zone: Beijing, Geological Publishing House, 119p (in Chinese).

Zheng, M.H. ed., 1989, An Introduction to Strata-bound Gold Deposits: Chengdu, Press of Chengdu University of Science and Technology, 266p (in Chinese).

Zheng, M.H. ed, 1994, Stratabound Gold Deposits of Exhalation Type and Turbidite Type: Chengdu, Sichuan Publishing House of Science and Technology, 273p (in Chinese).

Table 1. Summary of geological features of NW-Sichuan sedimentary rock-hosted disseminated gold deposits

Deposits	Dongbeizhai	Qiuluo	Laerma	Manaoke	Yichang	Pulongba	Lianhecun
Subtype	Au-As	Au-Sb	Au-U	Au-W	Au-Hg	Au	Au
Scale	L	M	L	L	M	S	M
Grade(ppm)	4 – 5	5 – 20	2 – 8	1 – 9	3 – 10	4 – 15	2 – 12
Tectonic setting	Western Qinling block	Luhuo-Daofu rift	Western Qinling block	Western Qinling block	Western Qinling block	Luhuo-Daofu rift	Western Qinling block
Ore-bearing strata	Upper Triassic	Upper Triassic	Lower Cambrian	Upper Triassic	Upper Triassic	Upper Triassic	Middle Devonian
Igneous rocks	Db (Mz)	Db (Mz)	Da (Mz)	No	No	Basic-ultrabasic rocks (Mz)	Grp (Mz)
Ore host rocks	Sl, Ss	Sl, Ss	Che, Sl, Da	Sl, Ss	Sl, Ss	Sl, Ss, basic-ultrabasic rocks	Sl, Ls, granite porphyry
Ateration phases	qt, cal, ser	qt, cal, ser, dol	qt, cal, ser, dick	qt, cal, ser, sid	qt, cal, ser	qt, cal, ser, dol	qt, cal, ser, ba, kao, fluor
Metallic minerals	py, rar, asp, Au, As, stib, po, cp, sp, cinn, mr, tn	py, stib, asp, Au, mr, tet, cinn	py, mr, stib, asp, Au, rar, orp, ura, cp, tet	py, sch, rar, asp, stib, Au	py, asp, cinn, rar	py, asp, cp, Bi, td, mr, cinn, po, sp, bis	py, stib, asp, po, cinn, rar
Trace element	As-Sb-Hg-Ba	As-Sb-Hg-Tl-Ba	As-Sb-Hg-Ba-Se-U-Pt	As-W-Sb-Hg	As-Sb-Hg-Ba	As-Sb-Hg-Tl-Ba-Bi	As-Sb-Hg-Ba

1. Abbreviations: asp = arsenopyrite, Au = native gold, As = native arsenic, ba = barite, Bi = native bismuth, bis = bismuthine, cal = calcite, Che = chert, chl = chlorite, cinn = cinnabar, cp = chalcopyrite, Da = porphyritic dacite, Db = diabase dyke, dick = dickerite, dol = dolomite, fluor =fluorite, Grp = Granite porphyry, kao =kaolonite, Ls = limestone, mr = marcasite, Mz = Mesozoic, orp = orpiment, ura = uranite, po = pyrrhotite, py = pyrite, rar = realgar, qt = quartz, sch = scheelite, ser = sericite, sid = siderite, Sl = slate, sp =sphalerite, Ss = sandstone, stib = stibnite, td = tetradymite, tet = tetrahedrite, tn = tennatite.

2. L = large gold deposit with gold metal more than 20 tons, M = medium-sized gold deposit with gold metal between 5 and 20 tons, S = small-sized gold deposit with gold metal less than 5 tons

Table 2. Electron probe analyses of native gold at the Pulongba deposit

Sample No.	Au	Ag	Cu	Fe	Pd	Pt	Bi	Ni	Te	Σ	Fineness
G220—4	86.2	13.3	0.2	0	0	0.3	0	0	0.1	100.1	866
G220—5	87.3	11.2	0	0	0	0.3	0.7	0.2	0	99.7	886
G220—6	84.8	13.4	0.2	0	0.1	0.4	0.2	0.2	0.1	98.9	864
G220—1	82.2	15.4	0.3	0.7	0	0.2	0	0.1	0.2	99.2	842
G220—2	81.1	17.6	0.2	0.5	0	0.4	0	0.1	0.1	100.0	822

Table 3. Trace element data in NW-Sichuan sedimentary rock-hosted disseminated gold deposits

Deposit	Dongbeizhai	Qiuluo	Laerma	Pulongba	Lianhecun
As, ppm	400 – 5400 (1000)	(500)	146 – 11028 (1535)	1366 – 2871 (2155)	497 – 11374 (4215)
Sb, ppm	0 – 0.2	100 – 1700 (600)	20 – 284 (83)	13 – 47 (31)	127 – 2052 (600)
Hg, ppm	0.5 – 1.2 (0.8)	(2.8)	7.7 – 44.5 (30.0)	0.3 – 4.6 (2.3)	18 – 161 (58)
Tl, ppm	(0.9)	(3.8)	n.d.	0.1 – 0.5 (0.3)	2.8 – 32.0 (9.8)
Ba, ppm	(470)	(80)	1665 – 7331 (5412)	36 – 344 (179)	1100 – 8550 (5798)
Ag, ppm	0.1 – 0.5 (0.2)	(0.9)	0.3 – 3.5 (1.8)	0.6 – 1.9 (1.3)	(0.1)

Averages are in parentheses. n.d. = not determined

Table 4. Characteristics of ore-forming fluids in NW-Sichuan sedimentary rock-hosted disseminated gold deposits

Deposits	Dongbeizhai	Qiuluo	Laerma	Manaoke	Pulongba
Subtype	Au-As	Au-Sb	Au-U	Au-W	Au
Inclusion features					
Type	V-L, L	V-L, L	V-L, L, V, CO_2	V-L, L	V-L, L
Diameter (μm)	3 – 10	2 – 20	5 – 20	5 – 15	4 – 30
Vapor percentage	3 – 30	2 – 25	5 – 95	5 – 15	5 – 20
Boiling	No	No	Yes	No	No
Gas type	CO_2, CH_4	n.d.	CO_2, CO, CH_4		CO_2, CH_4
Temperature (°C)	140 – 240 (175)	200 – 290 (243)	200 – 250	210 – 270 (240)	145 – 195 (169)
Pressure (Bars)	135 – 205	156 – 256 (193)	70 – 100	400	26 – 192
Salinity (wt % NaCl)	5.8 – 12.5	6.0 – 7.3 (6.8)	3 – 14	4.5	9.5 – 12.6
Density (g/cm^3)	0.92 – 1.01	0.84 – 0.88	0.85 – 0.92	0.85	0.94 – 1.00 (0.97)
pH	5.68 – 6.00	7.63 – 7.93	4.5 – 4.8	6.8	4.63 – 7.93
Log fO_2 (Bars)	-49 – -44	n.d.	-38 – -36	-38	-47 – -42
Log fS_2 (Bars)	-25 – -17	n.d.	-11 – -8	-12	-17 – -16

n.d. = not determined

Table 5. Metallogenic epochs of sedimentary rock-hosted disseminated gold deposits in northwestern Sichuan

Petrology	Analyzed target	Analyzed method	Age ($\times 10^6$a)	References
Pulongba deposit				
Olvine-diabase	Whole rock	K-Ar	154	Wang, 1995a
Gala deposit				
Gold ore	Whole rock	K-Ar	164	Zhang et al., 1998
Gold ore	Whole rock	K-Ar	158	Zhang et al., 1998
Gold ore	Whole rock	K-Ar	177	Zhang et al., 1998
Altered rock	Whole rock	K-Ar	208	Zhang et al., 1998
Altered rock	Whole rock	K-Ar	149	Zhang et al., 1998
Gold ore	Whole rock	K-Ar	163	Zhang et al., 1998
Gold ores, altered rocks	Whole rock	Rb-Sr	157	Zhang et al., 1998
Qiaoqiaoshang deposit				
Granite-porphyry	Whole rock	K-Ar	172	Hu, 1991
Gold ore	Whole rock	Rb-Sr	167	Zheng, 1994
Laerma deposit				
Gold ore	Quartz	$^{40}Ar/^{39}Ar$	49.5	Peng, 1992
Gold ore	Whole rock	U-Pb	79	Liu et al., 1996
Gold ore	Whole rock	U-Pb	117.1	Liu et al., 1996
Gold ore	Whole rock	U-Pb	73.1	Liu et al., 1996
Gold ore	Whole rock	U-Pb	66.4	Liu et al., 1996
Gold ore	Whole rock	K-Ar	57.1	Liu et al., 1996
Gold ore	Whole rock	K-Ar	127	Liu et al., 1996
Gold ore	Quartz	Rb-Sr	46	Ji et al., 1999

Table 6. Hydrogen and Oxygen isotopic data of minerals, rocks, and waters in NW-Sichuan sedimentary rock-hosted disseminated gold deposits

No.	Sample No.	Description	$\delta^{18}O_s$ (‰)	$\delta^{18}O_w$ (‰)	δD (‰)	T (°C)	No.	Sample No.	Description	$\delta^{18}O_s$ (‰)	$\delta^{18}O_w$ (‰)	δD (‰)	T (°C)
	Dongbeizhai						23	02	Spring water		-14.1	-92.4	51
1	CM48-2	Calcite	23.5	12.3	-73.7	170	24	03	Spring water		-13.9	-117.0	
2	CM48-40	Calcite	23.2	12.9	-75.5	187	25	04	Spring water		-13.9	-115.0	
3	CM48-62	Calcite	27.2	16.2	-66.6	175	26	90-7	Rain water		-15.6	-99.5	
4	IV-Ca_2-1	Calcite	25.3	13.6	-69.0	164		**Manaoke**					
5	IV-Ca_2-2	Calcite	25.1	13.4	-69.8	164	27	KW2	Quartz	23.6	13.8	-62.3	233
6	Hy-3	Pit water		-12.3	-95.3		28	KW4	Quartz	21.3	12.0	-65.9	244
7	Hy-5	River water		-12.0	-91.3		29	B39	Quartz	22.6	13.6	-67.8	249
	Laerma						30	B35	Quartz	23.6	14.6	-78.1	248
8	MC22	Quartz	16.3	10.7	-101.5	342	31	B16	Quartz	20.6	11.3	-77.6	242
9	L19	Quartz	20.1	12.0	-98.4	269		**Pulongba**					
10	L35	Quartz	20.9	12.2	-106.0	257	32	T172	Spring water		-18.0	-117.2	7
11	L76	Quartz	16.2	8.3	-97.4	274	33	T067	Spring water		-18.3	-122.6	25
12	L78	Quartz	17.3	11.4	-111.9	332	34	T145	Quartz	20.9	0.7	-117.8	105
13	T68	Quartz		-4.0	-73.9	327	35	T154	Quartz	21.7	6.8	-103.5	157
14	LA98	Quartz		-11.1	-93.6	251	36	T041	Limestone	24.5		-128.9	
15	LA6	Quartz		-2.6	-52.9	296	37	T058	Limestone	21.4		-103.6	
16	LE6	Quartz		3.6	-77.5	219	38	T043	Basalt	15.8		-81.4	
17	LE7	Quartz		4.2	-86.4	235	39	T049	Sandstone	15.5		-88.7	
18	MLE1	Quartz	21.2	13.2	-93.0	272	40	T063	Sandstone	16.4		-108.6	
19	MLE2	Quartz	19.4	10.9	-85.0	260	41	T065	Sandstone	17.4		-84.1	
20	MLE3	Quartz	23.4	12.9	-85.0	220	42	T051	Slate	15.7		-79.6	
21	W2	Spring water		-14.1	-94.4		43	T056	Diabase	10.6		-103.6	
22	90-6	Spring water		-14.3	-93.4		44	T089	Pyrolith	9.7		-119.2	

1.The oxygen isotopes of ore fluids are calculated by using the fractionation equations between quartz-H_2O and calcite-H_2O at corresponding temperatures (Clayton et al., 1972; O'Neil et al., 1969).

2.References: 1 –7, 18 – 31, Zheng,1994; 8 – 12, Zhang,1991; 13 – 17,Zhou,1991; 32 – 44,Wang,1995a

Table 7. Sulfur isotopes of minerals in gold deposits

Sample	No.	Sample number	$\delta^{34}S$, ‰		
			Range	Average	Derivation
Dongbeizhai					
Pyrite (I)	1	4	-1.9 – 3.1	1.8	2.1
Pyrite	2	17	-7.4 – 6.3	-0.1	3.8
Realgar	3	28	-14.6 – -2.8	-5.0	2.5
Stibnite	4	2	-5.4 – -4.9	-5.2	0.3
Qiuluo					
Stibnite	5	6	-4.8 – 2.5	-3.5	0.7
Laerma					
Pyrite (I)	6	8	9.5 – 32.1	17.1	7.1
Pyrite	7	6	-25.6 – 7.8	-4.8	13.4
Stibnite	8	2	-6.7 – 1.9	-2.4	4.3
Marcasite	9	2	-1.6 – 0.2	-0.7	0.9
Barite	10	6	2.4 – 28.3	14.6	8.6
Manaoke					
Stibnite	11	4	-15.3 — -6.1	-8.2	2.2
Realgar	12	1		-15.3	
Pulongba					
Pyrite (I)	13	2	-2.0 – 1.1	-0.5	1.6
Pyrite	14	5	-11.0 – 2.0	-3.1	4.3

Note: 1.References: 1-4, 6-11, Zheng, 1994; 5, 13-14, Wang, 1995a
2.Py (I) = Diagenetic pyrite

Table 8. Carbon isotopes in NW-Sichuan sediment-hosted disseminated gold deposits

Sample	No.	Sample number	$\delta^{13}C$, ‰		
			Range	Average	Derivation
Dongbeizhai					
Calcite	1	23	-4.7 – 2.7	-0.9	2.2
Limestone	2	6	0.3 – 3.3	2.1	0.9
Laerma					
Pitch	3	5	-27.4 – -10.3	-23.4	7.0
CO_2	4	1		2.0	
Manaoke					
CO_2	5	2	-4.4 — -3.7	-4.1	0.4
Pulongba					
Calcite	6	9	-12.7 – -1.3	-7.4	4.0
Dolomite	7	2	-3.7 – -1.2	-2.5	1.3
Limestone	8	2	-0.8 – 3.4	1.3	2.1

Note: 1. References: 1-5, Zheng, 1994; 6-8, Wang, 1995a
2. CO_2 = CO_2 in fluid inclusions of quartz

Table 9. Lead isotopic data of ores, minerals, and rocks in NW-Sichuan sediment-hosted disseminates gold deposits

sample No.	Sample name	$^{206}Pb/^{204}Pb$	$^{207}Pb/^{204}Pb$	$^{208}Pb/^{204}Pb$	Sample No.	Sample name	$^{206}Pb/^{204}Pb$	$^{207}Pb/^{204}Pb$	$^{208}Pb/^{204}Pb$
Dongbeizhai					Mop8	Che	18.798	15.626	38.592
IV-Sb1	stib	18.395	15.647	38.573	Mop9	Sl	18.635	15.707	39.019
IV-Sb2	stib	18.439	15.667	38.670	LM5	Stib	37.266	16.870	38.676
IV-Sb3	stib	18.384	15.605	38.440	LM3	ba	18.412	15.550	38.58
IV-Sb4	stib	18.410	15.643	38.559	LM5	qt	17.794	15.460	37.674
IV-Sb5	stib	18.407	15.626	38.498	**Manaoke**				
IV-Sb6	stib	18.412	15.619	38.478	KW2	qt	17.347	15.608	37.446
RZ-1	py (II)	18.392	15.673	38.436	KW3	qt	17.256	15.615	36.904
YM8-CM48	py (II)	18.386	15.571	38.281	KW4	qt	17.001	15.444	36.895
B481	py (I)	18.440	15.626	38.518	KW5	stib	17.330	15.591	37.408
P-53	Ss	21.064	15.779	38.918	KW6	stib	17.364	15.601	37.421
P-64	Ss	20.525	15.721	38.779	**Pulongba**				
P-51	Sl	18.804	15.683	38.889	T093-1	py (II)	18.57	15.71	38.8J
P-57	Sl	18.692	15.692	38.897	T168	py (II)	18.39	15.65	38.55
HSG-1	Db	18.595	15.492	38.585	T089	ore	18.43	15.64	38.52
H-B7	Db	18.471	15.569	38.774	T041	Ls	20.28	15.65	38.30
CM48-62	Ls	18.848	15.734	38.939	T058	Ls	20.92	15.69	38.26
Laerma					T043	Bas	18.76	15.52	39.36
Mop 1	ba	26.86	15.898	38.135	T051	Sl	18.69	15.57	38.67
Mop6	ba	31.602	16.138	39.087	T049	Ss	18.51	15.59	38.87
Mop3	py (II)	17.653	15.483	37.074	T063	Ss	18.45	15.60	39.01
Mop2	mr	18.418	15.615	37.836	T064	Ss	18.62	15.60	38.71
Mop4	mr	19.134	15.618	38.007	T065	Ss	18.77	15.61	39.02
Mop7	Da	27.945	16.176	36.644					

1. Abbreviations: ba = barite; Bas = basalt; Da = dacite; Db = diabase; Ch = chert; Ls = limestone; mr = marcasite; py (I) = diagenetic pyrite; py (II) = hydrothermal pyrite; qt = quartz; Sl = slate; Ss = sandstone; stib = stibnite.
2. References: Data of Dongbeizhai, Laerma, and Manaoke deposits are from Zheng (1994), those of Pulongba deposit are from Wang (1995a).

Table 10 Comparison of sedimenary rock-hosted disseminated gold deposits in NW-Sichuan with those in Nevada

Area	NW-Sichuan, China	Nevada, U.S.A*
General features		
Metals	Au; increased As, Sb, Ba, ± Hg, ±Ag, ±Tl ; W, U, Bi present in some deposit	Au; increased As, Sb, Ba, ± Hg, ±Ag, ±Tl ~100 times background; increased Pb, Zn, Cu <10 times background
Size (Mt)	0.1 to 15.36 Mt at 1.6 to 10 ppm; mostly 0.92 to 6 Mt at 3.4 to 8.0 ppm	<1 to >100 Mt at 0.65 to ~9.6 ppm; mostly 0.92 to 48 Mt at 0.96 to 5.6 ppm
Host rocks	Mainly Triassic, complex rock series such as fine-grained clastic, subvolcanic, and ophiolitic melange ones	Generally Pennsylvanian to Cambrian, silty to massive limestones and dolostones marl; Paleozoic mafic flows; hornfels; locally felsic dikes
Igneous and metamorphic rocks	Generally absent, when present Jurassic through Tertiary, intermediate to felsic	Generally absent, when present Jurassic through Tertiary, intermediate to felsic; skarns are present near a few intrusions
Structure	Located near the margin of a Precambrian craton, and experienced compression followed by extension; main ore-controlling structures are regional oblique-slip (thrust) faults	Located near the margin of a Precambrian craton, and experienced compression followed by extension; commonly at intersections of normal faults with favorable stratigraphy or thrust contacts
Alteration mineralogy	Mainly quartz and carbonate minerals, less deconatization and acid-leaching alteration minerals	Carbonate dissolution and/or quartz deposition, forming bedding and fault-controlled jaseroids and/or decarbonated zones; peripheral calcite vens and/or recrystallization of calcite or dolomite
Ore mineralogy	pyrite, arsenopyrite, marcasite, realgar, orpiment, stibnite, cinnabar, quartz, calcite and barite; scheelite, uranite and bismuth minerals present in some deposits	Quartz, illite, kaolinite, arsenical pyrite (2~6 wt % As), arsenopyrite, stibnite, realgar, orpiment, gold; postore barite alunite, jarosite
Gold occurrence	mainly sub-micron in size, closely associated with arsenian pyrite and arsenopyrite; micron-sized native gold present in oxidized and semi-oxidized ores of some deposits	mainly sub-micron in size, closely associated with arsenian pyrite and arsenopyrite
Age	208 and 46 Ma	Mainly 40 to 20 Ma, other ages possible (e.g., Jurassic)
Conditions of formation		
T (°C)	150 to 250, most between 175 and 225	Au ore stage 160 to 250, most between 190 and 225
Pressure	26 ~ 400 bars	300 to 800 bars
Fluid composition	Ore fluids 3 to 14 wt % NaCl equiv. with significant CO_2 and measurable CH_4; stable isotopes (from fluid inclusions and calculated from silicates and carbonates): δD = -118 to -53‰; $\delta^{18}O$ = -16 to +8‰	Ore fluids 0 to 6 wt % NaCl equiv. with significant CO_2 and measurable H_2S; preore fluids up to 20 wt % NaCl equiv.; stable isotopes (from fluid inclusions and calculated from silicates): δD = -130 to -155‰, $\delta^{18}O$ = -16 to +8‰

* Data mainly from Moiser et al., 1992; Arehart, 1996; Ilchik and Barton, 1997

Fig.1. Tectonic sketch map of the mainland of China, showing the location of two sedimentary rock-hosted disseminated gold belts.
Fig.2. Tectonic units of Kekexili--Bayankala region in NW-Sichuan, showing the distribution of sedimentary rock-hosted disseminated gold deposits.
Fig.3. Geologic map of the northwestern Sichuan, PRC, showing the distribution of sedimentary rock-hosted disseminated gold deposits and prospects.
Fig.4. Geological sketch map (A) and a typical profile (B) of the Dongbeizhai gold deposit (after Zheng, 1989).
Fig.5. Geological sketch map of the Qiuluo gold deposit.
Fig.6. Geologic sketch map of the Laerma gold deposit (simplified from Zheng, 1994).
Fig.7. Generalized geologic map of the Manaoke gold deposit (simplified from Zheng, 1994).
Fig.8. Geologic map of the Yinchang gold deposit.
Fig.9. Geologic map of the Pulongba gold deposit.
Fig.10. Geologic map of the Lianhecun gold deposit.
Fig.11. Mineralization stages and paragenesis of the Dongbeizhai deposit
Fig. 12. Mineralization epochs and paragenesis of the Qiuluo deposit
Fig. 13. Mineralization epochs and paragenesis of the Pulongba deposit
Fig.14. Lead isotope comparison between rocks and ores from Pulongba deposit during ore-forming period

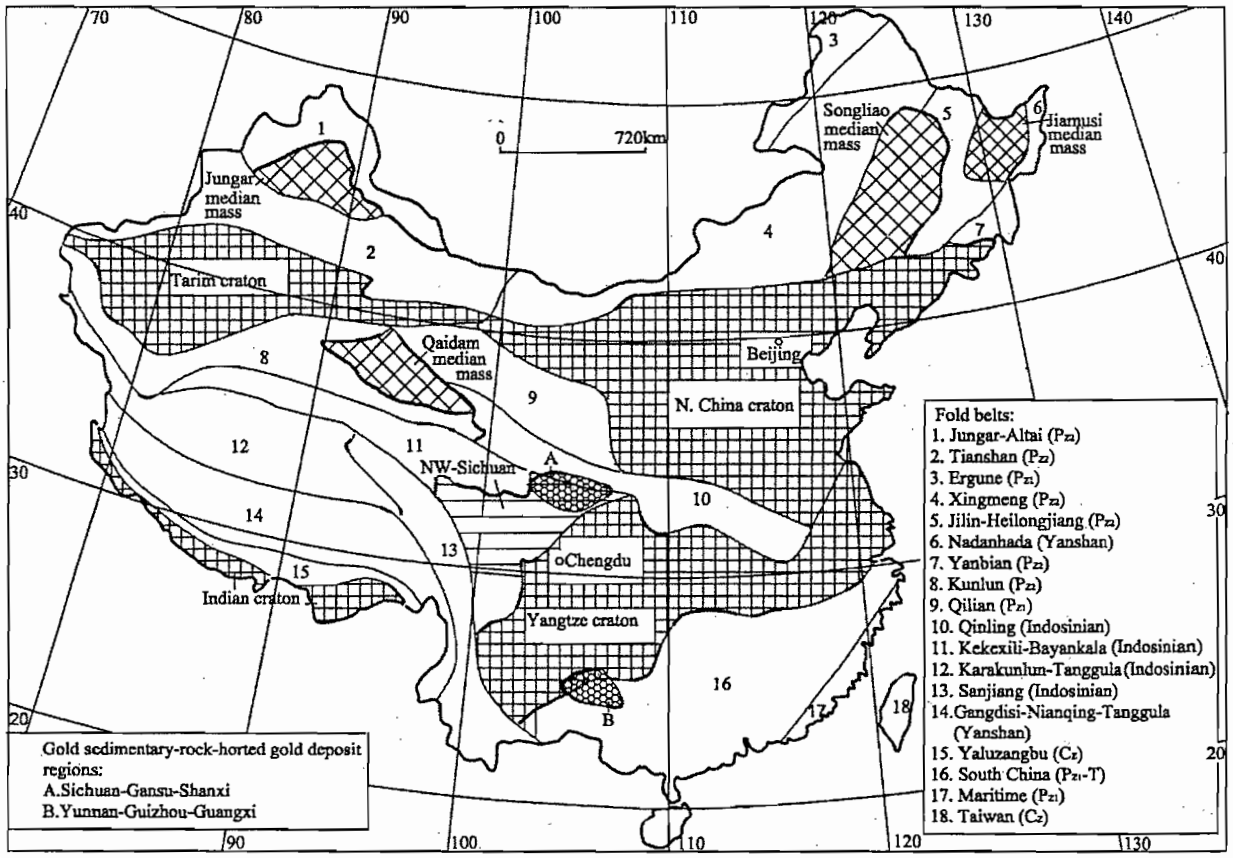
70
80
90
100
110
120
130
140
40
30
20
0
720km
Jungar median mass
Tarim craton
Qaidam median mass
Songliao median mass
Jiamusi median mass
Beijing
N. China craton
NW-Sichuan
A
Chengdu
Yangtze craton
B
Indian craton
Gold sedimentary-rock-horted gold deposit regions:
A.Sichuan-Gansu-Shanxi
B.Yunnan-Guizhou-Guangxi
Fold belts:
1. Jungar-Altai (Pz1)
2. Tianshan (Pz2)
3. Ergune (Pz1)
4. Xingmeng (Pz2)
5. Jilin-Heilongjiang (Pz2)
6. Nadanhada (Yanshan)
7. Yanbian (Pz2)
8. Kunlun (Pz2)
9. Qilian (Pz1)
10. Qinling (Indosinian)
11. Kekexili-Bayankala (Indosinian)
12. Karakunlun-Tanggula (Indosinian)
13. Sanjiang (Indosinian)
14. Gangdisi-Nianqing-Tanggula (Yanshan)
15. Yaluzangbu (Cz)
16. South China (Pz1-T)
17. Maritime (Pz1)
18. Taiwan (C2)

Fig-1

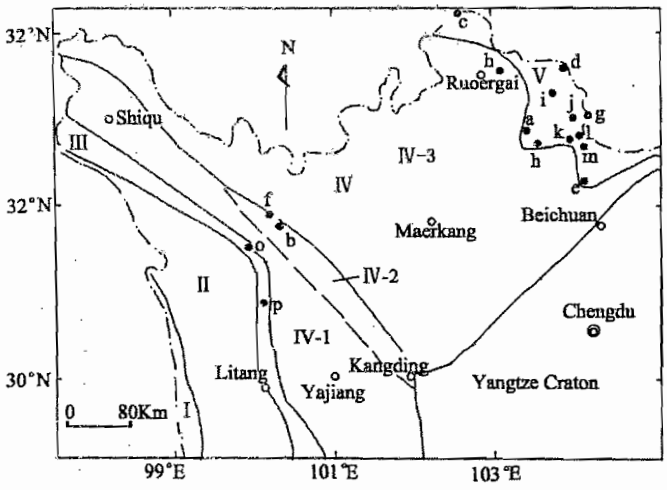

Structural unit:

I. Jinshajiang suture zone
II. Dege-Zhongdian block
III. Ganzi-Litang suture zone
IV. Kekexili-Yajiang block
IV-1. Yajiang fold belt
IV-2. Luhuo-Daofu rift
IV-3. Bayankala-post Longmenshan fold belt
V. Western Qinling block

Sediment-hosted disseminated gold deposits and their subtypes:

Au dominant subtype: f. Pulongba, g. Lianhecun, i. Erdaoqiao, j. Jiawuchi, k. Longdishui, l. Shuinuijia, m. Baxi, n. Zeboshan, p. Xionglongxi
Au-As subtype: a. Dongbeizhai, h. Qiaoqiaoshang
Au-Sb subtype: b. Qiuluo, o. Gala
Au-U subtype: c. Laerma
Au-W subtype: d. Manaoke
Au-Hg subtype: e. Yinchang

Fig.2

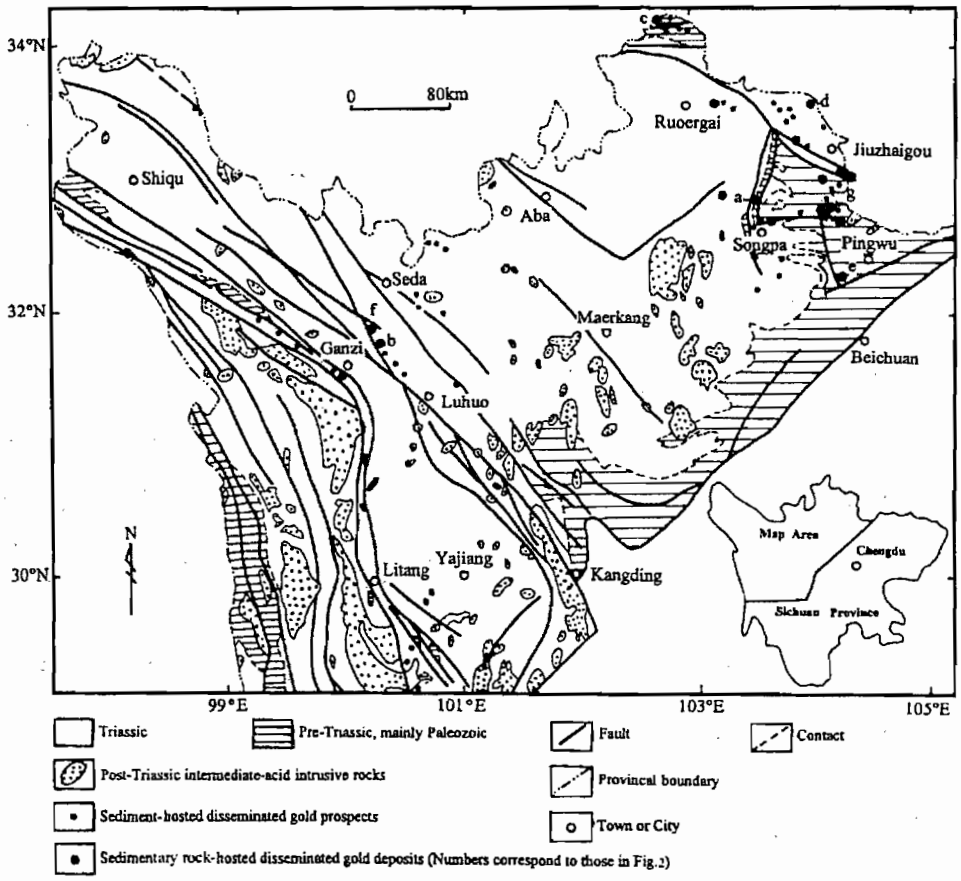
34°N
32°N
30°N
99°E
101°E
103°E
105°E
0 80km
N
Shiqu
Aba
Ruoergai
Jiuzhaigou
Songpa
Pingwu
Seda
Maerkang
Ganzi
Beichuan
Luhuo
Litang
Yajiang
Kangding
Map Area
Chengdu
Sichuan Province
Triassic
Pre-Triassic, mainly Paleozoic
Fault
Contact
Post-Triassic intermediate-acid intrusive rocks
Provincal boundary
Sediment-hosted disseminated gold prospects
Town or City
Sedimentary rock-hosted disseminated gold deposits (Numbers correspond to those in Fig.2)

Fig. 3

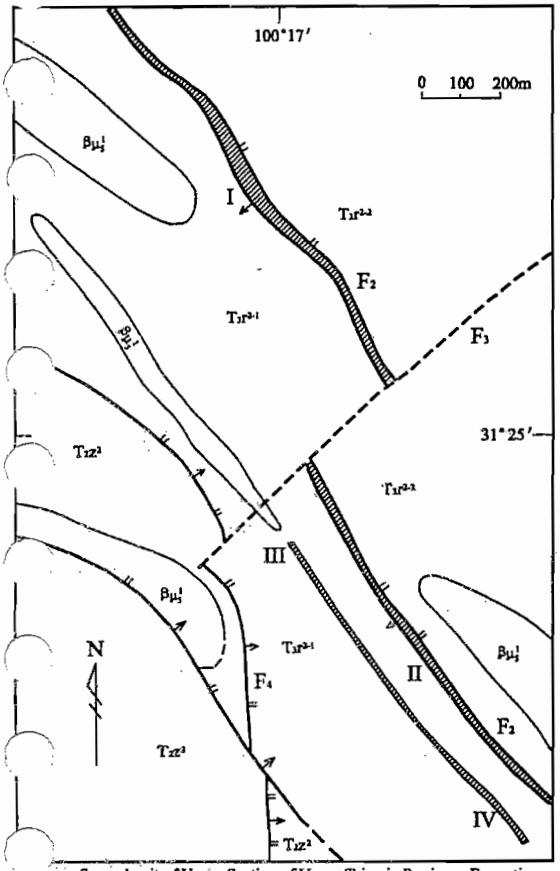

Second unit of Upper Section of Upper Triassic Runiange Formation (Slate intercalated with sandstone, chert and pelitic limestone)

First unit of Upper Section of Upper Runiange Formation (basalt intercalated with limestae and sandstone)

Upper Section of Middle Triassic Zagunao Formation (Sandstone, slate)

Indosinian diabase

Gold body

Fault

Contact

Fig.5

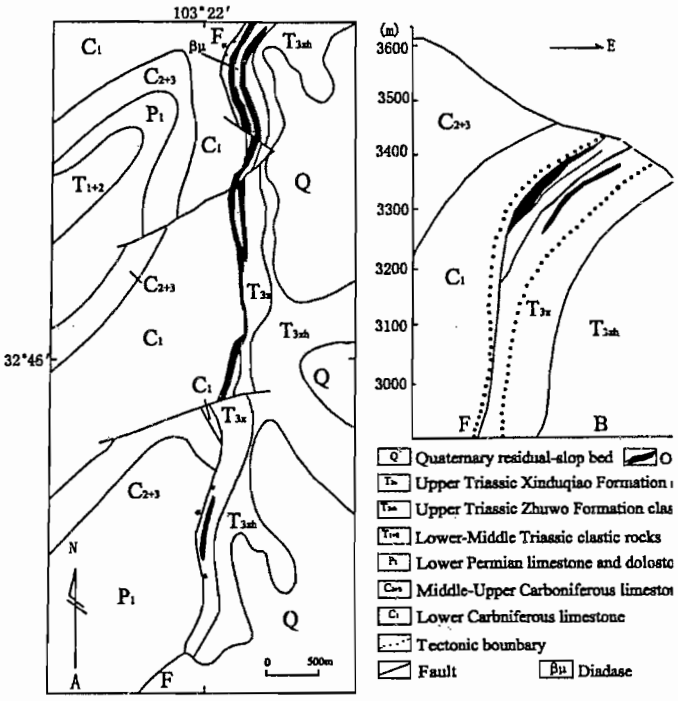

Fig.4

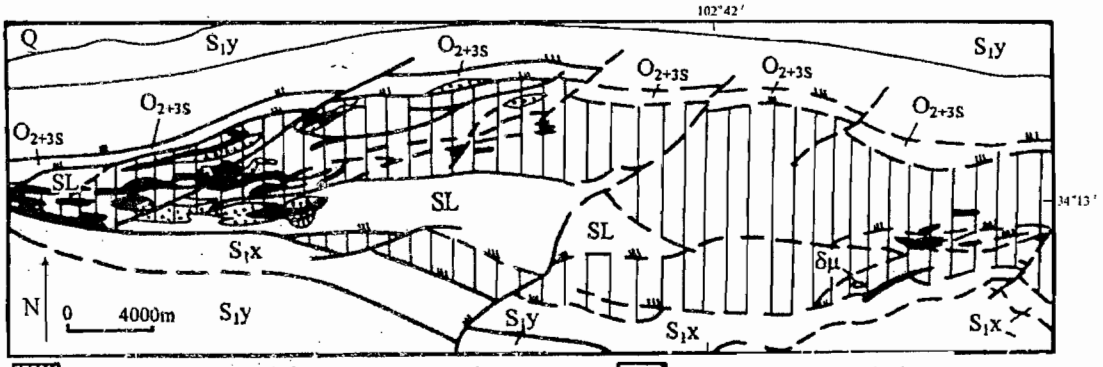

Chert of Lower Cambrian Laerma Formation

SL Carbonaceous slate and silty slate of Lower Cambrian Laerma formation

O2+3S Slate, chert of Middle-Upper Ordovician Sulimutang formation

S1x Limestone, chert and slate of Lower Silurian Xiadi Formation

S1y Lower Silurian Yancangou Formation

Q Quaternary residual-slop bed

Compresive--shear fault

Shear fault

Contact

Gold ore body with grade ≥3g/t

Gold ore body with grade from 1--3g/t

δμ Porphyritic dacite dyke

Fig-6

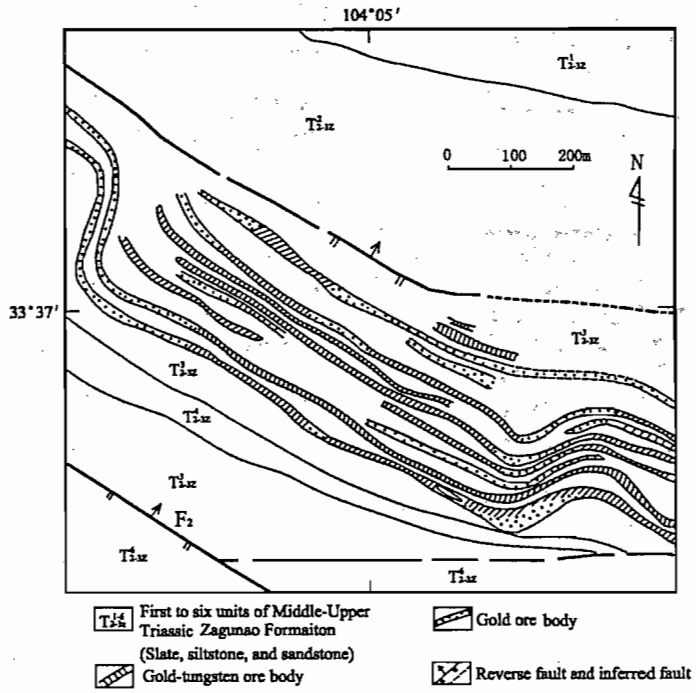
104°05′
33°37′
0 100 200m
N
F₂
First to six units of Middle-Upper Triassic Zagunao Formaiton (Slate, siltstone, and sandstone)
Gold-tungsten ore body
Gold ore body
Reverse fault and inferred fault

Fig.7

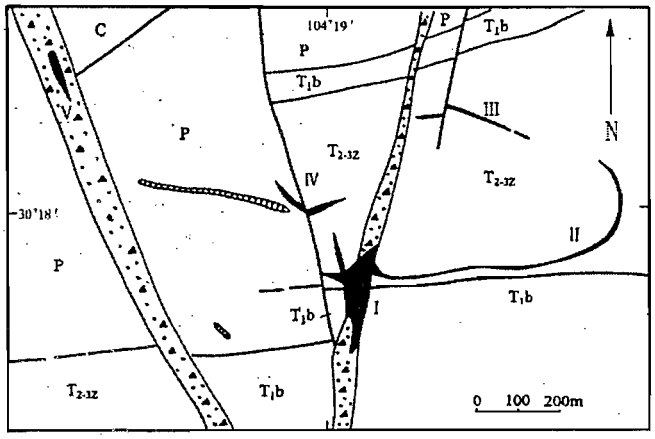

T2-3Z Middle-Upper Triassic Zagunao Formation (quartz graywack)

T1b Lower Triassic Bochigou Formation (slate, limestone)

P Permian (limestone)

C Carboniferous (limestone)

Gold ore body

Contact

Fractured belt and fault

Mercury ore body

Fig.8

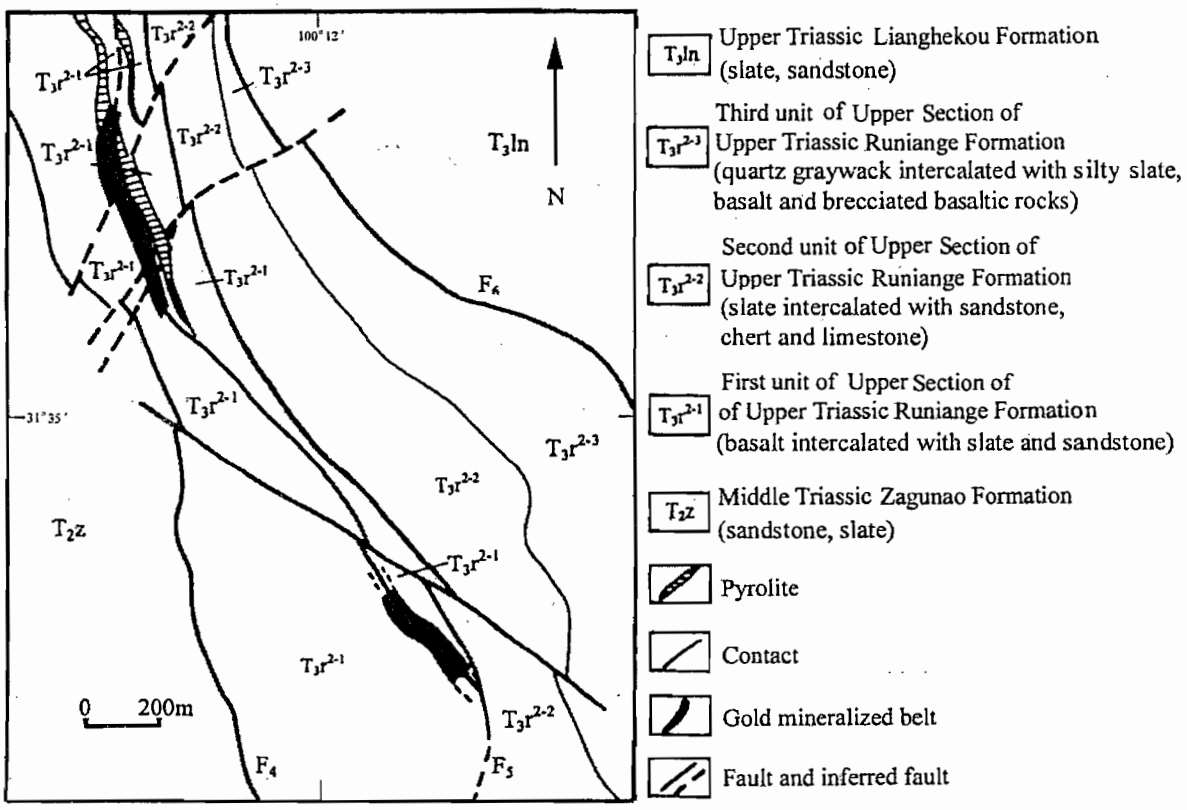
100°12'
31°35'
T_3r^{2-2}
T_3r^{2-1}
T_3r^{2-3}
T_3ln
N
F_6
T_2z
0 200m
F_4
F_5
T_3ln Upper Triassic Lianghekou Formation (slate, sandstone)
T_3r^{2-3} Third unit of Upper Section of Upper Triassic Runiange Formation (quartz graywack intercalated with silty slate, basalt and brecciated basaltic rocks)
T_3r^{2-2} Second unit of Upper Section of Upper Triassic Runiange Formation (slate intercalated with sandstone, chert and limestone)
T_3r^{2-1} First unit of Upper Section of of Upper Triassic Runiange Formation (basalt intercalated with slate and sandstone)
T_2z Middle Triassic Zagunao Formation (sandstone, slate)
Pyrolite
Contact
Gold mineralized belt
Fault and inferred fault

Fig. 9

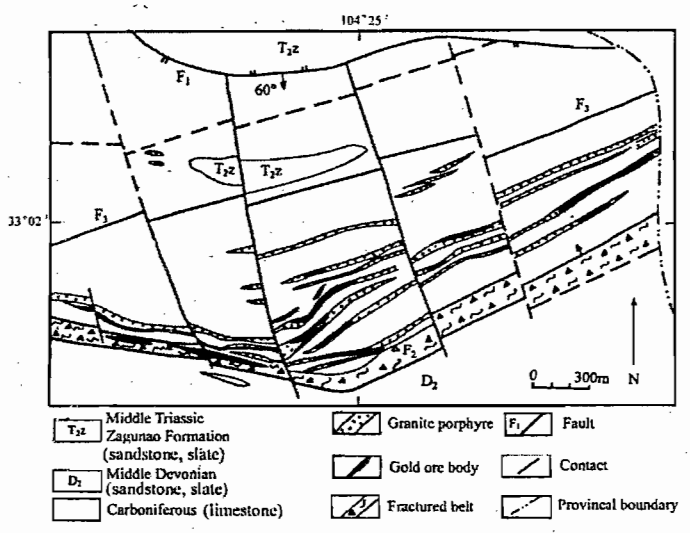
104°25'
33°02'
T_3z
F_1
60°
F_3
T_3z
T_3z
F_3
F_2
D_2
0 300m N
T_3z Middle Triassic Zagunao Formation (sandstone, slate)
D_2 Middle Devonian (sandstone, slate)
Carboniferous (limestone)
Granite porphyre
Gold ore body
Fractured belt
F_1 Fault
Contact
Provincal boundary

Fig.10

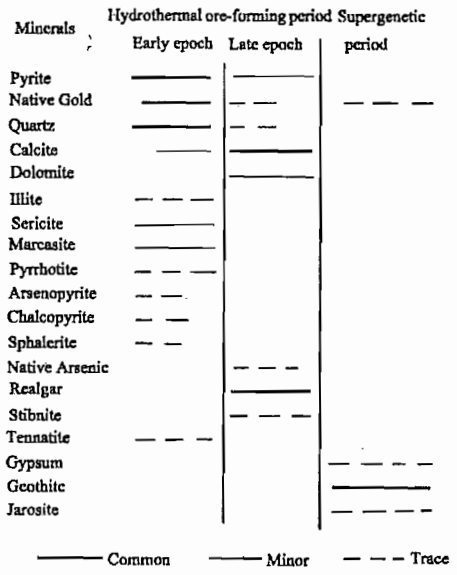
Minerals
Hydrothermal ore-forming period
Early epoch
Late epoch
Supergenetic period
Pyrite
Native Gold
Quartz
Calcite
Dolomite
Illite
Sericite
Marcasite
Pyrrhotite
Arsenopyrite
Chalcopyrite
Sphalerite
Native Arsenic
Realgar
Stibnite
Tennatite
Gypsum
Geothite
Jarosite
Common
Minor
Trace

Fig. 11

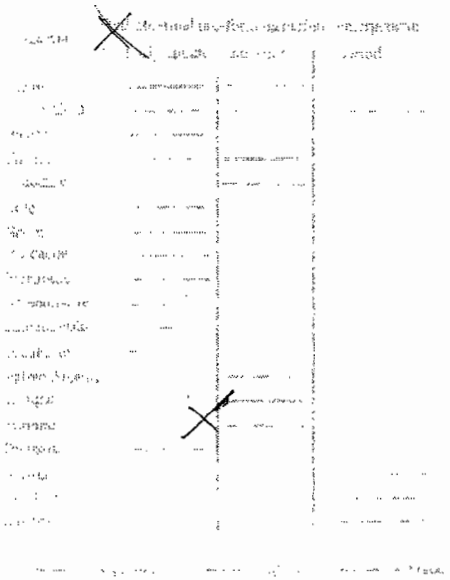

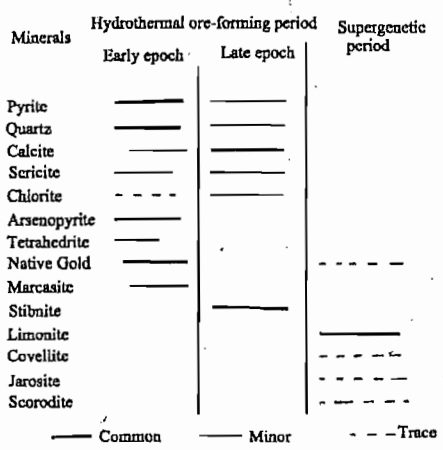
Minerals
Hydrothermal ore-forming period
Early epoch
Late epoch
Supergenetic period
Pyrite
Quartz
Calcite
Sericite
Chlorite
Arsenopyrite
Tetrahedrite
Native Gold
Marcasite
Stibnite
Limonite
Covellite
Jarosite
Scorodite
Common
Minor
Trace

Fig. 12

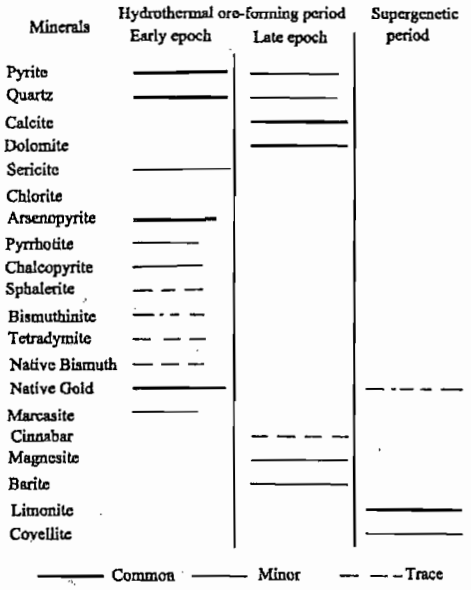
Minerals
Hydrothermal ore-forming period
Early epoch
Late epoch
Supergenetic period
Pyrite
Quartz
Calcite
Dolomite
Sericite
Chlorite
Arsenopyrite
Pyrrhotite
Chalcopyrite
Sphalerite
Bismuthinite
Tetradymite
Native Bismuth
Native Gold
Marcasite
Cinnabar
Magnesite
Barite
Limonite
Covellite
Common
Minor
Trace

Fig. 13

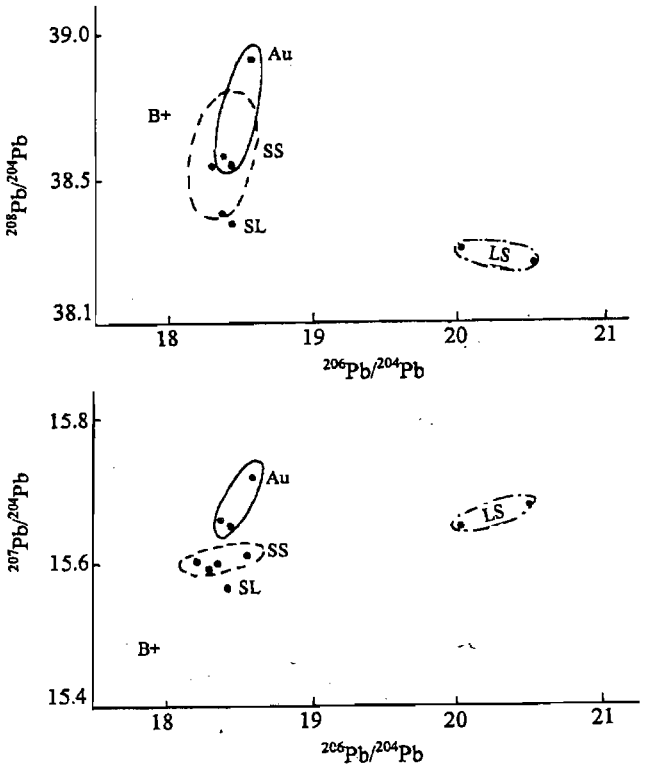

Au = Ore B = Basalt LS = limestone SL =slate SS =sandstone

Fig.14. Lead isotope comparison between rocks and ores from Pulongba deposit during ore-forming period

Tectonics and Gold Mineralisation in East China

T Zhou[1]

INTRODUCTION

China has been producing gold for more than 4000 years with gold production increasing substantially since the 1980s, from about 25 tonnes in 1980 to some 160 tonnes in 1998. More than 80 per cent of the gold production is from East China. However, complete information on eastern China gold has been rarely reported internationally. This is a general overview on the tectonics and metallogeny of gold deposits in East China. The geology of these gold deposits is compiled mainly from data and information reported in China, and is also based on the author's work in China from 1974 to 1986 and a recent visit to China.

TECTONICS OF EASTERN CHINA

The major Precambrian cratons in East China are the Sino-Korea and Yangtze blocks (Figure 1). The tectonic history and gold mineralisation in East China is largely controlled by the interaction between the Precambrian blocks and the Siberian block, the micro Precambrian block Cathaysia, as well as the Pacific oceanic plates. Deformation of accreted sequences between the Precambrian massifs has also played a role.

The Sino-Korea craton in East China underwent up to three orogenic periods during the Archaean, namely the Qianxian (*ca* 3.2 Ga), Fuping (*ca* 2.8 Ga) and Wutai (*ca* 2.5 Ga) orogenies (CGMC, 1990). During the Proterozoic, both the Sino-Korea and Yangtze blocks in East China underwent the Zhongtiao orogeny (*ca* 1.8 Ga). In addition, both of the blocks as well as the microcontinent Cathaysia underwent the Jinning orogeny (*ca* 1.0 Ga). During these orogenies, the rock units experienced extensive greenschist to granulite facies metamorphism, intensive migmatisation and widespread magmatism (Wang and Mo, 1995). Over three-quarters of gold deposits in China are located in the orogenic belts along the margins of these two major Precambrian continent blocks. Some of the deposits are directly hosted in Archaean greenstone-granitoid belts. The major Archaean blocks in East China, however, have also undergone multiple orogenic tectonism and magmatism along their margins since the Palaeozoic, and most of the gold deposits are believed to have formed as the result of these later orogenies (Chen, 1994; Zhai and Deng, 1996; Miller *et al*, 1998; Zhou, 1998).

During the Early Palaeozoic, both the Mongolian and Qinling oceanic plates were subducted beneath the Sino-Korea block from the north and south, respectively. This led to uplift of the Sino-Korea block and formation of the Caledonian fold belts as a narrow terrain along the northern border of the Sino-Korea block (Li *et al*, 1978; Wang and Mo, 1995). This uplift caused the major part of the Sino-Korea block to be exposed from the Middle Ordovician to the Middle Carboniferous, without receiving sedimentation.

In southern China, the area of Caledonian folding is located between the Yangtze and Cathaysia blocks. The strongest Caledonian orogeny probably occurred along the Shaoxing-Shaoguan convergent zone (Wang and Mo, 1995) although there are some arguments about Caledonian orogeny in southern China (Liu *et al*, 1994; Li *et al*, 1996).

1. Great Central Mines Limited and Centaur Mining and Exploration Limited, 210 Kings Way, South Melbourne Vic 3205.

The most important tectonic events in East China are the Hercynian and the Indosinian (Triassic) orogenies. The former led to merging of the Siberian and Sino-Korean blocks, forming the Xinganling and Yanshan fold belts (Wang and Mo, 1995), whereas the later led to merging of the North and South China blocks, forming the Qinling-Dabie-Sulu fold belts (Yin and Nie, 1993, 1996).

During the Yanshanian (208 - 90 Ma) and Himalayan (< 90 Ma) periods, the tectonic patterns were largely influenced by subduction of the Izanagi-Pacific plates under, and collision of the Indian continent with the Eurasian continent.

MAJOR GOLD PROVINCES IN EASTERN CHINA

Gold distribution appears to be patchy in China in terms of geography. However, when the data are put into the tectonic frameworks, the following gold provinces may be recognised (Table 1):

- *North China gold province* along the north margin of the Sino-Korea block;
- *Eastern Shandong (ie Jiaodong) gold province* along the SE margin of the China-Korea craton and the ultra-high-pressure suture zone between the North and South China blocks;
- *Qinling gold province* (mainly the Xiao Qinling sub-province) along margins of, and in the fold belts between the Sino-Korea and Yangtze blocks; and
- *SE China gold province* along the SE China fold belt.

East Shandong gold province

East Shandong gold province is the top gold producer in China, producing some three-quarters to one million oz a year. A quarter of Chinese gold reserves is hosted by rocks in eastern Shandong, with most deposits in an area of 3000 km^2 in the Zhaoyuan County. The total resource in East Shandong is about 25 - 30 million oz.

Tectonically, the East Shandong gold province is located at the southeast margin of the Sino-Korea craton, close to the northern border of the ultra-high pressure suture zone where the Yangtze block indented into the Sino-Korea block from the end of the Permian to the Early Jurassic (Yin and Nie, 1993). During the Yanshanian (Late Jurassic to Cretaceous), subduction of the Izanagi-Pacific plates under the Eurasian continent led to late magmatism.

The oldest rock unit in East Shandong is the Archaean East Shandong Group, with a thickness of about 6800 – 7900 m. It comprises granulite, gneiss, amphibolite, and biotite-bearing schists, dated at 2.94 - 2.67 Ga (Yu, 1984). The Archaean rock is unconformably overlain by Early Proterozoic Jinshan (3400 m) and Fenzishan (12700 m) Groups of metamorphosed ultramafic igneous, granulite, amphibolite, marble and schist, dated at 2.48 -2.03 Ga. The Late Proterozoic Penglai Group is 5000 m thick, and consists of slate, phyllite and carbonate rocks unconformably overlying the Early Proterozoic rocks. The Precambrian rock units are covered by up to 19 000 m of Mesozoic clastic, shale and volcanic rocks.

The Precambrian rock units were intensely metamorphosed, migmatised and intruded by mafic and felsic intrusions during the Wutai (*ca* 2.4 - 2.2 Ga) and Lüliang (*ca* 1.8 G) orogenies (Lü and Kong, 1993). Indosinian (270-*ca* 208 Ma) and Yanshanian (208 - 90 Ma) magmatism was extensive in eastern Shandong.

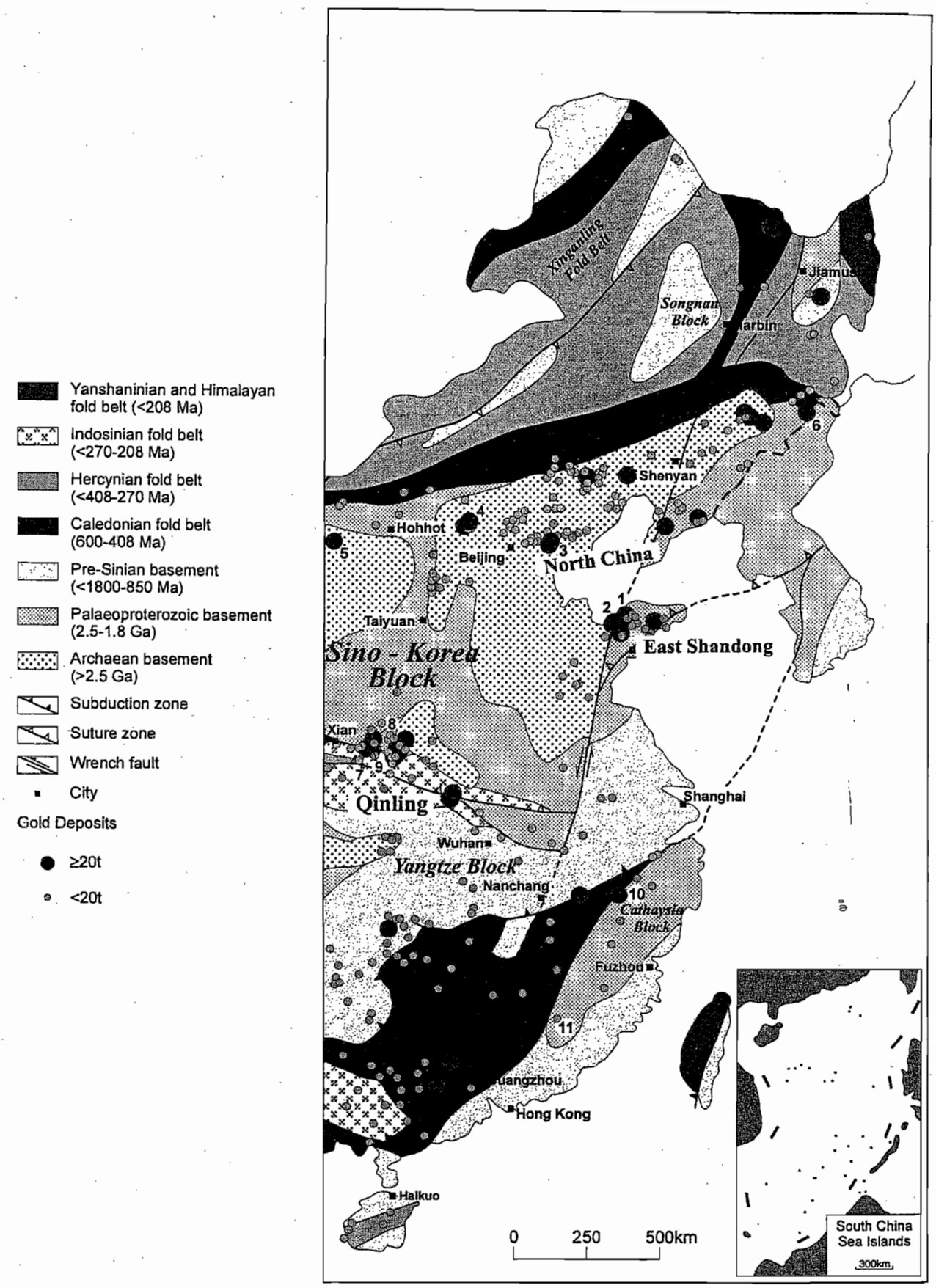

FIG 1 - Geology and gold distribution in East China. Tectonic background modified from Wang and Mo, 1995; Numbered deposits are listed in Table 1.

TABLE 1

Characteristics of some major gold deposits in East China.

Gold province	Deposit	Type	Host rock	Igneous rock age (Ma)	Resource (million oz)	Grade (g/t)	Data source
East Shandong	1. Linglong	q-vein	granite	165 - 125	4.1	9.7	1 and 2
	2. Jiaojia	shear zone	granite and Archaean metamorphics	165 - 125	3.7	6.1	1 and 2
North China	3. Jinchangyu	shear zone	Archaean metamorphics	197	3.3+	7.1	3
	4. Dongping	q-vein and q-feldspar-vein	Hercynian alkali syenite	Hercynian	3.3+	11.8	3
	5. Hadamengou	shear zone and q-vein	Archaean and Proterozoic metamorphics	Hercynian	2.0+	4.0	3
	6. Xinancha	qv/shz	Granite and metamorphics	Hycynian	1.2+	3 - 5	8
Xiao Qinling	7. Wenyu	q-vein	Archaean metamorphics	180 - 115	1.2+	7.0	4
	8. Dongchuang	q-vein	Archaean metamorphics	180 - 115	1.0+	8.2	4
	9. Yangzaiyu	q-vein	Archaean metamorphics	180 - 115	1.3+	11.4	4
SE China	10. Zhilingtou	q-vein and stockworks	Proteozoic metamorphics	Cretaceous	0.77 Ag: 61.2 t	12.0 306	5 and 6
	11. Zijinshan	breccia, vein and disseminated	Cretaceous trachydacitic to dacitic volcanic dome	125 - 105	0.3 Cu: 1 Mt	5.0 1 (%)	7

Notes:
Q-quartz; location of the deposits (ref the number) are shown in Figure 1; data source: 1-Zhou and Lü, submitted; Wang *et al*, 1998; 3-Miller *et al*, 1998; 4-Rui, 1998, pers comm; 5-Xu *et al*, 1995; 6-Pirajno *et al*, 1997; 7-So *et al*, 1998; 8-Zhou, unpublished data.

The gold province comprises seven large gold deposit (> 1.5 million oz), ie the Sanshandao, Linglong (number 1 in Figure 1 and Table 1), Jiaojia (number 2 in Figure 1 and Table 1), Xincheng, Fushan, Taishang and Daingezhuang deposits, eight medium size deposits (0.5 - 1.5 million oz), 80 small deposits and some 200 prospects. About 80 per cent of the gold deposits of East Shandong are spatially associated with the Yanshanian (Middle to Late Mesozoic) Linglong and Guojialing granitoids (Lü and Kong, 1993; Yang and Lü, 1996). There are primarily two types of gold deposits in East Shandong, namely quartz-vein and shear-zone types. The former is represented by the Linglong deposit, where gold occurs in quartz veins mainly within the Linglong granite. The shear-zone type is represented by the Jiaojia deposit, where gold is controlled by shear zones located largely along the contact zone between the granites and the Archaean amphibolite and TTG (Trondhjemite-Tonalite-Granodiorite) gneiss. Gold deposits directly hosted by the Archaean metamorphic rocks are concentrated in the Qixia area. Although it only comprises less than two per cent of the total reserve in East Shandong, it could potentially becomes important in the Qixia and Pingdu areas. Epithermal and unconformity-related gold deposits are also reported locally, although they are very small and insignificant in this area.

North China gold province

The North China gold province is a roughly EW-trending belt located in Inner Mongolia, northern Hebei, Liaoning and Jilin provinces. Nearly a quarter of the current Chinese gold resource is located in this region. The total resource was about 20 million oz in the early-1990s, and the accumulated resource has increased to some 25 - 30 million oz by now. Comparing with those in eastern Shandong, gold deposits are scattered over a much larger area, ie about 370 000 km^2, in the North China gold province.

The North China gold province is located along the northern margin of the Sino-Korea craton. Most deposits occur within the craton, and their distribution appears to be related to the Soulun-Linxi Hercynian suture zone. However, the effect of the Yanshanian oblique subduction of the Izanagi plate under the eastern China continent (*ca* 117 Ma) is emphasised in the Chinese literature, and this effect may need to be taken into account.

The Sino-Korea craton comprises the oldest rock units in China, dated from 3.8 to 3.6 Ga (Liu *et al*, 1992; Chen, 1994). Archaean and Early Proterozoic gneiss, schist, amphibolite and banded iron formation outcrop over about one-third of the area. Slightly metamorphosed Proterozoic quartzites, slates and limestones surround the uplifted basement. Gold deposits occur in areas which underwent Archaean, Hercynian and Yanshanian orogenies. Hercynian granitoids are widespread, and Yanshanian (208 - 90 Ma) granites mainly intruded in eastern part of the belt.

The principal deposits may be divided into two types, greenstone- and granite-hosted gold deposits. The former predominates in this gold province accounting for over 70 per cent of the resources. The main deposits (*ca* 1- 4 million oz) include the Jiapigou, Jinchangyu (number 3 in Figure 1 and Table 1), Xiaoyinpan, Jinchanggouliang, Paishanlou, Honghuagou and Hadamengou (number 5 in Figure 1 and Table 1) deposits. The main gold deposits wholly or partly hosted in granites (*ca* 1 - 2 million oz) are the Yuerya, Dongping (number 4 in Figure 1 and Table 1), Haigou, Baizhangzi and Xinancha (number 6 in Figure 1 and Table 1) deposits. There are also some

gold deposits hosted in low-grade metamorphic and volcanic rocks, mainly in the fold belts, including the Sidaogou, Beinaimiao, Ciweigou and Maoling deposits. The majority of these later deposits are slate-belt type. Although their size is usually less than one million oz, the potential for finding large deposits is thought to be significant.

Qinling gold province

The Qinling gold province is located along the south and north margins of the Sino-Korea and Yangtze blocks, respectively within the Henan, Shaanxi, Sichuan and Gansu provinces. In most Chinese publications this region is divided into three gold provinces, ie West Qinling, South Qinling and Xiao Qinling from west to east. This distinction is because of the different types of gold deposits in the three subprovinces. Only the Xiao Qinling gold province is reported here since the other two subprovinces geographically belong to western China, and are not part of the Pacific Rim.

The Xiao Qinling region is currently the second biggest gold producer in China, with a gold resource over 15 milliom oz. Tectonically, it is located between the Sino-Korea and Yangtze cratons, and may have formed as the result of suturing between the two cratons. However, there has also been a later influence from the subduction of the Pacific plate under the Eurasian continent (Guo, 1987; Wang and Mo, 1995; Zhai and Deng, 1996).

In the Xiao Qinling region (ie Henan and eastern Shaanxi), gold occurs in large quartz veins (a few m wide × 4000 m long) hosted in Archaean and Early Proterozoic high metamorphic rocks and greenstone belt. The greenstone belt underwent magmatism during the Xionger (1.55 - 1.38 Ga), Jinning (*ca* 1000 - 850 Ma) and Indosinian (Triassic) orogenies. Late Indosinian (*ca* 210 Ma) and Yanshanian granites (two populations of 148 - 182 and 130 - 100 Ma) are widespread. The main gold occurrences (*ca* 0.5 - 3 million oz) are represented by the Wenyu (number 7 in Figure 1 and Table 1), Dongchuang (number 8 in Figure1 and Table 1), Yangzhaiyu (number 9 in Figure 1 and Table 1), Tongguan, Tongyu, Sifangou, Dahu, Shanggong and Qiyugou deposits.

SE China gold province

The SE China gold province is located in the SE China fold belt, tectonically situated between the Yangtze Preambrian block and the Cathaysia Precambrian mincrocontinent (Figure 1).

Isotope ages of *ca* 2.5 Ga are reported from Zhejiang and Fujian, and Early Proterozoic basement rocks of amphibolite facies are widely distributed in the Cathaysia block (Wang and Mo, 1995). The block collided with the Yangtze block during the Jinning orogeny (*ca* 1.0 Ga) (Li *et al*, 1996), and probably underwent partial rifting during the Sinian (8.0 - 6.0 Ma). The rifted parts of the two blocks remerged to form the South China block during the Middle Caledonian (Wang and Mo, 1995). During the Middle to Late Mesozoic, subduction of the Pacific plate along the SE coast caused widespread Late Jurassic to Middle Cretaceous volcanism and granite intrusions (Guo, 1987).

The total resource in the SE China gold province comprises less than five per cent of the East China total gold. The gold is hosted either within inliers of the Proterozoic metamorphosed basement or in Mesozoic volcanic rocks and porphyry/granite. In the former setting, eg the Zhilingtou Au-Ag deposit (number 10 in Figure 1 and Table 1), Au-Ag mineralisation occurs in quartz veins or stockworks with rhodonite, chlorite and sericite alteration within biotite-plagioclase gneiss of the Proterozoic Chencai Formation (Xu *et al*, 1995; Pirajno *et al*, 1997). In the latter setting, eg the Zijinshan Cu-Au deposit (number 11 in Figure 1 and Table 1), high sulphidation epithermal Cu-Au mineralisation occurs around a dacitic volcanic pipe in the cental part of a trachydactic to dacitic volcanic dome (So *et al*, 1998). Both types of gold deposits were probably formed during the Late Mesozoic as a result of subduction of the Pacific plate under the South China continent.

SUMMARY

The major gold provinces in East China are the East Shandong, North China and Xiao Qinling gold provinces, with a minor amount gold in the SE China gold province. Formation of the major gold provinces appear to be controlled by the major tectonic movements in China. The major Precambrian cratons in China are the Sino-China, Tarim and Yangzi blocks, and the tectonic history of China is dominated by the interaction between these three blocks and with the Siberian, Kazakhstan and Indian blocks, and deformation of accreted sequences between the Precambrian massifs.

Apart from strong tectonic movements during the Late Archaean and Proterozoic, the major Archaean blocks have undergone multiple orogenic tectonics and magmatism along their margins since the Palaeozoic. The most important tectonic events are the Hercynian orogeny, which led to the start of the collision of the Siberia and Sino-Korea blocks which formed the Xinganling and Yanshan fold belts. The Indosinian orogeny (Triassic) led to merging of the North and South China blocks forming the Qinling-Dabie-Sulu fold belts. Many of the Chinese gold deposits are located along these two major tectonic belts. During the Yanshanian (208 - 90 Ma), the tectonic patterns and gold distribution in East China were largely influenced by subduction of the Izanagi-Pacific plates under the Eurasian continent.

ACKNOWLEDGEMENT

Thanks are due to my previous Chinese colleagues, Wenkui Guo, Zongyao Rui, Hongtao Zhang, Jingwen Mao, Fengjun Nie, Dequan Zhang, Jiqing Liu, Jishun Ren, Mengeng Liu, Lansheng Liu, Longri Min, Jun Zhou, Rongfu Pei, Guxian Lü and Jiashan Wu. G Neil Phillips, Richard Goldfarb, Yuming Qiu and Zhengxiang Li are acknowledged for some constructive discussions. Guoyi Dong and an anonymous reviewer are thanked for comments.

REFERENCES

CGMS (Commission for Geological Map of China, 1:5 000 000), 1990. Explanation Notes of the Geology Map of China 1:5 000 000, p 82 (Geological Publishing House, Beijing).

Chen, J, 1994. Greenstone belt gold deposits in China, in *New Development of Research on Gold Deposits of China*, (Ed: B Chen), pp 4-29 (Seismic Publishing House, Beijing) (in Chinese).

Guo, W, 1987. *Guide to the Metallogenic Map of Endogenic Ore Deposits of China* (1:4 000 000), p 72 (Cartographic Publishing House, Beijing).

Li, C Y, Liu, Y, Zhu, B C, Feng, Y M and Wu, H C, 1978. Structural evolution of the Qinling and Qilian Shan, *Scientific Papers on Geology and International Exchange*, pp 174-197 (Geological Publishing House, Beijing).

Li, Z X, Zhang, L and Powell, C McA, 1996. Positions of the East Asian cratons in the Neoproterozoic supercontinent Rodinia, *Aust J Earth Sci*, 43:593-604.

Liu, D Y, Nutman, A P, Compston, W, Wu, J S and Shen Q H, 1992. Remnants 3800 Ma crust in the Chinese part od the Sino-Korea craton, *Geology*, 20:339-342.

Liu, B and Xü, 1994. *Atlas of Lithofacies and Palaeogeography of South China*. 188pp (Science Press, Beijing) (in Chinese).

Lü, G and Kong, Q, 1993. *Geology of the Linglong-Jiaojia Type Gold Deposits*, p 253 (Scientific Publishing House, Beijing) (in Chinese).

Miller, L D, Goldfarb, R J, Nie, F, Hart, C Jr, Miller, M L, Yang, Y and Liu, Y, 1998. North China gold – A product of multiple oregens, *SEG Newsletter*, 33:1-12.

Pirajno, F, Bagas, L, Hickman, A H and Gold Research Team, 1997. Gold mineralization of the Chencai-Suichang Uplift and tectonic evolution of Zhejiang Province, southeast China, *Ore Geol Rev*, 12:35-55.

So, C, Zhang, D, Yun, S and Li, D, 1998. Alteration-mineralization zoning and fluid inclusions of the hingh sulphidation epithermal Cu-Au mineralisation at Zijinshan, Fujian Province, China, *Econ Geol*, 93:961-980.

Wang, H and Mo, X, 1995. An outline of the tectonic evolution of China, *Episodes*, 8:6-16.

Wang, L G, Qiu, Y M, McNaughton, N J, Groves, D I, Luo Z K, Miao, L C and Liu, Y K, 1998. Constrains on crustal evolution and gold mellogeny in the Northwestern Jiaodong Penisula, China, from SHRIMP U-Pb zircon studies of geanitoids, *Ore Geol Rev*, 13:275-292.

Xu, G, Yao, S, Zhang, C and Wang, P, 1995. A case study of the Zhilingtou gold-silver deposit, Zhejiang, China, in *Proceedings of the 1995 PACRIM Congress* (Eds: J L Mauk and J D St George), pp 645-649 (The Australasian Institute of Mining and Metallurgy: Melbourne).

Yang, M and Lü, G, 1996. *The Geology-Geochemistry of Gold Deposits of the Greenstone Belt in Jiaodong District*, China, p 228 (Geological Publishing House, Beijing) (in Chinese).

Yin, A and Nie, S, 1993. An indentation model for the north and south China collision and the development of the Tan-Lu and Honam fault systems, East Asia, *Tectonics*, 2:801-813.

Yin A, and Nie, S, 1996. A Phanerozoic palinspastic reconstruction of China and its neighboring regions, in *The Tectonic Evolution of Asia*, (Eds: A Yin and M Harrison), pp 442-485 (University Press, Cambridge).

Yu, H, 1984. Zircon age of the Penglai Group, Jiaodong Formation and the Geology, *bulletin of the Shenyan Institute of Geology Mineral Resources, Chinese Academy of Geological Sciences*, 9:45-50 (in Chinese).

Zhai, Y and Deng, J, 1996. Outline of the mineral resources of China and their tectonic setting, *Aust J of Earth Sci*, 43:673-685.

Zhou, T, 1998. Major gold provinces and tectonics of China, in *Geoscience for the New Millennium, 14th Australia Geological Convention*, p 496, (Abstracts Number 49, Geological Society of Australia).

Zhou, T and Lü, G, Tectonics, granitoids and gold deposits in East Shandong, China, *Ore Geol Rev* (under review).